2002

High temperature superconducting coils and devices: design, fabrication, and testing - for power applications

Frank Darmann
University of Wollongong

High Temperature Superconducting Coils and Devices: Design, Fabrication, and Testing – for Power Applications.

A thesis submitted in fulfilment of the requirements for the award of the degree

Doctor of Philosophy

from

University of Wollongong

by

Frank Darmann B.Sc (H) B.E (H)

at

Institute of Superconducting and Electronic Materials

and

The School of Electrical and Telecommunications Engineering

2002

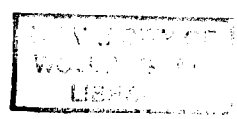

Candidate's Certificate

I, Francis A. Darmann, hereby declare that this thesis, submitted in fulfilment of the requirements for the award of Doctor of Philosophy, is wholly my own work unless otherwise referenced or acknowledged. The document has not been submitted for qualifications at any other academic institution.

Signed: _____

Frank Darmann

Date: _____

Table of Contents

List of Abbreviations

Abbr.	Meaning
HTS	High Temperature Superconductor
LN	Liquid nitrogen
sss	Sinusoidal steady state
rms	Root mean squared value of an sinusoidal AC signal
MBC	Mass boil off calorimeter
AC	Alternating current
Bi-2223	The superconductor: Lead doped bismuth strontium calcium copper oxide
DC	Direct current
Je	Engineering current density in units of A/cm^2
Ic	The current in a superconductor at which the electric field = 1 μV/cm
FS	Full scale
LIA	Lock-in amplifier
LI	Lightning impulse
p.u	Per unit system, as used in the electric power industry
n	Exponent in the DC voltage-current characteristic. *i.e* $V = (I/I_c)^n$
DQ	Double quench - a test where coils are rapidly cooled and warmed in LN
TC	Thermal or "slow" quench - a test where coils are slowly cooled and warmed
W	Watts or Joules per second
L_w	Twist pitch of filaments in a multi-filament superconducting wire
L_t	Twist pitch of filaments in a multi-filament superconducting tape
Q_h	Hysteresis loss of a superconductor in general
$Q_{h\perp}$	Hysteresis loss of a superconducting tape due to a field along the C axis
Q_c	Coupling current loss
w_{fc}	Width of the filamentary core section of a HTS tape
w_f	Width of an individual filament within a HTS tape
d_{fc}	Thickness of the filamentary core section of a HTS tape
d_f	Thickness of an individual filament within a HTS tape
w	Width of a HTS tape including the sheath
d	Thickness of a HTS tape including the sheath
λ_{fc}	The filamentary core fill factor = $w_{fc}d_{fc}/(wd)$
J_{fc}	Engineering current density of the core region = $I_c/(w_{fc}.d_{fc})$
f	The frequency of an oscillatory source of magnetic field
$\rho_\perp$	The resistivity of the matrix material for current flowing in the C direction
N	The number of filaments in a HTS tape
B_a	An externally applied AC field
B_p	The magnetic field amplitude of full penetration
β	The ratio of the applied field to B_p, i.e, $\beta = B_a/B_p$
T	Temperature in Kelvin
λ(T)	Thermal conductivity as a function of temperature

Abstract

A literature review of the state of the art of HTS AC losses and power devices determined that the subject of low AC loss HTS tapes required additional work and input and that these could be applied to HTS transformers to obtain a device with lowered AC loss compared to using straight filament tape. A procedure for manufacturing short lengths of twisted filament tape, with novel matrix alloys, and physically distinct filaments was developed. Two alloys were used for the matrix material and the range of twist pitches was from 4 to 20 mm. Tapes samples with twist pitches of 10 and 8 mm were produced with Ic's of 40 A. The AC losses were measured at power frequencies in fields up to 0.04 T using a pick-up loop and a lock-in amplifier technique. Control samples of HTS tapes with straight filaments were found to have an AC loss which was predicted very well by the established equations in the literature. Some twisted filament samples had an AC loss signature that showed a significant lowering of the losses in the range of 0.01 to 0.03 T. No straight filament samples, however, were found to have lowered losses, including those with novel matrix alloys. Suitable materials for use at liquid nitrogen temperatures that can electrically insulate HTS tapes were investigated. It was found that many commonly available materials can be used in liquid nitrogen, however, the application method and adhesives must be considered. A range of pancakes and coils were manufactured using those insulation materials found most suitable. A suitable construction technique was investigated to manufacture robust potted pancake and solenoid coils and these coils were found to give negligible degradation in the Ic after thermo-mechanical testing.

A liquid nitrogen mass boil off cryogenic calorimeter was designed and built incorporating a glass cryostat, a field coil, mass flow meters, and all non-metallic supports and frame. HTS solenoid and pancake coils were tested with AC transport currents of up to 40 A rms and with applied parallel fields of up to 80 mT peak in the range of 50-200 Hz. It was found that the hysterises losses of HTS coils could be measured with an uncertainty of ±0.5 W. The suitability of mass flow calorimetry at 77 K was demonstrated, and the AC loss results on different coils are presented. Induced currents were found to dominate the self field loss of a solenoid coil at 55 Hz, and hysteresis losses were found to dominate the loss at frequencies between 110 and 200 Hz. Hysteresis losses were found to dominate, however, in an applied parallel magnetic field at frequencies of between 55-110 Hz.

Issues regarding the practical construction of liquid nitrogen cooled HTS transformers were reviewed with respect to the relevant Australian standards and thermo-dynamic principles. The dielectric properties of liquid nitrogen and solid cryogenic insulation materials were reviewed and their electric field enhancement effects considered. It was found that liquid nitrogen had a higher breakdown voltage compared to transformer oil over comparable voltage clearances, by a factor of two to three. Electrostatic field mapping of a 100 kV solenoid coil revealed an electric field enhancement factor due to conductor radius of less than 30 %.

A dimensional analysis for the design of a 100 kVA, 3 phase, iron core, 6.6 kV/240 V, wye - wye connected transformer comprising HTS coils with Ag sheathed Bi-2223 HTS multifilament tapes was carried out. The mass, volume and tape length requirements were calculated over a range of core cross sectional areas and coil shape factors. Finite Element Methods software was used to map the magnetic fields throughout the winding volume of each design, and to estimate the hysteresis loss at full load. The analysis of

mass and volume with core area variation revealed the presence of distinct points, which minimised these quantities. However, these designs were impractical in reality owing to the significant length and cost of HTS tape that would be needed. It was also shown that the coil electrical losses in these designs were too high owing to the length of HTS tape required. By considering the factors of mass, volume, hysteretic loss, and HTS tape length and tape cost, a suitable design was found that was a compromise between all the factors involved. It particular, it was recognised that coils with a high shape factor had the lowest hysteresis losses. Assuming HTS tape was available with a modest Je of 2000 A/cm^2, it was found that the mass and volume of the transformer were reduced significantly compared to that of a conventional transformer of the same rating. The volume decreased from 206 dm^3 to 129 dm^3, and the dry mass decreased from 400 kg to 214 kg. The hysterises loss due to the parallel field profile dominated the loss in this design. The hysteresis loss due to the perpendicular field profile dominated the loss of the less suitable designs which had a lower shape factor. Approximately 50% of the total coil losses were due to less than 10% of the winding volume in these designs.

A primary HTS coil was wound with 1200 m of single HTS tape, and a secondary coil was wound with 6 HTS tapes in parallel each 50 m long. The Ic of each coil was 11 A and 215 A respectively (self field, 77 K), and each displayed a high exponential n value of 11 and 14 respectively, despite the long length and self field conditions. A proto-type transformer was constructed, complete with iron core, bushings, liquid nitrogen connections, and current leads. The equivalent circuit was calculated from room temperature measurements of the short circuit and open circuit parameters.

Acknowledgements

The research work reported in this thesis was carried out at the Australian Superconductors (AS) manufacturing facility under the guidance of the General Manager, Professor Tim Beales, and the Plant Manager, Dr. Miles Apperley. I thank them for encouraging me in this thesis and for the technical assistance which was freely given. I also thank Metal Manufactures Ltd, Port Kembla, for supporting AS and the Institute of Superconducting and Electronic materials (ISEM), and for contributing to the APAI scholarship which supported me.

Special thanks are given to Professor Dou of the ISEM who provided me with the scholarship and opportunity to enrol in a PhD course at the University of Wollongong.

I am grateful to Professor Chris Cook of the School of Electrical, Computer and Telecommunications Engineering who assisted me in the writing of this thesis, in providing advice regarding its content. I am also thankful to Chris Cook and Sarath Perera of the school for our many meetings during which I could present my work and obtain genuine feedback in a friendly and relaxed atmosphere. In particular I thank Sarath for the many references and texts which he loaned me.

The project was also supported by The NSW Department of Energy.

List of Publications

The refereed Journal papers published during the research of this work are listed as follows:

1. F.Darmann, "Design and loss calculations of a 100-kVA transformer employing multi-filamentary Bi-2223 Ag sheathed superconducting tapes", Cryogenics, Vol. 41, No. 9, pp. 611-621, 2001.

2. F.Darmann, "Determination of the AC losses of Bi-2223 HTS coils at 77 K at power frequencies using a mass boil off technique", Submitted and approved for publication in IEEE Transactions of Applied Superconductivity, 2002.

3. T.Hughes, F.Darmann, J.Horvat, S.X.Dou, "Reduction of the a.c. losses in Ag sheathed PbBi2223 tapes with twisted filaments", Physica C, Vol. 325, pp 77-82, 1999.

Foreword

The Case for Superconductivity

Most electrical devices manufactured to date employ pure metallic copper to conduct electricity along controlled paths. For the past century, the conductive properties of this metal has enabled the construction of generating plants and transmission lines to power large city populations and provide services at the receiving end such as electric light, linear traction, and rotational motion. This has in turn lead to the elimination of much of the fossil fuel burning in cities previously used to achieve these functions and has had the greatest contribution to cleaning up the air in the cities of the developed world.

Advancements in the efficiency of electrical power transmission, distribution, and rotating plant have mainly been through the use of ever increasing voltage levels, and the subsequent advancement in the electrical insulation materials employed. High voltage levels allow the current level to be lowered for the same electrical power rating, and therefore large reductions in losses can be achieved. This fact has dictated the development of the power transmission system world wide to the extent where power is now transmitted at voltages of up to 700 kV through a series of transformers. However, leveraging ever increasing efficiencies from the use of high voltages has been exhausted owing to the practical limitations and complexities of high voltage design.

The size and efficiency of electrical power devices is primarily dictated by the engineering current density at which the conductors may be operated. This rating is in turn dependent on the heat emitted by the conductors and the cooling power available for those conductors. Unfortunately, the increase in resistance of copper conductors with increasing temperature means that they must be de-rated compared with their room

temperature rating. Cooling of the conductors to decrease their temperature and therefore losses may only be employed to a very basic extent. Very rarely is active refrigeration used, as often the price, size, and power requirement of the refrigerator results in a device with no net additional benefits. The device is instead designed to use large enough conductors such that simple cooling is sufficient to reach a static temperature which does not impose a severe fire risk to the insulation materials employed. For high power transformers, generators, and motors, this often results in an extremely large device employing many tonnes of copper, iron, and insulating materials. Also, because these devices typically run at temperatures above ambient and use flammable insulations materials such as oil, the risk of fire hazard is ever present. Particularly for the electricity distribution network, a fire in a large plant item, such as a transformer or oil cooled cable, can result in a significant disruption to the electricity supply. Unfortunately, the hottest days of summer put the great loading on underground cables and transformers owing to the rapid growth in the use of air-conditioning and refrigeration plant. The higher ambient temperature on these days means that plant is less efficiently cooled. Hence, large plant is designed according to the expected loading on these hottest days, or, a short term overrating is allowed for a few hours that the plant may operate at without imposing significant loss of insulation life. The risk of a fire or of damage or significant loss of life that may result in a future fire is greatest on the warmest days of the year.

One way to solve all of the above problems would be to actively refrigerate the conductive parts of a power device. For example, at 77 K, the resistance of copper decreases by a factor of ten. This fact alone would immediately allow smaller power plant to be manufactured using the higher current density at this temperature. The constant temperature of operation would alleviate the problem of transformers and those

associated with the oil used in them. The problem with this argument is that the penalty associated with refrigeration is currently too large owing to fundamental thermodynamic principles, and from current practical limitations in refrigeration engineering.

The main penalty arises from the presently low refrigeration efficiency for temperatures around that of liquid nitrogen (77 K) and lower. At 77 K, this efficiency is typically 5-10 %, and the consequences of this is that any benefit from cooling copper conductors to 77 K is negated because the reduction in resistance is insufficient to justify the cooling power required. In addition, the economic cost and the complexity of cooling completely rule out this option. However, what if the resistance dropped by a factor of 10,000 ? Would refrigeration to temperatures of 77 K or lower then be practical for power plant in terms of cost and maintenance ? This is indeed the question faced by engineers since the discovery of High Temperature Superconductors (HTS) in 1987. Exhibiting zero dc resistance at temperatures below 110 K, and current densities of up to 20,000 A/cm^2 at 77 K, these materials have the potential to revolutionise the electricity and power industry if a positive answer to the above fundamental question is found. The subject matter of this thesis seeks to assist the engineering community in obtaining an answer to this question and to advance the knowledge and engineering uses of high temperature superconductors.

Chapter 1

Literature review

1.0 Introduction to superconductivity

This chapter reviews current HTS technology and its use in power engineering applications with reference to worldwide activities in this area. In addition to benefits of improved efficiency in existing applications and components, HTS provides the enabling technology for innovation both within existing systems and in the design of new systems. Significant attention has been paid in this literature review to applications and demonstrations of HTS devices so that a better understanding of the issues involved is gained and to assist the candidate in finding suitable areas of study and practical applications to explore and contribute to. In addition, the subject of losses which occur in HTS under alternating current (AC) conditions will be explored, and the works of some of the major contributors to this field will be reviewed. The essential technologies and measurement techniques are reviewed from both the practical and theoretical points of view.

Superconductivity was discovered in 1911 by Kamerlingh Onnes whilst working on the liquefaction of gases. Instead of an expected levelling off of electrical resistance in mercury approaching absolute zero, he found no resistance - a flow of electricity without power loss from the conductor. Subsequently, other characteristics were established including critical values of temperature, current density and magnetic field below which the material remains superconducting, and the Meissner effect - the exclusion of magnetic field from superconductors.

The great potential of superconductivity remained unexploited for over fifty years because, in the materials studied, the phenomenon was limited to within a few degrees of absolute zero. By the late 1950s considerable advances in theoretical understanding led to engineered materials with critical temperatures of 20-30K. Using these low critical temperature (LTS) materials, several years of widespread activity followed during which many applications of superconductivity were successfully demonstrated. These demonstrations established superconductivity as an enabling technology, e.g., for magnetic resonance imaging (MRI), but rejected superconductivity in place of existing technologies where the high cost of liquid helium cooling resulted in an unacceptably large size and scale of operation to break even, e.g., 1-5 GVA for transmission cables, above 5 MW for DC motors.

In 1986 researchers at IBM reported the discovery of ceramic superconductors [1.1] and reports soon followed of materials with critical temperatures above 77K, the liquefaction temperature of nitrogen at atmospheric pressure. These materials were immediately named High Temperature Superconductor materials (HTS) [1.2]. This created great interest world-wide both in the search for materials with ever increasing critical temperatures and because of the very significant reduction in the cost of cooling with liquid nitrogen compared with liquid helium, which had been required for LTS demonstrations. Since their discovery, development work on ceramic HTS materials is bringing their unique properties close to exploitation in many areas [1.3].

HTS materials are brittle polycrystalline copper oxide based ceramics with highly anisotropic properties and low thermal conductivity. Some fifty or more HTS materials have been reported and investigated and the search for materials with high-T_c continues. However current developments are concentrated almost entirely on the materials shown in Table 1.1 which lists their critical temperatures. These materials are frequently

referred to by the first letter of their constituents and/or their stoichiometric ratios i.e. $Y_1Ba_2Cu_3O_{7-X}$ is referred to as YBCO or 123 and the Bismuth materials are referred to as Bi-2212 and Bi-2223. The thallium and mercury barium copper oxides are still very much at the research phase but the Yttrium and Bismuth oxides are the focus of commercial HTS development.

FORMULA	NAME	ABBREVIATION	T_c (K)
$Y_1Ba_2Cu_3O_{7-X}$	Yttrium Barium Copper Oxide	Y-123	92
$Bi_2Sr_2Ca_1Cu_20_X$	Bismuth Strontium Calcium Copper Oxide (2212 Phase)	Bi-2212	80
$(Bi,Pb)_2Sr_2Ca_2Cu_3O_X$	Bismuth Strontium Calcium Copper Oxide (2223 Phase)	Bi-2223	110
$Tl_2Ba_2Ca_1Cu_2O_Y$	Thallium Barium Calcium Copper Oxide (2212 Phase)	T-2212	98
$Tl_2Ba_2Ca_2Cu_3O_Y$	Thallium Barium Calcium Copper Oxide (2223 Phase)	T-2223	125
$Hg_1Ba_2Ca_2Cu_3O_Y$	Mercury Barium Calcium Copper Oxide (1223 Phase)	H-1223	133

Table 1.1 HTS Materials and their Critical Temperatures

The most important property of a superconductor is its critical current density, J_c, above which energy is dissipated by the finite resistance of the material whenever a direct current flows just as in normal materials. The current that can flow through HTS materials is limited by weak links in their anisotropic and polycrystalline structure. Alignment of grains during processing of the materials can reduce the effect of weak links and increase the critical current. With alternating current, HTS materials exhibit hysteretic AC losses even in the superconducting state due to the non-reversible nature of the magnetisation of these materials.

The magnetic field dependence of the superconducting state is also anisotropic and can be enhanced by grain alignment. In all power applications the magnetic field, whether induced or applied, penetrates the HTS material whose ability to resist movement of the magnetic flux increases the critical current. This is referred to as "flux pinning". Above the critical magnetic field magnetic flux moves freely through the material which is no longer superconducting. Figure 1.1 shows the magnetic fields at which superconductors are required to operate in different applications and the rate of fall of J_c with increasing magnetic field.

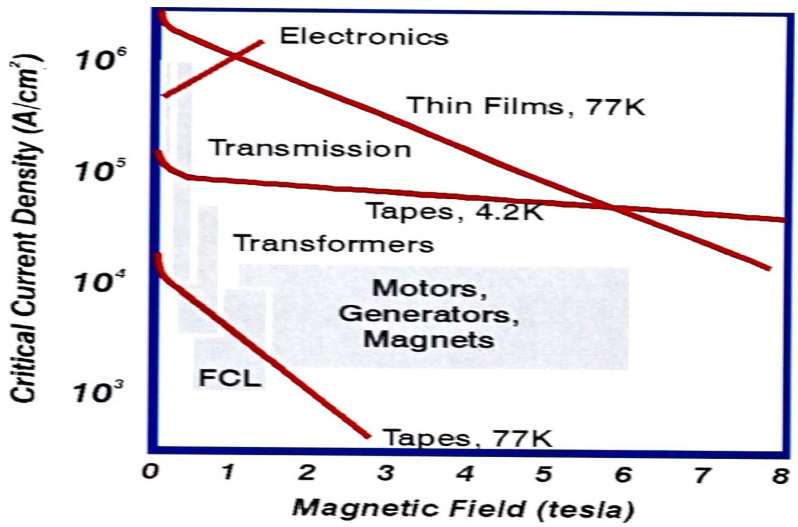

Fig 1.1 Jc requirements for applications. J_c vs magnetic field for HTS tapes at 77 K & 4.2 K and thin films at 77 K [1.3].

YBCO shows good intrinsic flux pinning. It is being developed commercially for use in some bulk applications such as current leads but cannot yet be processed into long length tapes. Various thin film deposition methods for producing YBCO tapes are currently being researched but are still at a very early stage of development, hence all power demonstrators so far have used the BSSCO materials in the conductors. BSCCO has a plate like structure, can be aligned to minimise weak links and this can be enhanced in a tape forming process.

Power applications of superconductivity depend on the availability of the material in long wires or tapes with J_c of at least 10^4 A/cm^2 as seen in figure 1.1. The manufacture of BSCCO HTS tapes using the powder-in-tube (PIT) technique has been established as the preferred processing technique to meet the required performance and has been studied significantly [1.4]. The PIT process encapsulates the superconductor in a silver or silver alloy tube which is then drawn to wire and rolled flat to provide single or multi-filament tapes. Appropriate annealing and heat treatment stages together with rolling ensure that the required microstructure develops. The silver is used because it is the cheapest metal that is benign to the superconductor material. The sheath provides mechanical strength as well as cryo-stability to the HTS material. Further improvements in both mechanical performance and cryostability result from the use of multi-filament as opposed to single filament tapes. The fabrication of multi-filament tapes with many thousands of micron size filaments has been developed for LTS superconductors. This technology base has been used to accelerate the development of HTS wires and cables of practical length. The economics for various applications, however, would benefit from an order of magnitude increase in current density as less superconductor would be required thereby lowering costs. Current densities in excess of 10^6 A/cm^2 are routinely achieved in thin films using these materials. Also, using PIT-type processing techniques, current densities approaching that of thin films are now being reported, albeit over small cross sectional areas [1.5]. This indicates that with further development and optimisation of the tape processing techniques it will be possible to obtain the required critical currents using these materials.

1.1 Power Engineering Applications of Superconductivity

1.1.1 Transmission

Electric power transmission is required to transfer electrical energy from a generating station or source to a consumer. It allows remote hydro resources to be tapped for electricity generation and vast coal reserves to be exploited without contributing to the pollution of the "air shed" of major cities. The efficiency of transmission is limited by conductor losses which can be reduced by limiting the current flow and operating at increased voltage. Typically, voltages of up to 500kV in cables and 765kV in bare overhead lines have been used to limit the current to a few thousand amps. Depending on the distances involved, the efficiency of transmission is between 95% and 99%. This allows economies of scale associated with large scale centralised generation to be exploited.

After generation at 6.6 to 22kV, the voltage is increased for transmission and then reduced to around 11/22kV and 415 volts which are more suitable for industrial and domestic users. Traditionally, this has been achieved using an AC power transmission network comprised of cables and transformers.

Transmission at high voltages increases the requirements for electrical insulation which can most economically be effected by the use of bare overhead conductors separated and cooled by air. Hence the familiar overhead transmission towers which span country sides and suburbs all over the globe.

Where high voltage transmission is required into city areas and where visible towers are unacceptable for either aesthetic reasons or in areas of high conservation value, the installation of underground cables is warranted. These cables are limited by thermal performance and require insulation of the conductors with either XLPE, or oil-impregnated paper pressurised with circulating oil. The expense of insulating and

protecting the conductors, excavation, installation and backfilling, increases the cost of underground cable systems significantly to about ten times that of their overhead counterparts.

Superconductors, which all require operation at cryogenic temperatures, offer no practical benefit for overhead transmission, but become attractive as the conductors in high voltage cables because of the reduction in losses. Cables with LTS conductors have been successfully demonstrated but were disadvantaged by the high cost of cooling with liquid helium [1.6]. Studies have shown, however, that HTS cables can transmit power at low loss with annual cost savings of up to 60% compared with conventional underground cables and for very high capacity cables, a capital cost saving of up to 30% may be realised [1.7].

Factors limiting the performance of HTS cables are conductor Jc, AC loss, cable self-field, and the heat loss through the walls of the cryostat. The fields generated by cables are amongst the lowest for any power application and so underground cable transmission may be among the first applications of HTS. However, to achieve the anticipated benefits which are indisputably and economically attractive, the current density of the tapes needs to be an order of magnitude greater than currently available over the required length.

An early application of HTS cables which may have less demanding current density requirements than above is expected to be the retrofitting of cables to increase transmission capacity within existing infrastructure. There are opportunities for both replacement of the cable in pipe-type systems and for increasing the capacity through existing ducts. This is in fact the case, as detailed by Harra, in Tokyo where the 2.5% annual growth in that city will see existing transmission requirements double in the next 30 years [1.8]. The existing ducts, currently carry 1000 MVA each, and are too small to

accommodate another conventional power cable at the proposed ratings of 600 or 1000 MVA but could house a 150 mm diameter cable. It has been reported that an HTS cable with a diameter of 130 mm operating at 66 kV could supply a further 1000 MVA. The predicted saving from the use of the existing ducts compared with new installations is 58%. In addition the need for substations at intermediate points is eliminated due to the very low voltage drop of HTS cables, reducing the total cost of substations by 28%. Furthermore, the HTS cable would require only 6% of the compensating shunt reactance compared to a conventional cable.

Traditionally DC transmission has always offered advantages over AC transmission in terms of simpler and cheaper conductor design without the need for reactive compensation. However, the high costs of rectification and inversion have limited the use of DC for transmission to particular situations such as submarine links, grid inter-ties etc. With superconductivity, DC offers the additional advantage of reduced copper losses compared with conventional HV DC. With HTS DC transmission, losses are very small even at the level of 2 kA, being under a W/m compared to several tens of W/m for conventional high tension lines and cables. The advantages of high voltage transmission then disappear, opening up the possible benefits of operation at lower voltages. These include simpler design based primarily on critical current performance and life extension of various components including insulators and switch gear. Prototype DC transmission models are already being investigated [1.9].

Reduced voltage transmission could offer radical change for the future design of systems. The timing for such change appears appropriate because the indications are that the economies of scale associated with the traditional approach to go to ever higher voltages have peaked [1.10-1.11]. As consideration is given to future load growth, questions must be asked such as: Can present systems design cope economically with a

load that may double in the next 30 years? What will be the most economical means to transmit this power?

1.1.2 SMES

SMES is a means whereby the excess base load generating capacity which exists at off peak times may be stored magnetically to provide instantaneous electricity during peak periods later the next day, referred to as load levelling [1.12-1.15]. The principle relies on the loss-less circulation of superconducting currents in a coil. The energy is effectively stored in the magnetic field of the coil. Necessarily, the AC supply must be rectified in order to store energy in a SMES unit, and be inverted to feed back into the grid. Despite this disadvantage, a SMES unit can achieve a round trip efficiency of up to 93%, with about half of the loss occurring as a result of the AC to DC conversion.

A major advantage of SMES is that the response time is very fast, about five AC cycles, limited by the switching speed of the solid state inversion/rectification components. This feature can provide enhanced transmission line stability through the judicious placement of SMES at various positions within a system. These include line voltage support by providing capacitive reactive VARS at the terminal station level, or spinning reserve fast load levelling by supplying real power at the generator level. The newly developed power inverters can effectively use storage to operate in all four quadrants of the power plane. Stabilisation applications requiring energy storage, which have lower energy requirements than those needed for load levelling, may well be the first utility application of SMES.

LTS SMES has already been demonstrated to stabilise an inter-tie line in the USA. The capacity of this unit was only 8.3 kWh but could supply 10 kW [1.6]. This unit ran successfully for 12 months between 1983 and 1984. Several other demonstration units

have been built including one in Australia [1.13]. LTS SMES units with only 0.416 kWh of storage are available commercially for around US$1M. These units, with up to a 0.75 MW rating, provide stability of voltage to industries which have stringent power quality requirements. Construction of a 5000 MWh utility scale LTS SMES is planned to begin in Japan in the year 2004 to fulfil a load levelling function. Such a system could provide 1 GW of peak power for 5 hours at a cost of around US$1B [1.15]. As a comparison, the cost of a new generating plant is also around US$1B for 1 GW.

1.1.3 Rotating plant

The two main losses in generators and motors occur in the rotor as copper loss and in the armature as eddy current iron loss. Because of the absence of DC losses, replacement of the DC field rotor winding with superconductors has been proposed. If the field generated by these windings can be made sufficiently large, machines can be designed with air cores replacing the traditional iron cores, thus greatly reducing size and weight in addition to reducing AC losses. In general, HTS may enable the miniaturisation of plant while increasing conversion efficiencies.

Compared with conventional machines, the reduced size and weight possible with HTS will reduce the capital cost of construction, whilst the low losses will provide savings in running costs. The results of a study carried out for a typical utility sized generator of 300 MW show that the cost of construction may be reduced by 15% through the incorporation of HTS in the rotor design, while saving over 80% in annual costs associated with losses [1.15]. Assuming the same reliability, the break-even point for HTS generators compared with conventional generators could come down to the MVA range.

A partnership between American Superconductor corporation and Rockwell automation has resulted in some very successful HTS motor development under the US DOE (Department of Energy) SPI (Strategic Partnership Initiative) [1.16]. A 125 hp motor working at 30 K was developed during phase I of the program, and a 1000 hp HTS motor using Bi-2223 HTS tape has been manufactured in-phase II. The 1000 hp motor fully represents the design issues to be addressed in the future 5000 hp motor also to be developed in-phase II. The losses have been reduced by half in a package with half the volume. Each pole of the 4 pole device contains coils with 4500 m of HTS Bi-2223 based wire with an Ic of 52 A (Self field, 77K). A total of 18000 m of wire was used.

1.1.4 Fault Current limiters

Protection schemes such as circuit breakers used to ensure safety of domestic and industrial users and to protect equipment at terminal stations and substations are an integral component of power distribution circuits. One critical design consideration of circuit breakers is their current rating under fault conditions. The ratings of these high voltage switches must be suitable to handle a worst case fault current caused by a number of possibilities such as line to ground, line to line, three phase line faults and lightning strikes. So too, many components in a power transmission system must be designed with suitable over ratings to cope with fault currents which may be up to 10 times rated current for short periods.

Calculation of the fault current level must take into account generator characteristics, line impedances, voltages, and conductor characteristics present, as well as large machinery and embedded generators which may be connected to the system. These machines contain large coils which feed a fault condition and are now being regularly

included in fault level calculations by power transmission companies. Hence, fault levels increase with industrial activity and expansion of the network.

Problems with circuit breakers include their cost, their vulnerability to be damaged on operation and their low speed of response - about 50ms or nearly three full 50 Hz cycles. Subsequent to a fault, the peak fault current, which may be up to twenty times rated current, occurs within milliseconds. System components may therefore be subjected to very high currents before the circuit breakers operate and must be designed accordingly. A proposal to incorporate faster circuit breakers to limit the fault current within the first two cycles, has been criticised because of insufficient utility experience and for not being fail safe in operation [1.17,1.18].

The incorporation of FCL's into a distribution system containing circuit breakers offers a practical solution to the above problems. FCL's can reduce the maximum fault current many times down to only about twice the rated current. Traditionally, FCL's are very large reactors and normal system currents flow continually through the FCL which therefore must incorporate large conductors, and tonnes of iron and copper which have associated losses.

To reduce the losses and reduce the overall size, a HTS FCL may be employed. These devices exploit the very fast switching (fractions of a cycle) between superconducting and normal states when a superconducting current increases above its critical limit and protect the system for those first few cycles long enough for the slower circuit breakers to operate. Prototype devices have already been built to demonstrate the possibility of a HTS FCL.

In one novel example, a saturable magnetic core is also used but with HTS windings used to energise two separate magnetic circuits [1.19]. The AC line current energises two conventional copper coils, which are in series, with one on each closed magnetic

circuit wired so as to oppose the flux in each produced by the HTS coils. The DC HTS windings saturate the cores and the AC coils produce a small perturbation about the saturation point. This results in the impedance being very small during normal operation because the iron is saturated and so the coil combination has little inductance so it acts like an air core inductance. When in fault, however, the large fault current in the AC windings drives each of the magnetic circuits out of saturation giving the coil combination high impedance. This effectively inserts a high impedance device in the network which is what is required to reduce fault currents. This device has a fast response to fault conditions and low reactance under normal operation. Two magnetic circuits are, however, required in order to limit the fault current in the positive half and negative half of the mains frequency cycle. The advantage of this design is that the line current is not conducted through the HTS coils and the HTS coils are operated with DC current so the standby losses are negligible.

1.1.5 Transformers

The largest utility scale conventional transformer offers efficiency greater than 99.5%, nevertheless, HTS can still offer clear advantages in reduced size and weight. A large 1000 MVA terminal station transformer typically consists of 150 tonnes of copper wire and has a total weight of 600 tonnes. In contrast, a HTS transformer of this rating would consist of a mere 80 kg of superconducting tapes and would weigh 110 tonnes [1.7]. It is also reported that, unlike the other applications discussed, HTS transformers are likely to have a higher initial capital cost due to the HTS tape content [1.20,1.21]. The reduced life cycle costs, however, more than make up for this disadvantage with the total lifetime cost coming in at 60% cheaper than that of conventional transformers. In fact, depending on the critical current and the AC losses of the tape employed, it has

been shown that for high power transformers above 100 MVA, the weight of HTS transformers to conventional can be reduced to just 60 %.

In order to compete with the very high efficiencies of conventional transformers, tapes must have very low AC losses and a minimum current density of 10,000A/cm^2 in a field of 0.2 Tesla over kilometre lengths [1.21]. Currently in LN the best BSCCO HTS tape can achieve a Je of about 20,000 A/cm^2 over lengths of up to 1 km in self field [1.22,1.23]. Nevertheless, proto-type HTS transformers have been designed and built in the USA [1.24], Japan [1.25,1.26], Germany [1.27], and Switzerland [1.28,1.29]. Two of these programs will be described here in detail as they use widely different operating temperatures.

Waukesha consortium, USA, [1.24].

This company, in association with Oakridge National Laboratory (ORNL), Intermagnetics General Corporation (IGC), IGC/APD cryogenics (APD), and Rochester Gas and Electric (RGE) have built a 1MVA, single phase 60 Hz, 13.8/6.9 kV, 75/145 A, HTS transformer using dip coated Bi-2212/Ag tapes. The iron core diameter was 28 cm, giving a core cross sectional area of 0.113 m^2 which is basically the same as for a conventional 1 MVA transformer. The coils are essentially square measuring 1.2 m in diameter and height. Only approximately 7 kg of HTS conductor was used in the design which incorporated a 25 K closed cycle refrigerator.

The number of partners involved in the program is indicative of the expertise that is required to develop these new types of Transformers. IGC supplied the HTS tape, ORNL specialised in AC loss measurements and some aspects of coil design, APD designed and installed the cryogenics. The expertise of Waukesha transformer and the

utility, RGE, was used to design a device that was practical and could be connected in the supply grid.

The Waukesha design used HTS coils in a cryo-cooled environment at 25 K which differs from most designs in the literature which employ sub-critical or critical liquid nitrogen (65 to 77 K). The dip coated 2212/Ag tape which was used is also unique since it is of lower cost than PIT Bi-2223 tape, and therefore the total ownership cost of the design will be less than that of a transformer manufactured from Bi-2223 tape and operated at 77K. The use of 2212 type tape necessarily required lower temperatures of operation because the Je at 77K of Bi-2212 tapes is lower than that of Bi-2223 tapes. The use of Bi-2212, however, was abandoned because of a lack of supply of the material and more recent proto-type coils have been manufactured using Bi-2223 PIT tapes. These coils were rated at 5/10 MVA. It is anticipated that 30 MVA, 138 kV transformers for the zone sub-station market will be available by 2005.

The most likely reason for employing a 25 K operating temperature was to reduce the tape cost and shift the expense to the refrigeration which is much larger at 25 K than at 77 K. In 1997, when the Waukesha program began, long lengths of HTS tape were less readily available than now. By operating at 25 K, the amount of HTS tape required was significantly reduced due to the increase in Ic. It can be estimated from the refrigeration co-efficient of performance (CoP) at 25 K that each W of loss requires 166 W of cooling power. Although a significant amount of information regarding the construction details and plans of this project are available in the literature, the ultimate efficiency achieved in the device at full load power was not available nor is it reported in the literature [1.24]. This may indicate that the efficiency of this HTS design compared to a conventional device may not have been demonstrated.

Kyushu University, Japan [1.25]

This university group, in association with Fuji Electric, and Sumitomo Electric have built a 500 kVA, single phase 60 Hz, 6.6/3.3 kV, 76/152 A, HTS transformer using Bi-2223 tapes operated in LN. The iron core diametre was 35 cm, giving a core cross sectional area of 0.0986 m^2 . This was much larger than the typical 20 cm diametre core size used in conventional 500 kVA transformers. The coils measured approximately 0.5 m in diametre and 0.75 m in height. The rating could be increased to 800 kVA when the coolant was sub-cooled to 66 K. The overall efficiency achieved at 77 K was 99.1 % at full load and 99.3 % at 66 K/800 kVA. A total of 2200 m of tape was used in the design with three tapes used to form the primary conductor and two used for the secondary.

A number of innovations were included in the winding structure to reduce certain components of the AC losses. Each tape in the multi-tape conductor was insulated with a glass fibre insulation tape. The individual tapes within the conductor were transposed 5 times in each layer. This technique is analogous to the continuous transposed conductor (CTC also known as Roebel bar) used in some transformer windings, and the usual techniques used in transformer coil manufacturing where transpositioning was included in-situ during winding.

The results of the literature survey on HTS transformers and calculations suggest that operation in sub-cooled nitrogen is the most efficient manner in which to design HTS transformers employing Bi-2223 HTS tape. At 25 K, the self field Ic increases by a factor of four compared to that at 77K. The cryogenic penalty, however, increases a lot faster, in fact, by a factor of 8, from 20 at 77K to 166 at 25K. By sub-cooling the nitrogen to 66 K, the Ic of the tape in the coils (self field) almost doubles, but the cryogenic penalty increases by only 50 %.

1.2 AC losses

1.2.1 Introduction

The subject of AC losses in superconductors is of great technological interest to researchers in the field of applied superconductivity. They are a key consideration in the design of practical superconductors in applications such as transmission cables, coils for transformers, pulsed magnet coils for magnetic-confinement in fusion reactors, and rotating electric plant such as motors and generators. The term AC losses has a somewhat different meaning to workers in different areas of applied superconductivity. To power electrical engineers, AC losses usually refer to those losses generated by transport currents varying sinusoidally at 50 or 60 Hz in either small fields as present in a transformer (<0.1 Tesla (T)) or large fields such as motors and generators (< 2 T). For someone designing a pulsed magnet coil, AC losses are those which arise due to the slow linear ramp up of the magnet current to fields up to 10 T or higher.

Three different types of AC loss occur in multifilamentary superconductor composites, namely, the hysteresis loss in the magnetically non-reversible superconductor, the classical eddy current loss in the normal metal matrix, and the coupling current loss in the matrix material between the filaments. The later loss is distinguished from classical eddy current loss because, part of their closed path coincides with the superconductor itself. Eddy current paths on the other hand flow purely in normal metal for the whole of their path. This definition will be used throughout this thesis.

1.2.2 General theory of AC losses.

The power loss density Q_v at any point in space due to any electromagnetic phenomenon may be generally determined by the dot product Equation 1.1 and the total power loss, Q, by Equation 1.2:

$$Q_V = E(r,t).J(r,t) \qquad \text{Eq. 1.1 } [W/m^3]$$

$$Q = \iiint E(r,t).J(r,t).dV \qquad \text{Eq. 1.2 [W]}$$

E(r,t) is the electric field vector at any point in space at time t and **J(r,t)** is the electric current density vector at point r at time t. **E** and **J** may also be represented by phasors to represent the case of sss varying electromagnetic fields and currents. In this case, the Equations 1.1 and 1.2 are integrated over one cycle and the result multiplied by the frequency, f, to give the loss. The integration must be taken inside a volume containing the material of interest. Another general Equation, which is integrated over a surface, the poynting vector, is used when only the fields E and H are known on that surface and is generally used in antenna design. Also, when no transport current is flowing in a magnetic material, it may be shown than the total loss is given in the sinusoidal steady state (sss) by Equation 1.3.

$$Q = \mu_o \oint M.dH \qquad \text{Eq. 1.3}$$

Where **M** is the net magnetic induction vector in the sample in response to an induction, **H**. Note that the dot product is taken in 1.3 so only knowledge of the component of **M** parallel to **H** is required.

Employing Maxwell's equations in their sss form, one may show that the AC energy loss per cycle is equal to the area enclosed by the hysteresis loop of M versus H, with $B=\mu_o H$. Therefore, Equation 1.2 integrated over 1 cycle must be equivalent to the area

inside the hysteresis loop, in Equation 1.3 With full knowledge of the two vectors, **E** and **J** in space and time, or the scalar material properties of net sample magnetisation parallel to magnetic induction, the total loss of a superconductor or any other material may be calculated.

When reworked, Equation 1.1 yields ohms law and the loss of energy in a resistor in a straight forward manner, because in a resistor, a very simple relationship exists between **E** and **J**. So too, in simple devices such as capacitors and inductors, where simple linear constitutive relationships exist between the current density and electric field, or induction and magnetisation, equations can be derived for the energy stored in them and this has lead to the everyday simplified description of these devices in terms of a single number, namely the capacitance, or inductance, and the specification of losses by the Q factor and loss tangent respectively.

Since the discovery of electromagnetism, engineers have condensed the particular properties of devices that demonstrate otherwise complicated electromagnetic properties, into a single number or set of simple equations that for practical purposes, describes the behaviour in an electric circuit or power device. This simplifies circuit design and allows simple specification of components that will give consistent electrical properties and responses between different manufacturers. The quantities **E**, **J**, or H and M, however, are generally not known for a superconductor under all circumstances and in particular, assumptions of the current density distribution throughout the superconducting volume must be made to solve Equation 1.1 or the magnetisation details modelled to solve Equation 1.3. For this reason, the losses in superconductors are not straight forward to calculate, and therefore as yet, no simple analogy to the common circuit elements fully describes these materials accurately under all circumstances.

Great progress has been made in the field of AC losses, however, in both LTS and HTS conductors in terms of both measurement technology and developing empirical equations [1.30-1.47]. The AC loss in simple HTS conductors can now be predicted to within 15% for sss excitations [1.43,1.44]. Just as not all properties or net loss of even a simple piece of wire can be specified by a single number or Equation under all electromagnetic circumstances, so too, not all electromagnetic properties nor the loss of HTS conductors can be exhaustively described by one equation. This is evident when trying to apply the usual approximations to the so called low AC loss HTS tapes that incorporate various alloying materials and twisted filaments [1.36-1.44]. Although not as common as straight filament tape, these HTS conductors represent the most practical method for reducing AC losses in high temperature superconducting power devices to date.

The low frequency (<500 Hz) low field (< 0.1 T) sss shall be assumed to apply in the discussion and analysis from here forth. We will not be concerned with those transient components of loss which occur when switching on a device, or when the current is ramped up to some final value.

If no transport current is present in the superconductor, then the total loss can be referred to as the hysteresis loss, in units of J/cycle/m and is equal to the area of the M-H loop. Neglecting small effects such as flux creep, the total AC loss is therefore made up of a number of components, namely, the superconductor loss, coupling current losses, and the eddy current loss.

The specific energy loss in the superconductor itself, Qs, expressed in J/ cycle/m is independent of the frequency in the regime of interest in this thesis. The hysteresis loss, expressed in W, is directly proportional to the frequency. This component of loss has

been greatly studied and has been found to be very well approximated in HTS tapes by the slab geometry approximation [1.31-1.35].

1.2.3 Slab Geometry

The simplest geometry to analyse theoretically is that of a rectangular slab, as shown in Figure 1.2, with side dimensions of 2a and 2b, with the dimension 'a' perpendicular to the field and critical current density, J_c, in a uniform field of peak strength B_m (peak to peak). The Bean critical state model was used to analyse this situation [1.35]. The widely adopted conventions shown in Figure 1.2 by the superconducting community naturally lead to one referring to the different components of AC losses as being attributed to the different components of magnetic field. Hence, the terms "parallel field loss", $Q_{//}$, and "perpendicular field loss", $Q_{\perp}$, arise. Other terms commonly used to

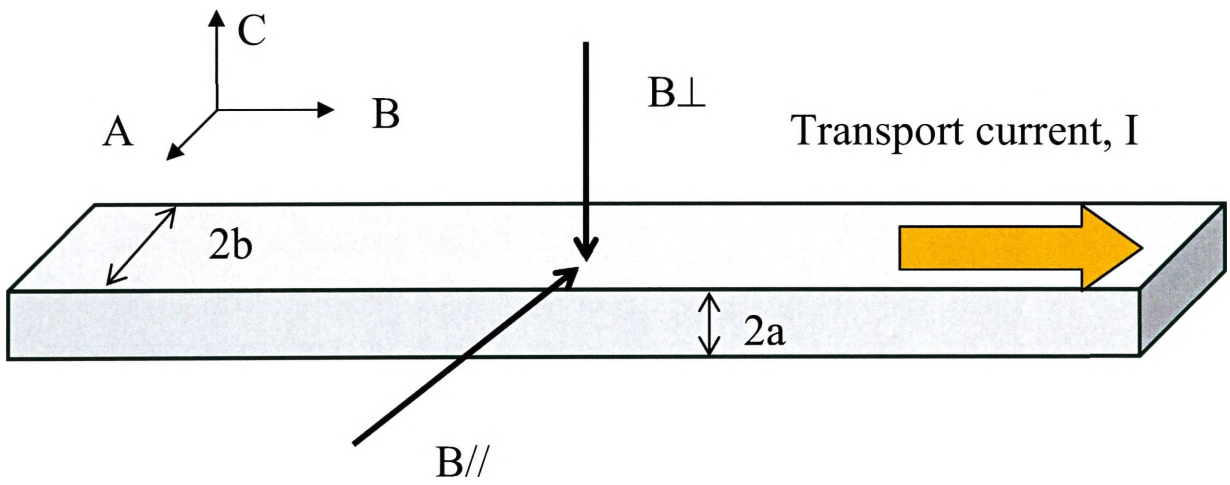

Figure 1.2. Schematic of a bulk superconducting slab showing the conventions used in the slab model. The thickness is 2a, and the width 2b. The "parallel field" is parallel to the wide side of the aspected superconductor, and the "perpendicular field" is perpendicular to the wide side.

distinguish vector quantities with respect to a superconductor slab or HTS tape are "parallel to the tape/slab" and "perpendicular to the tape/slab". For convenience, these terms will be used throughout this work as defined in Figure 1.2. In addition, owing to the near isotropy within the A-B plane, the term "Parallel to the tape/slab" will refer to any vector which is in the A-B plane of the tape or slab, as defined in Figure 1.2.

The simplest situation to analyse is the "infinite slab" in a parallel field, where 2b is extended to infinity, I = 0, $B_\perp$ = 0, and 'a' is the "half thickness" of the slab. The calculations may be separated into two different cases. That where the field penetrates the bulk superconductor, but not fully, and where the field has fully penetrated the slab. The volume integral of **E.J** in Equation 1.1 is straight forward to calculate in this case. Closed loop shielding currents flow in the sample in response to the oscillating applied field and are assumed to have a current density equal to Jc. Any un-penetrated region has a current density of zero. Due to the absence of any eddy and coupling currents, the electric field is simply given by $d\phi/dt$ where ϕ is the flux enclosed by the closed loop of the shielding currents. It also assumed that the electric field in the centre of the slab is E = 0, where the induced currents reverse. The losses per cycle in both these cases have been analytically derived by Wilson [1.31].

$$Q// = \left[B_m{}^2/2\mu_o\right]\beta/3 \qquad \beta < 1 \qquad \text{Eq. 1.4}$$

$$Q// = B_m{}^2/2\mu_o\left[1/\beta - (2/3)\beta^2\right] \qquad \beta > 1 \qquad \text{Eq. 1.5}$$

Where B_m= peak to peak field strength, $\beta = B_m/B_p = B_m/2\mu_o J_c a$. The value B_p is equivalent to the field required for complete penetration of the superconductor. It should be noted than the value of B_m is equal to twice the magnetic field amplitude, B_a,

or the "zero to peak" value, which is more commonly used to describe magnetic fields amplitudes. Hence, $B_p = \mu_o J_c a$ is the zero to peak parallel field required for full penetration.

Equations 1.4 and 1.5 are a commonly known result, and it should be noted that the first factor, $B_m^2/2\mu_o$ is the maximum energy stored in the AC field during one cycle occurring at the peak in the magnetic field cycle and the second factor may then be considered a loss factor, less than one, representing the amount of the maximum stored energy which is dissipated each cycle of the hysteresis loop. Despite the rather artificial nature of this ideal case, these two equations have been proven to be particularly accurate in practical AC loss measurements of HTS tapes where the field is applied parallel to the wide side [1.39].

1.2.4 Self field hysteresis losses with a DC current

The effect of a DC transport current, Jdc A/m^2, and an oscillatory field is to lower the value of AC magnetic field at which current penetrates all the way to the middle of the conductor. At this point, β no longer equals 1, but rather 1-I where I is defined as the normalised transport current (J/Jc). For $\beta < 1\text{-}I$, the same Equation holds for the slab geometry. For the next stage of $\beta > 1\text{-}I$, the loss is as follows:

$$Q = (B_m^2/2\mu_o)[(1+I^2)/\beta - 2(1-I^3)/3\beta^2] \qquad \beta \geq (1-I). \qquad \text{Eq. 1.6}$$

Where J_T = Transport current, I = normalised transport current, B_m = peak to peak field. The effect of transport current is to shift the peak loss to a lower value of β, while increasing the loss factor. The peak loss occurs slightly above $\beta = 1\text{-}I$. Since transport currents are often around 90 % of Jc, the analysis here has shown a potential difficulty

in obtaining low AC losses. In addition to the reasons above for using high β, this analysis adds further weight to this usage. In this situation, small increases in β due to operational changes may lead to disastrous increases in losses, especially if β is around the value of 1-I.

1.2.5 Twisting of filaments and AC losses.

Under certain circumstances, oscillatory magnetic fields can penetrate to the interior of multifilament superconductors and produce coupling currents [1.30-1.34]. Under these circumstances, the filaments or groups of filaments may behave as individual and distinct entities in terms of electromagnetic properties, rather than being coupled into one large monofilament like behaviour [1.38-1.40]. This can occur when using very low frequencies (less than a few Hz) due to the quasi-static nature of the field, or in very low linear ramp rates or in very low magnetic field amplitudes [1.33]. At power frequencies, however, and magnetic fields of reasonable amplitude (> 10 mT), the filaments in HTS tapes are completely coupled and would behave as a single large filament for electromagnetic calculation purposes [1.38, 1.39].

The solution to minimise hysteresis losses is to twist the filaments in some manner to de-couple them. Twisting allows the electromagnetic situation to induce coupling currents to flow between the filaments, and for the individual filament or groups of filaments to be penetrated by an external field as individual filaments rather than as one large monofilament. Eddy currents will not be reduced by twisting because the self field produced will be of substantially the same form, and in a plane perpendicular to the conduction axis, i.e. in the cross sectional area, and will form closed lines of field within the metal matrix. Hence, the induced eddy currents will be longitudinal, and the losses will simply depend on the fraction of metal in the cross sectional area. Coupling

currents, however, because of their nature, do not form closed loops within the superconductor cross section but rather flow between filaments. By twisting filaments together, the emf produced per twist will be zero since each half pitch will be of opposite emf. The diagram in Figure 1.3 will clarify this. The actual coupling will include a longitudinal ($\mathbf{J}_z$) and transverse component ($\mathbf{J}_x$). The Equation to solve is.

$$\frac{\partial \mathbf{J}_x}{\partial z} - \frac{\partial \mathbf{J}_z}{\partial x} = i\omega\mu\sigma\mathbf{H}_y \text{ from } \nabla x\mathbf{E} = -i\omega\mu\mathbf{H} \qquad \text{Eq. 1.7}$$

Although a solution for the coupling currents has already been obtained by Campbell [1.34], some insight may be gained from first principal considerations. One way to grasp how the coupling currents flow is to imagine the filaments untwisted, with the applied field twisted, so that the field in each section is reversed as shown in Figure 1.3. If the dimension 'a' is the thickness, then the field is applied parallel to the tape. If the dimension 'a' is the width, then the field is applied perpendicular to the tape. In both cases the coupling current will flow into the page in one half twist pitch and out of the page in the other. From considerations of this diagram, and some basic electromagnetic theory, one can immediately see that the magnitude of the coupling current must be directly proportional to the magnetic field because the driving emf is proportional to the field. Similarly, the coupling current magnitude will be proportional to the frequency, and conductivity of the matrix material. Also, the coupling currents will be proportional to the square of the twist pitch because the driving e.m.f is proportional to the area of the loop which the filaments make and the resistance of the loop length is also proportional to this dimension.

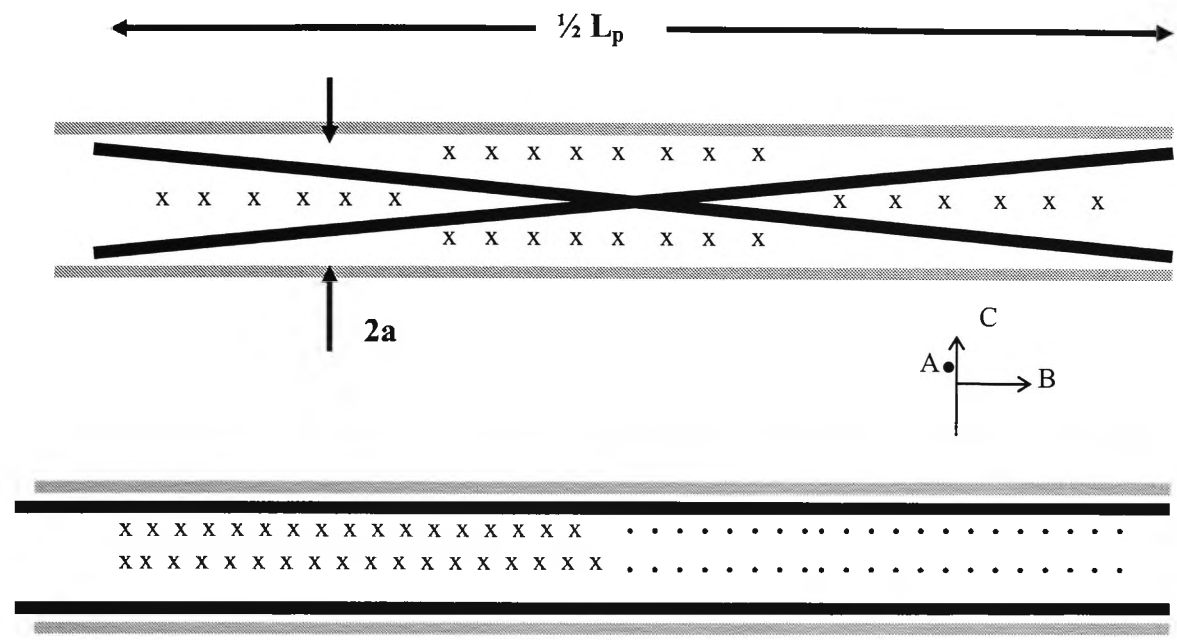

Figure 1.3. Schematic representation of two filaments in an HTS tape showing the longitudinal dimension over half a twist pitch. The applied AC field passes into the page. The twist pitch is L_p, and the thickness is 2a.

One way to understand how twisting breaks down the shielding nature of the filaments and allows coupling currents to flow is to think of the tape as purely a 2D object as in Figure 1.3 with just two filaments. The locus of each filament over a half pitch will encompass the central portion of the tape as well as the outer edges. The shielding currents which flow entirely within the superconductor leads to the hysteresis loss, however, since the filaments are now twisted about each other, the portion of the filament which is central to the tape will no longer be shielded from the external field as the twisting has forced shielding currents to enter the interior far earlier. Hence, the external field must penetrate the tape and coupling currents flow between the filaments. Another consequence of this is that because the shielding currents penetrate much earlier, the hysteresis losses will increase at low fields compared to the untwisted case and this has been observed experimentally [1.38]. The induced currents in the filaments

lead to local saturation to their Jc value, so all the extra coupling current must flow in the normal metal matrix for a part of their path which is the source of the coupling current losses.

1.2.6 Coupling current losses and designing for them

If the filaments in a HTS conductor are decoupled by twisting or other means such that the sinusoidal oscillatory flux penetrates the conductor and threads the filaments, then a coupling current will flow with an associated coupling current loss, Q_c.. This can be seen through Maxwell's equations:

$$-\oiint_S \frac{d\underline{B}}{dt} = \oint \underline{E}.dl = 1/\sigma \oint \underline{J}_{eddy}.d\underline{l} \quad \text{Eq. 1.8}$$

Where $B=B_m \sin 2\pi f t$.

The sss phasor relationships are given by:

$$-i\omega\mu \oiint_S \underline{H}.\underline{dS} = \oint \underline{E}.\underline{dl} = 1/\sigma \oint \underline{J}_{eddy}.dl \quad \text{Eq. 1.9}$$

$$Q_c = \iiint \underline{E}.\underline{J}.dV\,[W] \quad \text{Eq. 1.10}$$

$$Q_c = \sigma.\iint_S E^2.dS\,[W/m] \quad \text{Eq. 1.11}$$

Where $\omega = 2\pi f$ and i represents the imaginary number.

From the above equations, it may be seen that increasing the matrix resistivity will decrease the coupling current by the same factor, and since the coupling current loss is proportional to the square of the coupling current and resistivity, the loss is decreased by this factor too. The portion of the coupling current path which is lossy is the

transverse flow between the filaments, within the thickness of the tape, and is perpendicular to the tape. Hence, to reduce coupling losses within a multifilament tape, the technique is to sheath each filament in a higher resistance cladding [1.39]. Briggs has compiled a table of the resistivity of silver for each atomic percent of doping element [1.48].

Element	Increase in ρ ($x10^{-7}\Omega cm$) per At%	Element	Increase in ρ ($x10^{-7}\Omega cm$) per At%
As	84.6	In	17.8
Au	3.8	Pb	46.4
Bi	73	Pd	4.36
Cd	3.82	Pt	15.9
Cu	0.68	Zn	6.2
Sb	72.6	Ti	22.7
Ga	22.8	Sb	72.6
Ge	55.2	Sn	43.2

Table 1.2 The resistivity increase with alloying element in silver at 291 K. The resistivity of pure silver at 291K is $15.5x10^{-7}$ Ωcm.

Campbell has derived an analytical expression for the coupling loss between two filaments, and introduced the concept of a time constant ,τ, in which all the material and geometrical properties of the conductor are encompassed. The AC loss, in J/m^3 of superconductor is then expressed as a function of the peak field, frequency and τ.

Campbell also included an analysis of the situation where the tape geometry has one side very much larger than the other, and where the filaments are aspected, and include a twist pitch. This is exactly analogous to the modern low AC loss HTS tapes. To calculate the coupling loss, Campbell derived expressions for the induced electric fields E(x,y), in a rectangular conductor with filaments of twist pitch, p. The loss equation is then calculated directly from the integral equation 1.12.

$$\int \underline{E}.\underline{J}.dV \quad = \quad \int E^2/\rho.dV \quad \text{Eq. 1.12}$$

From the induced electric field and any point x,y the coupling current density at x,y , Jc(x,y) , may be derived from E/ρ and hence the coupling current may be derived by integrating J(x,y) over the cross section. The expression derived shows that the magnitude of the coupling current is indeed proportional to the square of the twist pitch L_p^2, frequency f, magnetic field amplitude, B, the conductivity, 1/ρ , and the geometrical factor, a/b.

Within the results presented here lie the mechanisms by which the AC losses associated with coupling currents may be decreased - increase the matrix resistivity and decrease the twist pitch as far as practical.

Oomen *et. al.* correctly argue that theoretical results based on slabs of superconductor and measurements made on straight filament tapes cannot be used to set the conditions by which filaments will de-couple [1.40]. There reasoning comes from the fact that coupling currents flow differently in twisted filament tapes than in straight filament tapes. This paper gives a graphical depiction of the direction of the coupling currents in straight filament and twisted filament tapes. In short, if the tape dimensions are 2a and 2b, perpendicular and parallel to the field respectively, then the coupling current path is b/a longer in twisted filament tape, and therefore the coupling current losses are a factor of a/b larger. Oomen makes use Campbell's equations to derive a practical set of conditions under which filaments will be de-coupled. The author asserts that when the coupling current becomes larger than the Ic, the model by which it was derived is no longer valid, and the transition to fully coupled filaments takes place. The result obtained is:

$$I_{coupling} = [L_p^2 a^2/(4\rho(a+b)].[\omega B_o/(1+\omega^2\tau^2)^{1/2}] \quad \text{Eq. 1.13}$$

The condition for full coupling is that $I_{coupling} > I_c$.

Some consequences of this result include the fact that in a parallel field of 1 Tesla, 50 Hz, the coupling current is 0.7 A in a pure silver matrix tape with a filament pitch of 10 mm. In a perpendicular field under the same conditions, the coupling current is calculated to be 521 A at 0.1 Tesla which is unreasonable. Under these conditions the coupling current would saturate the filaments much earlier, and further losses will be purely hysteretic and may be calculated from simpler models presented previously.

In a HTS tape with more than two filaments, the lossy part of the coupling current path between the filaments and through the normal metal matrix will not be as simple as Campbell has assumed in his analytical derivations. Hence, the simple or "Bulk" resistivity of the matrix cannot be used to correctly calculate the coupling current losses of a practical HTS tape. However, suitable approximations could be made if an "effective" resistivity, commonly referred to as the "effective perpendicular matrix resistivity", or $\rho_\perp$, could be calculated. This value would differ from the bulk value due to the fill factor of the tape and the actual path that the coupling currents follow.

Sumption and Collings discuss the difference between $\rho_\perp$ and that of the bulk matrix material [1.33]. They explain that the differences are due to 1. size effect, 2. filament-matrix interface resistance, and 3. current path effects that may reduce or enhance effects 1 and 2 and depends on the fill factor.

1.2.7 Transport current losses in arrays of superconducting tapes

The magnetisation losses of an infinitely broad and infinitely long stack of tapes have been derived by Müller [1.36]. The tapes are placed either in an X array (side by side, with edges in close proximity) or in a Z array (on top of each other, with the broad flat faces in close proximity). The physical situation is solved for the case of an AC transport current (expressed as the β fraction I_{AC}/I_c) with no other external fields applied. Although the mathematical derivation is valid only for an infinite number of tapes of infinite length and extent, Müllers calculations are the one most relevant to predicting AC losses of pancakes and coils consisting of a stack of pancakes. This is because the treatment includes the transport current (many only include magnetisation loss in an applied field). Hence, the parallel Z stack can be likened to a pancake and the case of a solenoid winding can be likened to the case of an X array.

The limitations of the model stem from the fact that the mathematical analysis uses parts of the Norris derivation (single tape AC loss, AC current, self field only) which in turn assumes fully coupled filaments and therefore rightly only includes hysteresis losses - not eddy or coupling current losses. Hence, no conclusions can be drawn from the findings regarding the benefit of increased matrix resistivity or twisted filaments.

The major results of Müller are described graphically. For the limiting cases when the distance between the tapes fall to zero, the results are in agreement with the infinite slab model and the Norris Equation. Müller's results will be analysed and discussed to provide an insight into the AC losses of pancakes and coils.

Case 1. Self field hysteresis loss of an infinite X array.

In this model, L is the distance between tape centres, d is the thickness of tape, and 2a is the width of tape. This situation is analogous to a long thin solenoid. The results show that as the tapes are brought closer together, the loss per tape decreases. The physical reason behind this arises from the fact that the closer the tapes come together, the smaller the perpendicular component of the magnetic field becomes at the edges of the tape. For example, when two tapes are brought together from a large distance apart, the fringe fields at the edge of one tape will be reduced as the other is brought closer to it.

Case 2. Self field hysteresis loss of an infinite Z stack

In this model, D is the distance between tape centres, d the thickness of tape, and 2a the width of tape. This situation is analogous to a pancake. The results show that as the tapes are brought closer together, the AC loss per tape increases. The physical explanation for this is due to the fact that the perpendicular component of magnetic field impinging on the edge of the tapes increases as the tapes are brought closer together. In an individual tape, the self field at each edge of the tape is essentially perpendicular to the tape. In a Z stack, the fringe fields produced by each tape add up in support of each other so that the field at the edge of any one tape is enhanced. Hence, the hysteresis losses per tape will increase as the number of tapes in the Z stack increases.

A closed form solution is not possible to calculate for the AC losses of a stack of pancake coils, since there is no closed form solution for the magnetic fields generated, and hence for the flux front within the tape. However, an approximate solution may be formulated using the equations of Müller.

Consider a Z stack of tapes, operating at $I_{AC}/I_c = 1$, at 50 Hz, with Ic = 100 A, and with no gap between the tapes, (the limiting case). The AC loss is 1000 W/m and even for

I_{AC}/I_c = 0.6, the AC loss is 200 W/m, which is still too large to construct practical devices. Hence the need to lower AC losses in HTS tapes, and why more effort needs to be put into tape development to address this issue.

1.2.8 The results of Carr

The total AC loss of an infinite slab in an applied parallel field with an in-phase AC transport current, I_t, has been calculated analytically by Carr [1.32]. Rabbers has rewritten the equations in SI units, and with normalised transport current, $i = I_t/I_c$, and magnetic fields, $\beta = B_a/B_p$. [1.51]. The model is not valid for transport current amplitudes greater than the Ic, and because the critical state model of Bean was used, an infinite value of the n exponent was assumed. Carr's equations, however, are useful for estimating the self field AC losses of coils where the transport current results in a magnetic field which is substantially parallel to each of the turns of tape. For the case of an applied field much greater than the penetration field ($B_a >> B_p$), the following equation applies:

$$Q_{tot} = \frac{2}{3}.\frac{B_p}{\mu_o}.B_a.[3 + i^2] \quad \text{Eq. 1.14}$$

In addition, because the expression for the hysteresis loss of a slab in a parallel field is known (Eq. 1.4 and 1.5), a transport current component of losses can be extracted by subtracting this component out, and assuming that the magnetisation loss is independent of the transport current. The results are shown in Equations 1.15 and 1.16 for two cases.

$$Q_{trans} = \frac{2B_a i^2}{\mu_o B_p} \quad (i \leq B_a/B_p \leq 1)\ [J/m^3/cycle] \quad Eq.1.15$$

$$Q_{trans} = \frac{2B_a i^2}{3\mu_o B_p} \quad (B_a/B_p >> 1)\ [J/m^3/cycle] \quad Eq.1.15$$

1.2.9 Eddy currents

Eddy currents, induced by time varying fields, contribute to the AC loss to a lesser extent unless high frequencies (>1 kHz) and fields (> 0.1 T) are employed. Eddy current losses can be safely neglected when measuring individual HTS tapes in the low field, low frequency regime. The power loss, in watts, contributed by eddy currents are proportional to f^2 and may be found using classical techniques already dealt with elsewhere [1.49,1.50]. Particularly useful are the equations given by Namjoshi, who derived closed form solutions for the eddy current losses in long thin conductors of arbitrary cross section [1.50]. Although the equations are derived for a normal metal conductor, they are presented in terms of the moment of inertia of the cross section and are valid for thin strips exposed to an applied field in an arbitrary direction. Rabbers explains that the eddy current loss in the sheath of an HTS tape may be obtained by calculating the moment of inertia of a hollow rectangle, which allows for the superconducting core [1.51].

1.3 Practical AC loss measurements

1.3.1 Introduction

Although valid theories that predict AC loss accurately have been derived, they do not cover all possible situations. In particular, even though the equations for the hysteresis

and coupling losses in a flat highly aspected tape have been derived, certain approximations and assumptions have been made that could lead to a significant difference between the actual and theoretical AC loss. A difference of 30 to 50 % is not unusual when measuring losses less than 1 mJ/cycle/m. This could have serious consequences in the design and sizing of the cooling plant required for a particular device. In addition, the mechanism of decoupling and the range of magnetic fields over which decoupling occurs is still not fully understood or predictable for HTS. The established equations for coupling losses also generally require a resistivity factor, which is really an effective resistivity because of the way coupling currents flow between the filaments. Currently, only simple approximations exist to estimate this factor and large variations between in-direct measurements of this parameter and predicted values occur.

Clearly, a practical measurement technique is required to confirm predictions of AC losses, to assist in the designing of practical lower AC loss tapes, and also for formulating empirical models of practical AC losses. In addition, a technique is required for measuring the net AC losses in prototype devices to confirm the models and measurements built from short length data.

1.3.2 Techniques of practical AC loss measurements

Direct determination of AC losses in superconductors requires the knowledge of the sample magnetisation or current density distribution and electric field in response to an external magnetic induction and transport current source. Without a transport current, only the response to a magnetic induction is required. In addition, only the in-phase component is important because the dot product in Equation 1.3 is zero for out-of-phase components.

The magnetisation of a sample in the presence of an AC magnetic field may be may be measured with an appropriate 'pick-up' coil of insulated wire. Open ended voltage contacts do not provide any information regarding the sample magnetisation or AC losses, which must be measured with a closed loop to ensure that all the flux associated with the magnetisation is included. This is due to the fact that the shielding currents, unlike transport currents, form closed loops within the sample being measured. Practically, measuring the sample magnetisation is then reduced to an exercise of measuring a voltage and its phase with respect to the AC excitation [1.37-1.42]. The AC loss is proportional to the in-phase component of the voltage, the magnetic field amplitude, and a constant which must be calculated from a model of the flux behaviour. In addition, precautions must be taken when winding the loop because a much larger out-of-phase component of voltage (the inductive response) will also be induced. This component can be reduced by winding a loop which folds back on itself so that an equal but negative inductive response is also included, or, by using a second coil, the "compensation coil", in the immediate vicinity of the pick-up coil.

The techniques that various groups have used to measure short tape sample magnetisation and total AC losses will be explored, including the lock-in amplifier technique, the integration of power supply sources, and the thermometric technique.

1.3.3 Lock-in amplifier techniques

Yang *et al.* used a saddle shaped pick up loop applied to the HTS tape and measured the fundamental component of the voltage that was in-phase with an applied field, and the third harmonic component of the voltage [1.38]. It was shown that the total AC loss may be obtained from the in-phase component, and that the hysteresis loss is obtained from the third harmonic component. An equation is required to convert the measured

"loss voltage" arising from the changing flux and the AC current in the sample into a loss value. This required knowledge of what the measured loss voltage actually represented and this required a model of the flux flow.

The advantage Yang's technique is that the hysteresis loss could be obtained independently of the total loss, so that any coupling current losses can be obtained from the difference.

1.3.4 Total loss using a figure 8 loop

The problem of including transport current loss is dealt with by Rabbers et. al by measuring the transport current loss in an external field using galvanic contacts in a figure 8 loop attached to the tape to eliminate the contribution to the voltage in the pick ups from the changing external field [1.43,1.44]. The magnetisation loss is then measured separately using an established technique such as the lock-in amplifier technique described above.

1.3.5 Total loss using the principal of conservation of energy

The combination of AC loss measurements described above to obtain the individual components of transport current loss and magnetisation loss are complicated and the technique is limited to the case where the magnetic field and transport current are in-phase, and of the same frequency. Introducing the possibility of a phase difference between the transport current and external field adds another degree of complexity into the measurements. This type of experiment is, however, extremely useful for the analysis of three phase cables where the fields from other phases are 120 electrical degrees out-of-phase with each other. This also occurs in transformers, but in this case,

there is an additional component of field on the windings due to the magnetising current which is 90 degrees out-of-phase with the transport current.

Ashworth presented a technique for determining AC losses that does not use the direct electrical measurement of a loss voltage [1.45] .Using the principal of conservation of energy, Ashworth proposed to determine the AC losses by integrating the voltage and current sources of each power supply in an experiment, as in Equation 1.16.

$$Q = \int_{Fieldcoil} v(t).i(t).dt \quad + \int_{Sample} v(t).i(t).dt \qquad \text{Eq. 1.16}$$

It does not matter which changing flux causes which loss component, if it links the circuit, the power supply must provide a suitable voltage in-phase with the transport current to drive the lossy component of current through the field coil circuit or the tape. The out-of-phase component simply provides the reactive component of voltage for the purely inductive response which will not contribute to a real power loss. The only problem remaining is the ohmic loss of the current leads – this is solved by measuring the transport current power supply voltage at the point where the current leads contact with the tape. The ohmic loss of the leads is therefore not included in the measured voltage. The coil power supply is a little more difficult to deal with conceptually, but in practice it is a simple matter. It should be noted that this technique is not limited to superconductors. Since no specific model of flux penetration or how the currents are flowing is used, the method may be extended to any magnetic material.

1.3.6 Thermometric technique

A thermometric technique has been used by Ashworth and Hardano to measure the total losses in HTS tapes under a wide variety of conditions, such as AC and DC magnetic fields and transport currents which vary in-phase with an applied field [1.46,1.47]. Ashworth states that this technique was developed specifically to overcome the problems of direct electrical type measurements and to dispense with the need for a model of flux flow to determine the losses. Ashworth's technique uses a type E thermocouple to measure very small (<0.2K) temperature rises in a thermally insulated HTS tape, which is exposed to various fields and may or may not have a transport current. The technique relies on a model of one dimensional heat flow. While the tape is encased and sealed in Styrofoam, the ends of the tape are exposed to the LN to form two iso-thermal points. The temperature rise across the tape then forms an inverted parabola with the maximum temperature occurring in the centre of the tape. Instead of solving the 1 dimensional heat flow Equation and relating temperature rise to AC loss empirically, the device is calibrated with a pure metal strip heater and DC current. The DC current produces a known power dissipation in the tape, and the central temperature rise is monitored by connecting the thermocouple leads in differential manner with the LN bath. Since sensitivities of mK are required for accurate loss measurements, this technique eliminates the problem of referencing the temperature to another external source which would introduce another uncertainty. The thermocouple has sensitivity of 2.6 μV/0.1 K which requires skill to measure accurately, but can be accomplished easily in a well equipped laboratory. Precautions had to be made to reject the induced voltage in the thermocouple wires due to the AC fields, and to limit the temperature rise to 0.2 K in order to minimise the increase in tape resistance.

The technique is otherwise straight forward and the authors present data of the AC losses in a HTS tape with externally applied AC field, AC transport current, and a variable phase angle between them. It was found that the loss is minimised with a 90 degree phase between the field and transport current, and is a maximum when they are in-phase which is the usual case for power devices.

1.3.7 AC results from the literature and their consequences

Yang showed for the first time that twisting of the superconducting filaments in Ag sheathed BSSCO tapes can effectively de-couple the filaments in an applied parallel magnetic field [1.38]. No evidence of de-coupling was observed in this paper when a perpendicular field was used, however, in subsequent work using tapes with alloy inter-filamentary matrix material, this phenomenon has also been found [1.41]. The reduction benefit found on individual tapes was about 1/6 of the straight filament hysteretic loss. This was consistent with the filaments de-coupling into 6 layers, instead of 37 individual filaments. It was found that the coupling eddy current loss dominated in twisted filament tapes, and the hysteretic loss dominated in straight filament tapes up to a critical field where full penetration of the filaments occurs, and the filaments couple once again. In this paper, this critical field was about 40 mT which was consistent with that predicted.

Leghissa and Oomen measured the AC losses of AgPd alloy matrix tapes with twist pitches of down to 6.5 mm [1.39,1.40]. A significant decrease in the AC loss in a parallel field was found for these tapes and good agreement was obtained between the measurements and theory at high field amplitudes. No reduction in AC loss, however, was observed for perpendicular applied fields and only purely hysteretic loss was detected. In this case, the coupling loss is not present as the loss was totally hysteretic,

and the filaments behaved as a single superconducting strip. Twist pitch and matrix resistivity had no effect on the loss at all. It was estimated that the matrix resistivity would have to be increased by a factor of 10 and the filaments have a twist pitch of 10 mm in order to decouple them in the presence of a perpendicular field of amplitude 10 mT.

Martinez et al, published the first paper to show de-coupling of filaments in multifilamentary HTS tapes exposed to a perpendicular field [1.41]. In this paper, Yang's technique of a saddle type loop and lock-in amplifier combination was used to measure the voltage across approximately 6.5 cm of tape. The total AC loss was then calculated from the fundamental component of the voltage, and the superconductor loss alone was calculated from the third harmonic using formulas derived by Yang and Martinez [1.42] The coupling current loss was then calculated as a difference between the two figures. The samples used had a silver gold alloy for the matrix and had twisted 37 filaments down to pitches of 4.4 mm. Although no effective matrix resistivity was calculated in the paper, the reduction in both the hysteresis loss of the superconductor and the coupling current loss in the twisted samples was clearly shown. The lowest losses were obtained for a sample that had a 4.4 mm twist pitch. The losses were measured in perpendicular fields up to a maximum of 80 mT peak field. For the 4.4 mm twist pitch sample, it was shown that the superconductor loss could be reduced by a factor of about 10 to 20 over the range of AC fields from 10 to 80 mT. The total loss, however, was reduced by a factor of just three at 10 mT compared to an untwisted sample. This difference was reduced to almost nil at 80 mT despite the superconductor loss still being a factor 10 lower than the conventional sample. The result is due to high coupling currents and therefore coupling current losses at higher fields.

Friend showed that the self field, transport current AC losses of AgAu matrix HTS tapes could also be reduced from that of un-twisted filament tapes by employing twisted filaments [1.52]. By using a Rogowlski coil and suitably arranged open ended galvanic contacts, Friend measured the in-phase component of the voltage with respect to the transport current to obtain the total loss. By also measuring the third harmonic component of the voltage signal, Friend was able to separate out the hysteresis loss component which dominated at high transport currents, but which were reduced compared to untwisted control samples for lower values of the current. This result has important consequences as a practical device will have both transport current and an applied field from the other turns of the device. Friend showed conclusively that it is possible to lower the AC losses from the former.

1.4 Conclusions

A literature survey of the field of HTS has been undertaken. The most promising candidates for possible power applications have been reviewed and discussed. The behaviour of HTS under AC excitation at power frequencies has been studied and practical techniques for measuring AC losses have been reviewed.

Through their theses' and papers, the combined theoretical works of Bean, Carr, Wilson, Yang, Rabbers, Oomen, Friend and Leghissa, would seem to have addressed AC losses in superconductors and highly aspected HTS tapes, however, two issues remain to be studied in greater depth.

Firstly, the issue of novel HTS tapes with alternate matrix materials and various twist pitches is not taken into consideration by the equations of Carr, or the work of Rabbers. Twisted filament tapes have been shown to give hysteresis losses which can be significantly lower than straight filament tape. The experimental results, however,

reveal that the AC losses cannot as yet be accurately predicted for differing matrix alloys and twist pitch. The analytical equations of Campbell and Carr, and the experimental procedures and results of Yang, Oomen, Friend, Rabbers, and Leghissa form an excellent starting point for investigating the effect of new matrix materials on the AC losses of short lengths of novel twisted HTS tape.

Secondly, it has also been found that there is a real need for research into AC HTS devices that employ coils and in particular, it is clear that the field of transformer technology could benefit significantly from HTS. It has also been found that the possible use of novel low AC loss tapes such as twisted filament tape in these devices needs to be investigated and new techniques developed for the suitable design of power devices which are to employ such HTS tapes. It has also been recognised that although the theoretical and practical AC losses of HTS tapes has been well covered, the literature lacks a methodical investigation into the practical AC losses of solenoid coils and pancakes.

To meet the above recognised inadequacies the following plan was executed, set out as the following Chapters in this thesis:

Chapter 2.

Investigate low AC loss tape manufacturing techniques and in particular twisted filament tape and the use of various different alloying elements. Particular attention shall be paid to ensure that the matrix of the prepared samples consists of distinct filaments, without inter-growths.

Chapter 3.

Source and experiment with insulation materials suitable for cryogenic applications. Establish the techniques for the manufacture of pancakes and solenoid coils. Carry out thermo-mechanical testing on the finished coils to verify their suitability for cryogenic applications.

Chapter 4.

Build and automate a short length AC loss measurement rig for the measurement of AC losses in novel HTS tapes made in the work of Chapter 2. In addition, build a cryogenic mass boil off calorimeter for accurately measuring the AC losses of HTS coils built in Chapter 3, under various excitations.

Chapter 5.

The electro-static design of HTS coils including field enhancement due to differing di-electric materials and conductor geometry become increasingly important for high power, (> 20 MVA), high voltage (> 110 kV) transformers. The coils must be designed according to a standard and built to withstand specified over-voltages and lightning impulses as dictated by those standards. Therefore, investigations into the suitability of HTS coil winding techniques and cryogenic insulation materials need to be discussed in terms of the over-voltage and lightning impulse requirements. The electrical insulating properties of LN also needs to be investigated in terms of the power frequency and lightning impulse breakdown voltage and the results summarised so that suitable insulation clearances can be allowed for in a LN HTS transformer design. The economics of cooling a transformer to LN and sub-LN temperatures also needs to be studied, as well as techniques for keeping the core sufficiently cold.

Chapter 6.

Using the knowledge gained from the previous experimental investigation, a 100 KVA transformer will be designed and modelled for use in LN. The design should be optimised for minimum weight and volume, while using appropriate approximations to estimate the total AC losses.

Chapter 7.

A primary and secondary solenoid coil will be manufactured from HTS Tape according to the optimised design. A single phase of the transformer will be constructed using the coil and tested at 77 K in order to prove the conclusions and design techniques established for HTS transformers in Chapter 6.

References

[1.1] J.G. Bednorz and K.A. Muller, "Possible high Tc superconductivity in the Ba-La-Cu-O system", Z.Phyz.B number 64, pp 189-193, 1986.

[1.2] M.K. Wu, J.R. Ashburn, C.J. Torng, P.H. Hor, R.L Meng, L. Gao, Z.J. Huang, Y.Q. Wang, and C.W. Chu, "Superconductivity at 93 K in a new mixed phase Y-Ba-Cu-O compound at ambient pressure" Phys.Rev.Lett. Number 58, pp 908-910, 1987.

[1.3] G. J. Sloggett, C.D. Cook, S.X Dou, N. Savvides and A.C.G. Secrett, "Opportunities in Power Applications of Superconductors", Electrical Engineering Congress, Sydney, November 24-30, 1994.

[1.4] M Lelovic, P Krishnaraj, N G Eror, A N lyer and U Balachandran," Transport critical current density above 10^5 Acm^{-2} at 77 K in $Bi_{1.8}$ $Pb_{0.4}$ $Sr_{2.0}$ $Ca_{2.2}$ $Cu_{3.0}$ O_y

superconducting tapes made by the Ag wire-in-tube method." Superconductor Science Technology No.9 pp 201-204, 1996.

[1.5] Y. Iijima, K.Kakimoto, M.Kimura, "Reel to Reel Continuous Formation of Y-123 Coated Conductors By IBAD and PLD Method", IEEE Transactions Appplied Superconductivity, Vol. 11, No. 1, 2001.

[1.6] E.B. Forsyth, "The Brookhaven Superconducting Underground Power Transmission System", Electronics & Power, number 30, p 383, 1984.

[1.7] A.M. Wolsky, "Advances in applied superconductivity: A preliminary evaluation of goals and impacts", ANL/CNSV-64, Argonne National Laboratory, Argonne, Illinois 1988.

[1.8] T.Harra, K.Okanawa, N.Ichiyanagi, S.Tanaka ,"Feasibility study of compact high Tc superconducting cables." IEEE Transactions on Power Delivery, Vol.7, No.4, 1992.

[1.9] T.P Beales, C.M Friend, W.Segir, E.Ferrero, F.Vivaldi, L.Ottonello, "A DC transmission cable prototype using high-temperature superconductors", Superconductor Science and Technology, No. 9, pp 43-47, 1996.

[1.10] R.F Hirsh, "Technology and Transformation in the Electric Utility Industry.", Cambridge University Press, 1989.

[1.11] C.J. Weinberg, J.J. Iannucci, M.M. Reading, "The Distributed Utility : Technology, Customer, and Public Policy Changes Shaping the Electrical Utility of Tomorrow.", Energy Systems and Policy. Vol.15, pp 307-22, 1992.

[1.12] D.Hoadley, A.Dabbagh, S. Moorthy, "Energy storage and conversion for renewable sources interconnected with the utility grid. Australasian Universities Power Engineering Conference." AUPEC '94, Vol.1, pp 192-9, 1994.

[1.13] H.C. Hay, M.F. Conlon, W.J. Bonwick," Development of a SMES device for application to problems of load unbalance", Electrical Engineering Congress. Sydney, Australia, 1994.

[1.14] C.C. DeWinkel and P.F Koeppe, "Superconducting Technology Offers Ride-Through Capability for Large Industrial Critical Process Loads", Proceedings of the American Power Conference, Illinois Institute of Technology, Chicago, Vol.2, p1252, 1992.

[1.15] R.F. Giese, T.P. Sheahen, A.M. Wolsky, D.K. Sharma, "High temperature superconductors: Their potential for utility applications.", IEEE Transactions on Energy Conversion. Vol. 7, No.3, 1992.

[1.16] G.Papst, B.B.Gamble, A.J.Rodenbush, R.Schöttler, "Development of Synchronous Motors and Generators with HTS Field windings", Applied Superconductivity, 158, Vol. 2, pp 1507-1510, 1997.

[1.18] W.J.S. Rogers, "Overview of Embedded Generators in Public Electricity Networks." IEE Colloquium on the effective response of a public electricity network to independent generators: Digest Number 93, Article 1, pp 1-5, 1993.

[1.19] J.X.Jin, S.X.Dou, C.Cook, C.Grantham, M.Apperley, T.P.Beales "Magnetic saturable reactor type HTS fault current limiter for electrical applications", Physica C, Vol. 341-348, pp 2629-2630, 2000.

[1.20] F.J.Mumford, "A Techno-economic study of High Tc superconducting power transformers", International Conference on Electrical Machines, 5^{th}-8^{th} September, 1994

[1.21] S.Hoernfeldt, O.Albertsson, F.Koenig, D.Bonmann, "Superconducting transformers", ABB Review pp 13-19, 1/1994.

[1.22] Superconductor Week, "ASC Reasserts $50/kAm Price Target; Sales Need to Reach 125 km/Year", Vol. 16, No. 5, 2002.

[1.23] A.P. Malozemoff, W.Carter, S.Fleshler, L.Fritzemeier, Q.Li, L.Masur, P.Miles, D.Parker, R.Parrella, E.Podtburg, G.N.Riley, M.Rupich, J.Scudiere, W.Zhang, (ASC) "HTS wire at commercial performance levels", IEEE Transactions on Applied Superconductivity, Vol. 9, No. 2, 1999.

[1.24] S.W.Schwenterley, B.W.McConnell, J.A.Demko, et. al. "Performance of a 1-MVA Demonstration Transformer", IEEE Transactions on Applied Superconductivity, Vol. 9, No.2, 1999.

[1.25] K.Funaki, M.Iwakuma, M.Takeo, K.Yamafuji, J.Suehiro, M.Hara, M.Konno, Y.Kasagawa, I.Itoh, S.Nose, M.Ueyama, K.Hayashi, K.Sato] "Preliminary Tests of a 500 kVA - Class Oxide Superconducting Transformer cooled by Subcooled Nitrogen", IEEE Transactions on Applied Superconductivity, Vol. 7, No.2, 1997.

[1.26] K.Funaki, M.Iwakuma, "Recent activities for applications to HTS transformers in Japan", Supercondor Science and Technology, Vol. 13, pp 60-67, 2000.

[1.27] P.Kummeth, R.Schlosser, P.Massek, H.Schmidt, C.Albrect, D.Breitfelder, H-W Neumüller, "Development and Test of a 100 kVA superconducting transformer operated at 77K", Applied Superconductivity, Vol. 1, No. 167, pp 1099-1102, 1999.

[1.28] M.S.Walker, S.P.Mehta, N.Aversa, "Transforming Transformers", IEEE Spectrum, pp 43-49, July 1997.

[1.29] A.Bitterman, "ABB connects HTS transformer to Geneva power supply network", Superconductor Week, Vol. 11, No. 6, P.1, March 1997.

[1.30] P. Sheahan, "Introduction to high temperature superconductivity", Plenum press, New York.

[1.31] M.Wilson, "Superconducting magnets", Oxford university press, 1983.

[1.32] W.J.Carr, "AC Loss and Macroscopic Theory of Superconductors". Gordon and Breach Science, New York, 1983.

[1.33] M.D Sumption and E.W Collings, "Transverse resistivities of Cu-Matrix and CuMn - Matrix Multifilamentary strands as functions of magnetic field and temperature", Advances in Cryogenic Engineering Materials, Vol. 40a, pg 807, 1993

[1.34]. A.M. Campbell. "A general treatment of losses in multifilamentary superconductors", Cryogenics, Vol. 22, pp 3-16, 1982.

[1.35] C.P.Bean, "Magnetisation of hard superconductors," Phys. Rev. Letters, Vol. 8, pp 250-253, 1962.

[1.36] K.H. Müller. "Self-field hysteresis loss in periodically arranged superconducting strips", Physica C, Vol. 289, pp 123-130, 1997.

[1.37] J.J. Rabbers, D.C. van der Laan, B. ten Haken, H.H.J. ten Kate, "Magnetisation and transport current loss of a BSSCO/Ag tape in an external AC magnetic field carrying an AC transport current", IEEE Transactions on Applied Superconductivity, Vol. 9, p 1185, 1999.

[1.38]. Y.Yang, T.J.Hughes, C Beduz, and F.Darmann. "Reduction of AC loss in Ag sheathed PbBi2223 Tapes with Twisted Filaments in External and Self fields", Physica C 310, p 147, 1998.

[1.39] M. Leghissa, "AC losses in high-temperature superconducting tapes and cables". Recent Developments in Applied Physics, Vol. 1, pp 89 – 118, 1998.

[1.40] M.P Oomen. "Decrease of Magnetic AC loss in Twisted-Filament Bi-2223 Tapes", Physica C 310, 137-141, 1998.

[1.41] E.Martinez, Y.Yang, C.Beduz, Y.B. Huang, "Experimental study of loss mechanisms of AgAu/PbBi-2223 tapes with twisted filaments under perpendicular AC magnetic fields at power frequencies". Physica C 331, pp 216-226, 2000.

[1.42] E.Martinez, Y.Yang, C.Beduz, "AC losses of twisted multifilamentary Bi-2223 tapes under AC perpendicular fields", Applied Superconductivity, Vol.1, No. 167, pp 731-4, 1999.

[1.43] J.J.Rabbers, B.ten Haken, O.A.Shevchenko, H.H.J.ten Kate, "An Engineering formula to describe the AC loss of BSSCO/Ag tape", IEEE Transactions on Applied Superconductivity, Vol. 11, No. 1, pp 2623/6, March 2001.

[1.44] J.J.Rabbers, B. ten Haken, H.H.J. ten Kate, "Measuring transport current loss of BSSCO/Ag tapes exposed to external AC magnetic fields", Physica C 310 pp. 101-105, 1998.

[1.45] S.P.Ashworth, M.Suenaga, "Measurement of AC losses in superconductors due to AC transport currents in applied AC magnetic fields", Physica C 313, pp 175/87, 1999.

[1.46] S.P.Ashworth, M.Suenaga, "The Calorimetric Measurement of AC Losses in HTS Conductors in Combinations of Applied Magnetic Fields and Transport Currents", Applied Superconductivity, Vol. 1, No. 167, pp 723/6, 1999.

[1.47] T. Hardono, C.D. Cook and J.X. Jin, Measurements of AC Losses in HTS Wires Exposed to an Alternating Field using Calorimetric Methods, IEEE Trans. on Applied Superconductivity, Vol. 9, pp. 813/6, June 1999.

[1.48] L.J.Briggs, "US National Bureau of Standards – Digest on Silver", 1932.

[1.49] V.Meerovich "Eddy current loss calculation in thin rectangular plates at cryogenic temperatures and its experimental verification", IEEE Transactions on Magnetics, Vol. 30, No. 6, 1994.

[1.50] K.V.Namjoshi, P.P.Biringer, "Low frequency eddy-current estimation in long conductors by using the moment of inertia of cross sections", IEEE Transactions on Magnetics, Vol. 24, p2181, 1988.

[1.51] J.J.Rabbers, "AC loss in superconducting tapes and coils", PhD thesis, University of Twente, Holland, October 2001.

[1.52] C.M.Friend, Y.B.Huang, "Self-field ac losses of a twisted multifilamentary (Bi, Pb)2Sr2Ca2Cu3O10/AgAu tape", Applied Physics Letters, Vol. 76, No. 26, pp 3983-5, 2000.

Chapter 2

Development of low AC loss tapes

2.1 Introduction

Figure 2.1 shows a simple dimensional description of a transverse schematic of a multifilament HTS tape and the conventions which will be used.

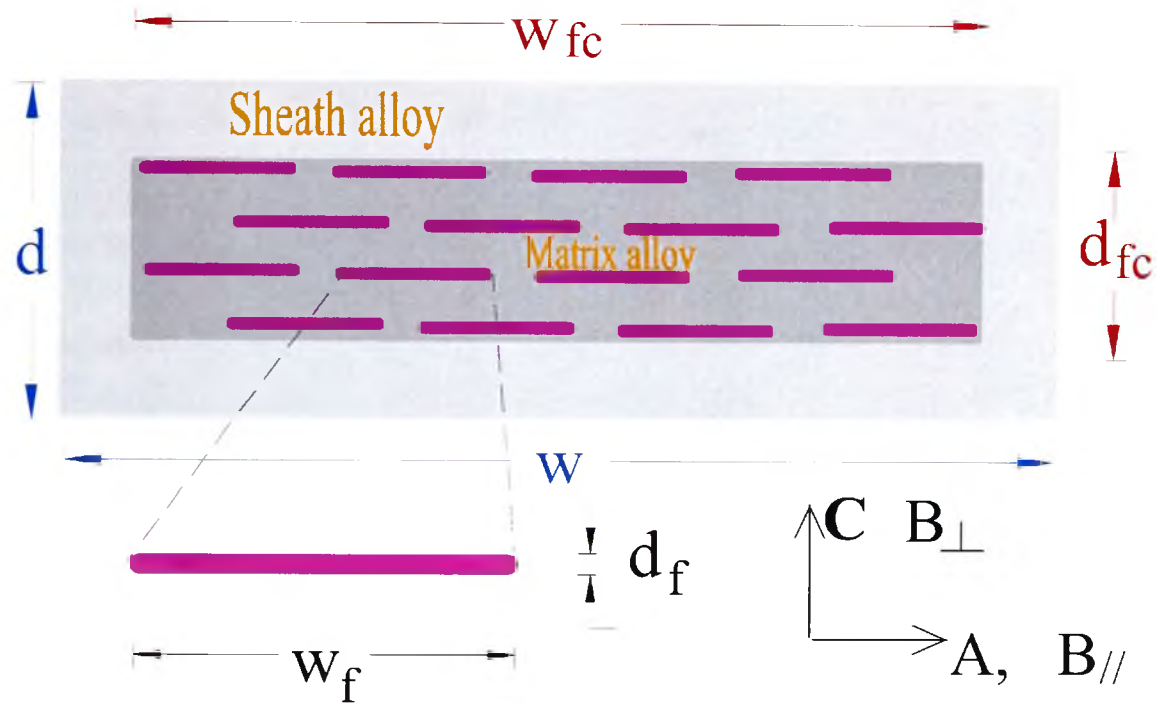

Figure 2.1 Symbols used to describe aspects of HTS MF tape, and the definitions of "parallel", $B_{//}$, and "perpendicular", $B_{\perp}$, directions of magnetic field used in this work.

Equations 2.1 – 2.3 describe the magnetisation loss, of superconducting material, arising from hysteresis in the superconductor formulated in terms of the above dimensions [1.39,2.1]. The units are J/cycle/m^3, where the volume is calculated for the whole HTS tape, not just the superconducting region.

$$Q_{//}(d_{fc}) = \frac{2B_a{}^2}{\mu_o}\left[\frac{\lambda_{fc}}{3}.\frac{2B_a}{\mu_o J_{fc} d_{fc}}\right] \quad \beta_{//} < 1 \qquad \text{Eq. 2.1}$$

$$Q_{//}(d_{fc}) = \frac{2B_a{}^2}{\mu_o}\left\{\left[\frac{\lambda_{fc}}{2}.\frac{\mu_o J_{fc} d_{fc}}{B_a}\right] - \frac{2}{3}\left[\frac{\lambda_{fc}}{}.\frac{(\mu_o J_{fc} d_{fc})^2}{(2B_a)^2}\right]\right\} \quad \beta_{//} > 1 \qquad \text{Eq. 2.2}$$

$$Q_{\perp}(w_{fc}, d_{fc}) = \frac{2B_a{}^2}{\mu_o}\left[\frac{\pi w_{fc}}{2\beta_{\perp} d_{fc}}\left(\frac{2}{\beta_{\perp}}\ln(\cosh\beta_{\perp}) - \tanh\beta_{\perp}\right)\right] \qquad \text{Eq. 2.3}$$

where

$B_p = (\frac{1}{2})\mu_o J_{fc}\ d_{fc}$ is the penetration field

$\lambda_{fc} = \frac{w_{fc} d_{fc}}{w.d}$ is the filamentary core fill factor

$\beta // = Ba / Bp \qquad \beta_{\perp} = B_a/B_d$

$B_d = \mu_o J_{fc} d_{fc}/\pi$

$J_{fc} = I_c/(w_{fc}.d_{fc})$

Corrections to these Equations are required to take into account the magnetic field effect on Jc, and also to accommodate the effect of a finite exponent in the V-I curve. These simple expressions however, predict hysteresis loss in isolated tapes to within about 15% in parallel and perpendicular fields up to 0.8 T, at frequencies below 1kHz [1.39]. Equation 2.3 was obtained by modeling the filaments as thin rectangular strips with homogenous Jc across the strip. Deviations between the measured values and those predicted by Equation 2.3 in particular, but also Equations 2.1 and 2.2, occur due to non-uniform Jc distribution of the material.

Parallel field hysteresis losses are so well described in straight filament tapes because the effect of coupling currents can be ignored and the effect of shielding between the filaments is small. The filaments themselves are indistinguishable, and are "coupled"

together so that flux penetration into the tape sample occurs in the same manner as in a monofilament tape or indeed a block of pure superconductor. Larger deviations in the perpendicular case arise when using Equation 2.3 in the small field regime (< 20 mT) due to the stacked nature of the filaments in a tape which leads to shielding between them.

In this chapter, twisted filament HTS tapes suitable for low field applications at power frequencies will be developed. Such devices as transformers, cables, and fault current limiters fit these criteria. The field amplitudes in these devices are limited to less than 0.4 – 0.5 T.

Most HTS tapes used in these devices will be in the fully penetrated state at 77 K. This is to make as much use of the tapes Ic as possible, while at the same time designing a smaller and less massive device as the conventional counterpart. The parallel field required for full penetration is usually less than 100 mT for the best HTS tapes available and about 50 mT on average, assuming the core region is about 300 microns thick, and a Jc of 35000 A/cm^2.

Equation 2.2 can be simplified to Equation 2.4 in the fully penetrated regime which shows that dimensionally, the hysteresis losses at each magnetic field amplitude depend only on the thickness of the core region, and the Jc.

$$Q_{//} = B_a \lambda_{fc} J_{fc} d_{fc} \quad \text{Eq. 2.4}$$

Equation 2.3 can be simplified to Equation 2.5 but only in the higher field case ($B_a >> B_p$) which shows that dimensionally, the perpendicular field losses depend only on the width of the core region [2.1].

$$Q_{\perp} = Ba[\lambda_{fc} J_{fc} w_{fc}] \quad B_a >> B_p \ [J/m^3/cycle] \text{ Eq. 2.5}$$

The ratio of the losses for applied fields in the perpendicular and parallel directions is obtained by dividing Equation 2.4 and 2.5, valid for $B_a >> B_p$.

$$\frac{Q_{\perp}}{Q_{//}} = \frac{w_{fc}}{d_{fc}} \quad \text{Eq. 2.6}$$

The aspect ratio for HTS tapes is typically of the order 10 to 20 due to the processing techniques required for high Jc tapes. Hence, the hysteresis losses occurring due to perpendicular components of magnetic field is a lot higher than that due to a parallel field of the same magnitude, and hence these components should be minimised in a good design.

Equations 2.4 and 2.5 show that the only way to reduce the hysteresis losses of multi-filamentary tapes in the low field, low frequency regime is to decouple the filaments. In the decoupled case, the quantities w_{fc} and d_{fc} may be replaced in the formulas with the dimensions of the decoupled regions. In the parallel field, the most likely decoupling mechanism is into layers parallel with the tape surface as first found experimentally by Yang [2.2]. In this case, the dimension d_{fc} may be replaced with the thickness of each layer which is considerably less than the thickness of the core. The losses of the layers are then multiplied by the number of layers to obtain the hysteresis loss of the entire tape. The following condition, Equation 2.7, must be satisfied in the first instance before it is possible for the total loss to be reduced.

$$N * Q(d_f) < Q(d_{fc}) \quad \text{Eq. 2.7}$$

where N is the number of decoupled regions. In the parallel field case, Equation 2.7 will hold because the gaps between the filament layers are distinctive and comparable to the filament width itself.

To a better approximation, Equation 2.8 must apply, which includes the coupling current expression in parallel fields:

$$N * Q\ (d_f) + Q_c < Q(d_{fc}) \qquad \text{Eq. 2.8}$$

The coupling current loss has been solved by Campbell and can be approximated by Equation 2.9 in the parallel field case for a pure silver matrix and for a thin strip [1.34].

$$Q_c \approx \frac{\pi^2}{8} B_a{}^2 . f . \frac{L_p{}^2}{\rho_\perp} \left(\frac{d_{fc}}{w_{fc}} \right)^2 \qquad \text{Eq.2.9}$$

Carr found that the effective matrix resistivity lies between the two extremes [1.32].

$$\rho(1-f)/(1+f) < \rho_\perp < \rho(1+f)/(1-f) \qquad \text{Eq.2.10}$$

Where ρ is the bulk resistivity of the alloy, and f is the fill factor of the tape.

Equation 2.8 and its consequences are the basic driving force behind the development of twisted filament tape with novel alloy matrices : to produce a tape with a small twist pitch ($Q_c \propto L_p^2$) and a higher resistance alloy matrix ($Q_c \propto 1/\rho_\perp$).

2.2 Development of twisted filament tape

The first step to producing HTS tape which has lowered AC loss at power frequencies and parallel fields is to develop a suitable manufacturing technique for twisted filament

HTS tapes. The literature shows that a twist pitch of 10 mm or less is required [2.2-2.8], and the following rule of thumb has been proposed, developed from Campbell's equation for coupling losses, which suggests the same [2.6].

$$Lp << \sqrt{\frac{d_f \rho \pi J_c}{f B_a}} \quad \text{Eq.2.11}$$

Kwasnitza gives an excellent description of coupling current losses and the conditions under which de-coupling may take place [2.8].

The most difficult task in achieving the required twist pitch is the establishment of a manufacturing process which yields Ic's of the twisted filament tape comparable to that of the straight filament tape. This is not a straight forward task, with most authors reporting some degradation in Ic for a 10 mm pitch and at least 30% degradation for finer twist pitches down to 5 mm [2.2, 2.4-2.7].

2.2.1 Experimental

The bulk of the experimental PIT procedure used in this work to develop twisted filament tape is outlined in Appendix 2.1. The twisting was carried out on the wire after the initial draw passes had been completed and before the first rolling operation. A range of different types of tapes with different filament numbers (37,75,127) and different alloys sheaths and matrices were employed. In addition, control samples with no twisting were always prepared to check for any degradation in Ic. The sheath materials explored included pure silver and a magnesium (Mg) alloy of silver. The matrix materials included silver alloys A and B (see Appendix 1). The Mg alloy sheath was used to strengthen the tape and the matrix alloys were used in an attempt to increase

the resistivity of the matrix. In all, 60 samples of 80 mm long tapes were prepared for this research work.

The twist pitch, L_w, imparted to the wire is given by Equation 2.12.

$$L_w = \frac{l}{n} \quad \text{Eq. 2.12}$$

Where l is the length of the wire sample being twisted and n is the number of half turns imparted to each end of the wire in mutually opposing directions. The final twist pitch of the outer layer of filaments in the tape, L_p, may be calculated from Equation 2.13

$$Lp = R.L_w \quad \text{Eq. 2.13}$$

Where R is the ratio of tape length to wire length and depends on many factors such as reduction rate, annealing schedule, and the initial wire diameter. Typically, R was approximately 2, so in order to achieve a twist pitch of 10 mm in the tape, a twist pitch of 5 mm was imparted in the wire immediately before rolling.

Samples of the initial wire and final tape were potted in epoxy resin for filamentary investigation using a Karl Zeiss microscope and Kontron™ image analysis software. The image analysis software was automated as part of this work to select individual filaments within a tape cross section, record all the filamentary dimensions, (d_f, w_f) and calculate the fill factor. The dimensions of the core, w_{fc} and d_{fc}, and the tape itself were also measured on this system.

Figure 2.2 shows a longitudinal cross section of a 1.54 mm diameter wire after twisting and before rolling and sintering. To prepare the mounted samples for the image analysis, only a small amount of silver was removed during polishing and only the outer layer of filaments were revealed in the wires and tapes.

Figure 2.3 shows a longitudinal cross-section of a twisted filament tape, showing the outer layer of filaments. To obtain this micrograph, a sample of twisted filament tape after final sintering was mounted flat and then polished carefully in the plane parallel to the a-b plane of the tape. This technique enabled confirmation of the final twist pitch in the outer layer of filaments in the tape using image analysis.

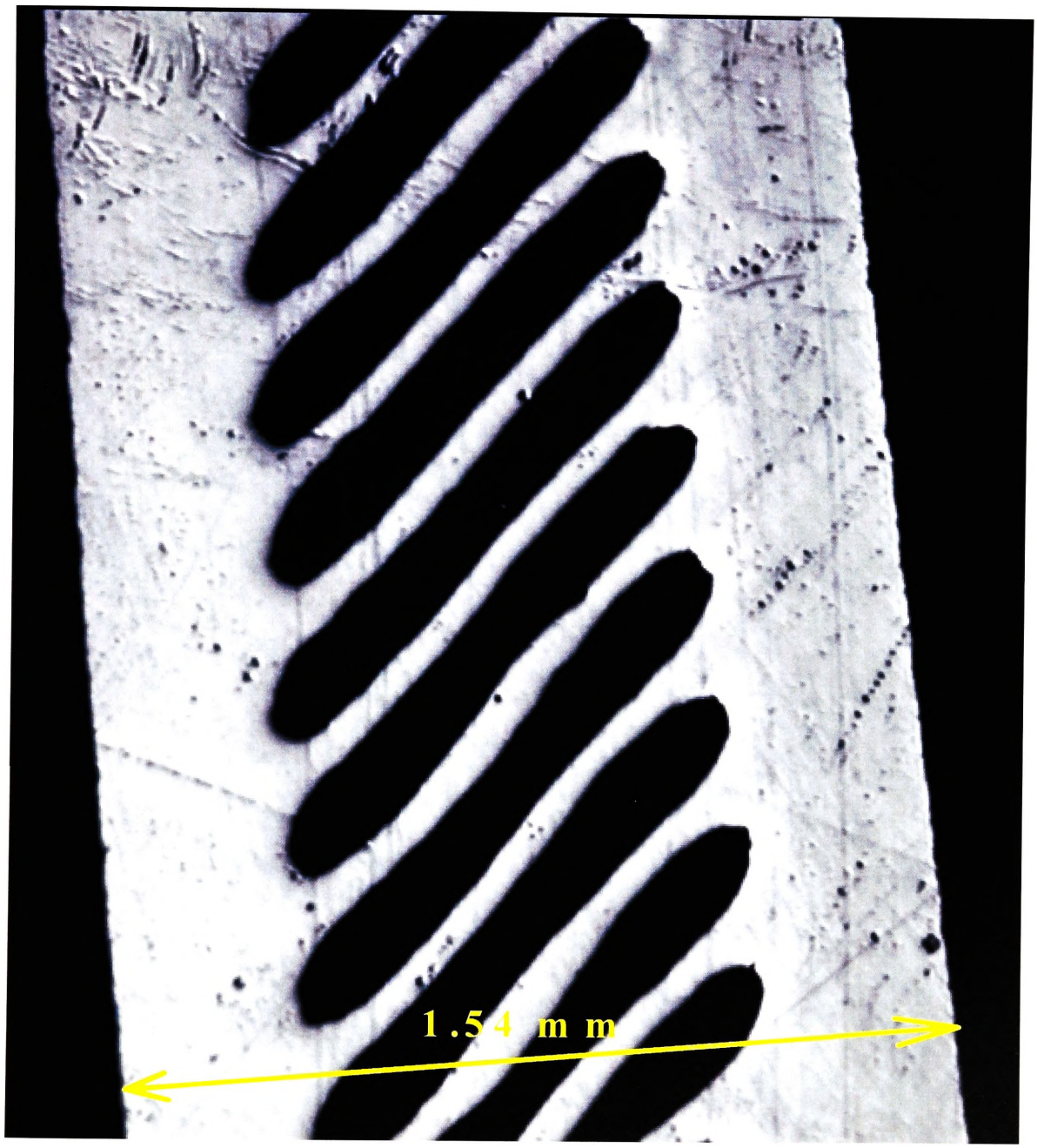

Figure 2.2. Optical Micrograph of a polished round wire with 37 twisted filaments. The wire diameter is 1.54 mm. The twist pitch is approximately 3.0 mm in this sample of wire. Pure silver sheath and matrix.

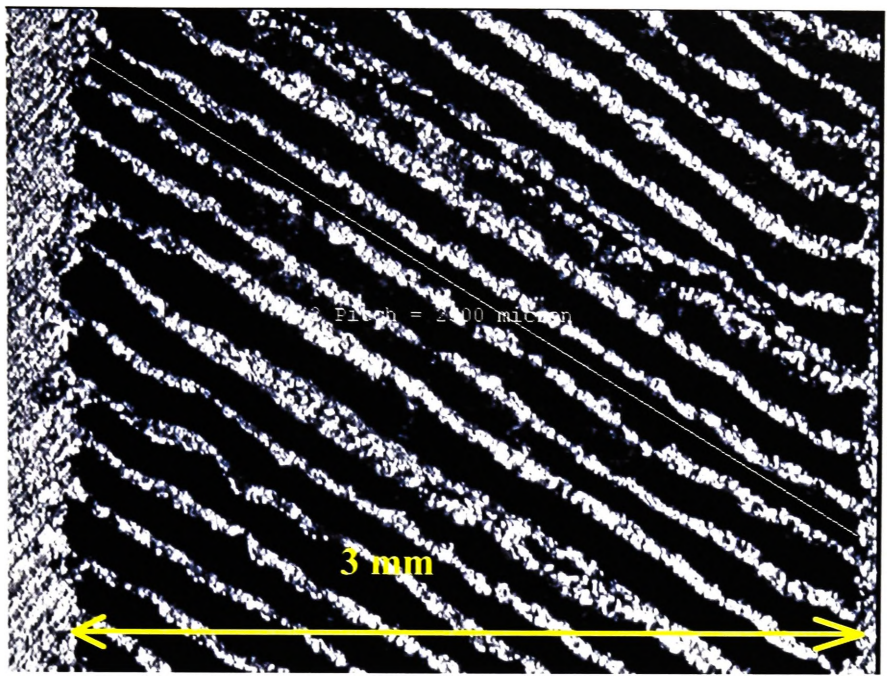

Figure 2.3. Optical micrograph of a longitudinal section of a 127 MF HTS tape after twisting, rolling, and final sintering. The outer layer of filaments are shown. The tape rolling direction is parallel to the page. The twist pitch was determined to be 5 mm.

2.2.2 Bridging

In order to fully decouple filaments into distinct regions and lower the hysteresis losses, the first condition that must be satisfied is that all the filaments or regions of filaments are physically separated by non-superconducting material. If this is not met, then it is possible for the whole multi-filamentary zone to behave as a mono-core filament, with no possibility of decoupling. This occurs when the filaments either coalesce during the drawing or rolling stages of processing, or they become connected to each other by inter-growths during the heat treatment stage. The merging of filaments together into one large cluster or many clusters is avoidable when judicious care is taken during the processing of the green wire and tape. Nevertheless, the drive for increased Ic through higher fill factors results in the HTS tapes of most companies containing significant coalescing of filaments.

For similar reasons, bridging of filaments is also a significant problem for the commercial production of low AC loss tapes. A high fill factor increases the likelihood of bridging between filaments, because the filaments are necessarily close together. Figure 2.4 shows an example of a typical alloy filament tape with bridging between the filaments due to inter-growths and coalescence.

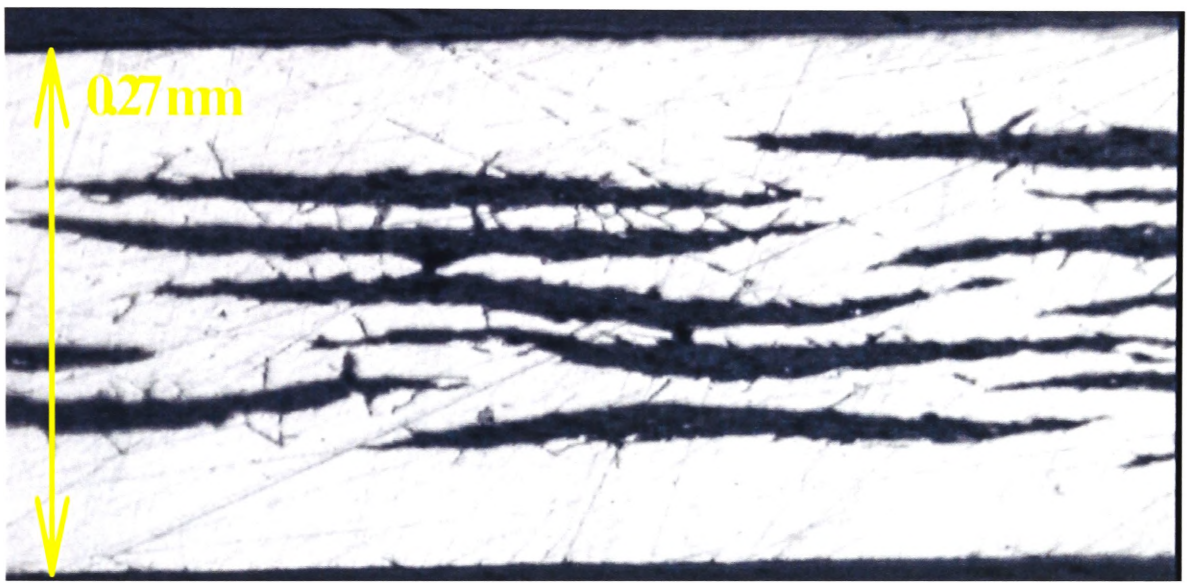

Figure 2.4. View of a section of twisted filament tape showing bridging between the filaments when alloy A was used for the matrix.

Bridging between filaments can sometimes be extremely difficult to detect since the evidence of this defect was not always evident in each mounted sample. A seven filament tape with low fill factor was made in order to prepare twisted filament samples without bridging, and to test various processing, and heat treatment techniques. Although microscope observations of the tapes revealed that they were nominally devoid of coalescence and bridging, low frequency magnetic field sweep measurements of the samples by Collings failed to detect the presence of any coupling currents (Figure 2.5), indicating that the filaments within the tested samples must be bridged.

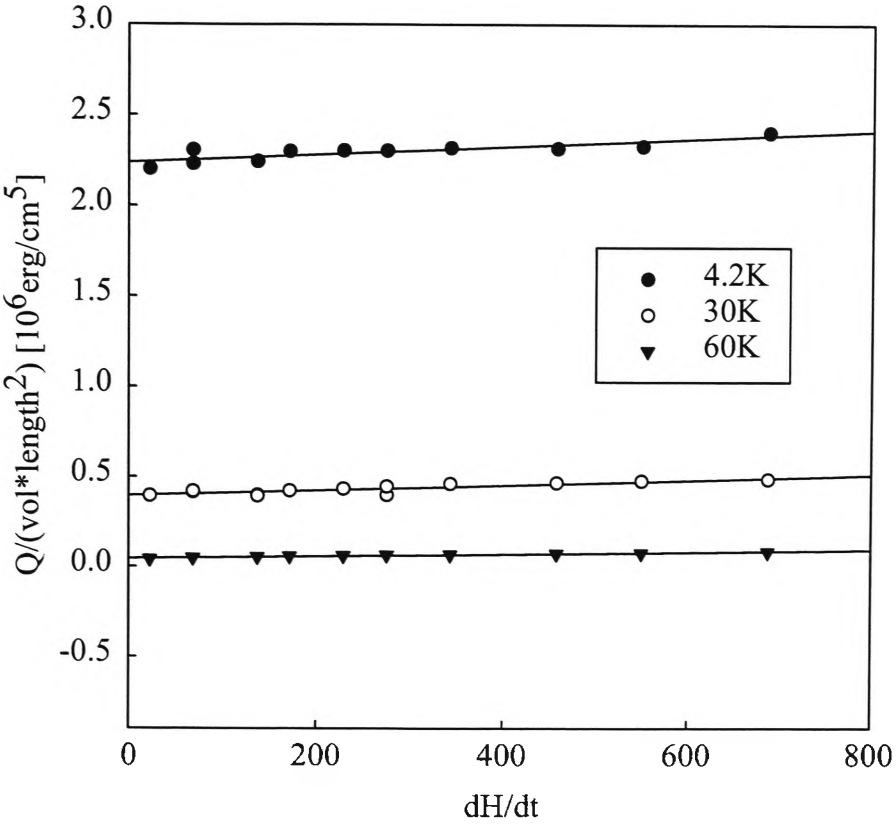

Figure 2.5. Plot of AC Loss versus field sweep rate for a seven filament sample of tape, courtesy of Collings and Sumption, Ohio State University, Ohio, U.S.

No coupling currents were evident by virtue of the fact that the loss was virtually independent of the sweep rate. Further microscope observations, however, revealed bridging of the filaments through coalescence of filaments (Figure 2.6) and intergrowths (Figure 2.7) in the measured samples along the length of the tape. This exercise shows the difficulty in guaranteeing any length of tape to be free of intergrowths and coalescence.

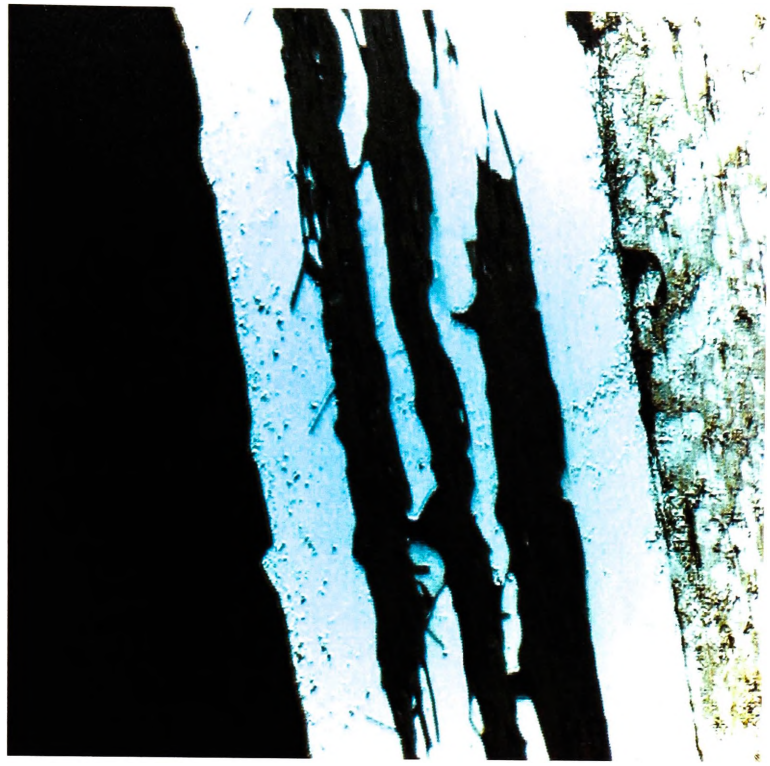

Figure 2.6. Transverse cross section analysis found that despite the low filament number and low fill factor, filament coalescence occurred in this sample.

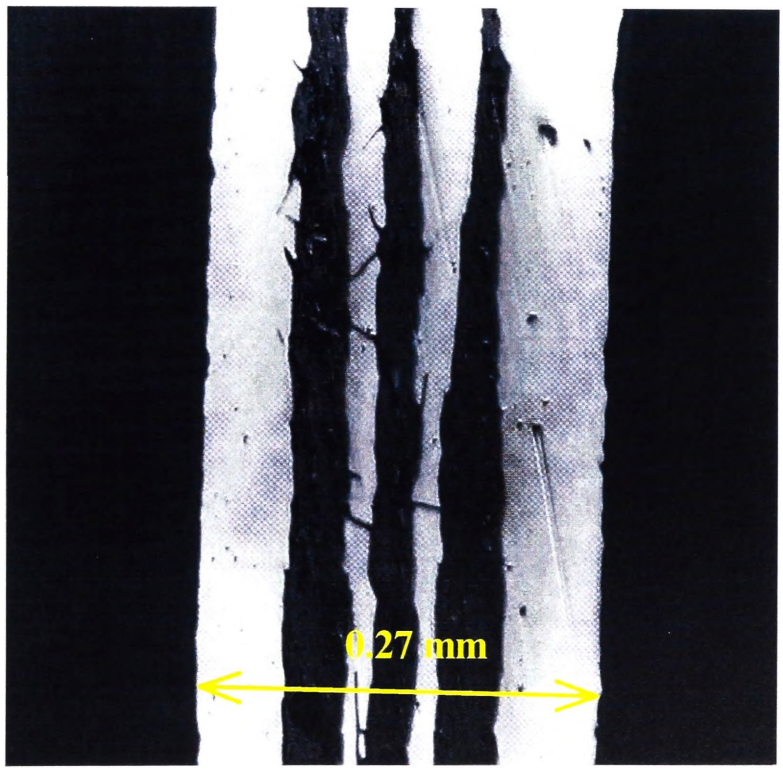

Figure 2.7. Transverse cross section of a seven filament tape made to avoid bridging between the filaments. Further optical investigation, however, found small intergrowths had occurred.

It was found that the bridging was more severe in tapes where alloy B was used as the matrix material. If the development of HTS tapes with lower AC losses is to be successful, then samples need to be developed with twisted filaments, a highly resistive alloy matrix, and a filamentary structure which is distinct and free of coalescence.

In general, it was found that by ensuring sufficient silver matrix material was present between the filaments, the coalescing of filaments could be largely avoided. The bridging problem was found to be significantly reduced by employing other suitable processing techniques outside the scope of the work reported here.

2.3 Results

Not all samples were found to have a suitable Ic for future AC loss characterisation and initial results revealed severe Ic degradation of the twisted filament samples to less than half the Ic of the control samples. As the twisting process was refined, however, the Ic after twisting was maintained compared to straight filament samples. Figure 2.8 summarises a selection of the Ic results obtained on over 30 samples of twisted filament tape fabricated in this work. In summary, tape manufactured with filament twist pitches down to 10 mm were manufactured with Ic's up to 40 A (Jc > 20 kA/cm^2), and a core which had physically distinct filaments. In addition, minimal degradation was achieved in samples with a twist pitch of 10 mm after suitable techniques had been perfected.

Samples of HTS tape with alloy matrices and physically distinct filaments with pitches down to 4 mm were also prepared with some success, however, a definite reduction in the Ic of these samples, compared with their alloyed control samples was noticed.

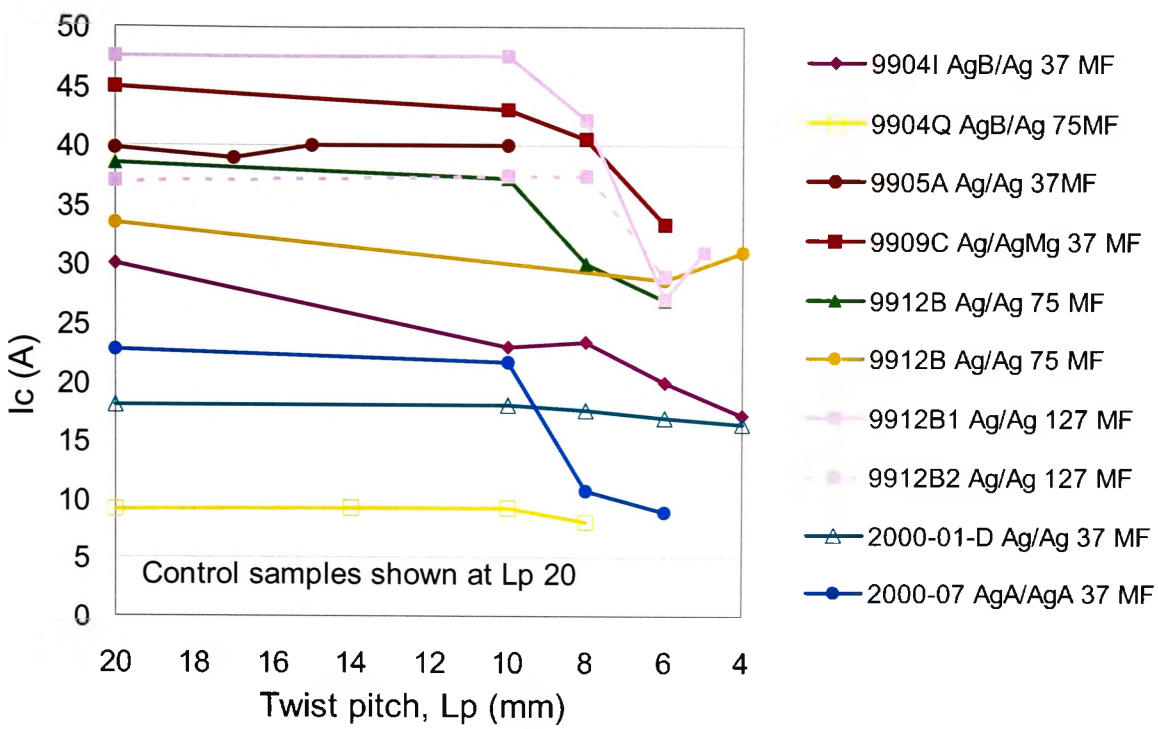

Figure 2.8. Plot of the development of twisted filament tape having various matrix and sheath alloy. The data points on the most extreme left represent the control samples. Example coding: **9909C Ag/AgMg 37 MF**. The year of manufacture is 1999, the month is 09, the matrix material is Ag, the sheath is AgMg alloy, and the tape has 37 filaments. Note: Sometimes twisting and completion of a tape sample and subsequent Ic measurement was obtained after the original date of wire manufacture. It also be noted that the results are sometimes influenced by the manufacturing process variables, for example, the Ic if sample 9912B1 increases at a pitch of 5 mm compared to the Ic at 6 mm twist pitch.

Filament twist pitches smaller than 10 mm in the tape resulted in degradation of Ic unless precautions were taken during the twisting procedure and in particular, the Ic degradation was most marked in samples of tape with filament pitches of 4-6 mm. With special precautions, however, twisted filament tape with 37,75, and 127 filaments, and pitches of down to 8 and 10 mm and Ic values of over 30 Amps were produced. Figures 2.9-2.11 show optical micrographs of typical results of this work, where filament coalescence and intergrowths were largely avoided in the twisted filament tapes and control samples.

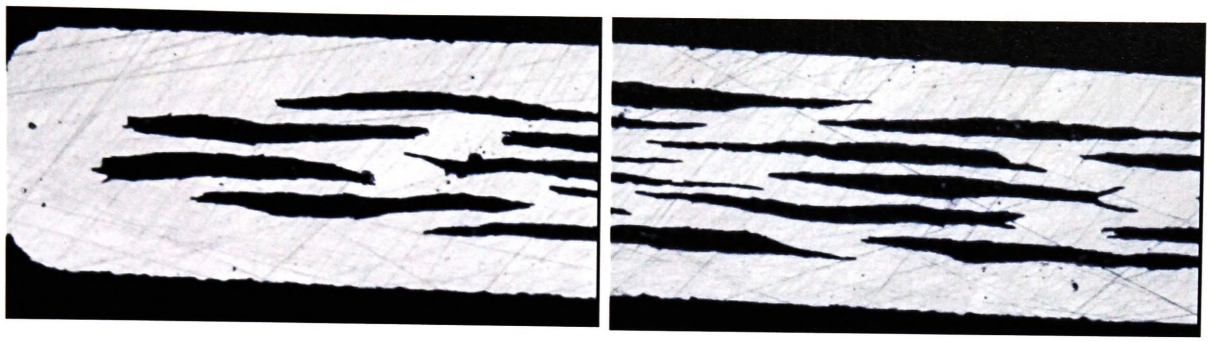

Figure 2.9. Optical micrograph of a cross section of 37 MF twisted filament tape produced without intergrowths or bridging (9904I AgB/Ag Lp=10 mm).

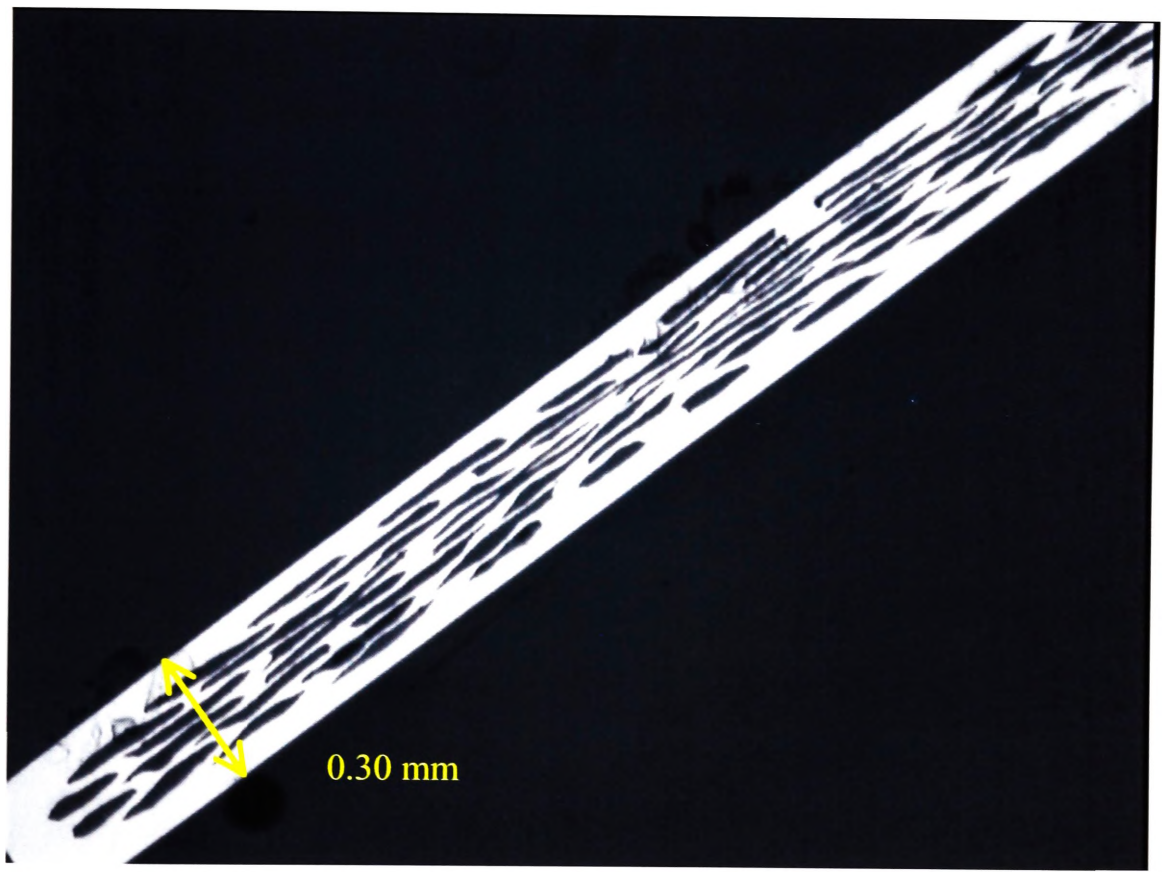

Figure 2.10. Optical micrograph of a transverse cross section of a 75 MF tape with no visible inter-growths and minimal coalescence (9912B, Lp = 10 mm)

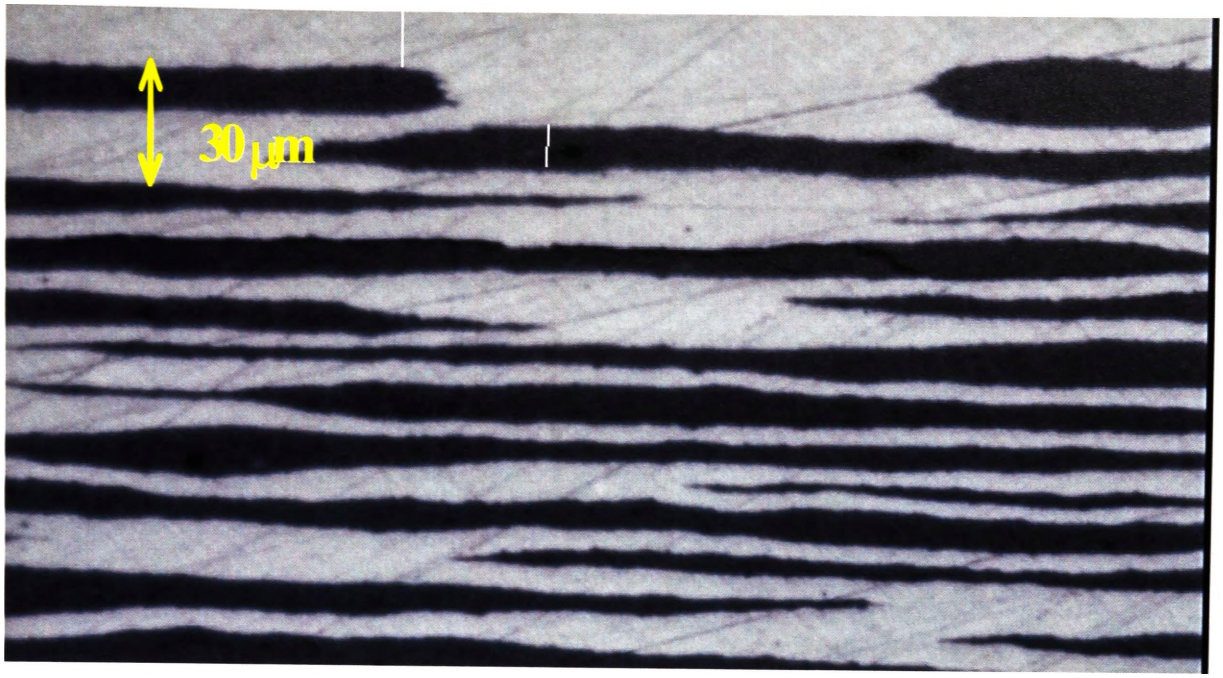

Figure 2.12. Optical micrograph of a transverse section of a portion of a 127 MF twisted filament tape made with minimal bridging. (9912B1 Ag/Ag, Lp = 10 mm)

2.4 Discussion

A manufacturing technique to produce twisted filament tape with distinct filaments that are not connected by bridges or coalesced, was developed over the course of circa two years. This requirement complicated the production of HTS tape considerably. The only way to achieve this requirement is with a lower fill factor tape which ultimately reduced the Ic of control samples by up to 30 %. The gains made in reducing the hysteresis losses by this technique may not justify the end use of twisted filament tape. A higher Ic is the best way to reduce overall device losses as the amount of HTS tape required can be reduced.

The ultimate aim of developing twisted filament HTS tape was to replace the current straight filament tape for AC applications where appropriate. It will be shown that HTS transformer coils can benefit from the use of twisted filament tape (See Chapter 6) when designed correctly. The techniques used to manufacture short pieces of tape for testing, however, may not be directly applicable to manufacturing longer lengths.

2.5 Conclusions

A more in-depth review of AC losses in multifilament HTS tapes revealed than the only practical method of lowering their AC losses is by the simultaneous de-coupling of their filaments through twisting and reduction of the subsequent coupling current losses through increased effective matrix resistivity. Hence, a technique for manufacturing short lengths of HTS twisted multifilament alloy matrix tape was developed, and improved to prevent filament bridging through the mechanisms of inter-growths and coalescence. Samples of multifilamentary HTS tape with twist pitches of 10 mm and alloy matrices were obtained with Ic's of greater than 35 A and with minimal Ic reduction compared to the controls. Samples with twist pitches of 4 and 6 mm were also successfully obtained in samples with alloy matrices, however, these were found to have up to 50% Ic degradation compared to the controls. A lower reduction in Ic of about 20 % was obtained for samples with pure silver matrices.

Use of an automated image analysis system was invaluable in determining whether a particular processing technique was successful in avoiding bridging. It was also found that the filament twist pitch of the outer layer of filaments could be measured to within ± 0.5 mm using this technique.

In summary, suitable novel samples with sufficient Ic were manufactured for future characterisation in a short length AC loss measurement system which will be developed as part of this research work.

References

[2.1] PhD thesis, S.H-R Clerc, Swiss Federal Institute of Technology, Zurich, "AC losses of mono and multi-filamentary High Tc superconducting tapes", Diss. ETH No. 11353, 1995.

[2.2] Y.Yang, T.J.Hughes, E.Martinez, C.Beduz, and F.Darmann, "Reduction of the a.c. losses in Ag sheathed PbBi2223 tapes with twisted filaments", IEEE Trans. Appl. Superconduct. Vol 9, p 821, 1999.

[2.3] T.Hughes, F.Darmann, J.Horvat, S.X.Dou, "Reduction of the a.c. losses in Ag sheathed PbBi2223 tapes with twisted filaments", Physica C, Vol. 325, pp 77-82, 1999.

[2.4] W.Goldacker, H.Eckelmann, M.Qulitz, B.Ullmann, "Effect of twisting on the filaments of multifilamentary BSSCO(2223)/Ag and Ag/Mg Tapes", IEEE Transactions on Applied Superconductivity, Vol.7, No.2, pp 1670-3, 1997.

[2.5] C.M.Friend, D.M.Spiller, Y.B.Huang, E.Martinez, "Low Loss Conductors for Power Applications", IEEE Transactions on Applied Superconductivity, Vol. 11, No. 1, pp 2196-2199, March 2001.

[2.6] P.F.Herrmann, E.Beghin, G.Duperray, D.Legat, A.Leriche, "Development of Twisted Bi-2212 and Bi-2223 Powder in Tube Conductors for ac Applications", IEEE Transactions on Applied Superconductivity, Vol. 7, No. 2, pp 2196-2199, 1997.

[2.7] H.Eckelmann, M.Däumling, M.Quilitz, W.Goldacker, "Investigations of the AC current loss of twisted and untwisted multifilamentary Ag/AgMg and Ag/AuBi(2223) tapes, Applied Superconductivity, Vol. 2, No. 158, pp. 1433-6, 1997.

[2.8] K.Kwasnitza, St.Clerc, R.Flükiger, Y.B.Huang, "Alternating magnetic field losses in high Tc superconducting multifilament tapes with a mixed matrix of Ag and BaZrO3, Physica C, Vol. 299, pp 113-124, 1998.

Chapter 3
Experiments with HTS coils

3.1 Introduction

Any coil which is to be used in a device requires tolerance to mechanical and electrical forces, and electrical stresses. The coils must be sufficiently robust, such that within reason, it is able to maintain the original current carrying capacity, dimensions, electrical insulation properties, and strength under operating conditions. In situations of high mechanical or Lorenz forces, it is customary to bind (or pot) the windings in an impregnating medium to prevent movement of the windings. In superconducting applications, this is especially necessary to prevent quenches and loss of current carrying capacity [3.1-3.8].

3.1.1 Coil engineering current density : effect of insulation.

When considering an insulation material for HTS tapes that are to form a coil, the Je of the coil will be reduced by a factor depending on the insulation thickness. Ultimately, the Je will determine the size of coil, eg. solenoid, magnet, or transformer, that is required for a given specification. A higher design current density allows for smaller devices to be built, and is the driving force behind the present research into superconducting wires and tapes.

The two possible methods are described below that reduce Je. A close packed structure is used to give maximum effective current density. Low Tc superconducting coils are wound very carefully to ensure that the close packed structure is achieved throughout

the whole cross section [3.20] and therefore a minimum reduction in the effective Je. Figure 3.1 shows examples of how round wires may be layed up in a coil winding.

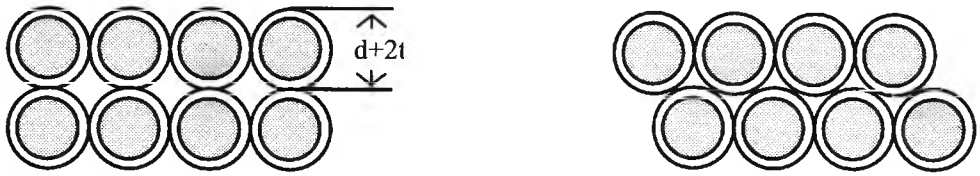

Figure 3.1 Diagram of the different structures possible with round wires

Figure 3.1 also shows the significant amount of volume available for impregnating varnishes to fill. For example, VAC low Tc superconducting wire (0.300/0.336) has a 28 % volume fraction available for impregnating varnishes [3.9].

When insulated tapes are considered, the reduction in Je may be found from equation 3.1, with the respective variables being defined in Figure 3.2.

$$\frac{Je(nett)}{Je(tape)} = \frac{wt}{(w+2t')(t+2t')} \quad \text{Eq. (3.1)}$$

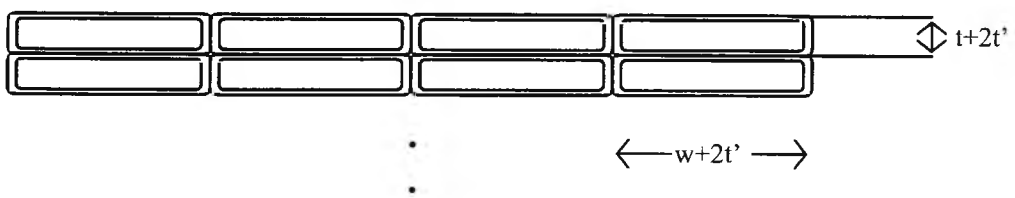

Figure 3.2 Schematic of HTS tape lay up in a coil showing insulation

For typical tape dimensions, e.g. w = 3 mm and t = 0.3 mm, and for an insulation thickness of t' = 0.1 mm, the current density will be reduced to 56% of the original tape, with no allowance for resin impregnation. Obviously, when large coils are considered, where size and volume are a major factor, and impreganating varnishes

must be used, such a reduction in Je is unacceptable. Hence, insulation thickness and incorporation of a binding agent is an important consideration [3.1]. In the above example, if a thinner insulation of 50 μm were used, then the effective current density would be decrease by 27.5%. Hence, the effect of insulation and resin coating thickness was an important consideration in this work. Cross sections of coils with various insulation and resin systems were taken in order to obtain the final volume fill fraction of HTS tape.

A technique that may be used to reduce the size of the coil due to the insulation requirements is to co-wind a number of tapes, n, together in parallel, with insulation around the entire set, rather than each individual tape. The coil may then be wound using this conductor, rather than individual tapes and the degradation in effective Je is reduced. The reduction in Je due to the insulation requirement was derived as:

$$\frac{Je(coil)}{Je(tape)} = \frac{wt}{(w+2t')(t+2t'/n)} \qquad \text{Eq. 3.2}$$

For thinner insulation, 25 μm, about five tapes arranged in parallel will provide the most benefit, increasing the effective Je from 80 % to 94 %. The disadvantage of the technique is that transpositioning of the tapes is required to reduce eddy currents for high current ramp rates and under sss conditions. This may be insignificant, however, compared to hysteresis losses, depending on the ramp rate.

3.1.2 General requirements of insulation for superconductors:

The two main coil fabrication techniques used for HTS tapes are referred to as the "react and wind" (R&W) and "wind and react" (W&R) methods . The former involves the fabrication of wire and tape to completion, including insulation. The latter method requires that the final coil be wound from partially or un-reacted HTS tape, and then heat treated to completion, with any insulation already in place. There are advantages and disadvantages of each type, and each technique is likely to be used in the design of different purpose devices.

Regardless of the technique used, the materials used for insulating the superconductor must ensure adequate turn to turn electrical insulation properties at cryogenic temperatures, and must not damage the conductor in the application process. They should minimise the overall size of a coil, and retain continuity and adhesion during coiling. In addition, insulation is also required for the layer to layer, and coil to cryostat potential differences, and must permit adequate cooling and cryostability of the HTS windings during operation and over the lifetime of the device.

Individual tapes within a larger magnet conductor may also be insulated, despite the fact that DC current is used. The reason for this, is to reduce the eddy currents during ramp up and ramp down sequences. During these procedures, eddy current losses and hysteresis losses will occur in each individual HTS tape. If the HTS tapes within a conductor are not insulated from each other, then transverse inter - tape eddy current losses will also occur [3.1]. This could be large compared to the hysteresis and individual tape eddy current losses and will lower the allowable ramp rate before instability occurs. Typically, it is these losses that limit the charge up time for large magnets. Any insulation applied to the windings, however, will impede the coolant to conductor heat exchange, and will lower the stability criterion. All these issues need to

be considered and resolved clearly when deciding on an insulation system for an HTS coil.

3.1.3 The Wind and React (W&R) technique

The most frequent insulating technique used for wind and react coils is to use "fibre" cloth to electrically insulate the windings, and a setting compound after reacting to pot the coil and impart structural stability [3.2,3.3,3.4-3.8]. In order to give a superconducting coil structural stability as well as electrical insulation, the Vacuum Pressure Impregnation (VPI) technique may be used. This technique relies on the absorption of epoxy into a "fibre" cloth and may be used to pot coils manufactured according to both R&W and W&R techniques. When it is applied to W&R coils, however, the cloth must be stable with respect to the sintering temperature.

When using the VPI method, all the "fibre" cloth insulation and re-enforcements are installed completely dry during the magnet assembly. The coil is then sintered to form the superconducting phase. After this, the coil is potted with an epoxy and an anhydride curing agent which is injected into the assembly, and the structure cured. A typical curing cycle, for example, is 1.5 hours at 135 °C.

Low Tc magnets wound with the W & R technique use a fine woven fibre glass and are sintered at around 750 °C [3.2,3.4,3.5]. However, the HTS tapes are commonly sintered between 820 and 920 °C in an oxidising atmosphere making this material unsuitable for HTS electrical insulation.

A more appropriate cloth to use is ceramic fibre insulation [3.5,3.6]. Haldar used a ceramic cloth insulation, followed by an epoxy to pot and electrically insulate 2223 tapes [3.6]. Haldar investigated appropriate fibre cloth for low Tc W&R coils include

quartz, ceramic, and R-glass. Haldar used cloth samples with a thickness of between 160 μm and 330 μm, with a fibre size of between 1 and 9 μm.

3.1.4 The react and wind technique

In this technique the tape has an insulation applied after all heat treatment procedures of the tape have been completed [3.10, 3.11, 3.13-3.19]. In addition, the coil may be potted in an epoxy resin for structural stability and to hold the insulation in place. This is the most popular technique in the literature as it allows a specialised product to be manufactured by a tape supplier, and coils to be made by a third party.

The insulation applied may be a polyester-amide-imide varnish or an enamel as used in conventional copper magnet wire [3.9], or alternatively insulating films may be used such as the various Kapton tape, polypropylene [3.10] , mica paper [3.4], and alumina paper [3.8]. Suitable materials with usual thickness, and breakdown strengths are tabled in the literature [3.10].

3.1.5 Advantages and disadvantages of the two coil fabrication methods:

The main advantage of using the R&W technique for coil fabrication stems from the fact that any insulation will not have to withstand elevated furnace temperatures. Some commercially available polymer based electrical insulation such as Kapton and Poly-amide-Imide can be used to insulate HTS tapes for use at 77 K and below [3.4,3.10]. The technology for applying varnish or film insulation is well established and results in a thin insulation layer of between 20 and 100 μm.

The disadvantage of the R&W technique is that the conductor is strained in the process which can decrease the Ic of the tapes. Strains of a few percent can completely destroy the Ic of a HTS tape with only around 60 % of Ic remaining after a 1% longitudinal

bending strain [3.11]. A level of about 0.2 % is commonly given as the maximum strain for 95 % retention of the un-strained Ic. This level of strain is achieved when a 0.3 mm tape is wound in a 15 cm diameter coil, and could be restrictive for some coil designs, and overly increase the size of coils wound in this manner. The degradation in Ic due to bend strain may be reduced by using multifilament tape. Using multifilament tape, the strain tolerance of HTS 2223 tapes has been shown to increase to 1 %. In addition, various alloying elements and high strength claddings can improve the strain tolerance further. Nevertheless, for some specific applications, such as insert magnets, which have a very small diameter of between 25 and 50 mm, the W&R technique is the only option [3.18]. By using W&R there is no degradation in the final electrical properties due to coiling strain. The final heat treatment heals any cracks in the filaments that may have formed during coiling and the tape is not subject to any extra strain after the final sinter.

A disadvantage of W&R coils is that thicker insulation is required than R&W. The required cloth thickness is around 200 to 300 μm [3.3,3.4]. The bore size must be taken into account, however, since if this is large compared with the annular thickness (inner radius-outer radius) the insulation thickness used has little consequence on the overall size of the coil.

3.1.6 Structural rigidity

Lorenz forces will be produced in coils due to the interaction of the current with the magnetic field. These forces tend to expand the coil in an outwards direction, and hence the HTS winding and insulation must combine to form a composite structure that can withstand these forces. Much work has been carried out in this area with Low Tc

superconductors for the international fusion reactor research collaborative (ITER) (International Thermo-nuclear Experimental Reactor) [3.13].

3.1.7 Thermal contraction

It has been found, that at cryogenic temperatures, the superconductor performance is degraded marginally if the electrical insulation makes adhesive contact to the conductor [3.14,3.15]. The low thermal contraction of the insulator compared to the metal sheathed superconductor effectively fixes the windings in place not allowing the conductors to compress in the cryogenic temperatures. This will put the superconductor in a state of compressive stress and reduce the critical current. This process is called training and is usually carried out by the manufacturer as part of the commissioning process. After one or two such processes, no further reduction in critical current should take place. Detailed analysis of the radial strain and the insulation tangential tension distribution throughout the layers of a large magnet coil has been completed by Karasik *et al.* [3.15].

The net thermal contraction of the dielectric insulation must be designed so that it contracts evenly with the conductor during the cool down period [3.16]. This means selecting materials that have a similar expansion co-efficient to the metallic sheath of the particular superconductor being used and avoiding those where a large difference exists. In high voltages coils, this is a problem as voids form between the dielectric and the outer conductor, and it is at these voids that partial discharges will occur, ultimately leading to breakdown of the insulation.

3.1.8 Quench requirements of DC coils

Quenches during operation of a coil may be caused by an attempt to exceed the critical current of the device, thereby causing thermal loss, and film boiling, followed by a temperature increase and normal conductivity.

Voltages developed during steady state operation of superconducting DC coils are small, and of the order of $2\pi R(I/I_c)$ μV, where R is the turn radius. Even for very large coils, this is of the order of μV and hence layer to layer and layer to ground voltages will also be small. High performance properties of the insulation are not critical during normal DC operation of coils. During charging of the coil, however, inductive voltages are significant.

A superconducting magnet should not be damaged by a quench and should be able to be restored to normal operation once it is re-cooled, therefore, any electrical insulation employed for layer to layer and coil to ground must be adequate to meet with these subsequently higher electrical stresses. If insufficient electrical insulation is used, then it may be damaged by the high voltages discharging through and hence have to be repaired or remade.

3.1.9 Calculation of electrical stresses

The calculation of the voltages developed in a particular coil design is critical to the choice of appropriate insulation. Critical voltages that must be known are the turn to turn, layer to ground, layer to layer or Pancake, and the current lead to ground voltage. In superconducting coils these are greatest when the coil is subjected to a ramp in current, or a quench where the stored energy in the coil is dumped very quickly into an external resistor. In these situations the current carried by the coil changes very rapidly and induces voltages according to $I(t)R(t) + L\delta I(t)/\delta t$. Hence, crucial parameters which

must be known are the maximum rate of current change, the coil inductance, and the quench or dump voltage.

Schwenterly provides an excellent review of turn to turn voltages developed in HTS coils and includes inter-turn voltage calculations for various coil types from pancakes to long thin solenoids and for "Brooks" coils (where winding thickness equals the coil length) [3.17]. The results of Schwenterly are important to this work, so a summary and discussion will be given here, along with further analysis that will highlight the compromise which needs to be made when choosing between pancakes and long solenoid type coils to achieve a certain magnetic field.

The result for the inter-turn voltage is given by equation 3.3,

$$\frac{V}{N}=\frac{N.I.E}{A^2 H(\Delta T)} \quad \text{where} \quad \{H(\Delta T)=\int_{T_i}^{T_f}\frac{Cv(T)}{\rho(T)}.\partial T \sim 3.0e16\} \qquad \text{Eq. 3.3}$$

and where,
N.I = total number of ampere turns in the coil,
E = total energy stored in the coil = $1/2LI^2$,
A = total area of stabiliser in a cross section of the coil (non superconducting),
Cv(T) = specific heat of the coil ($J/^{\circ}Cm^3$),
ρ (T) = ratio of silver resistivity to superconductor resistivity (~ 500).

The term H(ΔT) is referred to as the hot spot integral and is calculated using the temperatures before (Ti), and after (Tf), a quench. Taking the case of a very long solenoid coil, it is possible to calculate the stored energy simply. The quench voltage per turn in this case is given by :

$$\frac{V}{N}=\frac{I^3 N^3(\pi r^2)\mu_o}{l(A^2)}.K \qquad \text{Eq.3.4}$$

where
r = radius of coil,
l = length of coil,

K = constant,
N = number of turns,
I = current.

This indicates that the quench voltage per turn is proportional to the cube of the number of turns, however, a more appropriate equation is that which gives the quench voltage for a particular magnetic field strength design. Tomita [3.18] shows this to be as follows :

$$\frac{V}{N} = \frac{B_z^3 f(\varepsilon, \phi, \gamma)}{H(\Delta T)} \quad \text{Eq. 3.5}$$

Where the function f is dependent on the geometry only.

3.1.10 Ageing of insulation materials at cryogenic temperatures

The factors of quench voltage, frequency of quenches, and mechanical stress influence the ageing and eventual life of the insulation. Ageing of electrical insulation ultimately leads to breakdown of the insulation (it fails to insulate) and mechanical breakdown (it crumbles). For conventional devices, the factor that most influences the life of electrical insulation is determined by long term chemical deterioration. This factor is absent at cryogenic temperatures, and the major factor influencing an insulation's life is that of mechanical stress which can either shear or fracture tape insulations, and partial discharges which can result in cracking of the insulation material. Factors influencing the ageing of electrical insulation are outlined and discussed by Schutz [3.2], Karasik [3.15], and Takahashi [3.19].

Schutz reviews the subject of insulation ageing in cryogenic applications. References are given to works which study the effects of partial discharges, the dielectric properties of LN, the expected time to failure, and the stress capability of specific insulation materials.

Takahashi investigated the resistance in LN of insulating materials to partial discharge activity. The materials studied were, polycarbonate, polyethyleneterephtalate, celulosetriacetate, polytetrafluoroethylene, and polyethylene. All were characterised as having weak resistance to partial discharge degradation except polyethelene. Takahashi found that if the LN is not pressurised, thermally induced bubbles can result in excessive discharges occurring. It was recommended that the nitrogen pressure be greater than 200 kPa.

3.1.11 Specific examples and details of insulation used for coils in the literature

Tomita et. al. describe how pancakes are manufactured using W&R [3.18]. Two coils are integrated by inserting one coil inside the other coil to form double layered pancakes multiples of which are stacked to form the final coil. The advantage of the method is that ordinary organic Mylar tape may be used to insulate the tapes, and the advantages of react and wind are still maintained. The method was to co-wind with 0.8 mm thick polyethylene, which is removed after annealing at 100 °C for 1 hour. This leaves gaps of 0.8 to 1 mm between the turns of the Pancake during sintering, that will easily accommodate the 50 μm Mylar tape for insulation after the R&W heat treatment.

A 2.58 m bore, low Tc magnet coil is described by Karasik et. al [3.15]. The LTS feed wire for the coil is insulated with 0.2 mm thick epoxy fibreglass. During coil fabrication, liquid epoxy is applied on each layer of winding, and 0.1 mm fibreglass placed between the layers to give an impregnated fibre glass insulation. The 96 mm high coil consisted of 40 layers of 24 turns each, and was insulated from the metallic flanges of the coil former by 10 mm thick fibreglass plastic hoops.

Karasik included an analysis of the tangential tensions in the epoxy insulating layers. These layers are in a compressed state after reeling, and, because of thermal contraction, the insulation is stretched strongly after cooling of the magnet down to 4.2 K, the

largest tension of 21 MPa occured in the outer layer and the tension in the inner layer was 13 MPa. The extra tension under charging of the coil was negligibly small. Karasik explains that this level of stress has not yet induced cracking of the epoxy. The radial displacement of the winding under charging of the coil and the influence of the induced strain on the Ic were also investigated. The largest strain of 0.065 % occured in the middle layers and is therefore thought not to degrade Ic significantly.

Quench protection of the magnet winding is achieved with low resistance shunts in parallel with the winding, as apposed to high resistance's in series. At a quench, the current will flow through the shunt resistance's instead of the windings.

Schwenterly et al. [3.1] and Bruzzone [3.3] reported on the details of W&R HTS Pancake coils which used a multiple of HTS tapes in parallel. Schwenterly used 5 tapes in parallel and Bruzzone used 3 tapes co-wound in parallel.. The performance of the coils in liquid helium in ramped and static magnetic fields was assessed. Bruzzone found that the critical current per tape was comparable to that of short single tapes from the same batch, which indicated that W&R of multiple tapes in parallel does not lead to degraded individual tape performance. This is an important result as high current coils and conductors must be fabricated from multiple HTS tapes. Both Schwenterly and Bruzzone concluded that employing multiple co-wound tapes does not cause excessive eddy current heating or instability in liquid helium. They also noted that using multiple co-wound tapes increased the overall "winding current density", as discussed in section 3.1.1 above.

To insulate and pot a coil of PIT 2212 wire, Tenbrink used a ceramic fibre insulation which was then wound onto a sample holder of AgNiMg which had a thermal expansion coefficient matched to the silver [3.5]. Tenbrink braided the ceramic fibre

insulation very rigidly around the wire at a thickness of 100 μm. The 1.00 mm wire diameter increased to only 1.2 mm reducing the effective current density by just 30 %. Tenbrink found that during the 2212 sintering procedure, the ceramic fibre insulation acted like a sponge and sucked small amounts of the 2212 out of the matrix. This created an interruption of the HTS wire core and the coil had a resistive behaviour at 77. Moriyama et. al. investigated epoxy resins and curing agents for vacuum impregnation of superconducting coils for use at 77 K and 4.2 K. The factors investigated were those of shock resistance, shrinkage after curing, tensile adhesive strength, and tensile shear adhesive strength, frequency of quenches, and cracking resistance. Test coils were wound from polyvinyl formal (PVF) insulated superconducting wire of 1 mm diameter and potted with three different types of biphenol epoxy resins according to curing reaction (A = amine curing, B = accelerated amine curing, C = acid anhydride curing). It was found although resin A was superior in thermal shock resistance, quenches occurred more frequently. Also, the viscosity of resin A increased more rapidly during the impregnation process compared with that of resins B and C. It was concluded that resins B & C are the most suitable for larger superconducting coils.

3.2 Experimental techniques for winding Pancake coils

3.2.1 Introduction

A technique for providing electrical insulation between the turns of pancakes coils and making a rigid potted structure was developed by the author in this work. The technique consisted of co-winding various types and thickness' of composite insulation with HTS tape followed by curing of the embodiment. An initial batch of eight pancake coils was manufactured. The pancakes with small annular thickness [define as (OD-ID)/2] of approximately 50 mm and diameter of approximately 100 mm were physically rigid,

however, those pancakes manufactured with larger dimensions with ID approximately 200 mm and OD = 400 mm were found to be not mechanically rigid. Attaching current leads to the pancakes after curing was also difficult as the insulation had to be scraped away and a soldered joint made. This left the inner and outer turns vulnerable to damage. It was also noted that the coil fill factor was low.

In order to improve the mechanical rigidity of the pancake manufacturing technique and improve the coil fill factor, a plan was developed which incorporated new techniques and materials designed to overcome the deficiencies in the existing pancake manufacturing routine.

Many applications, such as transformers and magnets will only have a very small turn to turn insulation requirement. For example, in transformers typical turn to turn voltage requirements are only of the order of a few volts or tens of volts which does not require such thick insulation. In order to reduce the insulation gap between turns and investigate how it still may be used to impart ruggedness and isolation of turns, thinner insulation materials were sourced and pancakes wound and tested.

3.2.2 Experimental pancake manufacturing techniques

The initial eight pancakes were manufactured using a simulated coil winder which incorporated two variable speed AC drives, a free wheeling shaft for the insulation takeoff, and a cleaning mechanism for the HTS tape. Sufficient back tension was applied to the HTS tape such that if either motor was stopped, the HTS tape remained straight. Using the knowledge gained from these coils, a further twelve pancakes were manufactured on a dedicated coil winding machine to investigate more robust coil manufacturing techniques, integrated current leads, and thinner insulation materials with the objective of increasing the coil fill factor.

A number of different insulation systems, A, B, C, D, (See Appendix 2) were investigated to produce well insulated and mechanically rigid pancake coils. In addition, a number of different post winding, pre-cure treatments, PW1, PW2, PW3, (See Appendix 2) were attempted, to investigate their benefit for pancake coils. Table 3.1 shows the details of the pancakes from which the conclusions of this work were drawn.. Pancakes 11 and 12 were manufactured subsequently to test the suitability of a thinner composite insulation materials and had no post wind treatments. In addition, the best techniques and knowledge gained from pancakes 1 – 10 were incorporated into these pancakes. As indicated by the use of ½ in table 3.1, only half the turns of Pancake 1 and Pancake 2 had a post wind treatment.

Pancake No.	Insulation system	Tape length (m)	ID (mm)	OD (mm)
1	A+(1/2)PW2	110	200	300
2	A+PW1	140	200	323
3	A+PW1+PW2	74	200	273
4	A+PW1+PW2	72	200	270
5	A+PW2	49	200	250
6	B	31	200	250
7	B+PW1	68	100	240
8	B+PW1	69	100	242
9	B+PW1	45	200	262
10	B+(1/2)PW3	80	200	300
11	C	30	25	104
12	D	30	25	120

Table 3.1. Details and insulation techniques used for the experimental pancakes

Figure 3.3 shows the lay up of a batch of pancake coils before final enclosure in the vacuum bag and curing. A suitable temperature, pressure, and time that accommodated the curing requirements of the insulation systems (A, B, C, D) and post-wind treatments (PW1, PW2, PW3) was chosen.

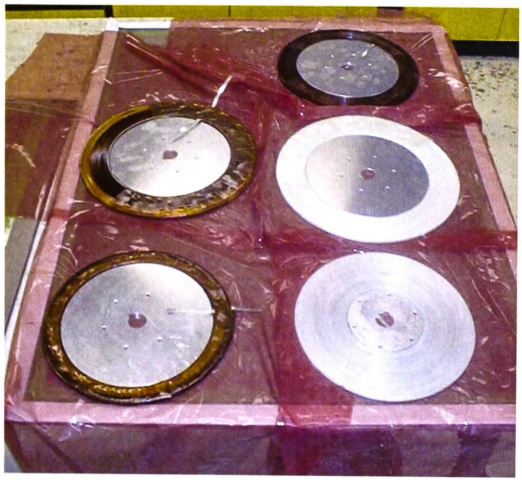

Figure 3.3. Set up of a batch showing pancakes from top right hand corner, down and to the left: Pancakes 2,10,8,5, and 1

3.3 Results

3.3.1 Observations of Pancake coils after curing

The first batch of 5 pancakes consisted of Pancakes 3,4,6,7, and 9 from Table 3.1 and are shown in Figure 3.4 after completion of the curing procedure. The pancakes were all rigid and survived quenching in LN without any visible cracks.

Pancake 4 was found to have good adhesion of the insulation system A to the outside faces of the Pancake. This was found to be better than on previous attempts at this technique without using treatment PW1.

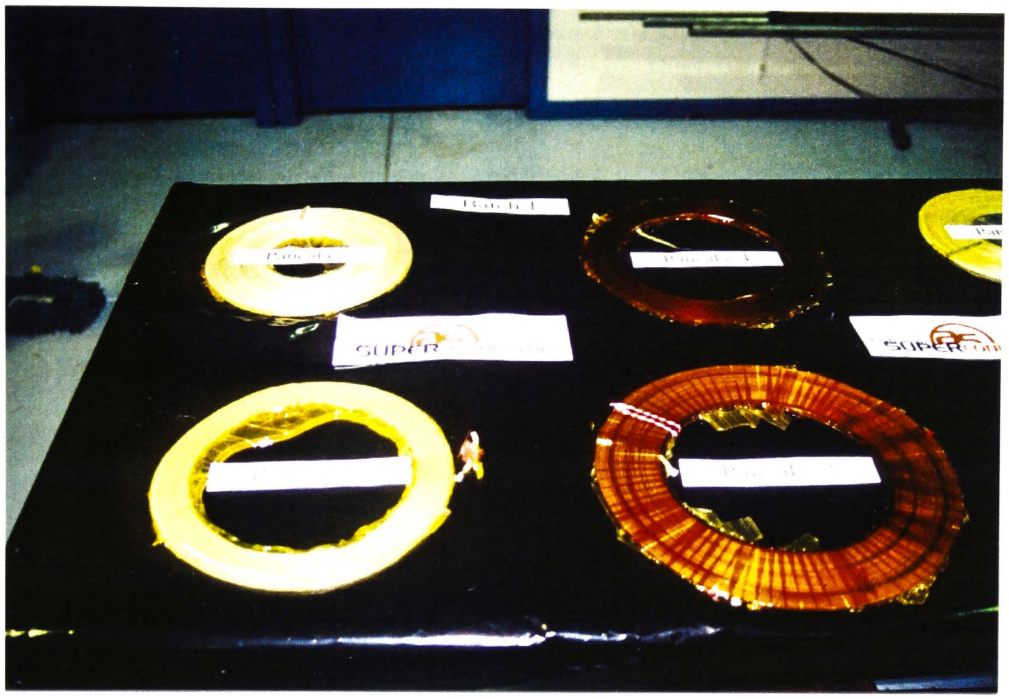

Figure 3.4. The completed first batch of cured pancakes 3,4,6,7, and 9

Pancakes 7 and 9 were found to be mechanically rigid and strong. They withstood normal handling and quenching in LN. The surface texture of the faces is rough due to the uneven width of the insulation tape used. All the turns are rigid and there was no tendency for the inner or outer turns to shear away from the main body.

Pancake 3 was the most successful of the pancakes in batch 1 insulated with system A. Treatment PW2 enabled the inner and outer turns to be firmly held in place, and the adhesion of PW2 to the outer faces of the Pancake was found to be excellent. The Pancake as a whole was rigid and mechanically strong. Some deformities, however, in the outer rim of the Pancake were noticeable. These were assumed to be due to the looseness of the original pancake winding. This problem could be avoided if the original winding was a lot tighter.

The results from the first batch of pancakes were used to refine the post wind treatments in a second batch. The coils in the second batch of pancakes are shown in Figure 3.5.

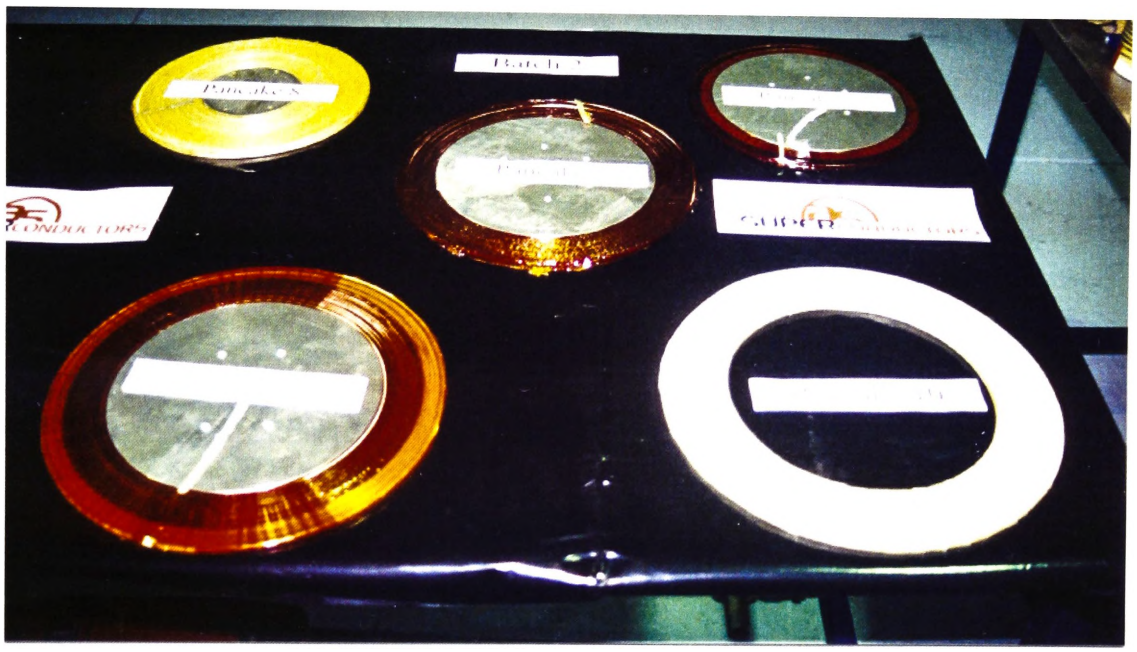

Figure 3.5. Second batch of panckes after curing. Pancake numbers 1,2,5,8,10.

Both the PW2 treated and non-treated sections of Pancake 1 (Figure 3.6) were found to be mechanically robust and self supporting under its own weight. However, after shipping and some mechanical handling, the inner turns of the section without PW2 treatment were found to be susceptible to peeling. The portion treated with PW2, however, remained intact. The adhesion of PW2 to the surface was excellent.

Pancake 5 showed much the same properties as that portion of Pancake 1 with the PW2 treatment. Due to the smaller annular thickness of Pancake 5 (25 mm), however, compared with Pancake 1 (50 mm), the treatment was more uniform in appearance.

Figure 3.6. Pancake 1 after curing

Pancake 2 demonstrated a similar mechanical rigidity to other pancakes. No excess PW1 is visible on the outside which meant that it formed an integral part of the composite Pancake structure. Pancake 8 showed the same level of mechanical rigidity as Pancake 2.

Pancake 10 (Figure 3.7) showed the best result of those pancakes for which insulation system B was used. Half the Pancake did not have the PW3 treatment and the inner turns of this portion were susceptible to peeling away. The other half was uniform and mechanically rigid due to the PW3 treatment.

In general, the combined treatments of PW2 and PW3 used in conjunction with the composite insulations A and B was found to impart mechanical rigidity to the turns of the pancake coils.

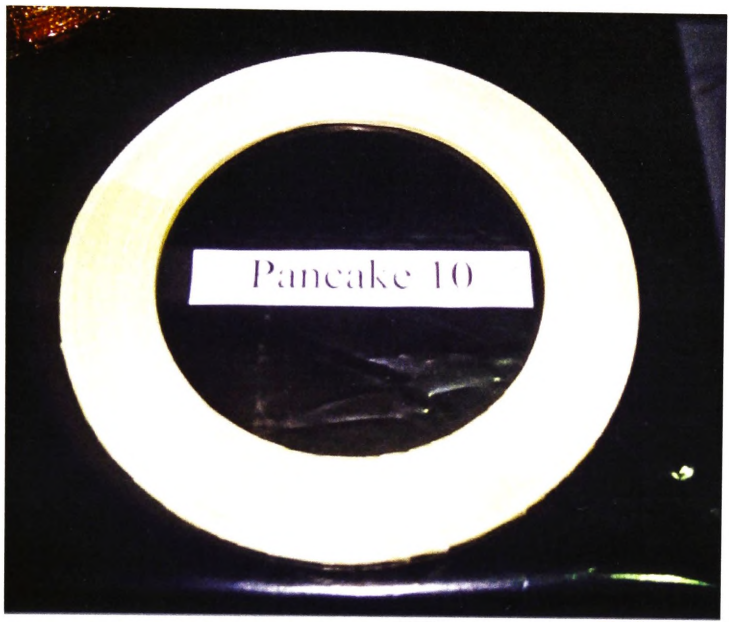

Figure 3.7. Pancake 10 after curing and removal of central disk.

3.3.2 Determination of Pancake coil fill factor

Although in this study no experiments were performed to assess the break down or partial discharge onset, a visual examination was performed over each cured Pancake with a microscope and image analysis system and the coil fill factor calculated from equation 3.4.

Coil FF = (HTS tape thickness)/(HTS thickness + final insulation thickness)] Eq. 3.6

Figure 3.8 and 3.9 show two representative images showing the insulation gap between the turns of HTS tape and the individual gap distances for Pancake 10 and Pancake 1 respectively. The coil fill factors were found to be 62% and 67 % respectively and a scan over the pancake faces showed no visible evidence of short circuits.

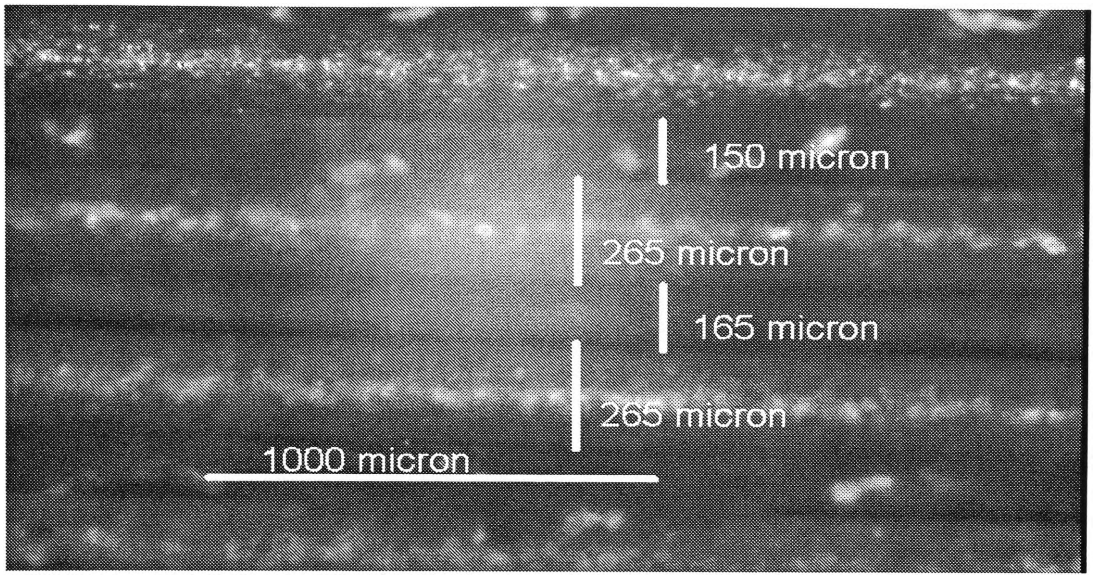

Figure 3.8. Pancake 10. Coil fill factor = 62 %

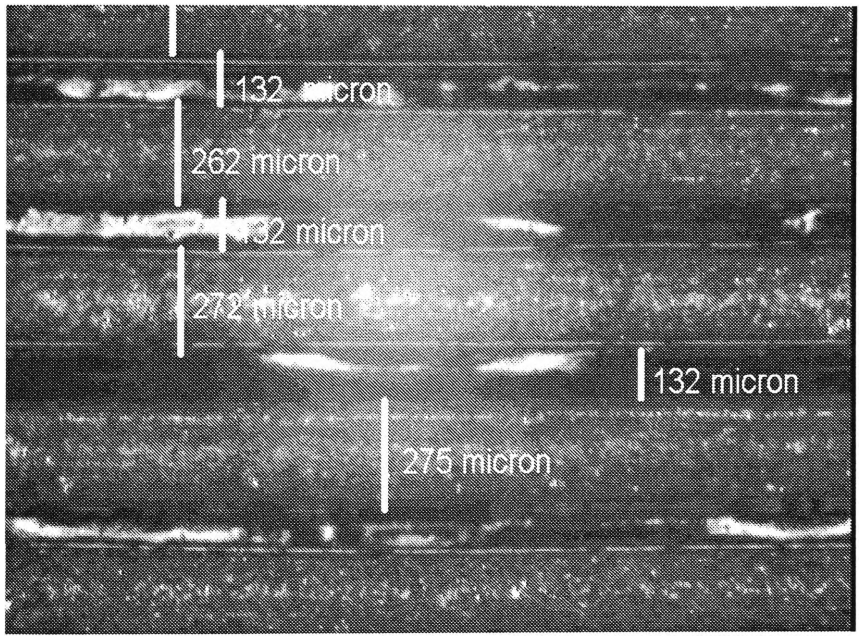

Figure 3.9. Pancake 1. Coil fill factor = 67 %

The estimated uncertainty in the thickness measurements is about ±10 μm due to the difficulty in assessing the boundary between HTS tape and insulation. Despite this, it can be concluded that both of these insulation thickness' are too great as the fill factor of conductor to coil cross section is less than 70%. This would severely limit the extent to which a HTS device can be made smaller. In order to have an acceptable 85 % fill

factor using 270 μm thick HTS tape, a final insulation gap of no more than 50 μm is required.

Pancakes 11 and 12 were inspected in a similar way. An image of tape insulation gaps was obtained as previously, and the coil fill factors calculated. The fill factor of Pancake 11 was 89 % and Pancake 12, 74 %. The thickness of the HTS tape at the points of measurement was 254 μm. Figures 3.11 and 3.12 show the images of the tape insulation boundary taken and the final thickness of insulation used to determine these fill factors.

Figure 3.11. Interface between insulation composite D and HTS tape in Pancake coil 12.

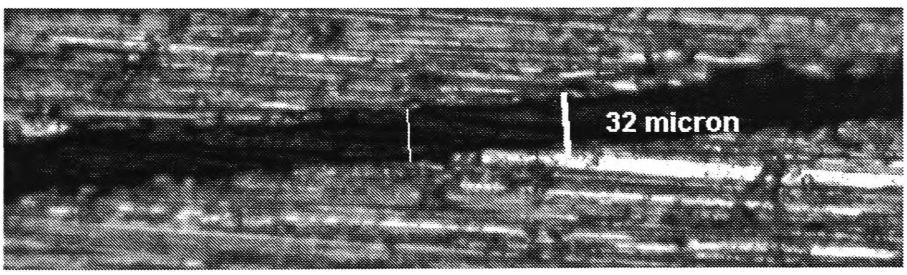

Figure 3.12. Interface between insulation composite C and the HTS tape in Pancake coil 11.

3.3.3 Thermo-mechanical testing of pancakes

The definitive test for a pancake insulation and potting medium is the ability of the pancake to maintain critical current and I-V characteristics after multiple quenches and thermal cycles. In an installation with power equipment containing HTS coils, the opportunities for a complete quench are remote; however, under exceptional

circumstances, for example, fault currents or loss of cooling, a quench may occur. To test the robustness of the HTS Pancake insulation and potting composites to quenches in LN, 4 point I-V measurements were made on the pancakes after various quench events. A double quench event (DQ) was defined as one where the complete coil was rapidly removed from the LN bath, warmed up to room temperature, and then rapidly cooled in LN. The I-V characteristics were taken before and after each double quench. This was the worst case of thermal shock that can be administered and is unlikely in practice. The more likely scenario in a practical installation is where a slow warm up of the coil is followed by a slow cool down of the coil after completion of works. In these experiments, this was typically accomplished over a period of an hour. The coil was then re-cooled by slowly immersing it in the LN bath over a period of 10 minutes. The typical rate of temperature change for the fast and slow cooling scenarios is shown in Figure 3.13, which was obtained using a resistance measurement technique and is only accurate to the Tc of the superconductor which is approximately 110 K.

Figure 3.14 shows the effect on the I-V curve of multiple double quenches performed on Pancake 1. The initial Ic was 13.4 A (77 K, self field).

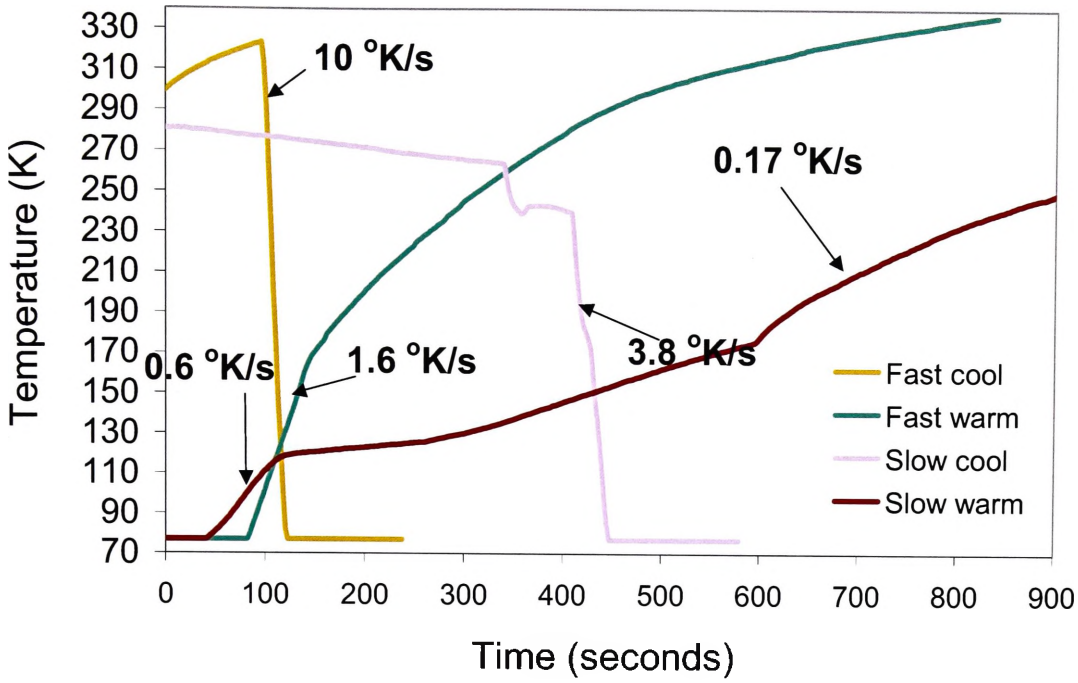

Figure 3.13. The rate of temperature change for double quenches and thermal cycles

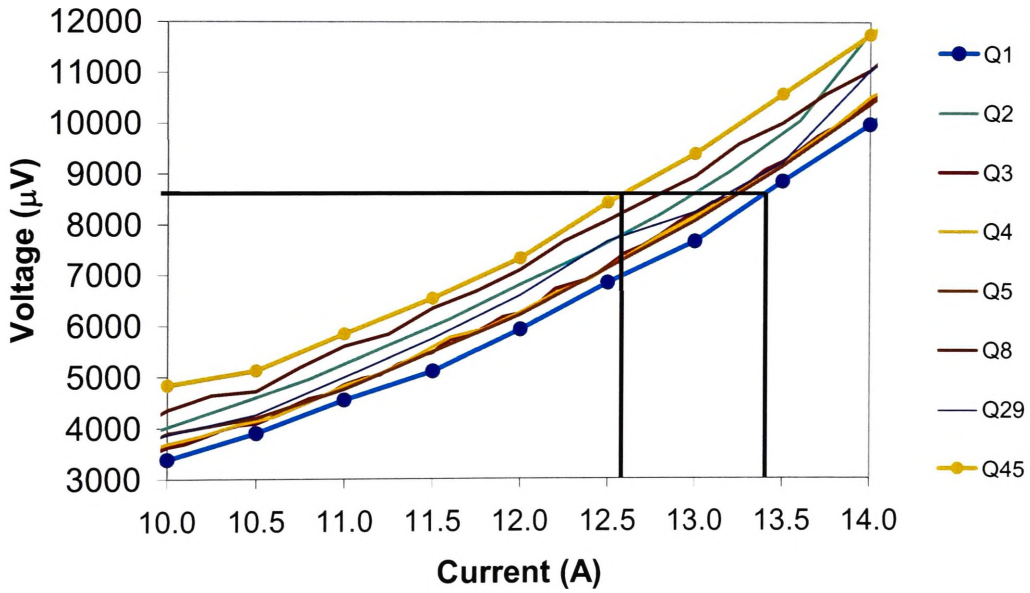

Figure 3.14. Effect on the I-V curve around the Ic of Pancake 1 after double quenches

The total drop in Ic after 45 quench events was found to be 0.8 Amps. Due to the severe nature of the quench, each quench was found to reduce the Ic slightly, by an average of 0.01 Amps or about 0.13 % of the initial Ic.

Figure 3.15 shows the I-V characteristics of Pancake 11 after each double quench and thermal cycle. The initial Ic was 10.7 Amps (77K, self field). The different effects of the double quench compared to the thermal cycle are obvious from the data. A double quench resulted in approximately 0.1 A reduction in Ic per cycle as found previously. The thermal cycles produce no discernable drop in Ic. Figure 3.16 shows a plot of the Ic after each cycling stage.

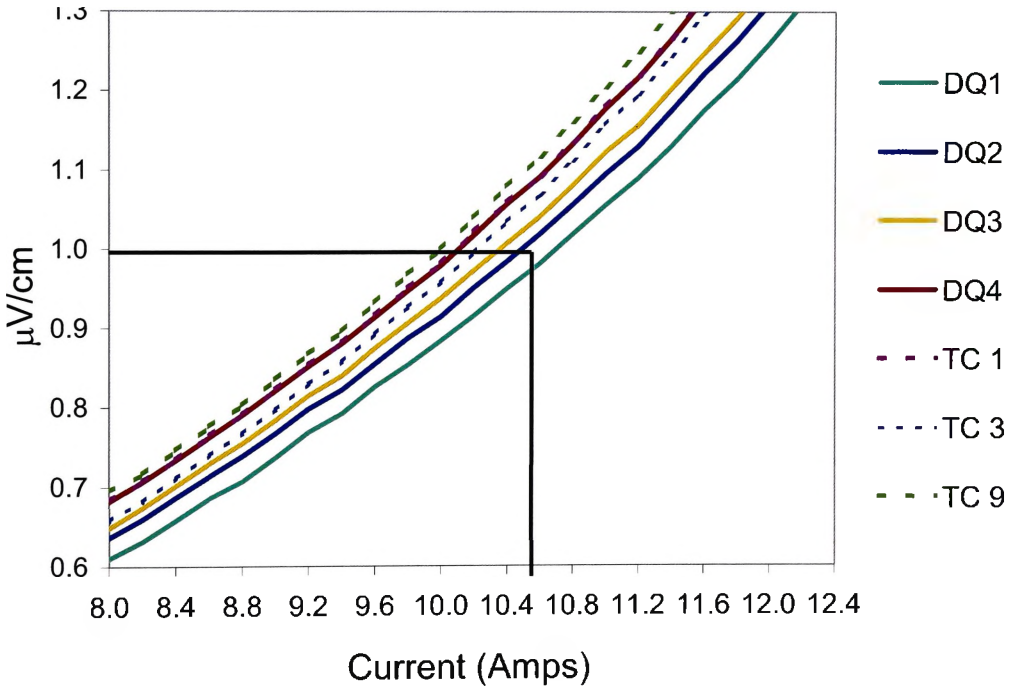

Figure 3.15. Effect on the I-V curve of Pancake 11 of double quenches followed by thermal cycling.

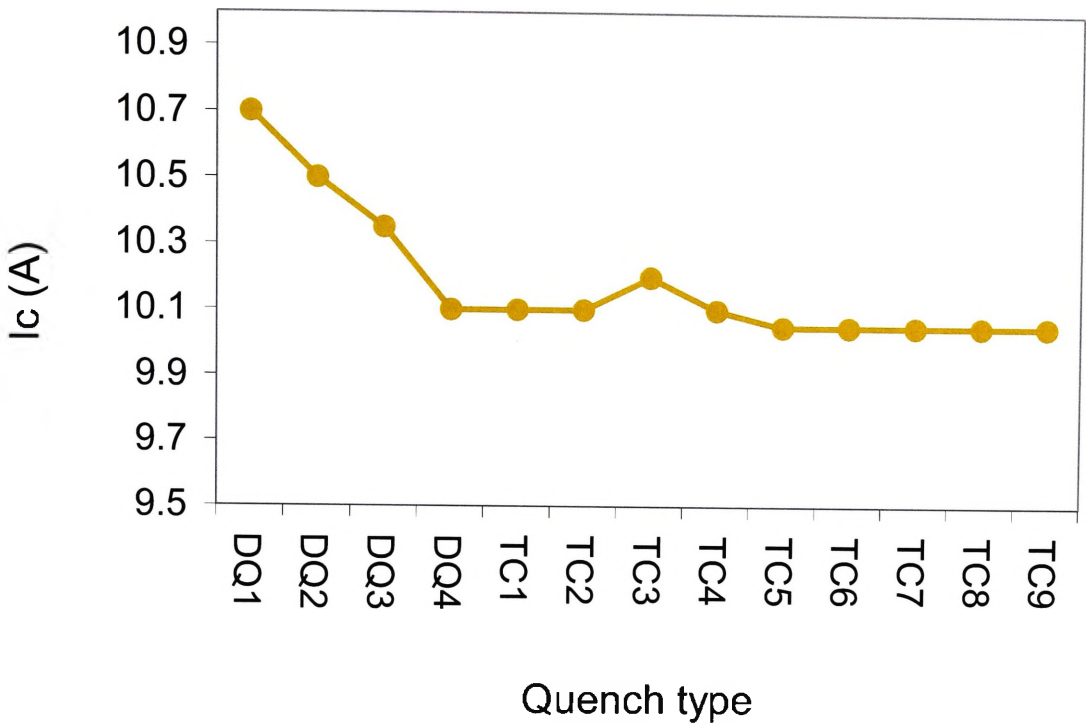

Figure 3.16. Effect on the Ic of Pancake 11 after each cycling stage

Figure 3.17 shows the effect on the Ic for each cycle and each type of cycle for Pancake 12. In this set of measurements, the thermal cycles were performed first and then the double quenches were subsequently carried out. The average Ic drop per double quench was 0.06 A, which is less than that for Pancake 1 and Pancake 11 (0.18 A/quench). The thermal cycling produced no net reduction in Ic, as was also found for Pancakes 1 and 11.

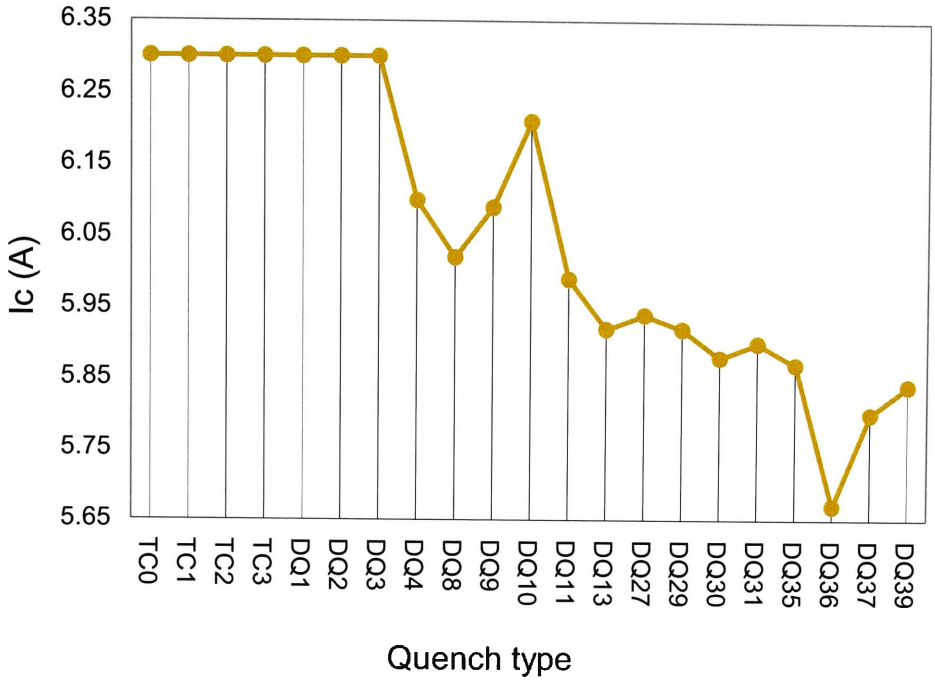

Figure 3.17. Ic of Pancake 12 after each thermal cycle and double quench

3.4 Solenoid coils

3.4.1 General winding technique

Using a purpose built coil winding machine, - a number of solenoid coils were wound with HTS tape using insulation composite A. The Ic was tested under thermal cycling in a similar way to that carried out previously on Pancake coils. Tables 3.4 and 3.5 show the details of these coils. The list of coils manufactured included a variety of shapes and sizes ranging from long thin solenoids, Figure 3.18, to low aspect ratio coils, Figure 3.19.

Coil Number	Length used	Layers	Turns/layer	Turns total	Voltage tap distance
					(m)
1	73	1	118	118	70
2	5	2	7	14	5
3	73	10	13	130	70
4	28.6	5	11	52	28
5	136	45	12	540	136
6	36	12	12	144	36
7	87	27	12	355	87
8	65	2	55	118	36
9	104	4	145	580	26
10	85.4	2	78	156	85

Table 3.4: Physical details of the HTS solenoid coils.

Coil No.	ID	OD	Coil (H)	Tape dimensions
1	175	176	360	0.22 x 2.2
2	175	176	30	0.22 x 2.2
3	175	180	30	0.29 x 3.0
4	175	180	30	0.29 x 3.0
5	79	135	44	0.29 x 3.0
6	79	110	44	0.29 x 3.0
7	79	82.5	44	0.29 x 3.0
8	175	176	180	0.29 x 3.0
9	104	106	360	0.29 x 3.0
10	174	175	296	0.29 x 3.0

Table 3.5: Physical details of the HTS coils manufactured

Figure 3.18. A selection of manufactured solenoid coils.

Figure 3.19. Coil 5: A low aspect ratio coil.

3.4.2 Thermo-mechanical testing of solenoids

In general, no reduction in Ic was observed owing to either thermal cycling or double quenching in LN. Due to the geometrical shape of the solenoid coils, it was possible to cool the whole mass more slowly than a Pancake coil. Figure 3.20 shows the rate of temperature change of Solenoid coil 8 during thermal cycling (TC).

Figure 3.21 shows the I-V curves obtained from successive thermal cycles of Solenoid coil 8 in LN. The Ic dropped by less than 0.1 A over 12 cycles.

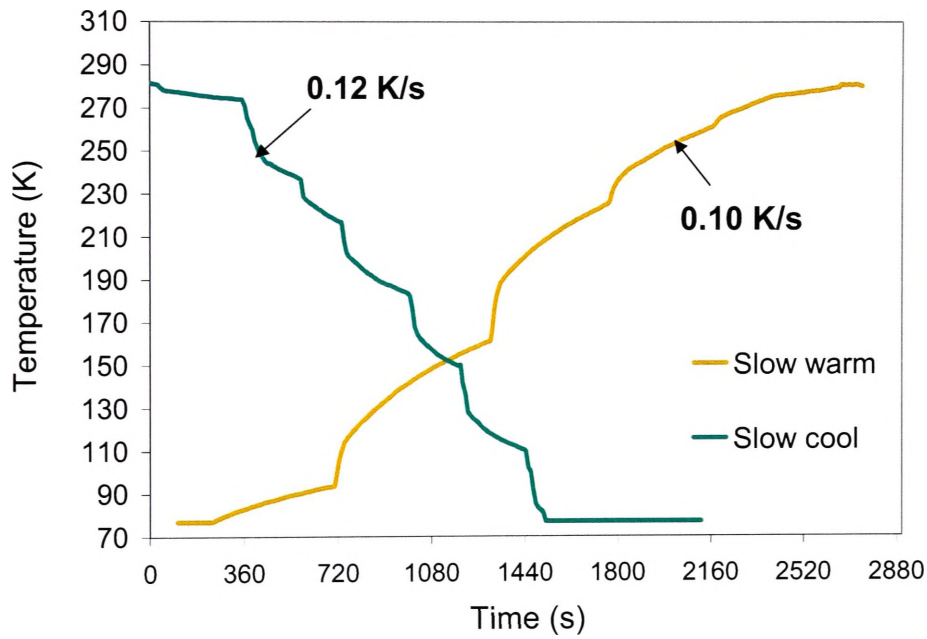

Figure 3.20. Rate of change of temperature for Solenoid coil 8 during thermal cycling

The Ic of Solenoid coil 10 after each thermal cycle and double quench is shown in Figure 3.22. The greatest Ic reduction of 0.2 A is caused by a double quench. The average Ic reduction per double quench, however, was just 0.04 A.

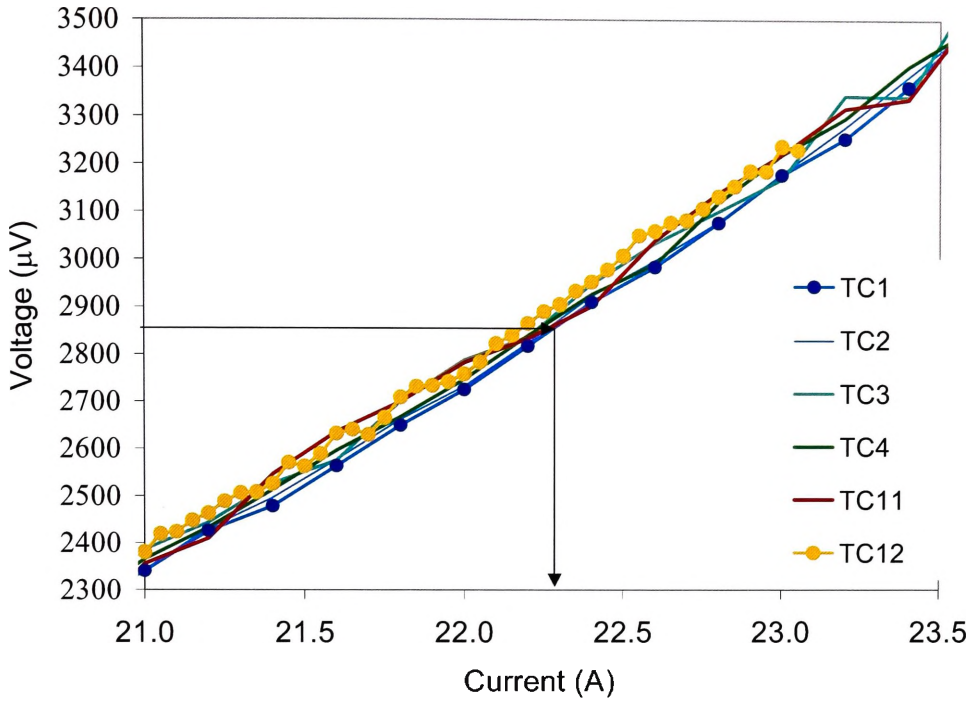

Figure 3.21. Plot of I-V curve of solenoid coil 8 in the vicinity of the Ic

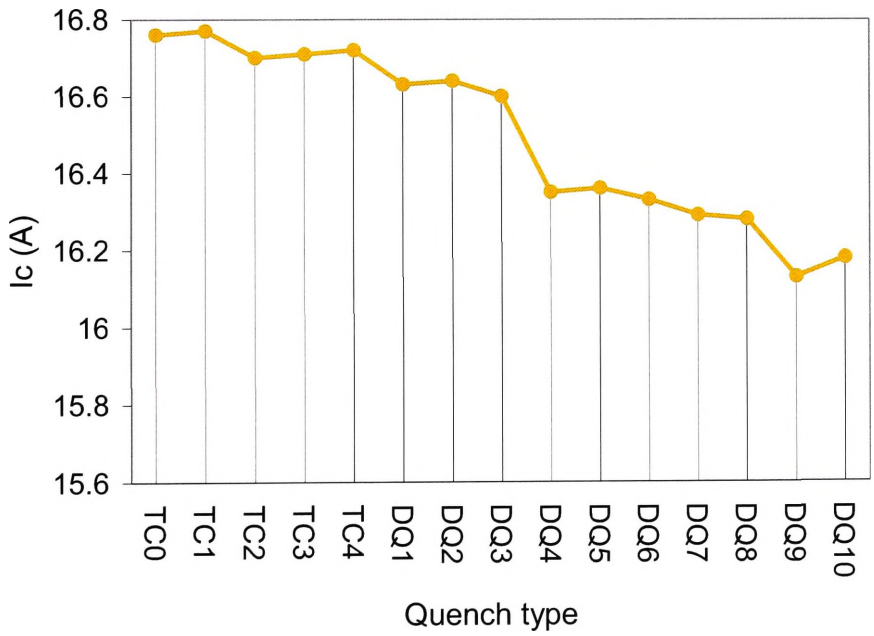

Figure 3.22. Plot of the Ic of solenoid coil 10 after thermal cycles and double quenches.

In the experiments conducted on pancakes and solenoids, the Ic before the winding of the coil was not available due to the complexity of measuring this on a long length. The Ic of the coils and pancakes was consistent, however, with the self magnetic field present, the Ic of the measured short lengths before winding, and the general capabilities of the company.

It is also noted that there are other types of tests which could have been conducted in these experiments relating to other failure mechanisms of HTS coils. For example, large fault currents, heating from poor restive joints, and other defects. As these are potentially destructive, it was chosen not to carry these out. The rating of the available power supplies were also insufficient for this purpose. It should also be noted that the double quenches performed in this work will test certain aspects of these destructive tests.

The n-value was measured during these tests at all stages, however, there was considerable scatter in the values and no direct conclusions could be drawn. For example, the n value both increased and decreased slightly (by about 1 or 2 from a value of 10) before after a double quench test. It is suspected that much higher values of n approaching 20 would be required to see trends and make conclusions using this parameter.

3.5 Conclusions

A method for the production of mechanically rigid and electrically insulated pancakes with high coil fill factor was successfully achieved. Of the techniques tried, the combination of composite insulation A or B with post wind treatments PW1 and PW2 respectively gave the best performance in terms of mechanical rigidity on Pancake coils with large radii (200-300 mm). It was found that the addition of PW1 to PW2 or PW3

was not necessary to achieve these properties. Pancakes exhibiting robustness were also achieved using PW1, however, these were not as aesthetic as those which had PW2 or PW3 treatment. While the coil fill factors achieved in these pancakes was less than 70 %, a higher fill factor of 89 % was achieved using composite insulation C.

The Pancake coils were found to have a very stable Ic with respect to the effects of cycling in LN. It was found that pancakes wound with insulation composite A could withstand up to 49 double quenches with only 0.8 A (6 %) degradation in Ic. A 0.4 A (0.38 %) reduction in Ic after 39 double quenches was found for pancakes wound with insulation composite D. Thermal cycling was found not to reduce the Ic value of pancakes insulated with any of the composite insulations used in this work.

Solenoid coils were found to exhibit a similar level of mechanical rigidity and maintenance of Ic after cycling in LN. The Ic of the solenoid coils was found not to decrease after 12 thermal cycles. An average decrease in Ic of 0.04 A (0.24 %) per double quench was found for Solenoid coil 10.

Overall, a successful manufacturing method of insulation and curing was developed to make practical pancake and solenoid coils. Extensive testing showed that these techniques provided coils with a good combination of mechanical strength, fill ratio, and insulation and that a stable Ic could be achieved even after arduous temperature cycling.

References

[3.1] S.W.Schwenterly, J.W.Lue, M.S.Lubell, M.S.Walker, D.W.Hazelton, P.Haldar, J.A.Rice, J.G.Hoehn Jr, L.R.Motowidlo, "Performance of Pancake coils of parallel co-wound Ag/BSCCO Tape Conductors in Static and Ramped Magnetic Fields", IEEE Transactions on Applied Superconductivity, Vol. 5, No 2, pp 507/11,1995

[3.2] J.B. Schutz, R.P. Reed, "Inorganic and Hybrid insulation materials for ITER", Advances in Cryogenic Engineering Materials Vol 40 B, pg 985, 1994

[3.3] P.Bruzzone, K.Nylund, W.J.Muster, "Electrical insulation system for superconducting magnets according to the wind and react technique", Advances in Cryogenic Engineering Materials, Vol. 36, pg 999-1006, 1990

[3.4] J. B. Schutz, "Dielectric strength of candidate ITER insulation materials", Advances in Cryogenic Engineering Materials, Vol. 40B, pg 1059/1066, 1994

[3.5] J. Tenbrink, H.Krauth, "Recent results on test windings and coils of Bi-2212/Ag HTSC wires", Advances in Cryogenic Engineering Materials Vol. 40 A, pg 305, 1994

[3.6] P.Haldar, "Fabrication and characteristics of a test magnet from HTS Bi-2223 silver clad tapes", Advances in Cryogenic Engineering Materials, Vol. 40 A, pg 313, 1994

[3.7] H.Moriyama, Y.Inoue, H.Mitsui, Y.Sanada, "Several properties of impregnating epoxy resins used for superconducting coils". Advances in Cryogenic Engineering Materials, Vol. 38, pp 339/46, 1992

[3.8] S.Hayashi, T.Egi, T.Hase, K.Shibutani, R.Ogawa, Y.Kawate, "Oxide superconducting magnets operating near 20 K", Advances in Cryogenic Engineering Materials, Vol. 40A, pg 319/25, 1994

[3.9] Vacuumschmelze round wire type S1, SL-012 Information Brochure.

[3.10] B. M. Weedy, S. G. Swingler, "Review of tape materials for cable insulation at liquid nitrogen temperatures", Cryogenics Vol. 27, pp 667/672, 1987

[3.11] N. Savvides, "Strain dependence of the critical current density of Bi-2223 multifilament tape conductors", M^2S -HTSC IV, Grenoble, 5-9 July,1994

[3.12] J. Yau and N Savvides, "Strain tolerance of multifilament Bi2223/ Ag composite superconducting tapes", IEEE Transactions on Applied Superconductivity, Vol. 5, No 2, June 1995.

[3.13] J.B.Schutz, R.P.Reed, "Inorganic and hybrid insulation materials for ITER", Advances in Cryogenic Engineering Materials, Vol. 40B, pp 985/92

[3.14] E.B.Forsyth, "The ageing of electrical insulators at cryogenic temperatures", IEEE Transactions on Electrical Insulation, Vol. 28, No 5, Oct 1993

[3.15] V.R.Karasik, O.A.Kleshnina, A.A.Konjukhov, V.A..Malginov, V.V.Matokhin, M.V.Sidorov, V.S.Vysotsky, "Design of high current density superconducting magnet with 2.58 m bore", Advances in Cryogenic Engineering, Vol. 37, part A pg 409/416.

[3.16] "Properties of plastic tapes for cryogenic power cable insulation". Internal report by A.C. Muller, pp 339/63. Brookhaven National Laboratory, Upton New York, USA

[3.17] S W Schwenterly, "Simple estimate of stored energy and conductor insulation withstand requirements for advanced solenoid magnet designs." Advances in Cryogenic Engineering Materials, Vol. 39, pg 805

[3.18] N.Tomita, "Development of superconducting coil using Bi-2212/Ag tapes", Advances in Cryogenic Engineering Materials, Vol. 40A, pg 297

[3.19] Y.Takahashi, "Deterioration of insulating plastics by partial discharge in liquid nitrogen", Record of 5th Int'l Cryo. Eng. Conf, IPC Sci. & Tech. Press Ltd, UK, pp 224-228, 1974

[3.20] M.Wilson, "Superconducting magnets", Clarendon Press, Oxford, pp. 313-314, 1983

Chapter 4

Measurement of AC losses in tapes and coils

4.1 Introduction

The AC losses of short lengths of standard, straight filament HTS tapes at power frequencies and in the sss regime have been studied extensively [4.1 – 4.7]. The conclusion of previous work was that the hysteretic losses of single tapes are very well predicted by approximations previously developed for thin strip LTS tapes.

Despite this considerable progress, the approximations made by the formulas describing the AC losses do not adequately predict the losses occurring when different alloys of silver are used for the matrix materials, and when the filaments are twisted. It is possible to calculate the losses for the fully coupled and uncoupled states, and these form a lower and an upper estimate of the AC losses respectively. The difference between these two limits is great and approximately n, the number of filaments in the HTS tape. As previously explained, an approximation can include the coupling current loss, however, there can be a factor of 2 or 3 difference in the losses owing to the variability of the effective matrix resistivity. Clearly, to investigate the effectiveness of twisted filaments, and/or matrix materials, on the lowering of AC losses in short length tapes made in this work, a suitable measurement system has to be used.

In this work, a short length, automated AC loss measurement system was constructed and several types of HTS tapes manufactured in this work (Chapter 2) were characterised in

parallel AC fields. The system was based on the lock-in amplifier (LIA) technique as described by Yang and in Section 4.2.The AC losses in novel tapes are not predicted well and the loss depends to a high degree on the filament twist pitch, the cross sectional uniformity, and the alloy sheath materials. Discrepancies of up to 50% between samples with slightly different physical characteristics were found to exist. This uncertainty in the AC losses of individual tapes also manifests itself when trying to predict the AC losses for an AC coil design. Hence, in addition to the short length AC loss rig, a cryogenic mass boil off calorimeter was constructed. To characterise the AC losses, the rate of nitrogen boil off from HTS coils sealed in a cryostat with pool boiling liquid nitrogen was measured. A number of coils were characterised under various conditions.

4.2 Short sample measurements – the lock in amplifier technique

4.2.1 Experimental set up

The short length AC loss rig consisted of a Helmholz coil to supply the AC field, a sample holder with an integrated phase coil to measure the AC magnetic field, an HTS tape sample with saddle pick up coil, and a LIA. A number of phase coils were wound from 50 μm copper wire with a varnish insulation. Although a number of phase coils were wound for the different versions of improved sample holders, for simplicity, only the details of one will be described. For example, one phase coil was wound with 100 turns, and had a cross sectional area of 21 x 1.8 mm^2. The turns area product (N*A) of this particular phase coil was 1.25 x 10^{-3} turns.m^2. A large number of turns were used to improve the accuracy of measuring the magnetic field. All phase coils were approximately of this size and number of turns. Both round and square phase coils were used with equal success.

The field coil was a Helmholz coil wound from 2.0 mm diameter enameled copper wire. This coil was rated at 15 A and could provide a peak field of up to 50 mT. The central magnetic field of the Helmholz coil can be calculated from:

$$B_{pk} = \frac{\sqrt{2}}{2\pi} \frac{V}{f.N.A} \quad [T] \quad \text{Eq. 4.1}$$

Where V is the rms value of the voltage induced in the phase coil. The field constant was independently found to be approximately 3.8 mT/A, but this was not used in the experimental measurements as Equation 4.1 gave a more accurate magnetic field magnitude.

A specially designed sample holder constructed from phenolic fabric was used to hold the samples of HTS tape and the phase coil, as shown in Figure 4.1. A single turn saddle coil made from 50 μm enameled copper wire was placed on the HTS tape sample. Appropriate voltage taps and a ground lead were made with the saddle coil to ensure that the length of copper wire between each voltage tap and the earth was of equal length, Figure 4.2. The voltage leads were twisted tightly to avoid a net additional induced terminal voltage, as shown in Figure 4.2.

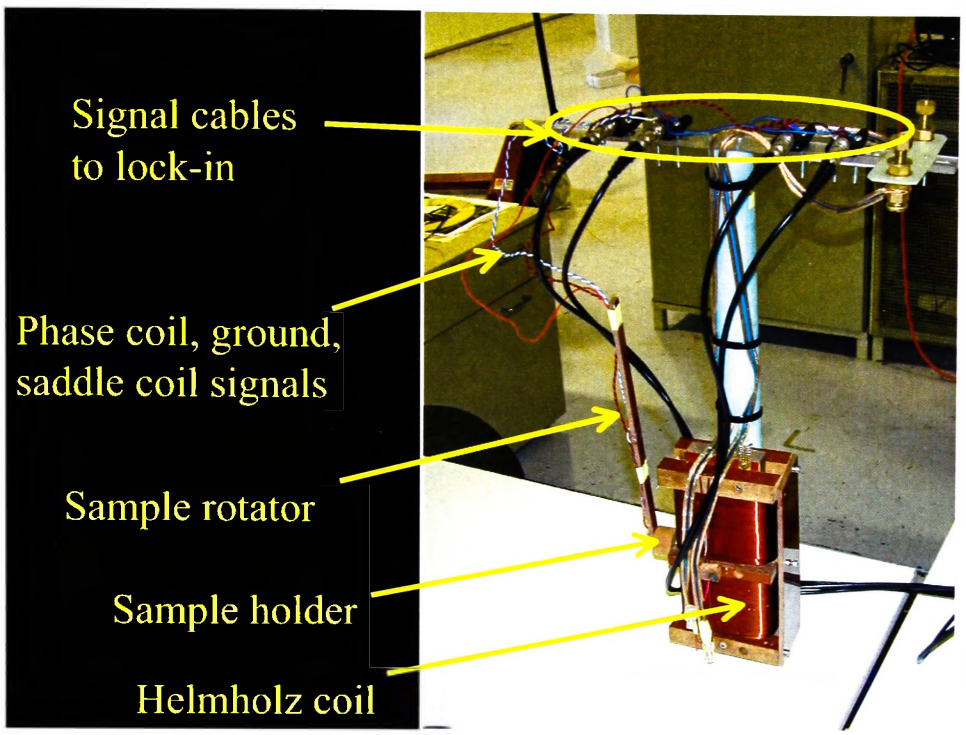

Figure 4.1. The sample coil holder and magnet assembly

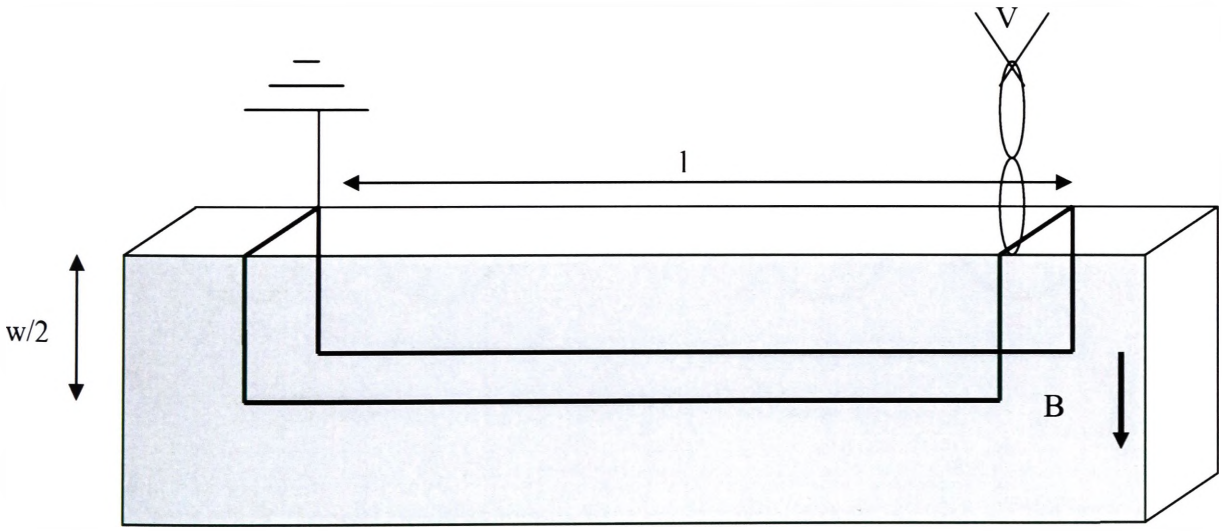

Figure 4.2. Diagram of the saddle coil on an HTS tape. The tape width w, and the sample length l. The magnetic field is parallel to the page, and the voltage, V, gives the magnitude and phase of the AC field.

This arrangement was used so that the stray voltage induced in each of the lines was equal to, and of opposite polarity and therefore, cancelled in the measurement. The voltage leads of the phase coil were also tightly twisted. The two phase coil leads, the two saddle coil leads, and the earth lead were all brought out of the magnetic field and connected to co-axial leads which went to the LIA inputs.

The LIA was a dual input type, with phase detection and a 24-dB/octave input filter. A time constant of 3 s was used to measure the phase coil voltage and saddle coil voltages. The earth lead was used as the shield on the co-axial cables, and the voltage signal of each pair was connected to the central conductor of the co-axial cable. Both inputs of the LIA were used, and the differential mode was employed to obtain the phase and magnitude of each signal. A separate switch was used to toggle between each signal. In this way, the noise measured from the saddle coil was minimised. A pictorial diagram of the connection arrangement is shown in Figure 4.3.

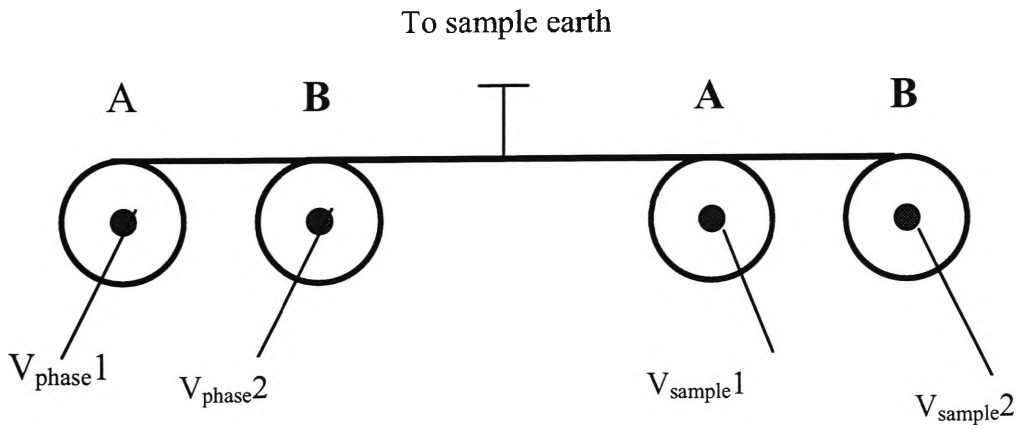

Figure 4.3. Technique for connecting each voltage wire of the signal pair and phase coil pair with the ground wire. The differential mode (A-B) was used to measure each signal voltage with the sample ground used as a shield on each input.

Other, simpler combinations of connections were tried, but frustratingly were found to give noisy results despite being reported to be successfully used by other groups. By using the

differential mode option on the LIA, the noise induced in each voltage tap from stray fields and other sources was effectively cancelled before the filter stage. The relatively long time constant of 3 s was found to be necessary, even though it slowed the measurements acquisition considerably.

The results measured on the LIA could be displayed as either X-Y components or as an R-ϕ vector. The resolution of the phase was 0.01^0 and the voltage resolution was 0.01 μV rms, which was obtained under the conditions of the experimental arrangement. An audio amplifier was used to power the Helmholz coil at frequencies between 43 and 169 Hz. The input signal for the audio amplifier was supplied by the LIA itself, and the internal phase locking mode was used. Hence, the phase of the measured signals was relative to the phase of the Helmholz coil field. An external power supply with a square wave output for lock-in purposes (a 5 V signal can be accepted by the LIA) was also tried, and the external locking mode used. However, this was found to be inappropriate, as it had too high an harmonic content for this application, which required very pure AC magnetic fields to obtain meaningful results. The experimental set up is shown in Figure 4.4.

The measurement system was automated using a GPIB card and IEEE protocols and was controlled by Labview™ 5.1.

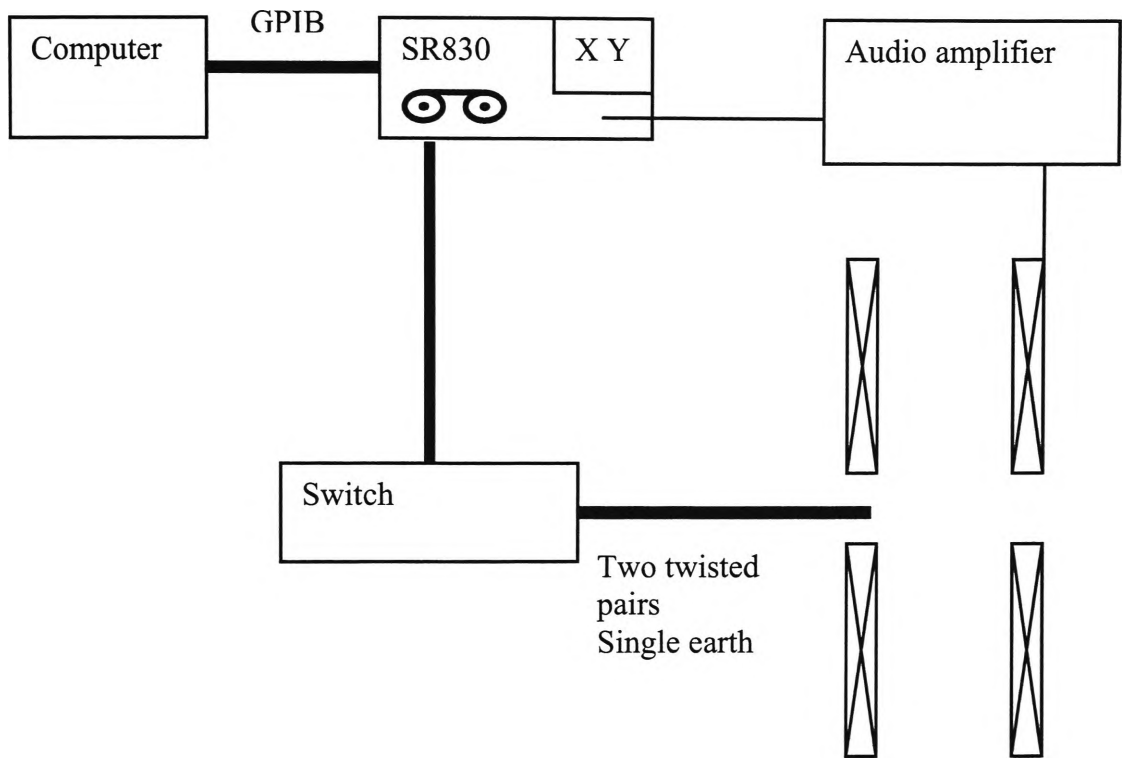

Figure 4.4. Experimental arrangement of the LIA technique for measuring short length AC losses.

The equations that convert the measured sample voltage into an AC loss are well known, and are given by Yang [1.38].

$Q_{total} = (\sqrt{2}).(B/f.\mu_o).w.V'$ [J/cycle/m] Eq. 4.2

$Q_{hystr} = \alpha(\sqrt{2}) .(B/f.\mu_o).w\ V_{3rd}$ [J/cycle/m] Eq. 4.3

Where B is the applied field, μ_o is the permeability of free space, w is the sample width, α is a constant, V' is the per unit length rms voltage component in phase with the applied

magnetic field and orthogonal to the phase coil voltage vector, and V_{3rd} is the third harmonic of the total induced voltage in the saddle coil.

The technique used to obtain the in-phase component of the signal voltage was to adjust the phase of the oscillator voltage output, Vosc, to be equal to that of the phase coil by using the auto-phase function on the LIA. Using this feature, all subsequent measurements of the sample signal on the Y channel were then the appropriate in-phase value, V', to be used in Equation 4.2. The auto-phase feature, however, was found to be accurate to only 0.01^0, and better than 0.0001^0 accuracy was required for this technique to work satisfactorily. In order to achieve this accuracy, it was found that the only way was to record the X and Y values of the phase coil voltage and sample saddle coil voltage and then perform a vector manipulation to obtain the in-phase component of the latter. The inductive component of the saddle voltage will be about 100 times greater than the loss component. Hence, to ensure the best accuracy, the nominal phase was arranged to be approximately at 45^0, as displayed on the LIA, so that both the X and Y values could be read with the same resolution and uncertainty. Figure 4.5 shows a vector representation of the voltages measured and how these relate to the phase of the magnetic field.

The Equation used to obtain the loss voltage, V' is:

$$V' = V_{saddle} .\sin[\tan^{-1}(\frac{V_{sy}}{V_{sx}}) - \tan^{-1}(\frac{V_{py}}{V_{px}})] \quad \text{Eq. 4.4}$$

Where V_{sx}, V_{sy}, V_{px}, and V_{py} are the x and y components of the saddle coil voltage, and the phase coil voltage, respectively, as measured by the LIA.

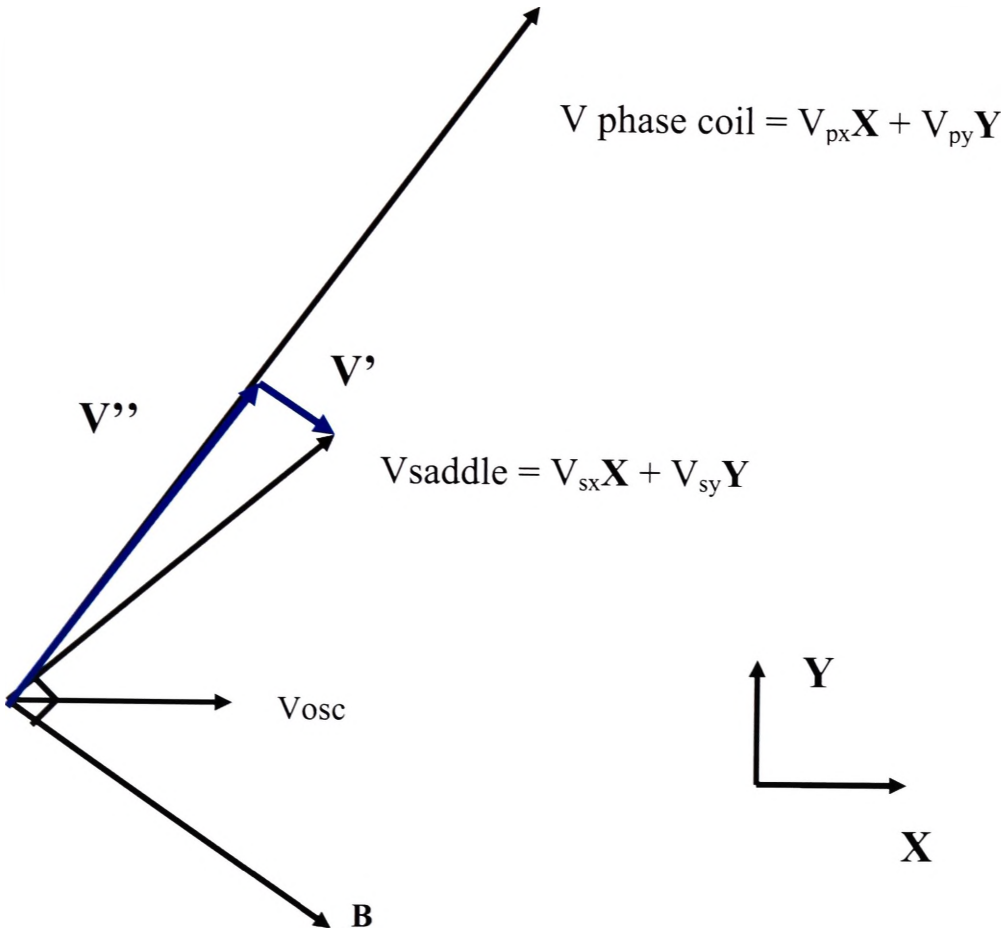

Figure 4.5. Vector diagram showing how the phases relate to each other. V' is the voltage of interest required to obtain the hysteresis loss and is in phase with the applied field B.

To confirm that the experimental measurements were within reasonable limits, and to check for gross errors and inconsistencies, the expected hysteresis loss for straight filament, pure silver matrix tapes was always plotted along with the measured values. In addition, the AC loss of the fully decoupled state was also calculated and plotted. The two loss curves then provided the two limits within which all the results were expected to fall. This technique was also helpful for identifying differences arising from any novelty in the prepared

samples. To do this, the full cross sectional details of a tape must be known as shown in Chapter 2. In order to accomplish this, sections of each tape sample were mounted in epoxy and polished. A cross sectional image was taken using an image analysis system and software. Using macros written as part of this work, the thickness, d_f, and width, w_f, of all the filaments in the sample were measured and averaged, and the core dimensional extents (d_{fc}, w_{fc}) were measured manually. These dimensions, and equations 2.1 to 2.3 then enable the maximum total loss to be plotted. Using Equation 2.9, the minimum hysteresis loss could be obtained, which pertains to the case where the filaments are fully decoupled.

A large number of samples were manufactured and characterised in the short length AC loss rig over the course of the three year period, and the experience gained through these measurements led to the improvement in the methodology, metrology, and in the way the samples were prepared and mounted. These intermediate stages of development, although interesting from an experimental point of view, will not be discussed here. Rather, the latest and most refined techniques and results will be presented. In addition, the data presented will be simplified to just three types of samples, which cover the range of interesting results, rather than presenting every result. The results on these three sample types cover the cases of control samples with straight filaments, twisted filaments and a pure silver matrix, and twisted filaments with an alloy matrix respectively. The sheath materials were found to have no effect on the measurements.

4.2.2 Case 1. Control samples

The control samples had straight filaments and were all processed together to eliminate possible sources of batch to batch variability. Two typical control sample AC loss measurements at a frequency of 43 Hz are shown in Figure 4.6. The Ic values did vary, which meant that the theoretical (fully coupled) loss line also changed slightly.

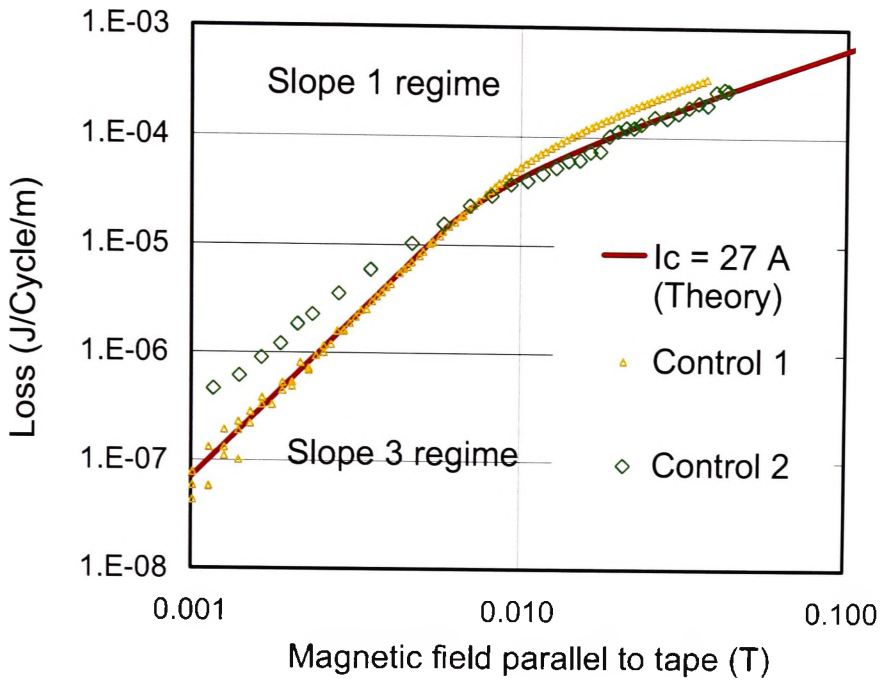

Figure 4.6. A representative set of data of the AC loss of two different control samples. Control 1 = 9904I (Ic = 30 A) and Control 2 = 2000-07 (Ic = 23 A).

As a guide to the eye, the theoretical loss calculated on the basis of a sample with an Ic of 27 A, and the same core thickness was included.

In general, the results and trends were consistent with the theory discussed in Chapter 1. The slope 3 regime (below full penetration) and slope 1 regime (above full penetration) predicted by equations 1.4 and 1.5 are clearly shown, and the penetration field was about 8mT (peak), which was also as predicted. This data showed that the theory of the LIA technique and the sample set up was correct. Absolute values of loss varied by as much as 30% particularly at the lower field values (< 10 mT). Considering that a loss of less than 0.5 mW/m, or 0.01 mW absolute, were being measured, then the accuracy achieved was within reasonable limits. At fields above 20 mT, where losses of about 5 mW/m or 0.1 mW absolute were being measured, the agreement was generally better.

Errors were detected during the initial stages of data acquisition, in particular, the so called "negative phase error" type, which resulted in severe dips in the loss eventuating in a null result (Figure 4.7). This error was very obvious and was quickly corrected by reversing the phase coil or saddle coil polarities or by re-starting the measurement. This did not always work, and Figure 4.7 shows successive attempts to measure the AC losses of a control sample.

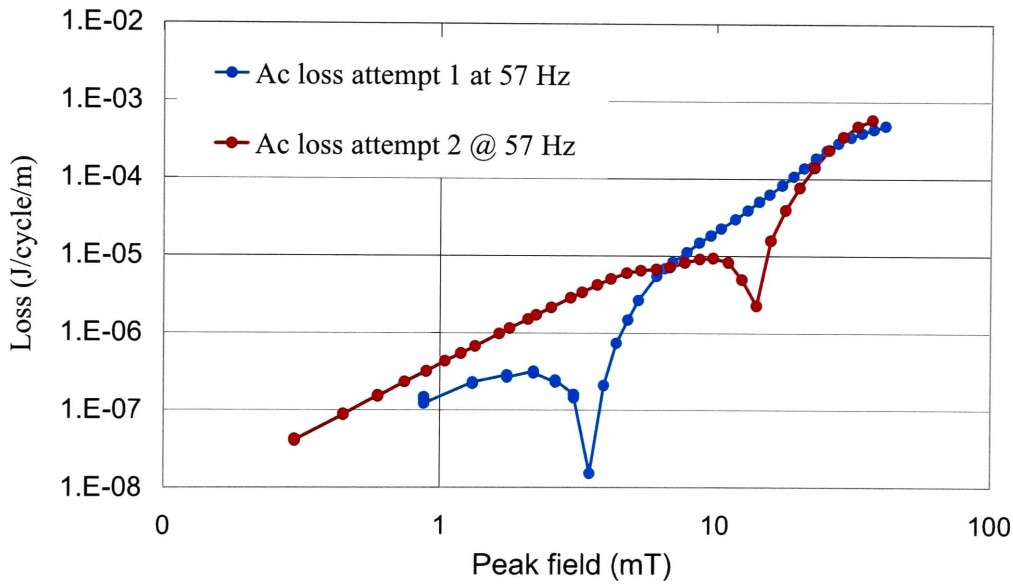

Figure 4.7. The distinctive negative phase error.

The dips correspond to points where the vectors V_{saddle} and V_{phase} coincide in the same phase.

4.2.3 Case 2. Twisted filaments with a pure silver matrix.

Fifty samples of pure silver matrix twisted filament tape were manufactured with twist pitches varying from 4 to 10 mm and filament numbers of 37, 75, and 127. As discussed previously, the de-coupling of filaments can only effectively occur when the filaments are physically well separated from each other in the matrix. Samples prepared with a higher number of filaments (> 37) complicated the manufacturing in that they tend to have many bridges and inter-growths, which can consolidate the core into effectively one large filament. Hence, no extra benefit was found for lowering AC losses by having a larger number of filaments. It was found that 37 filaments was the optimum number for lowering losses of twisted filament samples and maintaining Ic. Figure 4.8 shows the AC loss signature of a twisted filament tape.

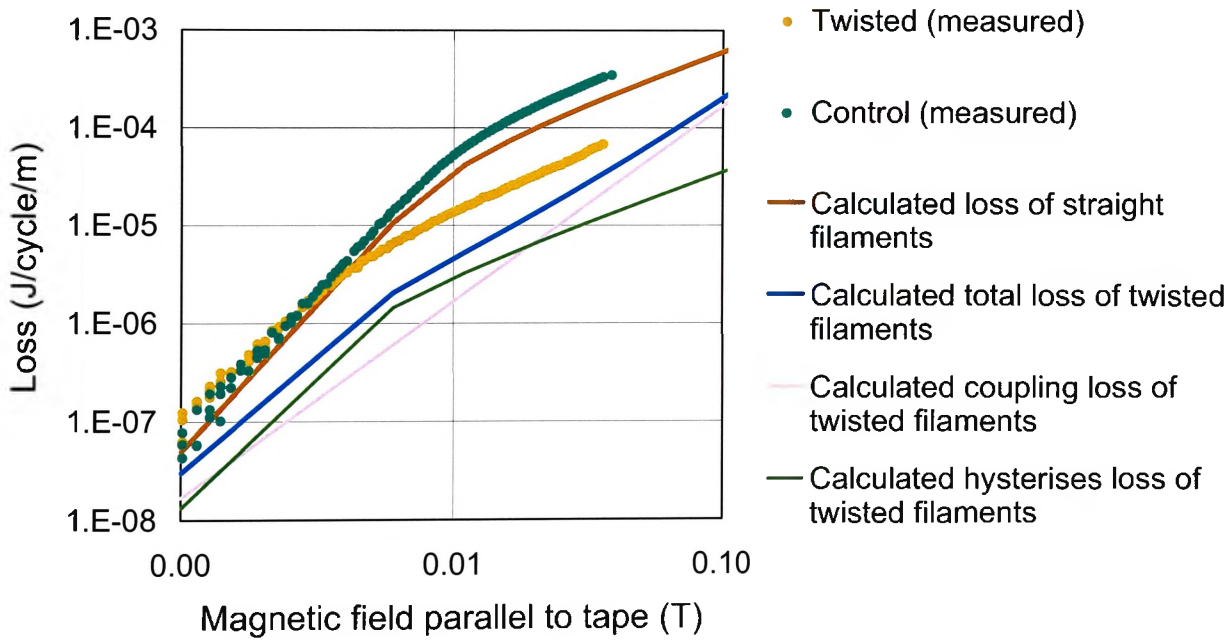

Figure 4.8. AC loss of a 37 filament, pure silver matrix, twisted filament tape sample. Samples 9909C Ag/AgMg 37 MF, Control (Ic = 45 A) and Lp = 10 mm (Ic = 42 A).

It was also found that only those twisted filament samples with a relatively high Ic (> 40 A) showed a lowering of AC losses. For samples with a lower Ic, only a marginal benefit was obtained. Figure 4.9 shows the AC loss signature of a sample with an Ic of 18 A.

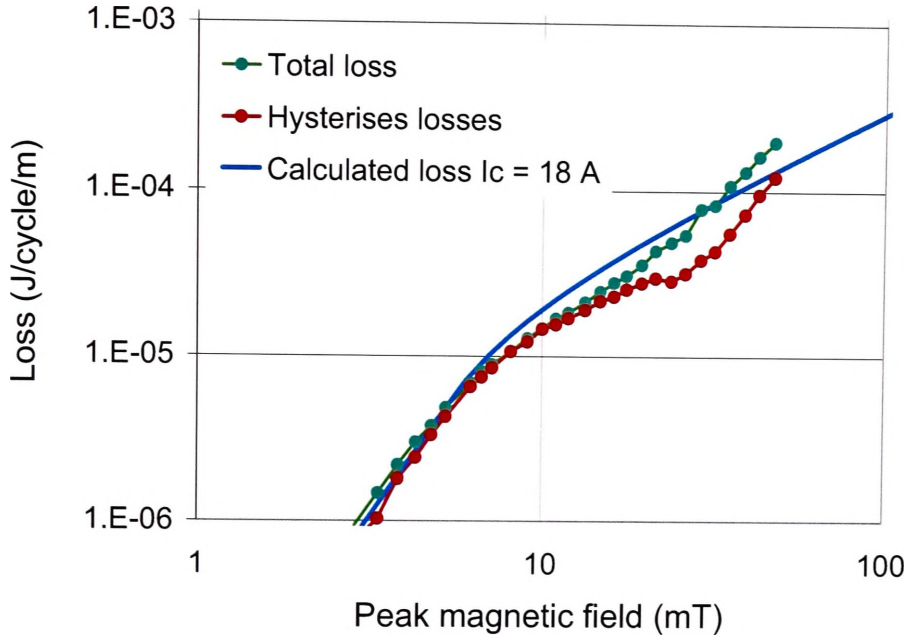

Figure 4.9. AC loss signature of twisted filament, P = 10 mm, Ic = 18 A.
Sample 2000-01-D Ag/Ag 37 MF.

4.2.4 Case 3. Alloy matrix, twisted filaments.

Samples of 37 twisted filament tape incorporating two different silver alloys as the matrix material between the filaments were prepared as described, in Chapter 2. The two different alloys of silver were Alloy A and Alloy B. The most successful samples prepared in terms of Ic, well separated filaments, and AC loss signature had 37 filaments. The results of the AC loss measurements at 45 Hz on a sample with Alloy B is shown in Figure 4.10 along with the theoretical upper and lower limits (fully coupled and uncoupled).

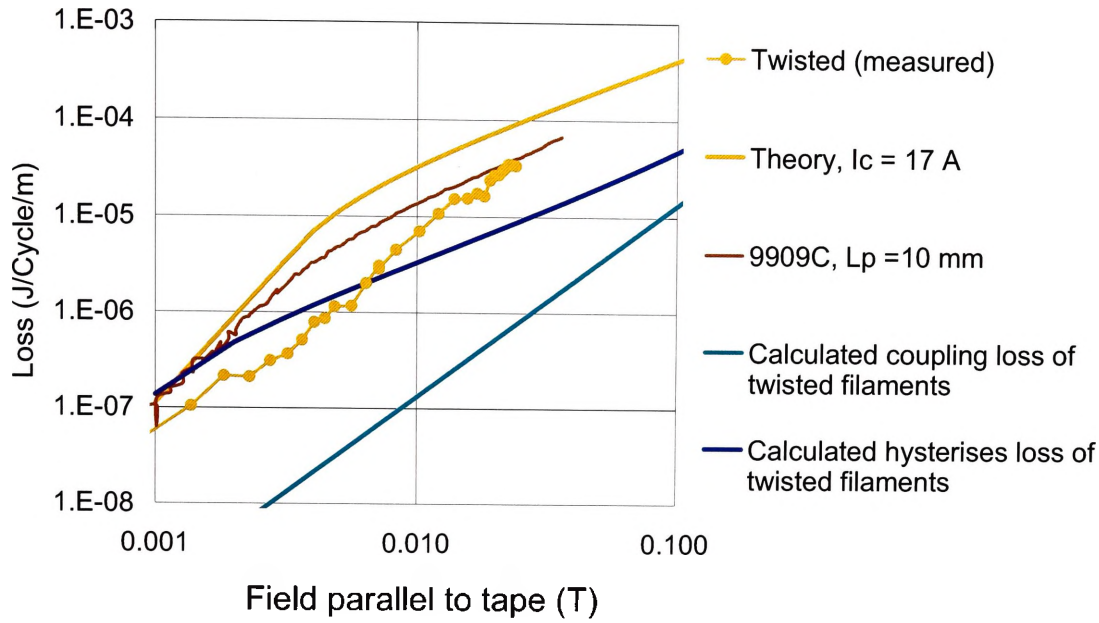

Figure 4.10. AC loss signature of twisted filament sample, 9904I AgB/Ag 37MF, Lp = 4 mm, Ic = 17 A. Equations 2.1,2.2 were used for the calculations. The coupling loss was calculated using equations 2.9, 2.10.

The best result from the twisted pure silver matrix samples is also included as a guide to the eye. As can be seen, by using Alloy B as an alloying element, the AC losses at lower magnetic field amplitudes was reduced further to almost that of the fully de-coupled state. At higher magnetic fields, the losses reverted to almost the same as that of the pure silver matrix twisted filament control samples.

The results at 43 and 87 Hz on the AgA matrix samples (Alloy A) are shown in Figure 4.11 for a twist pitch of 10 mm. This alloy was not successful in reducing the AC losses, despite the experimental evidence in the literature. Further experimentation with this alloy, especially the weight percent addition in silver, may yield better results, but this is outside the scope of this work.

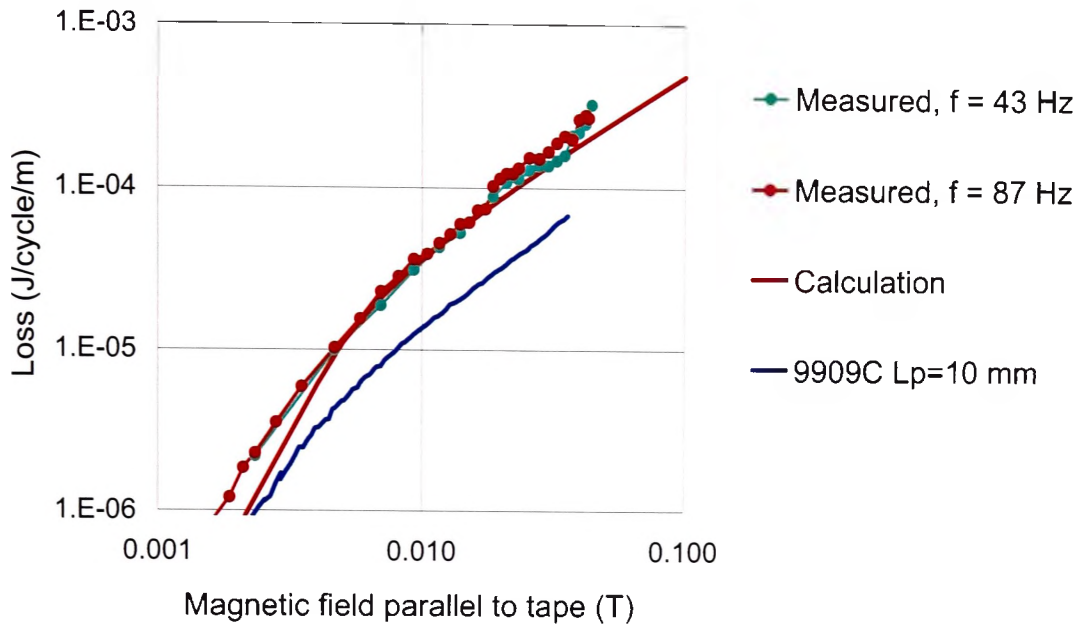

Figure 4.11. Measured and theoretical losses of sample 2000-07 37 MF with twisted filaments (Lp = 10 mm, Ic = 22 A). The measured total losses of 9909C are also included.

4.2.5 Case 4. Degradation in AC loss properties owing to rapid quenching

A source of measurement error in the technique was from the degradation in AC loss properties owing to rapid quenching of the samples. This arises when many different measurements are taken on the same sample over an extended period and the sample was re-quenched frequently. Without taking care, some degradation in the sample could occur and this is immediately obvious as soon as the results are taken. Figure 4.12 shows the AC loss results on a sample before, and after an event which caused some degradation in the AC loss profile. As can be seen, the damaging event has destroyed the characteristic AC loss signature.

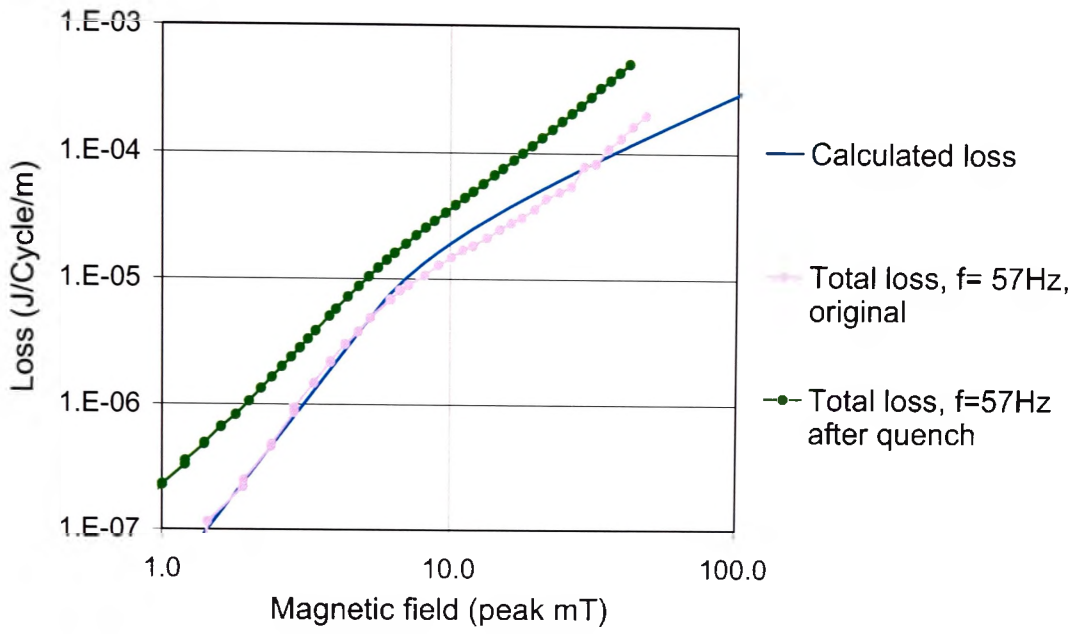

Figure 4.12 AC loss before and after a rapid quench that damaged the sample.

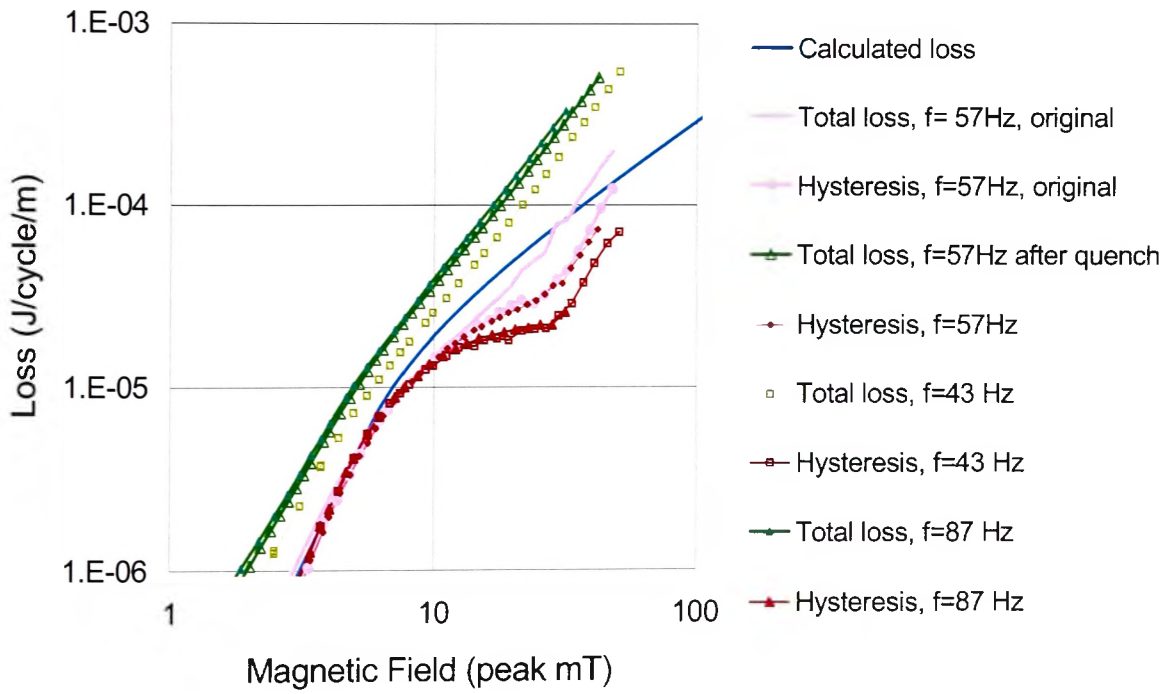

Figure 4.13. AC loss and hysteresis loss measurements at various frequencies

In order determine what is physically happening with the sample, a number of AC loss measurements were taken at different frequencies. Figure 4.13 shows these results. As can be seen, the hysteresis loss component decreased which means that the Ic decreased. There was no provision for measuring the Ic *in-situ* with the sample arrangement to confirm this, however, the total loss in J/cycle/m increased with the frequency of the applied field in an approximately linear manner which can be attributed to induced current effects.

4.2.6 Conclusions on short length AC loss measurements

A short length AC loss measurement apparatus was built, and a number of different types of HTS tape samples were characterised in parallel fields and at power frequencies. The AC losses of straight filament tapes was found to be well predicted and agreement between measurement and theory of better than 20% was obtained in some samples. All the AC loss signatures on undamaged twisted filament samples were found to be between the appropriate limits obtained from the theory for fully coupled and fully de-coupled states. Twisted filament samples of tapes with Alloy B matrix, 37 filaments, and Lp = 10 mm were found to be suitable for substantially lowering the total AC losses in parallel fields. Samples of this tape are suitable candidates for characterising in perpendicular fields, and eventually for making low AC loss coils.

Variations in HTS tape quality and parameters, such as the Ic, n value, overall tape dimensions, core dimensions, and filament dimensions and arrangement effects the AC loss of HTS tapes. This uncertainty will also manifest itself when calculating or designing the AC loss of a large power coil containing perhaps thousands of meters of HTS tape. Damage during coil winding procedures can also effect the AC loss. Hence, the net AC loss of a

significant length of tape will be substantially different from that predicted by the measurements on a few centimeters of tape. The degree of difference may be used as a benchmark as to the quality of the manufacturing route and the consistency of physical and electrical properties along the length of the tape.

Clearly, a technique for measuring the AC losses in coils is required.

4.3 Determining the AC loss characteristics of coils using a cryogenic calorimeter

4.3.1 Introduction

The lock-in amplifier technique proved to be very useful for the measurement of short length AC losses in HTS tapes, however, the method has its drawbacks, and in particular, in the sensitivity of the results to phase shifts. In addition, the total AC loss in the presence of a transport current, and magnetic field that are out of phase, is not directly measurable.

The LIA technique does not allow for the transport AC losses of coils to be measured directly because of the difficulty in interpreting the meaning of the voltage signal obtained. If an HTS coil were to be measured using a voltage measuring technique, then the question as to where and how, to place the voltage taps must first be answered. In conventional electrical engineering, wattmeters are used to measure the losses in devices, and low power factor wattmeters are also available. However, they are not accurate enough for the measurement of the small AC losses in superconducting coils.

A suitable technique that can accurately measure the total AC losses in a superconducting coil immersed in a boiling cryogenic liquid is mass boil off calorimetry. Basically, if a cryogenic vessel containing a HTS coil is sealed, and the boil off gas flow measured very accurately, then the total electrical loss of the coil may be determined by Equation 4.5.

$$\frac{dm}{dt} = \lambda(Q_{tot} - Q_q) \quad ,\lambda = 199.0\ \text{kJ/kg} \qquad \text{Eq. 4.5}$$

Where dm/dt is the mass boil off flow rate in kg/s when the system has reached steady state, λ is the latent heat of vapourisation of the cryogen, and Q_q is the background boil off rate without any excitation of the superconducting coil.

A measurement of 1 SLPM (standard liter per minute) is equivalent to 3.71466 W of heat input into the liquid nitrogen. By measuring dm/dt and the background boil off rate very accurately, Q_{tot} may be obtained for a variety of HTS AC coil transport currents, externally applied magnetic fields, DC transport currents, and combinations of these.

4.3.2 Experimental set-up of the mass boil off calorimeter

The experimental set-up of the mass boil off calorimeter (MBC) device is shown in Figure 4.17. A copper field coil is placed around the cryostat in which the coil under test is placed. With this arrangement, a combination of AC and DC background fields and coil transport currents may be applied to the coil under test. The phase between the AC background field and the transport current is also variable. A pulse width modulated (PWM) power supply with a variable resonating capacitance and an audio amplifier/oscillator set are available to supply the HTS coil and/or copper field coil.

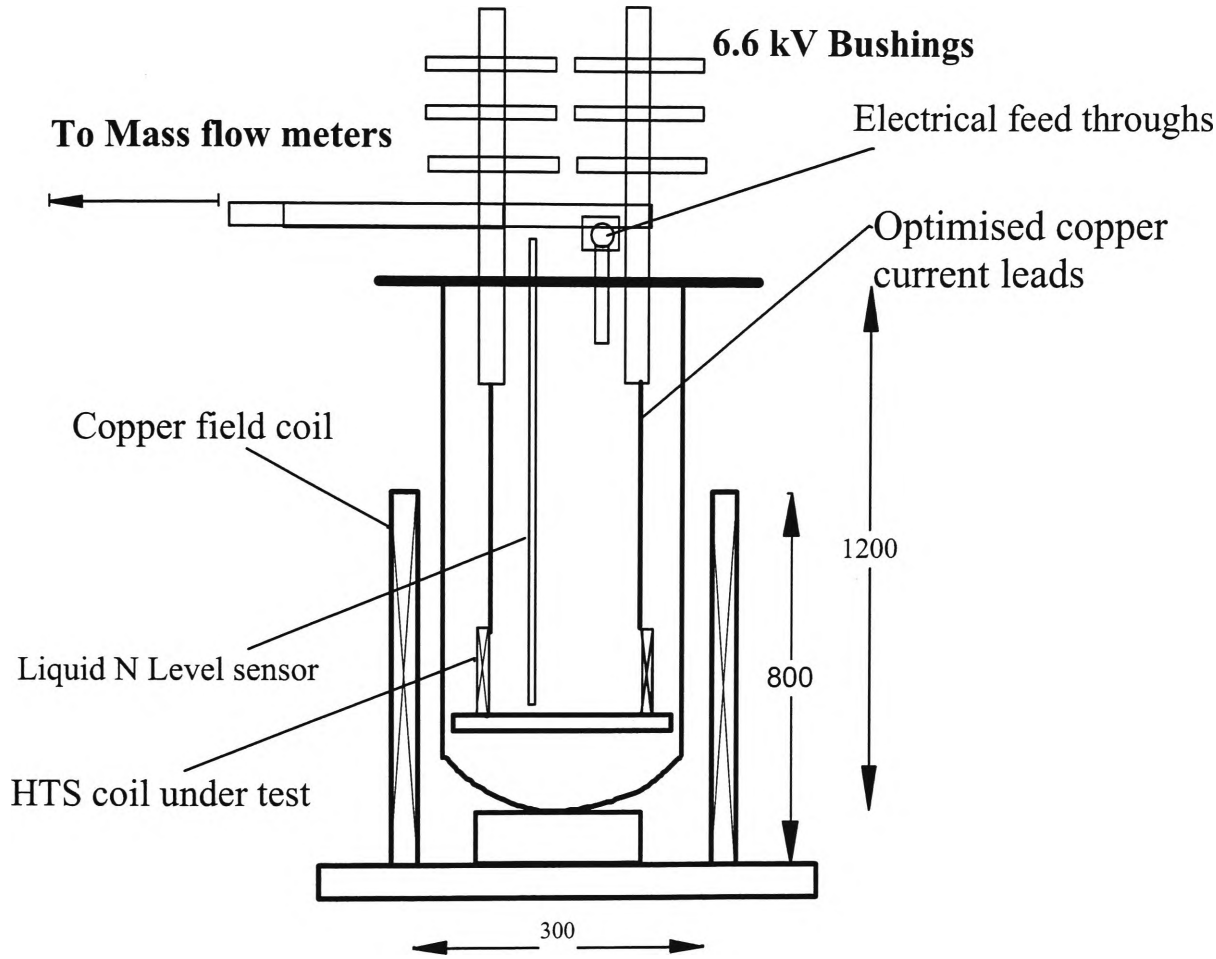

Figure 4.17. Schematic drawing of the MBC

4.3.3 Coil holder, cryostat arrangement, and current leads

A mass boil off calorimeter for measuring the AC losses of HTS coils was designed, constructed, and automated as part of this work. The coil holder, cryostat, field coil, and power supply are shown in Appendix 3.1. Extensive use of non-electrically conductive materials was employed throughout the construction of the MBC. This was to avoid the induction of eddy currents in external devices which could lead to additional mass boil off which would be difficult to correct for when measuring the total boil off rate.

The cryostat was manufactured from glass, as this is the component which is closest to the HTS coils under test and the field coil, and therefore, the most vulnerable to induced eddy

currents. Significant eddy current losses of approximately 100 W in stainless steel cryostats of the same dimensions were calculated from FEM analysis. The most significant proportion of the eddy current loss occurred in the base of the vessel, with only slight losses in the vertical walls.

Sealing the coil holder to the top lip of the glass cryostat was essential for correct data acquisition, however, this proved difficult since only minimal force could be used, and no flange was available as in stainless steel cryostats. To overcome this problem, a gas tight seal was made using two different techniques. The first technique consisted of a tight fitting double O-ring arrangement to secure the coil holder to the inside wall of the cryostat (Figure A3.3, Appendix 3.1). The second technique used a greased silicone gasket between the coil holder and the top rounded lip of the cryostat. An external bolting arrangement with springs was used to apply a constant and reproducible force between the coil holder top, the greased gasket, and the top lip of the glass cryostat.

Conventional copper current leads optimised for use at 20, 50 , and 100 A were designed and manufactured to power the HTS coils in the cryostat. A single copper rod of appropriate diameter was used for each lead. The optimisation used the well established techniques found in to minimise the total heat leak from 300 K to 77 K by suitably designing the cross section such that the sum of the contributions from the I^2R copper resistive loss of electric conduction and the thermal heat leak are minimised [4.8- 4.12]. Equation 4.6 approximates the appropriate heat equation to use. The component due to vapour cooling of the leads was neglected in this calculation.

$$Q = \frac{A}{l}\int_{Tc}^{Th} \lambda(T)dT + \frac{1}{A}\int_{xl}^{xh} I^2\rho(x).dx \quad \text{Eq.4.6}$$

where:
A is the cross sectional area of the conductor, and is assumed constant,
$\rho(x)$ is the resistivity of the conductor along the length, x,
T_h and T_l are the hot and cold end temperatures respectively,
l is the length of the current lead,
$\lambda(T)$ is the thermal conductivity of the copper as a function of temperature,
I is the rms transport current in the lead.

The effect of vapour cooling is not represented in Equation 4.6, because the vapour flow is low (about 3 g/min) and not concentrated around the leads for the whole length up to the 300 K point, hence, this complicating factor was ignored.

To obtain the optimum diameter, the energy balance Equation was solved and the minimum found either numerically or by using simplifying assumptions such as the Wiedmann Franz law. The thermal heat leak integral may be calculated for copper from standard tables [4.10], however, a reasonable approximation may also be obtained if the thermal conductivity of copper is considered independent of temperature in the range 300 K to 77 K. Then, the value of 400 W/m/K may be used [4.3]. The final optimised results for the three current leads are shown in Table 4.1, assuming a perfect heat transfer from the copper lead into the nitrogen liquid. The details of the calculations are given in Appendix 3.2.

	Length (mm)	Optimum diameter (mm)	Optimum cross sectional area (mm^2)	Thermal Leak, per pair (W)
20	1100	2.83	6.286	1.71
50	1100	4.473	15.714	4.27
100	1100	6.326	31.43	8.54

Table 4.1. Data on the three optimised current leads used in the MBC.

The heat leak was estimated to be 0.0427 W/A/lead and hence the heat leak of a pair of 50 A optimised current leads is 4.3 W.

4.3.4 Mass flow meters

It has been reported in the literature that one of the major disadvantages of the mass flow technique for measuring AC losses is that the sensitivity of the meters themselves that leads to large uncertainties in the measurement, and hence, the final AC loss [4.3,4.4,4.13]. However, it will be shown that if a multiple of mass flow meters are used having the appropriate characteristics for this application, then an uncertainty of ± 0.5 W may be obtained, depending on the experimental circumstances.

Two sensitive mass flow meters were obtained with full scale (FS) readings of 20 SLPM (standard liters per minute) and 5 SLPM, equivalent to an FS measurement of approximately 19 and 74 W, respectively. These mass flow meters rely on the pressure drop across a laminar flow element to determine the mass flow. The two mass flow meters were connected in series, with the 5 SLPM meter being used to accurately determine the background losses of the cryostat, and the 20 SLPM meter used to determine total boil off rate when the HTS coils are energized. The mass flow data was collected remotely by measuring the voltage output from the meter, which was calibrated to read 5.000 V for each full scale output. The actual temperature of the measured gas was also available as a voltage output. A remote tare function was included to enable re-zeroing of the meters before each measurement.

These meters met the requirements of resolution, accuracy, external data collection capability, insensitivity to temperature and pressure differences of the gas flow, and

functionality at virtually zero pressure drop. These mass flow meters gave an output of mass flow in SLPM so that the reading was corrected to the equivalent flow of gas at 25 °C and 1 atm, allowing for simple calculation of the mass flow in grams/minute. The resolution of the meter outputs was 1 mV, which is equivalent to a loss of 3.72 mW for the 5 SLPM meter, and 14.9 mW for the 20 SLPM meter. This resolution was sufficient for the characterisation of HTS coils that contained about 30 m of tape.

The accuracy was specified as being better than 0.5% of FS and a linear interpolation from a calibration report was used to improve the accuracy to 0.1% of FS. Other types of mass flow meters were located which could also provide 0.1% FS accuracy, however, these also had additional uncertainties of 0.5 % of the reading, and 0.05 % of the FS reading for each degree that the temperature varied from the temperature of calibration. The expected uncertainty with different types of meters was calculated for the case of a coil with 20W of loss and a background loss of 18W. A 10^0 temperature difference from the calibration temperature was assumed. Table 4.2 compares the uncertainty of the AC loss obtained from the two types of mass flow meters, representing the worst and best cases found.

	FS flow	FS error	Uncertainty	Additional errors	**Total uncertainty in AC loss**
	SLPM (W)	±%	±%	±(%FS per ^{0}C)	**±W (%)**
B	20 (74)	0.1	0.5	0.05	**1.2 (6)**
A	20 (74)	0.5	0	0	**0.5 (2.3)**
A	5 (18.5)	0.5	0	0	**0.1 (0.6)**

Table 4.2 Calculation of the final uncertainty in the AC loss obtained from two different mass flow meters.

As can be seen, although Type B had a low uncertainty in the reading, additional uncertainties lead to an unacceptably high error in the final AC loss obtained. Five different meters were checked in this way, and four did not meet the required accuracy.

The most important factor in obtaining a low uncertainty in the AC loss is to choose the full scale reading of each meter to be as close to the experimental values being measured. In this work, the LN level was adjusted so that the 5 SLPM meter could be used to measure the background loss, and the 20 SLPM meter used to measure the total loss. It is ultimately the FS rating, and the uncertainty in this, which limits accuracy of the mass flow technique. By using multiple meters in series for the different regimes of mass flow, however, the use of this technique can be extended with good certainty.

Finally, a correction was applied to the mass flow meter readings based on the linear interpolation of the calibrated values, which allowed individual readings of mass flow to be made with an uncertainty of approximately ±0.07 W on the 20 SLPM meter.

4.3.5 Power Supply for field coil and HTS coils

It was recognised very early on in the project that a specialised power supply would be required in order to power the field current in the short length AC loss rig, the transport current through the HTS coils in the mass flow AC loss rig, and the field current for the conventional coil surrounding the cryostat. The current would need to be of variable frequency and sufficiently large current to produce the required magnetic fields.

The problem with supplying an AC current, to what is essentially a large inductance, is that the voltage requirement is significant owing to the reactive VARs that must be supplied. The voltage required to supply a coil with inductance, L, with a current, I, at frequency, f, is given by Equation 4.7 :

$$V = 2\pi fLI \quad \text{Eq. 4.7}$$

The field coil, had an inductance of L= 64 mH, and therefore required 0.8 MVAR at 200 Hz to supply 100 A at a frequency of 200 Hz. Clearly, in order to minimise the cost and complexity of the power supply, a resonant technique had to be used employing capacitors to supply the VAR requirement of the coils.

To achieve this, a variable frequency PWM power supply was specified, and used in this work along with a suitable bank of capacitors. Two possible ways of using the capacitors were available: either in series with the load coil, or in parallel. The former reduced the voltage requirement of the power supply, while the later reduced the current requirement.

A bank of eight sets of capacitors, each with 100 μF capacitance, was placed in series with the supply current to the coil. The capacitors were interconnected in a multitude of ways to allow any combination of capacitance from zero to a maximum of 800 μF. This allowed for a resonance with a wide range of coil inductances. Appendix 3.1 shows the physical capacitor layout. Approximately 90% resonance was achieved with the current slightly lagging the voltage, so that the overall load remained inductive.

The power supply was capable of providing 3140 V at a current, I, at frequency f such that Equation 4.8 holds:

$$fI \leq 5000 \quad A/s \quad \text{Eq. 4.8}$$

The specifications were 100 A at 50 Hz into a 100 mH coil, or 25 A at 200 Hz into a 100mH coil. The frequency range was limited to between 50 and 200 Hz. The total harmonic distortion (THD) was guaranteed at less than 0.5%, but was found to be better than 0.1 % for the majority of experiments.

4.3.6 Field coil for cryostat

A copper field coil was designed in order to supply a uniform field in a cylindrical volume within the cryostat. The coil sat around the glass cryostat in ambient air and is sufficiently distant so insignificant thermal transfer occurred. See Appendix 3, Figure A3.4.

The field coil was designed with a suitable inductance, 65 mH, and current to be conveniently compensated for by the PWM power supply, while still providing a useful AC magnetic field. An HTS coil was placed in the cryostat with its axis parallel to the field coil axis. The length of the field coil, 740 mm, ensured that the region around its center had a uniform magnetic field parallel to the longitudinal axis. In this way, an HTS coil placed centrally with the field coil encompasses all the HTS tape in the same parallel field. Figure 4.18 shows the vector field plot of the internal region of the field coil, and Figure 4.19 shows the magnitude of the radial and axial fields in the center and at one quarter coil height (185 mm). Both show the magnetic field with a 45 A rms field coil current.

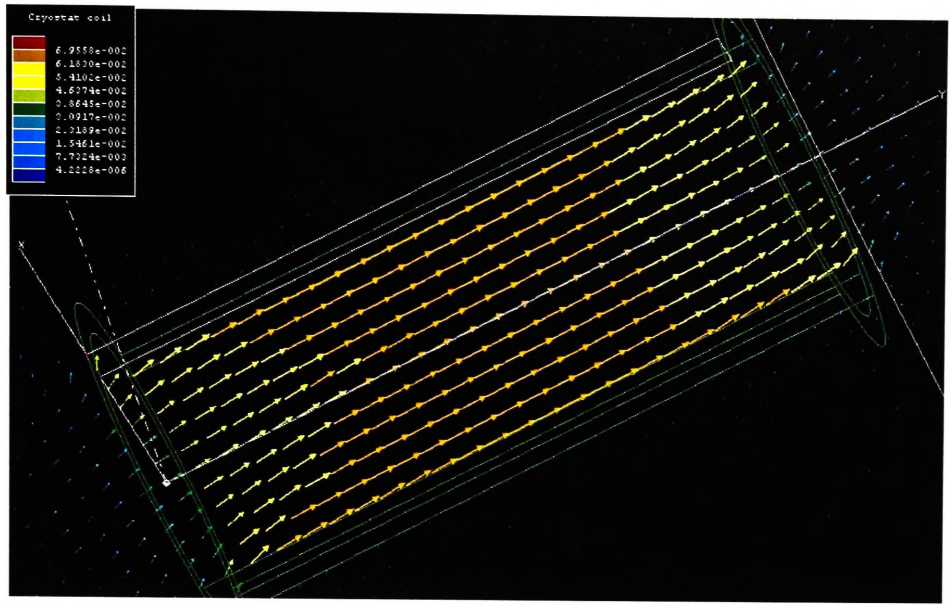

Figure 4.18. Vector plot of field coil in the cryostat volume with a 45 A rms field current

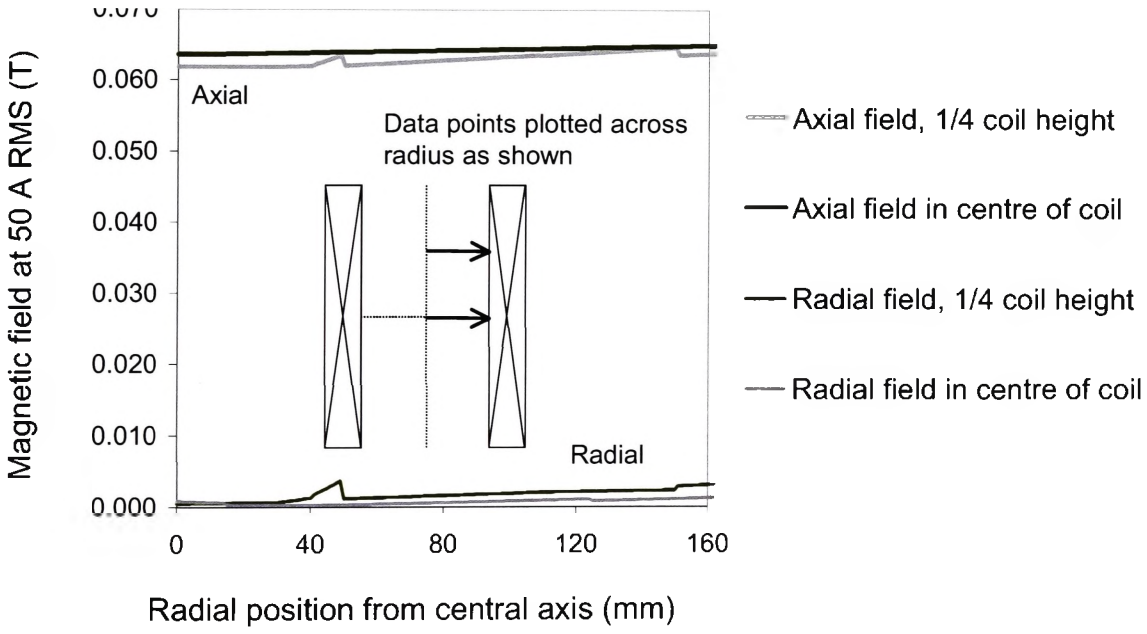

Figure 4.19. Axial and Radial components of the field coil at 45 A rms excitation

A maximum of 70 mT (peak) was available in the middle of the cryostat, and coils up to 300mm axial length were placed in the central volume and subjected to a parallel AC field. At 100A rms coil current, the temperature on the inside surface of the coil was just 80 °C.

4.3.7 Data acquisition

In this work, the MBC was automated using Labview™ software and National Instruments hardware to establish a user interface between the mass flow meters, LN level, gas flow valve, and PWM power supply. Figure 4.19 shows an example of the user interface which was developed over a period of three years.

Figure 4.19. Picture of the MBC automation screen interface. A typical result is shown.

Two charts (only one shown) indicated the output of each mass flow meter. The AC loss at each value of current was taken by first measuring the off set flow rate with the valve closed. This procedure allowed for any drift in the mass flow tare. Although the mass flow meters have an automatic tare function, it was found that it was better to allow the mass flow meter to drift to a steady state value, rather than tare it off for each measurement. The solenoid valve was then opened and the background loss measured. The current in the field coil or in the HTS coil was then stepped, and the mass flow monitored until a steady state reading was achieved within a small limit. The net AC loss was then obtained from the difference in the measured loss values.

4.4 Results of measurements using the mass boil off calorimeter

4.4.1 Commissioning of the system

The first commissioning experiment to be conducted was to determine the effectiveness of the silvered glass cryostat. The cryostat was operated at a fill level of approximately 60% for all experiments. It was found that the background heat leak at this level of liquid nitrogen was about 21 W. This value decreased gradually to about 14 W when less than 40% full. The loss potentially negated the purpose of having a high resolution flow meter with a small full scale (5 SLPM, or 18.5 W FS equivalent), so measurements on small coils were taken with only a 20% LN level where the background loss was 10 W, and the incremental loss of the coil could be measured close to the FS of the 5 SLPM meter. This ensured good accuracy in the data. Larger coils required a higher liquid nitrogen level and the measurements were closer to the FS level of the 20 SLPM meter.

The second commissioning experiment was to measure the effect of stray losses from the metallic components which could not have been replaced with non-metallic equivalents. With no HTS coil in the cryostat, and with the current leads taken out and all other metallic components in place (phase separator, LN level probe, pressure gauge funnel), the maximum magnetic field was applied with a 70 % fill of LN. No extra component of loss above the background was detected in this experiment. Stray losses were neglected for all other experiments in which the current leads were removed. Hence, using non-metallic structures as far as possible successfully prevented stray losses.

To measure the effect of the heat leak and resistive loss components of the current leads on the background loss, the leads were short circuited in the cryostat, without the presence of a HTS coil, and the total loss measured across the AC current range of interest. At a constant level of LN, the heat leak into the cryostat owing to the thermal conductivity of the copper was constant and therefore neglected. By measuring the total boil off with, and without the current leads, this component of heat leak was found to be approximately 5.3 W, which is close to that predicted by the design (4.3 W). The boil off rates measured over a 24 h period are shown in Figure 4.20.

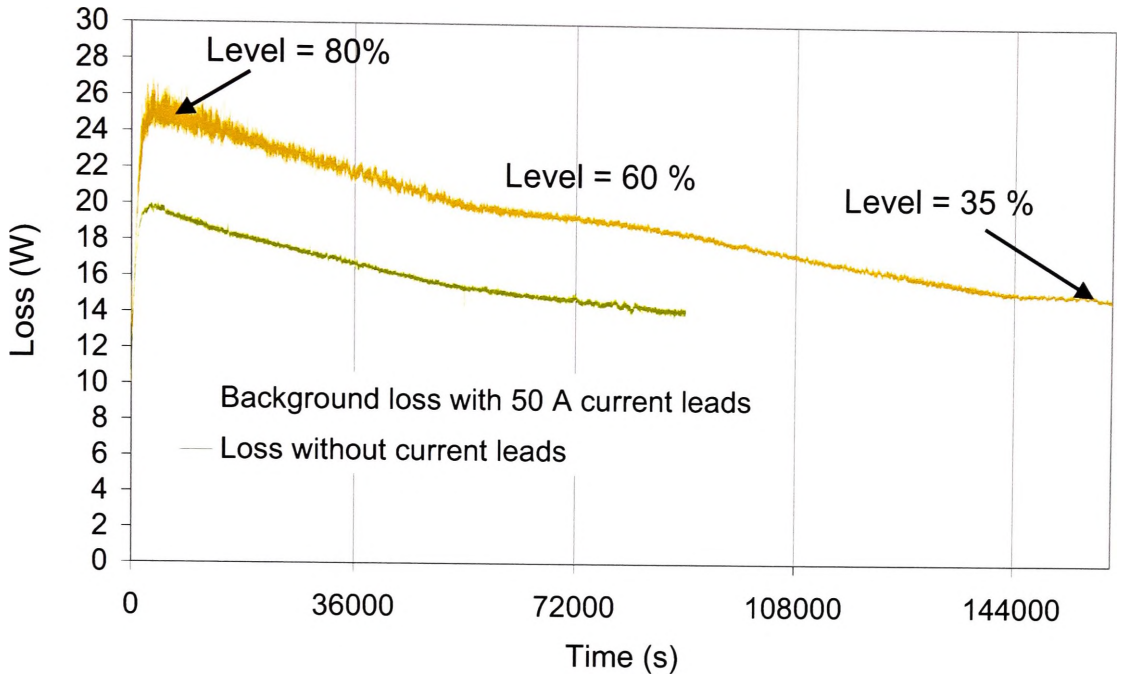

Figure 4.20. Background loss of the MBC cryostat with and without 50 A current leads.

The room temperature DC resistance of the current leads, including the joint was 4.3 mΩ determined by a four probe DC current technique. With the cryostat 60% full, which was the most common fill level for running the experiments, the total DC resistance of the current leads was found to be 1.64 mΩ corresponding to a 4.1 W resistive loss. With a 40% fill of LN, the DC electrical resistance was found to be 2.00 mΩ, which corresponded to a 5 W resistive heat loss. Hence, a small correction was made which depended on the level of LN. If this was not allowed for in the measurements, an error of ±0.5 W was incurred. Alternatively, measurements were taken at an approximately constant level of LN so that the 5.0 W correction was always constant. Both techniques were used in this work depending on the length of time require for complete characterisation of the HTS coil. Figure 4.21 shows the DC resistive loss of the current leads with LN levels of 60 % and 40

% as well as the joint loss. Equation 4.9 gives the relationship of resistive current lead loss in terms of fill level and the AC rms current.

$$\mathbf{Q = [8x10^{-4} - F.(2x10^{-3})].I^2} \quad (0.6 \geq F \geq 0.4) \text{ Eq. 4.9}$$

Where Q = current lead loss in mW, F is the fractional fill level, and I is the DC or rms current level. To take into account the small variability in the joint loss between different experiments, a DC calibration of each coil was completed at about 10% of the Ic. This calibration took into account the actual joint loss for each coil measured. A joint loss of 0.87μΩ was generally achieved at 77 K measured using a 4 probe DC current technique. It was found that this component of loss was negligible at up to 50 A current at 50 Hz, and was therefore not taken into account during measurements at lower values of current.

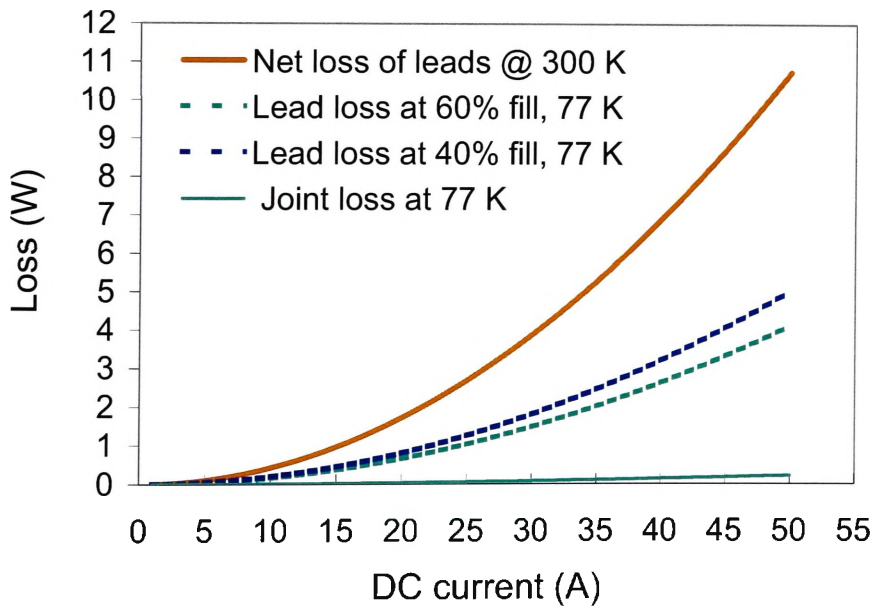

Figure 4.21. Current lead loss as a function of DC current or rms current level

4.4.2 Step response of the system

It was found that the MBC system required a significant time for the steady state to be established. Figure 4.22 shows the measured loss of a HTS coil for a step in the field coil current, (no current leads inserted).

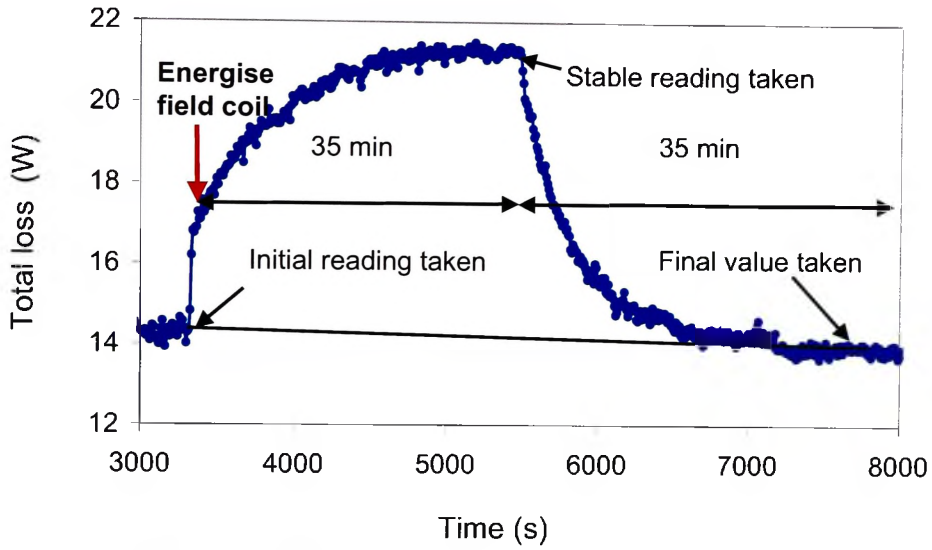

Figure 4.22. Response of MBC to a step in the magnetic field amplitude

The time constant of the rising and falling transient period was approximately 10 min and each AC loss measurement took 70 min to be taken accurately. A similar response was also observed in the background flow after connecting the gas flow pipes from the bushings to the mass flow meters, and when opening the gas valve.

During the period of stabilisation, the relative pressure inside the vessel increased gradually to 1 psi. During the stabilisation period, the loss measurement, as indicated on the mass flow meters, was not a true loss value of the HTS coil, as some of the energy lost by the coil went into the stored energy of the pressurised nitrogen gas in the cryostat rather than flowing out of the pipe work through the mass flow meters. The sum of the energy loss

indicated by the mass flow meters and the rate of increase in stored potential energy of the gas equaled the net loss in the system (HTS tape and background). Only after the pressure in the vessel has stabilised and remained constant, did the mass flow readings indicate the total losses of the system. Appendix 3.3 details further consequences of this feature on the final uncertainty in the measured AC loss of a coil, and shows in detail that the final AC loss of a coil may be determined with an uncertainty of ±0.5 W.

4.4.3 AC loss of solenoid coils

A three layer HTS coil, Solenoid coil A, of length 240 mm was wound with silver sheathed Bi-2223 tape, using insulation composite A. Other details are shown in Table 4.3

Property	**Value**	**Property**	**Value**
HTS tape core thickness	0.24 mm	Layers	3
HTS core width	2.8 mm	Turns/layer	60
Ic, 77 K, self field	18 A	Total turns	180
Jc of coil, self field	6.1×10^7 A/m^2	Bp (//,Tape)	0.009 mT
n (77K, self field)	12		
Tape length	135 m		

Table 4.3: Details of Solenoid A.

In this experiment, only the coil losses owing to an applied parallel AC magnetic field were measured, and hence, the current leads were not used. The losses were measured with the PWM power supply at 53 Hz and as a check compared with a 3 phase, 50 Hz, 20 Amp variac using a single line to line output. The results, shown in Figure 4.23, obtained using the variac output and the PWM supply at 53 Hz were consistent after allowing for the effect of the small difference in frequency. This indicated that there was a negligible effect from the presence of the small harmonic content in the PWM output.

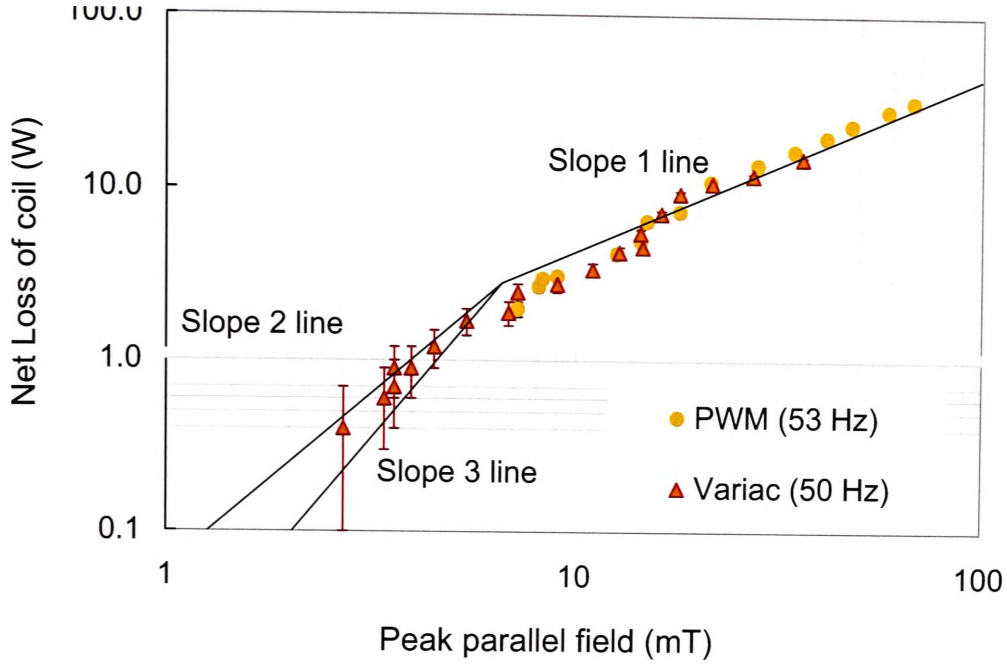

Figure 4.23. AC loss of a solenoid coil in a background AC field as measured by the MBC.

In this experiment, Solenoid coil A can be considered as a long thin slab in an applied parallel field for the determination of AC losses. The field was parallel to each turn of tape. The results at 50/53 Hz for applied fields greater than 15 mT follow a slope 1 characteristic as derived from the critical state model for an infinite slab. A slope of between 2 and 3 was found, however, for fields below 6 mT.

A two layer solenoid coil with integrated current leads, Solenoid B, was wound with 85 m of HTS tape in order to allow the AC losses to be measured for separate transport current and applied fields, and to confirm the results obtained for Solenoid coil A. The details of this coil are shown in Table 4.4.

Property	Value
HTS tape core thickness	0.24 mm
HTS tape core width	2.8 mm
Tape length	85 m
Ic of coil , 77 K, self field	16.2 A
Ic (0), 77K, zero field	18.0 A
Jc(0) of coil, 77 K	7.41×10^{7} A/m^2
n (77 K, self field of coil)	6.0
Resistance (300 K)	3.1 Ohms
Turns	156
Layers	2
Interlayer separation	50×10^{-6} m
Inside diameter	0.174 m
Coil height	0.296 m
Tape penetration field Bp	0.011 T

Table 4.4. Details of solenoid coil B

The measured AC losses of Solenoid B due to separately applied transport current and applied field are shown in Figure 4.24, as well as the measured DC transport current losses.

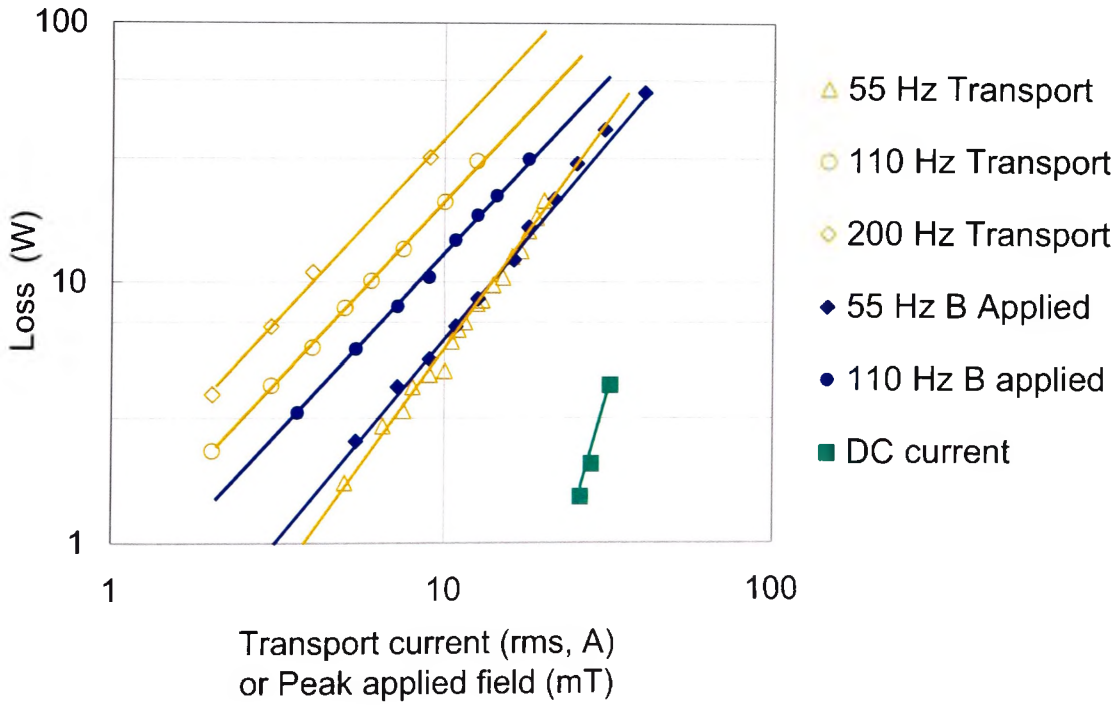

Figure 4.24. AC losses of solenoid coil B with separate transport current and applied field

The measured DC transport current loss of solenoid coil B was found to be small enough to neglect over the range of AC transport currents considered. The slope of the DC loss curve above the Ic was determined to be 7 which was consistent with the n value, 6, of the coil measured in the DC self field.

The measured AC loss of solenoid coil B in an applied parallel AC field was found to have a slope of 1.4 in the frequency range 55-110 Hz. In addition, it was found that the measured losses in applied parallel field increased by a factor of approximately two when the frequency of the applied field was doubled from 55 Hz to 110 Hz. This indicated that the coil had an AC loss which was hysteretic in nature. However, unlike Solenoid coil A, the slope of the curves were 1.4, rather than 1.0, as predicted by the critical state model.

There are two possible explanations for the observed slope of 1.4. If the double layer of tape is considered as a coupled system, then the penetration field of the equivalent slab is 22 mT, not 11 mT as calculated for the individual tape. Hence, the values of the field in figure 4.24 are all below the penetration field of the slab and the observed slope is between the expected values of three and one. It is neither three or one due to the complexity of the coupling between the tape layers, and the non-uniform Jc distribution across the tape thickness. However, the results from Solenoid coil A do show a slope 1 characteristic at fields above 15 mT, which is far lower than the penetration field of the equivalent slab for that coil (27 mT), so the coupled tape explanation does not seem to be consistent at least for these two solenoids.

A second possibility is that the relatively low n value of the Solenoid coil B is altering the slope from a value of 1 to 1.4. The critical state model assumes a high n value. Rabbers found experimentally that the slope of the loss curve for individual tapes is greater than 1 above the penetration field for finite n values [1.51].

The measured transport current losses of Solenoid coil B were found to have a more complex relationship with frequency. They were found to increase by a factor of four when the frequency was doubled from 55 Hz to 110 Hz, indicating that the losses from induced currents dominated the loss at this frequency. An increase by a factor of just under two occurred, however, when the transport current frequency was increased from 110 Hz to 200 Hz, indicating that the induced currents had saturated the superconductor, causing further losses to behave more like a penetration type loss mechanism of a fully saturated superconductor and therefore hysteretic like in nature. Obviously, different mechanisms of AC transport current loss in a solenoid coil exist at different frequencies. The two tapes of the Solenoid coil B conductor were not individually insulated, but rather in galvanic contact (the layers were insulated). This would allow, depending on the contact resistance, not only induced coupling currents between the filaments of an individual tape, but also coupling currents between the separate cores.

4.4.4 AC transport current loss of a pancake coil

A pancake coil was wound with a single HTS tape with the details shown in Table 4.5.

Property	**Value**
HTS tape core thickness	0.24 mm
HTS tape core width	2.8 mm
Tape length	40 m
Turns	140
Ic of pancake , 77 K, self field	6.0 A
Ic (0) (calculated)	9.0 A
Jc (0), 77K (calculated from Ic(0))	3.7×10^7 A/m^2
Inside diameter	0.025 m
n (77K, self field of pancake)	6.5
Outside diameter	0.118 m

Table 4.5. Details of pancake coil characterised in the MBC.

The transport current losses of the pancake were measured in the MBC at a frequency of 50 Hz, Figure 4.25. The transport current loss of the isolated tape (the Norris ellipse) is also included in Figure 4.25 [4.14], as is the DC loss of the coil, as calculated from the DC V-I curve, and the eddy current losses which were calculated using the equations of Namjoshi and Biringer [1.50]. These are included to discount their effects on the results. The AC loss data in Figure 4.25 was fitted to an I^2 relationship going through the origin, for transport current amplitudes below Ic, and extrapolated to higher currents. This fitted line is included in Figure 4.25. In addition, approximations based on the infinite slab model and the results of Carr are included in Figure 4.25 [4.14]. The estimated field free Ic, (Ic(0)) of the pancake was used in these calculations [4.16].

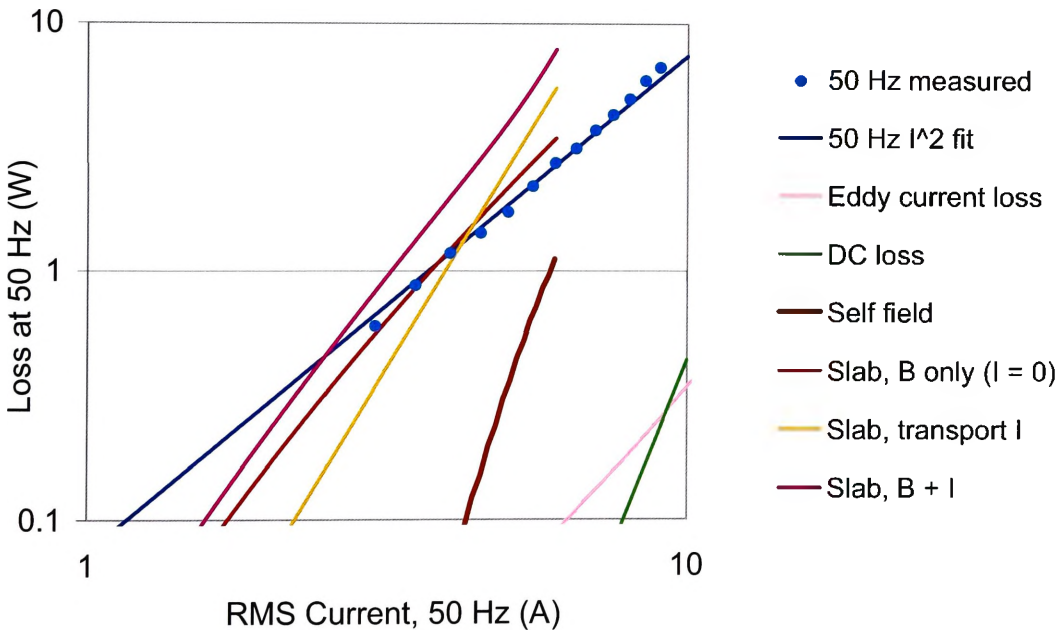

Figure 4.25. A comparison of the 50 Hz measured AC loss results and the various calculated approximations for a pancake coil.

The results of the AC losses on the pancake coil can be explained by considering the components of the magnetic field on each turn that result from the current in the coil. Each turn of the pancake has a parallel component of magnetic field in addition to the transport current, and a smaller perpendicular component of magnetic field. Hence, to estimate the AC losses, the pancake can be considered as an individual piece of straight tape with both a transport current and an applied parallel field, which is non-uniform across the length of the tape, but approximately uniform across each turn of tape length. The peak self field of the pancake was calculated to be 3.8 mT/A parallel to the tape. Both the parallel and perpendicular components of the magnetic field were calculated for each turn as a function of the radial position across the coil using an FEM software package. The self field AC loss of the pancake coil was estimated by summing the contribution to the total loss from each turn of the pancake for each value of transport current considered.

The calculations of AC loss are terminated at I = 6.0 A because the equations of Carr are not valid for transport current amplitudes larger than the Ic. Although the resolution of the MBC device restricts accurate data in this area to seven points, the agreement is reasonable. The measured results are generally lower than those predicted by the model. This is most likely owing to the fact that the self field amplitudes used to approximate the AC losses were calculated at the surface of the pancake and the internal magnetic field experienced by each turn of tape will be lower than this, due to the nature of the field produced by a pancake. This will in turn reduce the magnitude of the shielding current response and hence lead to lower losses than predicted.

4.4.5 Discussion

The aim of this part of the work was to prove that the AC losses of HTS coils can be accurately measured within reasonable time limits and uncertainty at power frequencies using a calorimetric technique based on mass flow meters. It has been shown that the system described here is capable of measuring AC losses in HTS coils from 0.5 to 50 W with an accuracy of ±0.5 W. The system can be connected to any sealed cryostat in which a HTS coil sits in LN and the losses may be determined under a variety of conditions.

The disadvantage of this type of system is the time required to obtain an AC loss measurement. This delay was reduced by maximising the size of the pipe work, avoiding 90 degree bends in the pipe work, and by reducing the bushes and other connections. The MBC technique also required a significant length of tape, at least 30 m, for meaningful results to be achieved. Another disadvantage is that the temperature at which experiments are conducted is limited to the boiling point of the available cryogenic fluid.

The major advantage of this measurement technique is the ability to measure the AC losses of a coil with independent applied magnetic field and transport current, each of which may contain a DC offset and a phase difference, although this was not explicitly tested in this work, which is on going. This is a difficult task using purely electrical means. The other advantage is that each loss mechanism is included in the result, so the losses of the real devices are known immediately without having to calculate or estimate them from data taken on short lengths of tape.

The variable frequency supply determined whether induced currents or hysteretic effects dominated the AC losses. In particular it was found for a long thin solenoid coil (Solenoid

coil B) that while the parallel applied field losses were hysteretic in nature at 55 Hz, the transport current losses were dominated by induced current effects at the same frequency.

4.5 Conclusions on the mass boil off measurement system

A mass boil off calorimetric system was built and used to characterise a number of coils in LN. The accuracy and range of the system was found to be suitable, and was extendable by including multiple mass flow meters in series with the gas flow line. A long time constant was found due to the time taken for the cryostat to pressurise against the pipe work. This extended the measurement time to about 70 min per point, and added to the uncertainty in the determined AC losses. The uncertainty of the system was determined to be ±0.5 W.

The accuracy and range of a liquid nitrogen mass boil off system was found suitable to characterise the AC losses of pancakes and solenoids with as little as 30 m of HTS tape.

The transport current losses of a two layer solenoid coil were found to have both linear and quadratic dependencies on the frequency of the transport current between 55 and 200 Hz.

The applied parallel field losses were found to be of a hysteretic nature between 55 and 110 Hz.

The transport current AC losses of a pancake coil were measured and found to be approximated well by using the analytical expressions for the hysterises losses of an infinite slab, for low values of current.

References

[4.1] M.P.Oomen, J.Rieger, M.Leghissa, H.H.J. ten Kate, "Magnetic ac loss in multi-filamentary Bi-2223/Ag tapes", Physica C, Vol. 290, pp 2891-2900, 1997.

[4.2] J.J.Rabbers, B.ten Haken, O.A.Shevchenko, H.H.J ten Haken, "An engineering formula to describe the AC loss of BSSCO/Ag tape", IEEE Transactions on Applied Superconductivity, Vol. 11, No.1, pp 2623-2626, 2000.

[4.3] O.A.Shevchenko, J.J.Rabbers, A.Godeke, B. ten Haken, H.H.J ten Kate, "AC loss in a high-temperature superconducting coil", Physica C, Vol. 310, pp 106-110, 1998.

[4.4] G.Coletta, L.Gherardi, F.Gomory, E.Cereda, V.Ottoboni, D.Daney, M. Maley, S. Zannella, "Application of electrical and calorimetric methods to the a.c.loss characterization of cable conductors", IEEE Transactions on Applied superconductivity, Vol. 9, No.2, pp 1053-1056, June 1999.

[4.5] C.F.Friend, "AC losses of HTS tapes and wires", Studies of High Temperature Superconductors, Vol. 32: AC Losses and Flux Pinning in High Temperature Superconductors, ed. A. Narlikar, Nova Science Publishers, NY, pp. 1-61, 2000.

[4.6] M.Iwakuma, K.Finaki, K.Kajikawa, H.Tanaka, T.Bohno, A.Tomioka, H.Yamada, S.Nose, M.Konno, Y.Yagi, H.Maruyama, T.Ogata, S.Yoshida, K.Ohashi, K.Tsutsumi, K.Honda, "Ac Loss Properties of a 1MVA Single-Phase HTS Power Transformer", IEEE Transactions on Applied superconductivity, Vol.11, No.1, pp 1482-1485, March 2001.

[4.7] V.Sokolovsky, V.Meerovich, M.Slonim "Eddy current losses at cryogenic temperatures", IEEE Transactions on Magnetics, Vol.. 29, No. 3, May 1993, pp 2095-2098

[4.8] D.E.Daney, "Handbook of Cryogenic Engineering", J.G.Weisend II Ed. PA:Taylor and Francis, ISBN: 1-56032-332-9, pp 365-441, 1998.

[4.9] Y.L.Buyanov, A.B. Fradkov, I.Yu. Shebalin, "A review of current leads for cryogenic devices", Cryogenics, pp 193-200, 1975.

[4.10] M.A. Green, "A design Method for Multiple tube Gas-Cooled Electrical leads for the g-2 Superconducing Magnets", Advances Cryogenic Engineering, Vol. 41a, pg 573, 1996.

[4.11] M.N.Wilson, "Superconducting Magnets", Chapter 11, pg 258. Oxford scientific publications, pg 256, Clarendon Press, 1983.

[4.12] P.F.Herrmann, "Handbook of Applied Superconductivity", Vol.. 1, pp 810-811, IOP publishing Ltd, ISBN 0 7503 0377 8, 1998.

[4.13] J.J.Rabbers, "AC loss in superconducting tapes and coils", Ph.D thesis, University of Twente, October 2001.

[4.14] W.J.Carr, Jr., "Ac loss from the combined action of transport current and applied field", IEEE Transactions on Magnetics, Vol. 15, p 240, 1979.

[4.15] W.T.Norris, "Calculation of hysterises losses in hard superconductors carrying AC curents: isolated conductors and edges of thin sheets", Journal of Physics D, Vol. 3, p489, 1970.

[4.16] F.Darmann, R.Zhao, G.McCaughey, M.Apperley, T.P.Beales, "Calculation of the critical current in pancake coiled long length Bi-2223/Ag tapes in non-uniform local magnetic fields perpendicular to the grain alignment axis", Cryogenics, Vol. 39, pp 445-451, 1999.

Chapter 5

Electrostatic and thermal design considerations for LN HTS transformers

5.1 Australian standards for transformers, AS 2374, "Power Transformers"

The higher current density of HTS conductors can lead to a reduction in the size and weight of transformers. An HTS transformer however, must be designed to pass various tests as outlined in the Australian Standards 2374 (AS 2374) documentation [5.1]. Although there is no section in AS2374 that pertains specifically to HTS transformers using LN as a dielectric, many aspects of the standards can be directly applied to HTS transformers. These include the following:

- AS2374 Part3. Insulation levels and dielectric tests which includes the power frequency (PF) and lightning impulse (LI) tests of the complete transformer.
- AS2374 Part 3.1. Insulation levels and dielectric tests – External clearances in air
- AS2374 Part 5. Ability to withstand short-circuit
- AS2374 Part 6. Transformer and reactor sound levels

In addition, the iron core temperature rise (not specified in AS2374), and the consequences of keeping the nitrogen in a liquid state will be studied in this chapter.

5.2 Insulation clearances

5.2.1 Introduction

The LN used in HTS transformer applications must form the dielectric between the primary and secondary coils and will also form part of the electrical insulation for all the other clearances in the electrostatic design. Hence, a general discussion of the dielectric properties of LN is warranted.

In general, the four main requirements of a dielectric liquid are as follows:

1. It must show a very high resistivity.
2. The dielectric losses must be very low .
3. The liquid must be able to accommodate solid insulators.
4. The breakdown strength must be high .

Liquid nitrogen is an excellent electrical insulating fluid, as it has no charged carriers and shows a very high resistivity [5.2]. Compared to oil, there are no breakdown products from partial discharges and it is non-flammable and environmentally benign. However, it is the breakdown characteristics that are the most important consideration for HV coil design.

5.2.2 Permissible electrostatic fields and clearances in oil filled transformers

In order to realise the promise of smaller and lighter transformers from the implementation of HTS, the electric stress clearances required for a LN design must be similar to, or not significantly greater than those employing oil or gas as the dielectric, so that the maximum benefit of HTS can be obtained. Two types of tests are stated in AS 2374 which transformers must pass, namely, the induced voltage test where the coils are subject to about twice the rated voltage and the LI test [5.1].

The permissible electrostatic fields used in oil filled transformers have been well documented and are well known through decades of experience. Fundamental knowledge of the breakdown characteristics of LN, however, is still the starting point in determining the permissible clearances.

To check whether the use of LN has any electrostatic disadvantages compared to transformer oil for the major insulation clearances, it is helpful to first list the axial and radial voltage stress used by designers for oil filled transformers [5.3,5.4]. The usual break down figures for oil are between 10 and 15 kV/mm measured using standard ASTM electrodes placed 2.5 mm apart [5.3,5.5]. Practical design considerations mean that such a high average field is not normally used and a suitable safety margin must be included when calculating clearances. Table 5.1 shows the safe average electric stress for different situations within an oil insulated transformer when the oil is restricted to channels less than 8 mm wide. These values are used to calculate the appropriate clearances required to a first approximation.

Situation	**Conditions**	**PF**	**LI**
		kV/mm	KV/mm
Average radial stress between windings	End entry	4	10
Average radial stress between windings	Centre entry	4.8	12
Phase to phase radial stress	End entry	2.8	7.3
Phase to phase radial stress	Centre entry	3.2	8.3
Axial stress towards yokes		1.5	4.0
Vector stress		6.8	18

Table 5.1. Average electric fields used to calculate the minimum clearances in oil filled transformers [5.3-5.5,5.12,5.13]

Higher stress on the oil is allowed using detailed electrostatic design, especially by employing barriers to restrict the oil column width to less than 8 mm.

The minimum clearance for each situation is calculated by Equation 5.1.

$$g = (V/\sigma) + x/(\varepsilon_1/\varepsilon_2) \quad \text{Eq. 5.1}$$

where :
g is the minimum clearance required for each situation given in Table 5.1,
V is the power frequency or LI test voltage,
x = total thickness of solid insulation across the clearance g with dielectric constant of ε_1,
σ is the stress limit in kV/mm from Table 5.,
$\varepsilon_1/\varepsilon_2$ is the ratio of the relative dielectric constants of barrier material to dielectric liquid.

The first half of Equation 5.1 is the basic clearance if no other materials were present. The appropriate stress limit for oil from Table 5.2 should be used for σ. The second half of Equation 5.1 represents that portion due to field enhancement effects arising from the differing materials which may be present, for example, press board and oil or Kapton and LN. This effect is discussed in section 5.2.5.

Using five 3 mm thick barriers, the clearance required between the primary and secondary in a 132 kV transformer is 55 mm, and the clearance to the higher voltage coil to the yoke is 84 mm [5.3].

5.2.3 Permissible average electrostatic fields in LN HTS transformers

There is no equivalent list of average electrostatic fields for LN HTS transformers as given in Table 5.2 for oil filled transformers. However, a great deal of experimental work has been carried out on the performance of LN and cryogenic gaseous nitrogen (CGN) under high voltage standard tests using a variety of electrode configurations [5.6-5.13]. Hence, reasonable assumptions must be made based on the breakdown data for LN under various experimental situations. Then, the clearance requirements may be calculated.

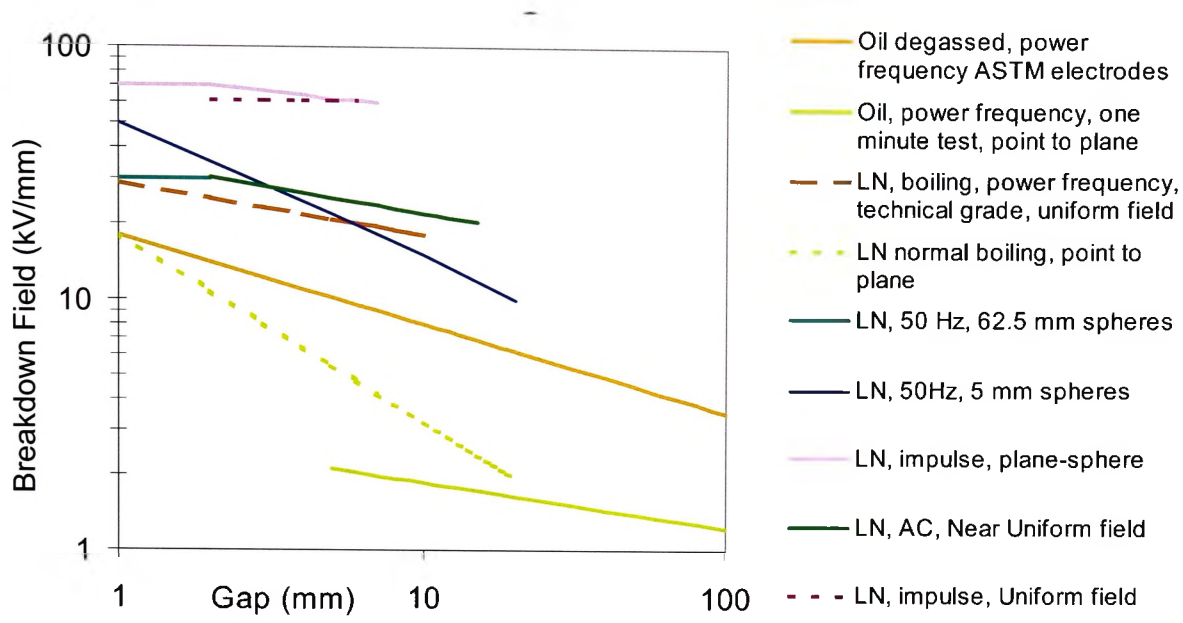

Figure 5.2. Comparison of breakdown strengths of LN and transformer oil [5.6-5.12]

The short term breakdown for LN in a near uniform field may be estimated from Equation 5.2, and in a point to plane gap by Equation 5.3 [5.6, 5.7].

$V_b = 29.d^{-0.2}$ Eq. 5.2 for d<10 mm

$V_b = 15.d^{-0.74}$ Eq. 5.3 for d<20 mm

Where
V_b is the breakdown voltage in kV/mm, and
d is the spacing in mm for a point to plane gap for d<20 mm

These equations are plotted in Figure 5.2 along with others available in the literature. Figure 5.2 also shows the other data available in the literature for various testing conditions of LN and as a reference a breakdown curve for degassed oil [5.3]. The data available for LN shows that the breakdown strength under both power frequency tests and impulse testing is about 3 to 4 times higher than that of transformer oil depending on the electrodes. Hence, it is safe to consider that the rules of thumb established for the electrostatic design

of high voltage oil filled transformers can also be used to determine the clearances required for LN HTS transformers. A general rule of thumb established is that all insulating parts of a LN HTS transformer, whether solid, liquid, or gas may be assumed to have a breakdown strength of 6.1 kV/mm for PF tests and 15 kV/mm for LI tests [5.12].

5.2.4 Materials used in oil filled and LN HTS transformers

There are a number of solid insulators which can be used in LN including Bakelite, Phenolic fabric and various other epoxy/fabric composites [5.2]. These are necessary in the design of high voltage transformers for use as barriers against electrical stresses between coils and from each phase to the earthed core components. Typically, in a conventional transformer they are manufactured from pressboard in large cylinders [5.3,5.4,5.5]. The cylinders are placed between the coils to reduce the maximum oil ducts gap between phases and coils to less than 8 mm.

Table 5.2 summarises the dielectric properties of the insulation materials used in oil filled transformers and those suitable for use in LN HTS transformers [5.2,5.4].

Material	ε_r
Oil	2.2
Paper	3.5
Pressboard	4.4
Varnish	3.0
Bulk insulation	3.0
LN	1.44
CGN	1.002
HTS insulation	3.0-3.5
Composites	3.0-3.5

Table 5.2. Relative dielectric constants of materials used in oil filled and LN filled transformers [5.2,5.4].

5.3 Electric field enhancement effects

5.3.1 Introduction to field enhancement

The electric fields discussed above are the average stresses within a transformer. The other issue in coil design is that of the vector stress or total stress on a conductor, which requires a detailed design to calculate its value. The vector stress is limited to 6.8 kV/mm under the power frequency test in an oil filled transformer [6.1]. To conform to this value, various field enhancement effects must be controlled at the dielectric to conductor/insulation interface. There are four types of field enhancement which must be designed for in all transformer coils, namely, the combined effects arising from edge enhancements, coil geometry, material permittivity ratios, and conductor geometry. Coil edge enhancement is solved by using metallic shielding rings, and is usually only required on coils operating at 110 kV and above. Each of the other effects was studied in more detail.

5.3.2 Field enhancement in transformer coils due to coil geometry

To investigate geometrical field enhancement in transformer coils, it is useful to write down the equations describing the effect between two concentric cylinders to model the case of a primary and secondary coil effect on an iron core. When no insulation is present on the conductors, the field between two cylinders can be estimated from Equation 5.2.

$$E = U_m/[x\ln(R/r)] \quad d >> r \text{ [kV/mm]} \quad \text{Eq. 5.2}$$

Where:
E is the field between the two cylinders [kV/mm],
R is the radius of the larger cylinder [mm],
r is the radius of the smaller cylinder [mm],
x is the distance to any point between the cylinders ($r<x<R$), and
U_m is the voltage between the cylinders [kV].

In transformer designs, the value of R and r will usually be of the order of 1 m and the value of R-r will be about 10 mm in a 100 kVA/78 kV DIL design and 38 to 55 mm in a 30 MVA/550 kV DIL design. Under these conditions, Equation 5.2 simplifies to that of the field between two large plates, as given in Equation 5.3.

$E = U_m/(R-r)$ Eq. 5.3.

Hence, for a reasonable range of transformer coil sizes, the average electrostatic fields can be simply calculated using Equation 5.3 and the fact that the coils are actually cylinders can be neglected in the calculation. Hence, there is no electrostatic field enhancement between transformer coils owing to the geometry of the coils.

5.3.3 Field enhancement owing to the permittivity differences between materials

In the case of an insulated round wire and a plane boundary, Equation 5.4 may be used to find the electrostatic field at any point, x, between the wire and plane [5.5].

$$E_x = \frac{U_m}{x\left\{\frac{\ln[\frac{R}{r}]}{\varepsilon_2/\varepsilon_1} + \frac{\ln[\frac{d}{R}]}{1}\right\}} \quad \text{Eq. 5.4}$$

where:
U_m = maximum voltage applied between tape conductor and ground plane,
R = radius of the round wire including insulation [mm],
r = radius of bare wire [mm],
d = distance from centre of conductor to ground plane [mm],
ε_2 = relative dielectric constant of the insulation covering the tape,

ε_1 = relative dielectric constant of the liquid nitrogen or dielectric liquid,
x = distance from the centre of a conductor to a point outside the conductor [mm],
E_x = field gradient at point x [kV/mm].

Equation 5.3 is arranged to show the effect of the insulation on the wire. The field enhancement due to the different dielectric properties of Kapton and LN is represented by the factor $\varepsilon_2/\varepsilon_1$. For the oil and pressboard combination, this factor is 2.0 and for a Kapton and LN combination this factor is also 2.0. Hence, there is no increase in field enhancement effects in LN HTS transformers compared to conventional transformers.

5.3.4 FEM analysis of field enhancement effects owing to conductor geometry

The second term in the denominator of Equation 5.4 describes the field enhancement owing to the conductor itself. Typically, the ends of solenoids are shielded with a metallic ring to increase the effective radius of curvature of the coil edge, and to prevent discharge or breakdown at these points. This component of the electrostatic field enhancement effect is called the edge enhancement and it has a practical conventional solution.

In any transformer, a field enhancement effect on the coil surface arises from the conductor winding itself. To investigate this effect in prototype HTS transformer coils, a solenoid coil, which included the geometric details of the HTS conductor, was analysed using FEM techniques. The stresses at the conductor edges along the coil were calculated and compared to the average stress to a ground plane. A suitable model consists of a 2 D X-Y planar geometry with HTS tapes extending in length to infinity in the Z direction, as shown in Figure 5.3. The coil was modelled as a line of conductors each with a width of 3.3 mm. In the model, a ground plane was placed at a distance of 38 mm away. However, it was found that an image coil 76 mm away was more suitable to use in the FEM model. A total

of just 16 tapes was found to be suitable in order to study the field enhancement effect of individual conductors. It was found that including a large number of HTS tapes in the model (>32) led to a problem requiring too much computer memory and time to solve. Including too few HTS tapes in the model (<8) led to the conductor field enhancement being obscured by the much larger coil edge field enhancement. The detail of two tapes in close proximity is shown in Figure 5.4 which also includes the mesh used to calculate the electrostatic fields.

The coil was assumed to be at a nominal test voltage of 100 kV, which gave an average field of 2.63 kV/mm away from the coil edge effects and from the immediate proximity of the HTS tape. Approximately 5000 mesh triangles were required within a 3 x 3 mm^2 area around the tape junction in order to accurately calculate the field enhancement, and a total of 100,000 mesh triangles was used in the model. The detail of the inter-layer insulation spacing was not included in the model, as it will be shown that the field enhancement effect is extremely limited in its spatial extent. For this reason, also, only a single layer of the coil was included in the model, as subsequent layers would not influence the field enhancement. The graphical result from the FEM modelling is shown in Figure 5.5 for two tapes in the middle of the coil, away from the effects arising from the edge of the coil.

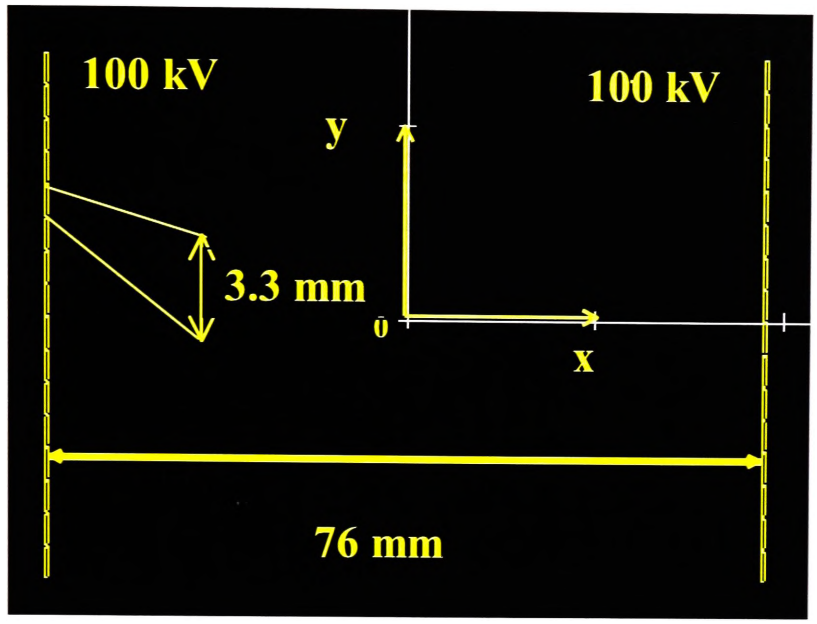

Figure 5.3. 2D model of a coil with 16 HTS tapes extended in the Z direction into the page.

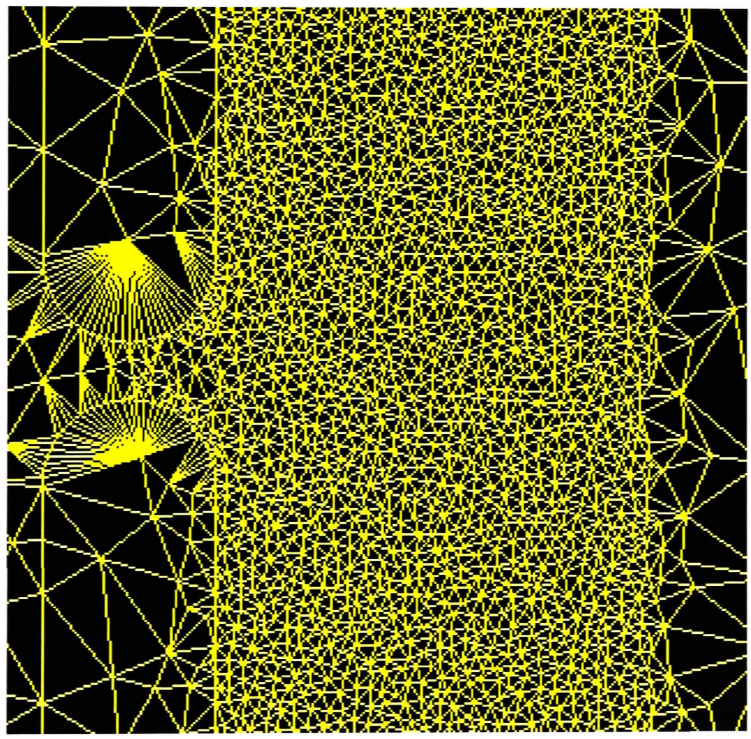

Figure 5.4. FEM mesh used to calculate the field enhancement effects in the model coil.

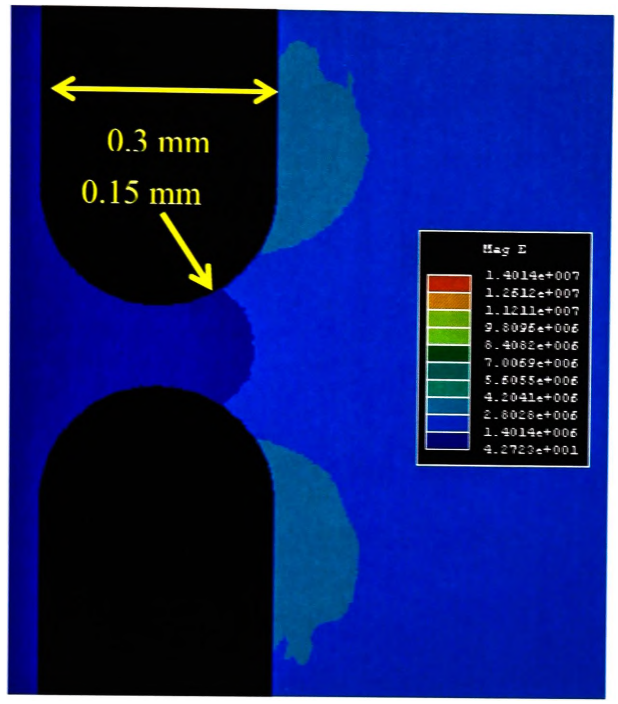

Figure 5.5. Magnetic field in the region of the HTS tape in the model coil.

It should be noted that this result arose only because of the static charging of the coil, and no induced voltage is included. The calculation of the vector stress would require the inclusion of the latter. However, for clarity, it was left out in this analysis.

A small field enhancement effect can be clearly seen. Figure 5.6 shows the effect more clearly by plotting the stress along vertical lines on the tape surface and at 0.1 mm above the tape surface. The coil edge effects can be seen and these are significant as expected being 9.3 kV/mm or an approximate field enhancement factor of 3.6. Figure 5.7 shows the stress at the surface of the coil in the centrally located conductors away from the influence of the edge effects. A maximum field enhancement effect of 30% was found, which is not significant in the design of a superconducting coil.

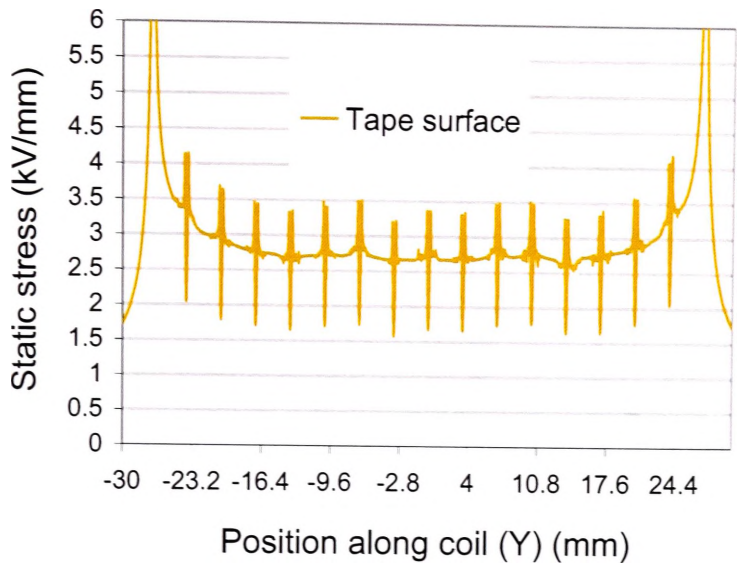

Figure 5.6. Electric stress along the surface of the model coil.

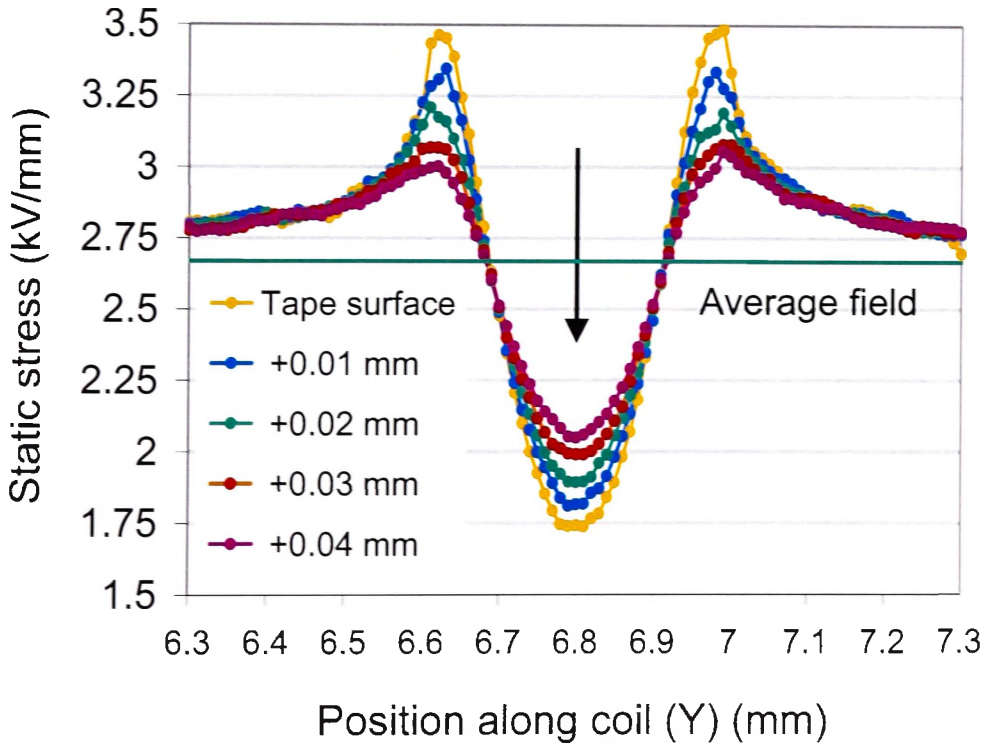

Figure 5.7. Detail of field enhancements away from coil edge effects

The situation changed somewhat when an insulation coating on the conductors was considered, except the maximum field enhancement occurred at the insulation to dielectric interface instead of on the tape surface. Figure 5.8 shows the 2D mesh used on the same model coil, but with a 0.05 mm continuous coating of insulation around each HTS tape with an ε_r of 3.5. The background was assumed to be air with an $\varepsilon_r = 1$. A pair of 10 mm diameter metallic corona rings were included at the ends of the coil model to reduce the coil edge effect and to provide a better resolution of the tape field enhancement effect. A finer 2D mesh consisting of 1000 triangles in a 0.3 x 1.0 mm^2 wide zone was required to yield accurate results, and this can be seen in Figure 5.8 near the junction of the tapes. A total of 127,000 mesh triangles was used in the model. The average stress in the insulation is 0.75 kV/mm, which was reduced from that in the bulk dielectric of 2.68 kV/mm by the ε_r factor of 3.5.

Figure 5.9 shows a plot of the stress versus distance along the coil surface (y) at various positions (x). Away from local field enhancements, the average stress on the tape surface of 0.75 kV/mm can clearly seen, as is the average stress on the insulation surface of 2.68 kV/mm.

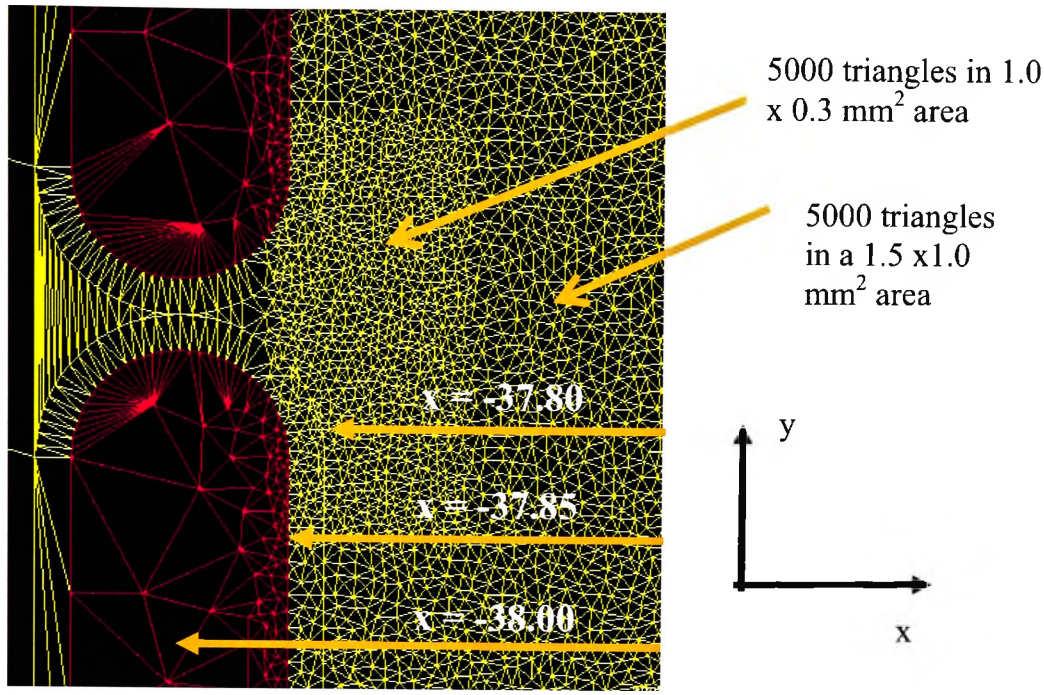

Figure 5.8. Detail of mesh used to calculate the field enhancement for an insulated tape

The maximum electrostatic stress found between the tapes away from the coil edge effects was 3.3 kV/mm on the insulation surface, which represents a field enhancement of 25% above the background of 2.63 kV/mm. Again, the coil edge effects can be clearly seen, but these are greatly reduced due to the inclusion of corona rings, and the extent throughout the rest of the coil was virtually eliminated.

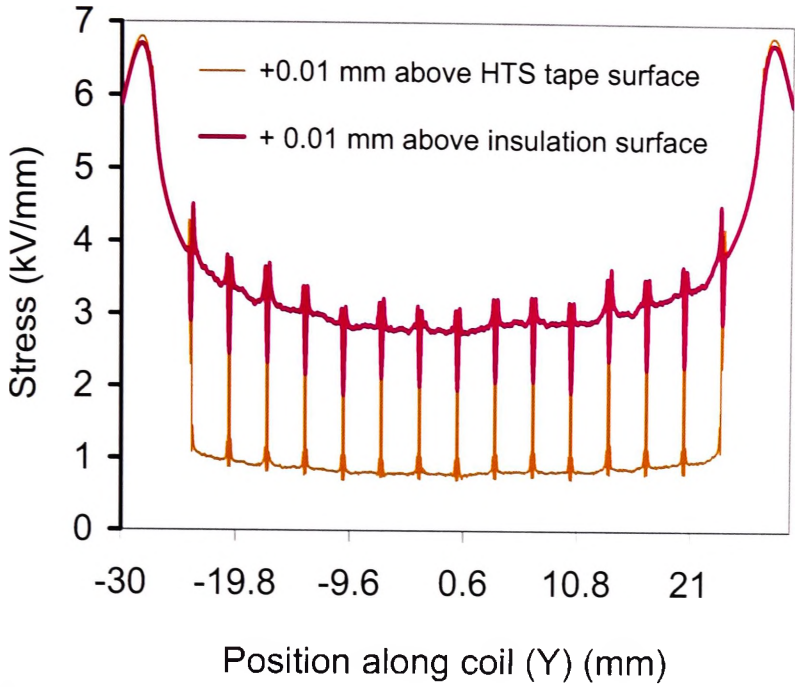

Figure 5.9. Plot of electrostatic stress along the model coil surface.

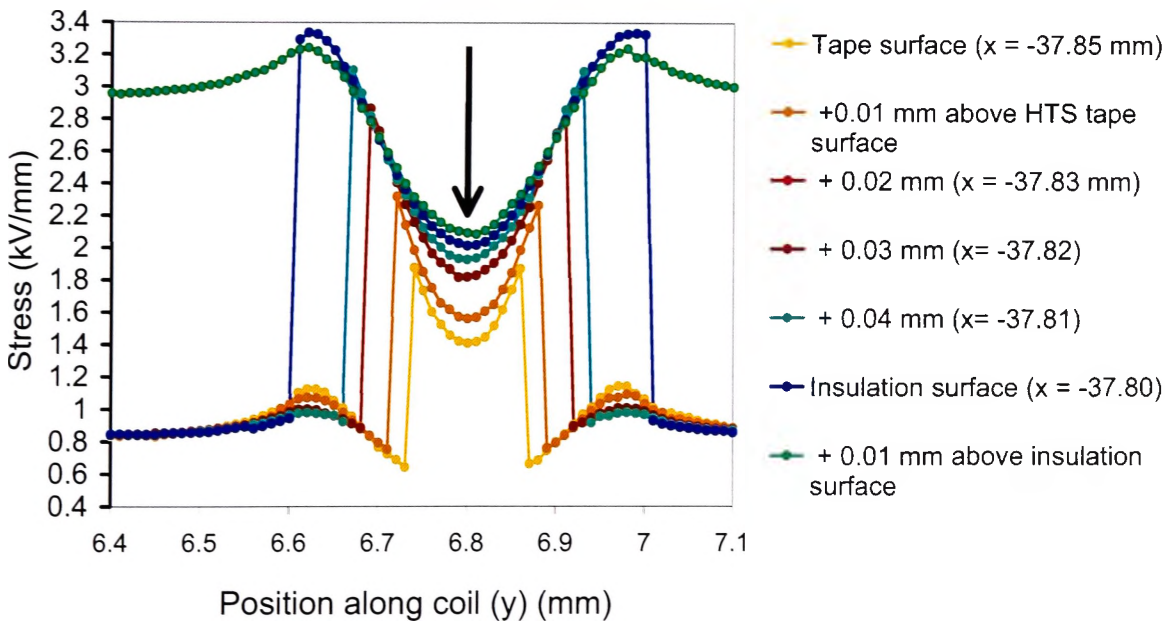

Figure 5.10. Close up of the stress along the tape and insulation surfaces near the boundary between two adjacent tapes.

The intersection of the two tapes is indicated by the arrow in Figure 5.10, and has a local minimum in the stress. The peak stress was located at 0.17 mm from the middle of two adjacent conductors, or 0.12 mm away from the tip of the conductor. The maximum field enhancement was located just under the insulation surface, where the stress reached was 3.3 kV/mm. Compared to the average stress in the insulation of 0.75 kV/mm, this represented a field enhancement of a factor of 4.4. However, compared to the average stress in the dielectric between the coils and ground plane (2.68 kV/mm) this represented only a 23% field enhancement.

In conclusion, no adverse coil surface field enhancement was found, and the electric stress can be well accommodated by LN and other readily available materials.

5.4 Designing for lightning impulse

The most uniform LI distribution across transformer coils was achieved by using a solenoid winding [5.4,5.5]. The LI distribution across a pancake stack of windings, a so called 'disk' winding, leads to a very non-uniform LI distribution with most of the impulse appearing across the first and second disks [5.5]. Conventional primary coils, however, for the most common power transformers are usually disk windings. A disk winding is preferred primarily to eliminate the complex insulation technique that would be required for a multi-layer solenoid winding. This insulation would be bulky and cumbersome, especially at the individual layer ends where flashover between layers would be difficult to prevent. One solution found is to employ a so called "butterfly", or "Diablo" winding, as currently used by Alstom [5.4,5.18]. This is not commonly used, however, by other transformer manufacturers.

In a disk winding, the test voltage across the coil is distributed across the whole height of the coil as shown schematically in Figure 5.11. A typical test voltage for a 132:11 kV power transformer would be either a short duration power frequency test voltage of 230 kV or a LI test of 550 kV peak. The greatest voltage stress during the LI test is between the top two disks, but these only have a fraction of the total turns in them, so the voltage will only be of the order of kilovolts or tens of kilovolts during LI, and not the full 550 kV. Various winding techniques exist to reduce the voltage across the first few disks.

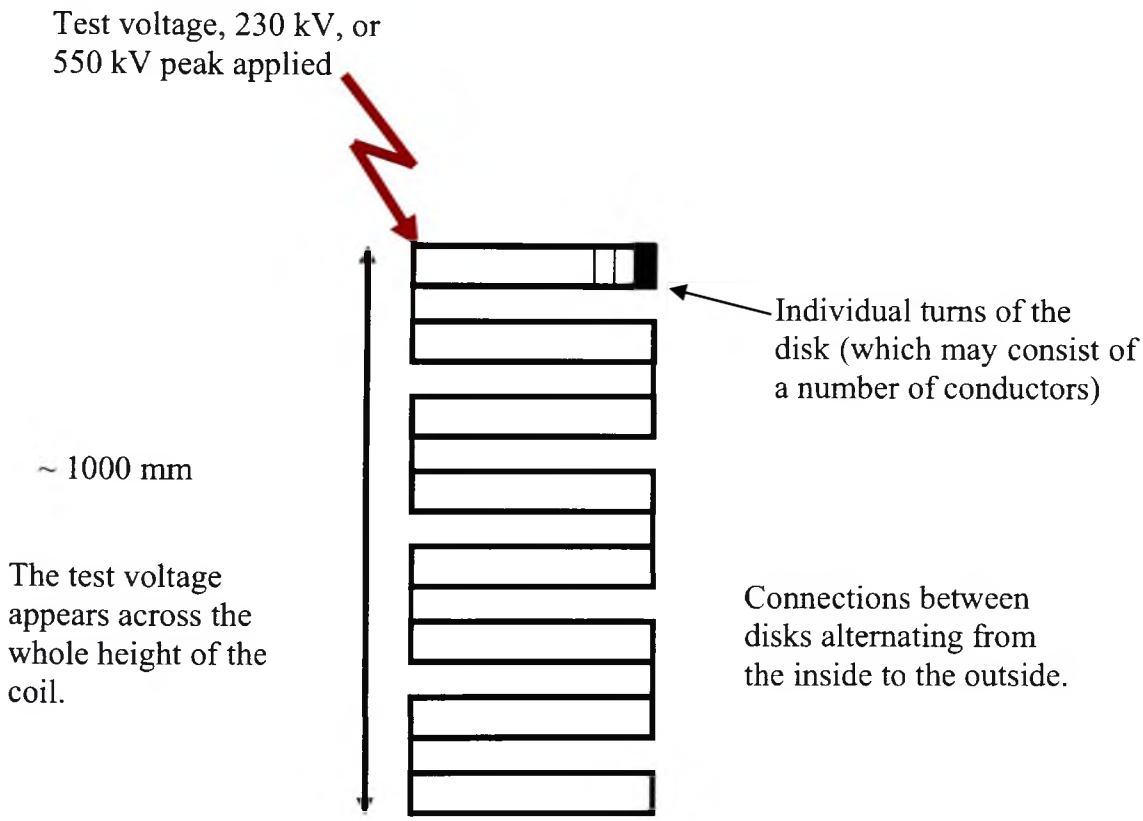

Figure 5.11 Conventional disk winding showing eight disks.

Disk windings require significant handling and physical contortions of the copper conductors in order to be wound in a single length in a neat manner suitable for transformer

coils. For example, each second disk must be turned inside out after winding so that the inner turn becomes the outer turn, and outer turn becomes the inner turn. This is to facilitate winding in a continuous manner, and not to transpose conductors, although this is also incorporated in the disk winding. In addition, the conductors must be bent in the plane parallel to the width of the conductor in order to proceed from one disk pair to another without making a joint.

If a high voltage winding were manufactured as a solenoid, the full 132 kV or test voltage, would appear across the top of the winding, which will be much less of a clearance than the height. Figure 5.12 shows a schematic of this situation. A short creep path exists between the two ends entirely though LN which would be impractical to eliminate with barriers.

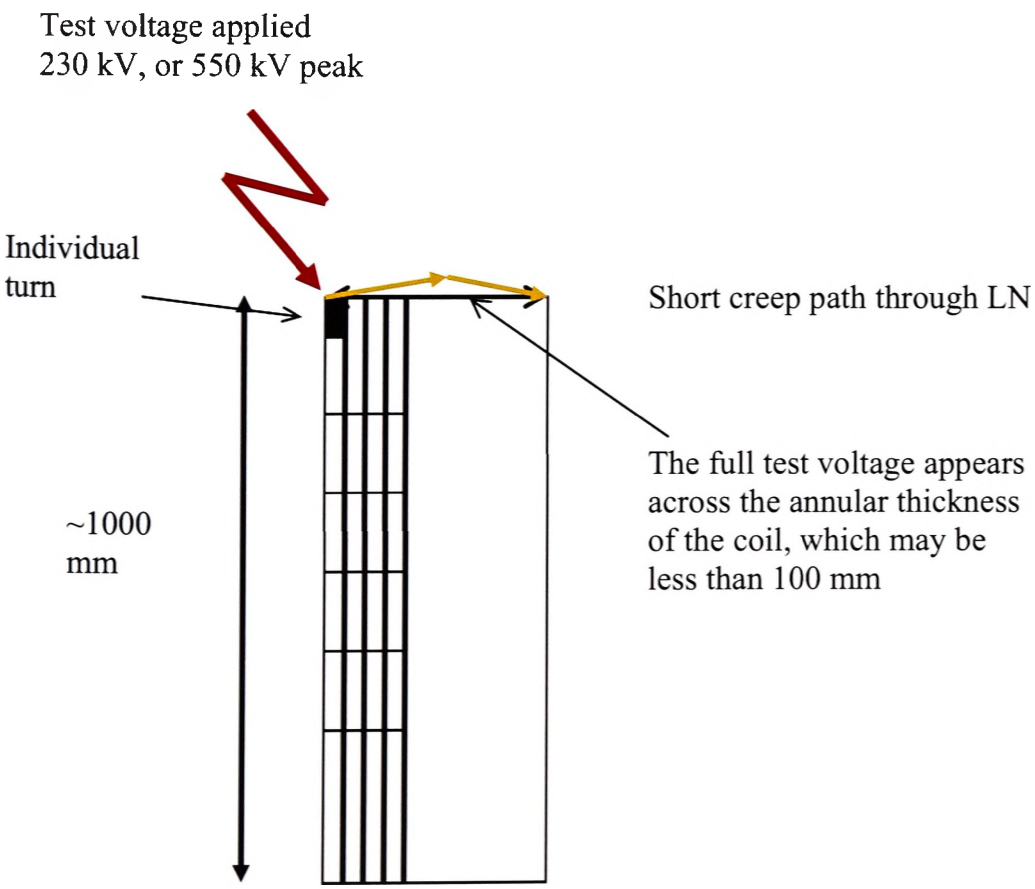

Figure 5.12. Schematic of a solenoid winding showing creep path

HTS conductors cannot be subjected to the level of mechanical manipulation that copper conductors are subjected to during the winding of transformer coils. The unit length of HTS may also not be available in more than 1000 m lengths, which means a completely continuous HTS winding may not be possible. Clearly, a technique is required that allows for a high voltage HTS coil to be wound such that the clearances and barriers required are not excessive.

One way to wind a high voltage HTS primary coil and avoid the above mentioned manipulations is to simulate a disk winding and use a series of electrically connected double pancakes. A double pancake is analogous to a pair of consecutive disks in a disk type winding in that the terminations are both at the inside or outside of the disks. The double pancakes would then be connected in series with normal conductors or other HTS conductors with resistive joints. Double pancakes must be used instead of single pancakes to avoid connections that run parallel to the plane of the pancakes. Double pancakes allow connections to be all on the outside or inside of the stack, thus avoiding cross leads traversing down the radial length of the coils which will pick up flux.

The disadvantage of double pancake stacks, however, is that in large transformers, the number of connections will be quite large, and may approach the hundreds. The connections are sources of dissipation which add to the losses. The estimated joint loss from 500 double pancakes in a 30 MVA transformer could be as high as 2 kW, which would require 32 kW of input power to remove, using a cryogenic penalty factor of 16.

Clearly, a solenoid winding has significant advantages over the double pancake connected arrangement for HTS windings; however, a high voltage HTS solenoid winding suffers from the same electrostatic problems mentioned earlier for conventional solenoid coils. The addition of a solid inter-layer dielectric which extends beyond the top of each layer is

possible. However, the LN would still have significant stress and the interlayer dielectric would have to be very thick or very long to the extent where the complete winding becomes very large.

In order to wind a high voltage solenoid coil and avoid the adverse stresses it is proposed that high voltage coils be wound as a series of inter-connected solenoids in top-down manner analogous to the disk winding. The complete coil would have all the beneficial properties of a disk winding, but without any of the disadvantages. It would be called a ***hybrid disk-solenoid*** coil, because each disk is replaced by a short solenoid with a fraction of the total turns of the whole coil. Figure 5.13 shows a schematic of this type of coil.

In the hybrid disk-solenoid winding the normal power frequency voltage between any two windings within a solenoid is reduced by the number of solenoids in the whole stack, n. The radial extent of the winding is the same as if it were wound as a conventional solenoid, and hence, the voltage stress is reduced by the same amount. If there were n solenoids, then the stress within each between the first and last turn would be reduced by a factor of n compared to the conventionally wound technique. The number of solenoids is dictated by the unit length of HTS tape available so that no joints occurred within any individual solenoid.

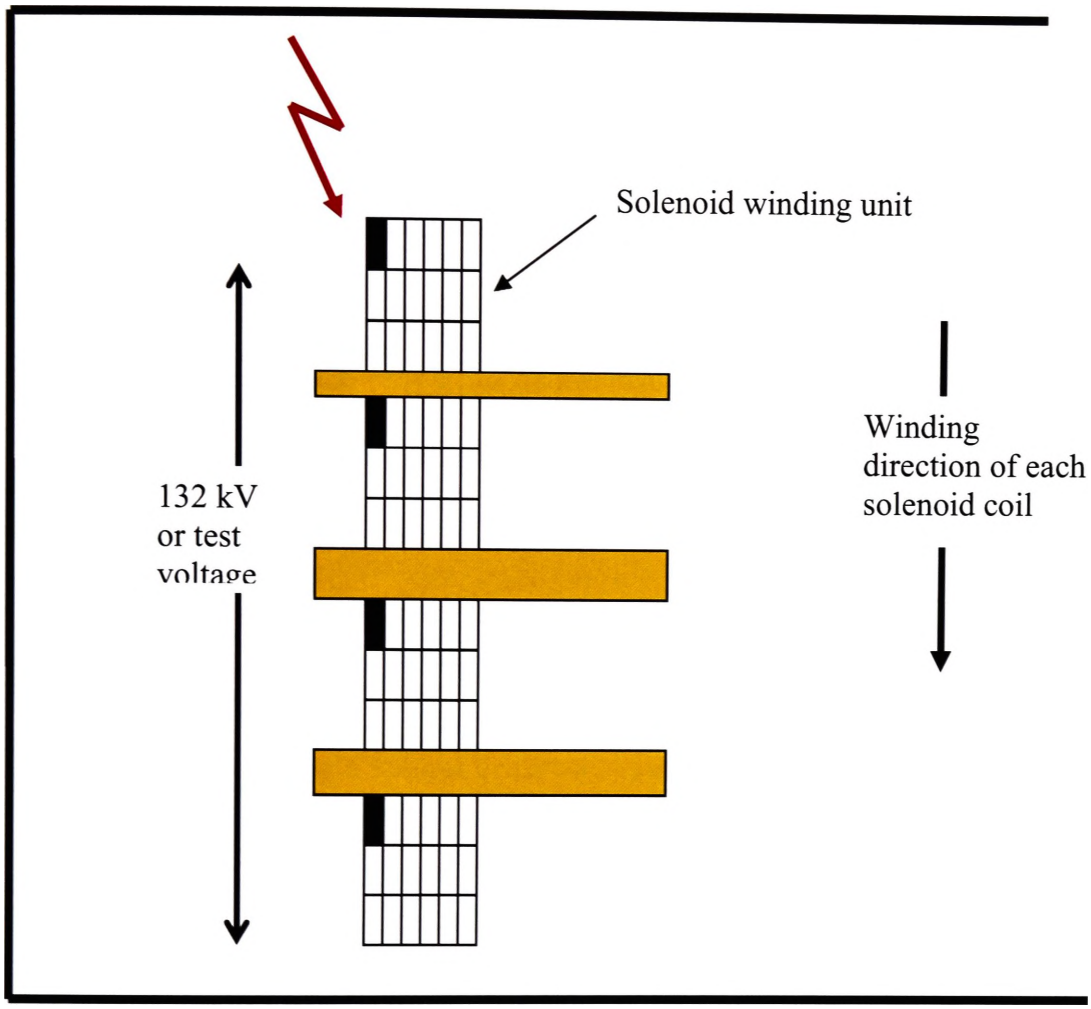

Figure 5.13. The hybrid disk-solenoid winding showing just four solenoids out of approximately 10 to 15.

The clearance between the coil subsets can be optimised using the LI voltage distribution. In a delta primary winding, the clearance between subsequent solenoids would be smaller at both ends widening to a larger gap in the middle, and in a star winding, it will be smaller just at the high voltage end. Optionally, a solid dielectric washer may be placed between the solenoids to increase the electrical strength, however, this would have to co-ordinated with the LI distribution across the top two coils.

5.5 Temperature rise of the magnetic core

AS2374 states that the iron core temperature "shall in no case reach a value that will damage the core itself, other parts, or adjacent materials". It was established that for commercially available cores, the maximum surface temperature must be less than 120 °C, and the absolute limit of temperature anywhere in the core is 145 °C [5.13]. These values are governed by the thermal properties of the insulating varnish between the laminations. Both of these limits must also be adhered to in the LN HTS design, as the core will be made of the same materials as those in a conventional transformer.

The above values ensure that under steady operating conditions, the oil does not ignite or release significant volumes of gas. In a conventional transformer, the magnetic core and coils are usually cooled by a natural or directed flow of oil, which is in turn cooled by an external radiator that may require cooling fans. Both the surface temperature and the central temperature of the core must be calculated in a transformer design. For small diameter cores, a one piece core is usually sufficient, however, for larger cores, above 50 cm in diameter, cooling channels must usually be incorporated within the core to limit the inner core temperature. Equations exist for calculating the surface temperature rise and central core temperature rise for iron laminations in contact with oil. These maximum limits must be achieved with rated current and with a 5% over voltage [5.13]. In a LN HTS transformers, however, the same temperature rise limits must be met. If required, forced air cooling of a core may be provided simply and cheaply with little overhead, and channels within the core, as in conventional designs may also be provided for the forced air.

To investigate core cooling, a simple core model for a substation style transformer was drawn, as shown in Figure 5.14, and the temperature rises approximated using the fundamental equations of heat transfer. A core diameter of 0.20 m^2 cross section was used

in the calculation. Using the calculated iron loss of 15 kW, the core surface and interior temperature were calculated with natural convective cooling and forced air cooling.

To simplify the calculations, the yokes and limbs were assumed to be cylindrical. Other dimensions are given in Table 5.5. The equations used to calculate the surface temperature and the interior temperature rise are given in equations 5.4 and 5.5 respectively. Equations 5.6-5.8 are used to obtain the convective heat transfer co-efficient for cooling of a cylinder in a cross flow of air [5.14].

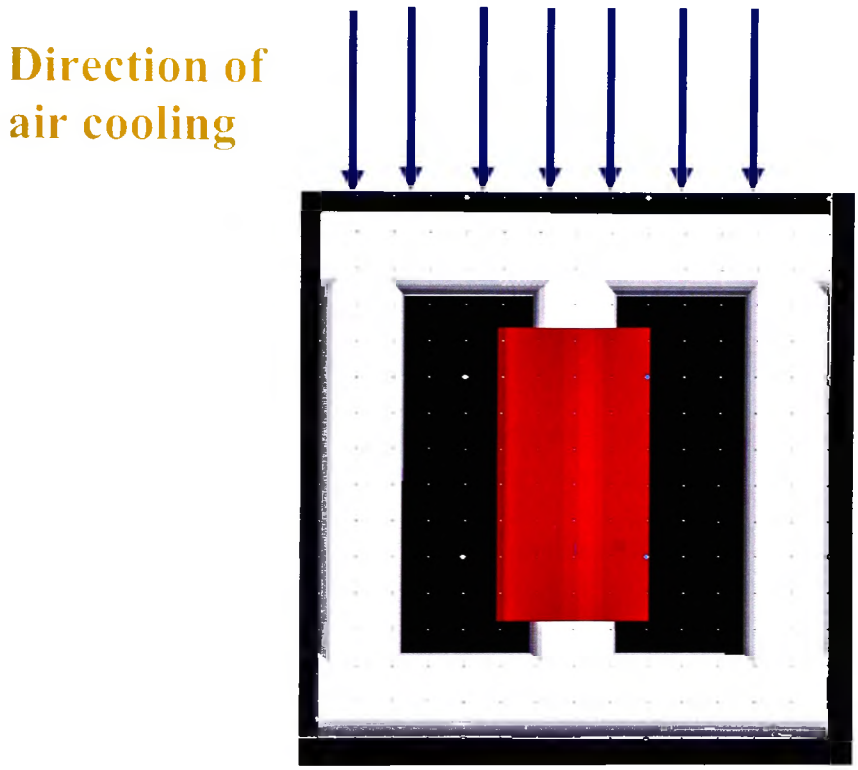

Figure 5.14. Model core to investigate the cooling requirements with 15 kW of core loss.

Parameter	Value	Unit
Iron Loss	15	kW
Yoke length	2.1	m
Limb length	2.0	m
Core diameter	0.50	m
Yoke Surface area	6.6	m^2
Limb surface area	9.4	m^2
Ambient temperature	30	^oC
Volume of iron	2.00	m^3

Table 5.5. Iron core details used to calculate the temperature rise.

$dQ/dt = (h_{conv}+h_{rad}).A.(T_s - T_{amb})$ Eq. 5.4
$T_{centre} = T_{surface} + (dQ/dT).D^2/16\kappa$ Eq. 5.5

$Re = VD/v$ Eq. 5.6
$Nu = CRe^mPr^n$ Eq 5.7
$h_{conv} = Nu.k/D$ Eq 5.8

where
Re = Reynolds number,
Nu = Nusselt number,
V = velocity of cooling air [m/s],
v is a constant, $15.89x10^{-6}$ m^2/s,
Pr = Pradlt number ~ 0.70 for temperatures less than 400 K,
n = 0.37, m = 0.7, C = 0.076, k = 2.63e-2,
h_{conv} = convective heat transfer [$W/m^2/K$],
h_{rad} = radiative heat transfer ~ 6 $W/m^2/K$ at the temperatures of interest,
dQ/dt = rate of heat loss [W],
D = core diameter,
A = surface area available for cooling.

For simplicity, the radiative heat transfer was estimated to be a constant 6 $W/m^2/K$, over the temperature of interest. It was also assumed that only the yokes were available for cooling as the limbs will be completely shrouded in the cryostat, although arrangements may be made to cool the limbs directly. Clearly, a more thorough study of core cooling would need to include a full FEM model to calculate the temperature profile in the entire core.

Considering the high thermal conductivity of iron laminations parallel to the varnish layer, however, no significant temperature differences across the limb length are expected.

Using the design dimensions given in Table 5.5, the heat transfer co-efficient was calculated to be 11 W/m^2K with static convection. Under these conditions, the core surface temperature was calculated to be 110 °C if both the yoke and limb surface areas are available for static cooling. Hence, it is not possible to dispense with active core cooling altogether.

Using a flow of air at 10 m/s (36 km/h) across the yokes only, an average heat transfer co-efficient of 30 W/m^2K was calculated and a surface temperature of 100 °C. These calculations show that core cooling does not pose a problem for the LN HTS transformer design and straight forward solutions exist for dissipating the core heat and limiting temperature rises.

5.6 Noise levels

The permissible noise levels of power transformers are covered by AS2374 part 6. Either the 'A' weighted (air weighted) sound pressure level, L_{pA}, or the A weighted sound power level, L_{WA}, is used to quantify the noise level [5.16-5.18]. The former is expressed in decibels [dBA] relative to a reference noise pressure of 20 μPa, and the latter is expressed in decibels relative to a sound power level of 10^{-12} W. The noise limit for transformer sound power levels (L_{WA}) as stated in AS2374.6 varies between 77 and 93 dBA respectively.

It has been found by tests on open circuit, and up to full load, that the vibration and noise of a transformer originates in the core, and not to any appreciable extent in the current carrying coils [5.17]. It has also been established that the main cause of noise is from the

expansion and contraction of the core laminations, referred to as magnetostriction. The magnetostrictive displacement is typically as little as a few parts in a million [5.17]. The magnetostriction is independent of the magnetisation polarity and hence the extension and subsequent contraction occurs twice per magnetisation cycle. The lowest frequency in the core vibration and sound emission spectrum is 100 Hz for 50 Hz power transformers and not 50 Hz, as might be expected.

Equation 5.10 may be used to estimate the core noise levels of a 3 limb transformer [5.1,5.16].

$$L_{core} = 40.B_{pk}+20.\log_{10}(C)-K \quad \text{Eq. 5.10}$$

where:
L_{core} is the noise power level in dBA,
B_{pk} is the peak field [1.75 T],
C = centre distance between core limbs [mm],
K varies with frequency, yoke design, baffles. For example, K = 58 at 50 Hz without baffles, and 60 with baffles.

If a transformer design is too noisy, then dampers can be added which increases the factor K in Equation 5.10 by 2 or 3 dB. More drastically, and at the expense of a larger transformer, the peak field in the iron core is often reduced from 1.75 T to 1.6 T to save about 4 or 5 dBA [5.13].

The reduced dimensions of the iron core in LN HTS transformers for the same power rating will reduce the noise level. For example, if the factor C is reduced from 1000 to 800 mm, then the noise level will drop by approximately 2 dBA.

Liquid nitrogen filled HTS transformers will differ in their noise characteristics in two main ways from oil filled transformers. Firstly, the damping effect of the LN differs from that of

the oil, and the noise level of the cryo-cooler differs from that of the fans used in conventional transformers. Each of these issues was addressed, and it will be shown that LN HTS transformers will have a lower noise level than a conventional oil filled transformer of the same rating.

The noise level of the cryo-coolers commonly used for nitrogen re-liquefication with a cold power rating suitable for large power transformers is of the order of 66 to 75 dBA [5.17]. Hence, the noise of the cryo-cooler is not significant with the noise levels of the transformer. Equation 5.9 can be used to determine the total noise level of the combined transformer and cryo-cooler when one is placed directly on top of the other [5.1].

$$L_{tot} = 10.\log_{10}[10^{Lcool/10}+10^{Ltrans/10}] \quad \text{Eq. 5.9}$$

where
L_{tot} = total noise power level of the cryo-cooler and the transformer,
L_{cool} = noise power level of the cryo-cooler,
L_{trans} = noise power level of the transformer.

For example, a conventional transformer with a noise level of 88 dBA can be compared with an HTS transformer having a noise level of just 86 dBA which would require a cryo-cooler which will have a noise level of 75 dBA [5.19,5.20]. The total noise power level of the combined cryo-cooler and transformer was calculated to be 86.2 dBA which is only 0.2 dB above that of the HTS transformer alone and 1.8 dBA below the conventional.

In conclusion, it has been shown that the noise level of the cryocooler does not add significantly to the noise of a LN HTS transformer, and that the reduced limb-limb spacing will reduce the core noise by around 2 dBA.

5.7 Cooling options for LN HTS transformers

In a LN cooled HTS transformer, the coil losses are all absorbed by the latent heat of the liquid. The vapour produced, which will be at 77 K, is re-liquefied by a cold head. The cooling power of the cold head at 77 K will determine the losses the coils may have in order to maintain thermal stability. If the losses are greater than this amount, then the cold head will not be able to keep up with vapour produced, the pressure will build up, and the level of LN will decrease. Eventually, the coil will become resistive and fail. Also important are the so called "hot spot" losses. As has been shown, the losses in a standard HTS solenoid coil are not evenly distributed owing to the radial component of field at the edges of the coil. The edges represent a higher proportion of losses than the rest of the coil, and the cooling at these places must be sufficient such that liquid contact can be maintained, or at least that the vapour zone does not become unstable.

Large LN re-liquefication systems are commercially available with tens of kilowatts of cooling power at 77 K. In these large systems, about 16 kW of input power gives about 1 kW of cooling power at 77 K [5.19-5.21]. They are extremely reliable, and require general maintenance every five years. Individual units have lasted up to 25 years [5.19,5.20]. The technology is mature, and has been mainly developed by the food and medical industries.

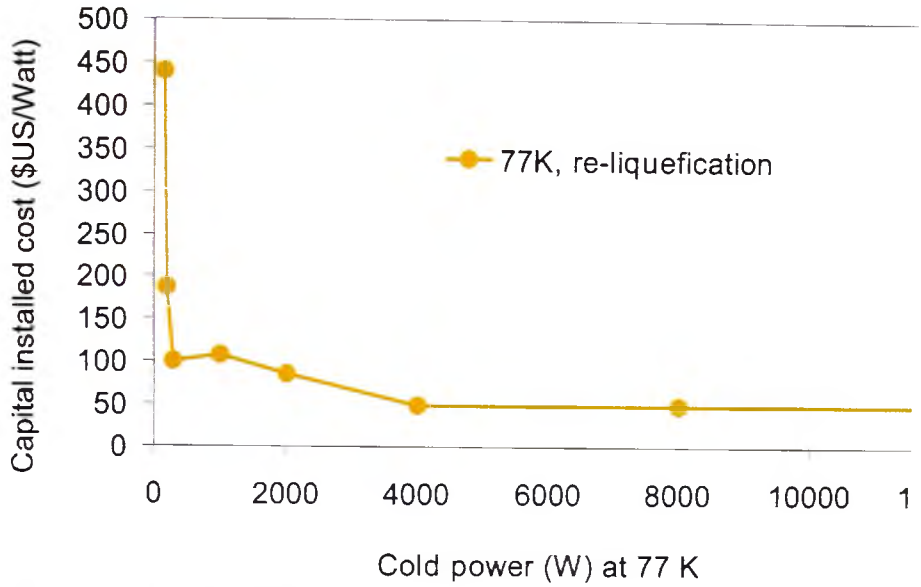

Figure 5.15. Capital cost of cooling system using a Stirling cryo-cooler at 77 K [5.20].

One particular cooling option for LN uses a cold head to re-liquefy the nitrogen gas. The cold head is cooled using helium gas at a pressure of 20 bar which is expanded in a piston arrangement through the Stirling cycle [5.19,5.20]. The cold head is placed in a vapour zone above pool boiling LN, and the re-liquefied nitrogen simply falls off the cold head back into the liquid volume. This system requires a compressor and cooling water. The ultimate efficiency of this type of cooling varies between 4.5% for small systems of less than 1 kW power, to 9.1% for systems with greater than 2 kW of cooling power [5.19]. Figure 5.15 shows how the capital cost of cooling using this system varies with the cooling power [5.19-5.21].

Another option is to use a simplified air liquefaction system, where the nitrogen gas itself is compressed and expanded in a reverse Brayton cycle to re-liquefy it. The advantage of this system is that no cooling water is required and no helium is required as the nitrogen gas itself is the working fluid. However, the disadvantage is that the nitrogen gas boiled off

must be compressed to 10 bar before expansion and liquefication in the turbine which necessitates a separate holding tank. A regular recharge of LN is also required to compensate for leaks through the high pressure seals.

Other cooling options are sub-cooled liquid nitrogen at 65 K, or forced flow liquid nitrogen at either 77 K or 65 K. In the sub-cooled option, the HTS device heat results in a slight increase in the liquid temperature to around 70 K. This heat is then removed by a cryo-cooler external to the system. The forced flow option includes a pump operating at up to 1 – 5 bar which pumps the 77 K or sub-cooled liquid around the HTS device. The forced flow, sub-cooled option requires two buffer tanks, one to act as a phase separator on the warm side, and one to store the 65 K sub-cooled LN [5.19,5.20]. The installed capital cost profile of these systems are shown in Figure 5.16, and the efficiency characteristics in Figure 5.17. As can be seen, in large (> 4000 W) systems, the cost of sub-cooling to 65 K is about twice that of simple re-liquefication being about US$100/W compared to US$50/W. However, the Ic(0) of HTS tape at 65 K is about 1.8 times that at 77 K which will reduce the tape length required, thereby reducing the heat load, and allowing a smaller cryo-cooler to be purchased. The cryogenic penalty of using that cryo-cooler at 66 K, however, will be about 50 % higher that at 77 K. These facts illustrates the point that the overall efficiency, cooling technique, capital costs, and running costs need to be evaluated to produce the most cost effective and reliable solution possible.

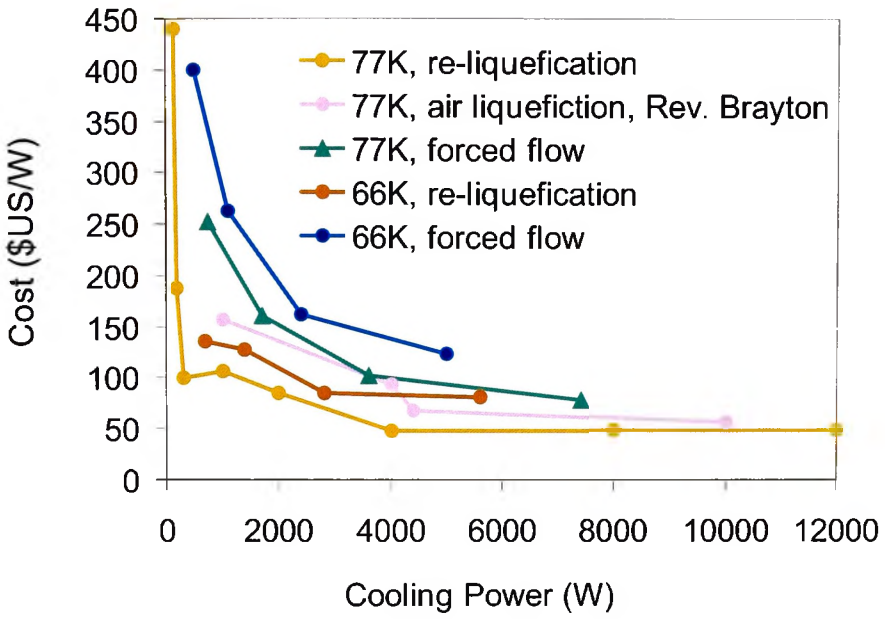

Figure 5.16. Capital cost of various types of LN cooling [5.20,5.21]

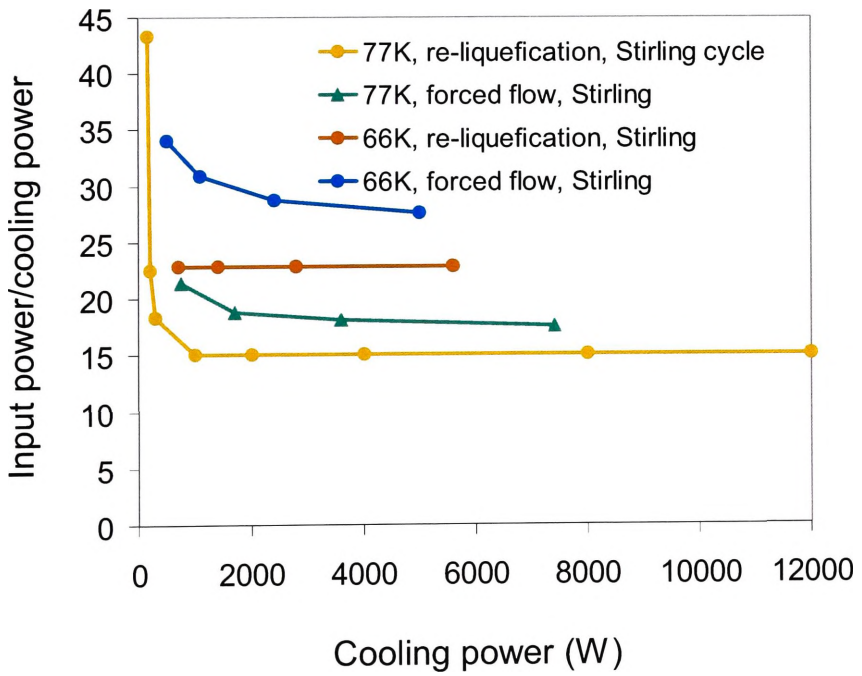

Figure 5.17. Efficiency of various types of cooling at 66-77 K

5.8 Conclusions

The main issues dealing with the design of high voltage and high power LN HTS transformers have been investigated. The electrostatic design has been investigated, and it has been shown that LN performs better under high electric stress than conventional transformer oil. The consequences of this are that the electrostatic design of a LN HTS transformer is similar to a conventional transformer, and this result will be used as the basis of a 100 kVA transformer design. The issue of field enhancement was analysed using FEM analysis of a model coil in the vicinity of the conductor insulation surface. A maximum enhancement of just 30% was found, and would have a negligible effect on the electrostatic design.

A new type of winding was described which addressed the different operating and handling techniques required for HTS tape, and provides the designer with an option for handling the coil end creepage requirement. The hybrid solenoid-disk winding permits high voltage solenoid coils to be wound with the flexibility to design for a suitable lightning impulse voltage distribution.

The issue of how to handle the heat produced in a LN HTS transformer was discussed. It was found that the core heating could be addressed by simple convective cooling. Using ambient air blowing at 10 m/s across the yokes, it was found that the temperature rise of the core could be kept below 75°C which is safely within the AS2374 requirements.

The cost and sizing of available cryo-coolers for closed circuit cooling of the LN bath cooling the HTS coils was investigated. The most practical size of cryocooler was found to be greater than 4 kW, which puts the size of the transformer in the 10 MVA + range. The cost of replacing the HTS coil loss was found to be $US50/W at 77K.

Finally, it was estimated that LN HTS transformers are approximately 2 dB quieter compared to conventional transformers because of decreased limb – limb spacing.

References

[5.1] Australian Standards, "Power transformers", AS 2374.1-AS2374.8.

[5.2] D. Evans, "Turn, layer and ground insulation for superconducting magnets", Physica C, Vol. 354, pp 136-142, 2001.

[5.3] "Insulation regions of the main transformer insulation", Electrostatic plots and brochure material, Weidmann sales information, Germany, pp 8-16.

[5.4] "High power transformers and shunt reactors", company literature published by Alsthom Atlantique, 25 rue des Bateliers, 93404 Saint Omen Cedex, France.

[5.5] L.F.Blume, A.Boyajian, G.Camilli, T.C.Lennox, S.Minneci, V.M.Montsinger, "Transformer engineering" 2nd edition, John Wiley & Sons New York, 1951.

[5.6] J.Gerhold, "Properties of cryogenic insulants", Cryogenics Vol. 38, No. 11, pp 1063-81, 1998.

[5.7] J.Gerhold, "Dielectric breakdown of cryogenic gases and liquids", Cryogenics, pp 571-584, Oct. 1979.

[5.8] H.Goshima, N.Hayakawa, M.Hikita, H.Okubo, "Area and Volume Effects on Breakdown Strength in Liquid Nitrogen", IEEE Transactions on Dielectrics and Electrical Insulation", Vol. 2, No. 3, pp 376-384, 1995.

[5.9] B.Y.Seok, H.Komatsu, M.Kushinaga, J.Suehiro, M.Hara, "Pressurising and Sub-cooling Effects on Electrical Breakdown of Ln2 in Modelled HTS Coils", IEEE Transactions on Dielectrics and Electrical Insulation", Vol. 8, No. 6, pp 1016-1024, 2001.

[5.10] H.Goshima, T.Suzuki, N.Hayakawa, M.Hikita, H.Okubo, "Dielectric Breakdown Characteristics of Cryogenic Nitrogen Gas above Liquid Nitrogen", IEEE Transactions on Dielectrics and Electrical Insulation", Vol. 1, No. 3, pp 538-544, 1994.

[5.11] S.W.Schwenterly, "High-voltage testing of superconducting power apparatus", Cryogenics, Vol 38, No. 11, pp 1115-1122, 1998.

[5.12] P.Caracino, M.Lakner, H.Okubo, O.Tonneson, B.Wacker, "Superconducting and insulating materials for HTS power applications", Pirelli Lab. public document, Dept. of Material Innovation, Pirelli, Viale Sarca, 222, 20126, Milano, Italy.

[5.13] Personal communication, Ravvi Ravindran, transformer design engineer, formerly of ABB Australia, Alsthom U.K. (retired).

[5.14] F.Icopera, D.P.DeWitt, "Fundamentals of Heat and Mass Transfer", Published New York : Wiley, 3rd edition. 1990.

[5.15] B.Fallou, J.C. Bobob, E.Carvounas, Z.Crotoru, "Insulation components for high voltage cryoelectric equipment, CIGRE report International Conference on Large High Voltage Electric Systems, Paris 1974.

[5.16] N.G.Trinh,Y.Menard, "Audible noise generated by power transformers of a substation", IEEE PES Summer meeting, Portland, OR, Paper A76 pp 473-9, 1976.

[5.17] A.J.King, "Reduction of the noise of iron-core transformers and chokes", Chapter 29 in book by C.M.Harris, "Handbook of Noise Control", McGraw-Hill 1979.

[5.18] C.T.Nguyen, R.Beauchemin, "Keeping down the volume", IEEE Potentials, pp 37-40, 1991.

[5.19] J.G.Weisend, "Handbook of Cryogenic Engineering", Taylor & Francis, London, 1998.

[5.20] F.Diogardi, Stirling public document, February 2002.

[5.21] Personal communication, Air Liquid personnel, France.

Chapter 6

Design of a 100 kVA 6.6 kV/240 V HTS transformer

6.1 Introduction

Current conventional transformer design no longer requires a focus on the broad dimensional aspects such as core size, copper winding dimensions, or insulation thickness and spacing. The judicious choice of these broad characteristics of transformers have long been standardised and written in a form where a basic solution can be arrived at very quickly. The only reason why this has been able to develop is because the physics of copper, iron, and insulation materials is mature and the properties of these materials are well defined. For example, the resistance of copper, the B-H loop of cold rolled silicon steel, and the dielectric constant, loss tangent, and break-down properties of insulation materials in oil and air are known, reproducible, and standardised.

There have been significant improvements in the materials and the way they are manufactured and used, for example, insulation and core materials. These advancements have allowed the development of dry-type transformers, which use advanced high temperature insulation materials. The iron losses have decreased owing to better processing through cold rolling, grain orientation, and connection techniques between the iron core yokes and limbs. The development of continuous transposed conductor has also significantly reduced eddy current losses in the copper and simplified the coil winding procedure. However, incremental improvements in modern transformers

pertaining to the efficiency generally achieve less than 1 kW of loss savings for a 20 MW 3-phase transformer which has up to 160 kW of total losses at full load [6.1,6.2].

In contrast, the design techniques and parameters for the electromagnetic and electrostatic design of HTS transformer are not as well developed, primarily because HTS materials behave differently to ordinary conductors and they are relatively new. The existing equations and design principles cannot simply include superconductors because they are so fundamentally different and new design principles have to be developed. The main difference in HTS transformer design is that the coil losses are fundamentally linked to the vector components of the magnetic field distribution across the coil, whereas in conventional design the losses due to the field distribution account for only a small contribution to the overall loss.

Given the advanced maturity and high efficiency of conventional transformers, it is fair to ask why change the state of affairs and introduce superconductors and unknowns such as cryogenics, compressors, and new conductors whose properties are not described by the old equations? The driving force comes from a need to make these devices cheaper in the long term, safer than they are currently, longer lasting, and more efficient.

The Je used in the design of conventional oil filled transformers with copper conductors is typically in the range of 200 to 350 A/cm^2 . With HTS conductors, typically capable of current densities in the range of 2,000 to 20,000 A/cm^2 without resistive voltage, potential reductions in the mass and volume of transformers is possible.

This chapter will be devoted to the design of a 100 kVA 6.6 kV/240 V WYE:WYE LN HTS transformer. This was chosen because it represents a real life situation. It is the least likely stage of power transformer ever to be replaced with the new technology,

however, for the purposes of this thesis, the design represents a sufficient challenge and many details that arose are pertinent to larger, higher voltage transformers.

In the absence of any leakage reactance specification, efficiency, noise, or size requirements, a range of possible solutions, governed by a set of practical constraints, were investigated. The constraints used in the design, based on the off line full 3 phase version, were as follows:

1. A reasonable amount of HTS conductor between 1500 and 2500 m per phase.
2. A footprint not larger than a conventional (1100 x 660 mm).
3. A overall height not greater than conventional (1140 mm).
4. An iron core cross section size less than conventional (150 cm^2).
5. Total losses of 3 phase device not more than conventional (2%, 2 kW).
6. A leakage reactance of less than 50%.
7. A 3 limb iron core with a fixed iron core flux density of 1.75 T peak.
8. A coil operating temperature of 77 K.
9. A lower dry mass than conventional (440 kg).

In addition, concentric primary and secondary coils of equal height were assumed and this design aspect will be justified later in this chapter.

Equation 6.1 was used to determine the iron core flux required which was re-arranged into the familiar form of Equation 6.2.

$$E = d\lambda/dt = -Nd\phi/dt \quad \text{Eq. 6.1}$$

$$E = 4.44 f N B_{pk} K A \quad \text{Eq. 6.2}$$

where:
E = 6.6 kV for the primary coil and 240 V for the secondary coil,
f = frequency of operation, 50 Hz,
N = number of turns of either coil,
B_{pk} = Peak flux density present in the iron core = 1.75 T,
K = "K ratio" of iron to total area of the core, and
A = total cross sectional area of the laminated iron core in m^2.

Equation 6.2 has an infinite number of solutions. By fixing f, E, B_{pk}, and the K ratio, the unknown variables are reduced to two, namely N and A. An infinite number of solutions still remain, however. In addition, for each solution set {N,A}, an infinite number of different coils may be designed. It was useful to characterise each possible HTS coil with two further parameters, namely, the primary coil shape factor, S, and the total length of conductor per phase, L. The shape factor was defined as the ratio of the height of the primary coil to the outside diameter of the primary coil. The four parameters, {N,A,S,L} define the basic parameter set of the transformer and were used throughout this chapter to refer to a specific design.

From the possible set of solutions, {N,A}, not all values of {S,L} work very well in practice. For designs employing conventional conductors and passive or forced oil cooling, the failure of most solution sets is that the transformer cannot be kept sufficiently cool. In this work, most solution sets {N,A,S,L} required a large HTS content and had high AC losses, or were overly large in size.

It was the physical and electromagnetic constraints that ultimately reduced the infinite set of solutions {N,A,S,L} to a very small set. The properties of the superconductor and the cooling technique ultimately decided the final solution for the four parameters. In addition, the Je, electrostatic clearance requirements, and cryostat size determined the core window size, footprint, and volume. In arriving at a final set of solutions for

{N,A,S,L} particular attention was paid to the coil hysteresis losses and the length of superconductor required, as these determined the ultimate efficiency.

Two possible solutions for {N,A} were found, each requiring 1500 m or 2500 m of HTS conductor per phase respectively. The next design step investigated was how the primary and secondary phase coils could be manufactured to meet the loss specification. The range of S considered was 1/8 to 5, and the range of L considered was 1500 to 2500 m. Three different coils with shape factors of ½, 1, 2, each with L = 1500 or 2500 m were found to be appropriate for detailed design work. This resulted in total of six possible designs. Using FEM software, the magnetic fields within the winding of each of these designs were calculated and the hysteresis losses estimated.

For each of the six designs, the dimensions and all details were calculated allowing the core loss and leakage reactance to be found. To summarise, the transformer design steps were as follows:

1. Dimensional analysis to determine a sub set of {N,A} meeting the constraints.
2. FEM analysis of various coil shape factors to arrive six designs, {N,A,S,L}.
3. Calculation of coil losses, efficiency, and full dimensional details for each design.
4. Selection from the six designs of a final transformer to construct.

The detail of each of these steps follows.

6.2 Dimensional analysis

For a given transformer rating, in order to reduce the volume and mass from those of a design employing conventional conductors, the iron core cross section must be reduced, which necessitates a larger number of turns. The physical reason behind this lies in the mutual flux linking the coils. With reduced core area, the flux available is reduced, which must be compensated for by more turns to increase the flux linkage to the required amount. For a given value of A, the coil and iron core dimensions can be calculated if all the other variables, such as insulation thickness, cryostat dimensions, and other clearance requirements are designed or selected according to the operating voltage.

The intelligent choice of the primary and secondary turns, coil dimensions and iron core diameter is the first step in designing a transformer. Once this is decided, in addition to the spacing requirements and the tape length, the magnetic circuit details may be calculated. Owing to the specific properties of the HTS conductor, it was found appropriate to introduce a new parameter, namely the coil shape factor, S. The shape factor will dictate the actual shape of the magnetic circuit, the mass and volume of the complete transformer, and the amount of tape required. This may be expressed symbolically as,

$M = f(S,A,L,\Lambda)$ Eq. 6.3
$V = g(S,A,L,\Lambda)$ Eq. 6.4
$L = h(A,S,\Lambda)$ Eq. 6.5

where:
M is the total mass of the coils and iron core,
V is the volume of a complete enclosing box,
L is the total length of HTS tape required,
S is the shape factor which will be approximately the same for the secondary coil, and
Λ represents all the fixed variables.

In this analysis, the variables represented collectively by Λ are fixed, as they only depend on the particular voltage of operation and are given in detail in Appendix 4.1. It should be noted that the usual transformer design parameter of volts per turn is not used explicitly in these calculations. Instead, a new variable, the shape factor S was chosen so that useful insights into appropriate HTS coil design may be gained [see Appendix 4.2].

One way to proceed towards a final design and to fix N and A was to plot M,V, and L over a realistic range of core areas, A, and use these plots to decide on the most appropriate values of A and S for a fixed set of parameters, Λ. Alternatively, L may be fixed or limited to a certain range dictated by cost limitations. The dimensional analysis to be presented here will utilise these two techniques by plotting M,V, and L over a realistic range of A and S.

To assist in this procedure, a program was written in Visual C which included all the fixed and free variables required to calculate the dependent variables. The program developed in this work, enabled a one-off spot design to be calculated for a given core area, A. Alternatively, and more usefully, any of the free variables were able to be stepped from a minimum value to a maximum value with a specified step size. Usually, the core area was stepped. Appendix 4.3 shows the front pages of this program and a brief explanation.

6.3 Estimation of the AC loss and the overall transformer efficiency

The average specific AC loss of HTS tape (expressed in W/m) within a transformer depends on the frequency, the magnetic field on each turn of the tape within the coil, and the transport current. All these factors must be considered if a design is to have acceptable electrical losses.

The total electrical losses, Q_{tot}, arise from the total hysteresis in the superconductor itself, $Q_{h.tot}$, the classical eddy current loss in the metal sheathing of the tapes, Q_{eddy}, and the iron core, Q_{iron}, and the transport current loss, Q_{trans},. The total loss may be expressed as in Equation 6.6.

$$Q_{tot} = Q_{h.tot} + Q_{eddy} + Q_{iron} + Q_{trans} \quad \text{Eq. 6.6}$$

The calculation or estimation of each component of Equation 6.6 for a HTS transformer coil set will be discussed. It should be noted that the dynamic resistance loss is not calculated as part of this analysis as the design is such that the peak transport current amplitude is less than the critical current and this results in a much smaller component of dynamic resistance.

6.3.1 Calculation of Hysteresis loss, $Q_{h.tot}$

The hysteresis loss of a coil is estimated by initially calculating the magnetic field pattern across the volume of the coil, translating this into a distribution of parallel and perpendicular fields on each turn of HTS tape, calculating the hysteresis loss for each turn, and then summing the results. The magnetic field pattern was found using an FEM package. The magnetic field distribution calculated is that due to the transport current in the turns of the coil, not just the self field of the individual tape.

The hysteresis loss must be estimated by calculating the individual contributions to the loss that arise from the separate parallel and perpendicular fields. Figure 6.1 shows one turn of the tape (either the primary or the secondary) in a coil with an iron core and the orientation and symbols for the magnetic fields at a point (r', z', ϕ') within a turn of the coil.

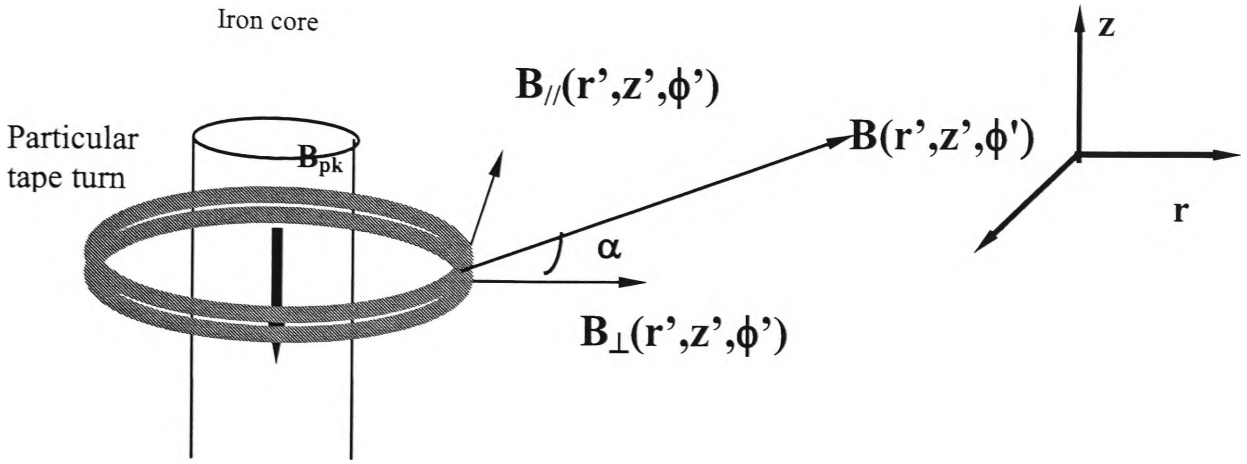

Figure 6.1. Schematic of an iron core limb and a coil turn and the conventions used

To simplify the calculation of the total coil hysteresis loss, each turn of the coil was assumed to be perfectly circular, *i.e.*, the slight helical nature of the windings was ignored. Also, the field on each turn was assumed to be invariant with ϕ, *i.e.,* it has cylindrical symmetry. This is a good approximation for cores manufactured from many stepped laminations, but will not be strictly correct for cores with a square profile.

For HTS tapes with untwisted filaments, the hysteresis loss of each turn may be estimated by initially calculating the loss contribution from the parallel component (in the r-z plane) and perpendicular component (in the r direction) of the magnetic field on the turn, assuming that no transport current is flowing. These loss equations have been conveniently parameterised by Campbell [1.34], Carr [1.32], and Leghissa [1.39] in terms of tape properties, such as core widths, thickness and the Ic.

The actual field on each turn, will not be in either of these planes, but will be at some angle to them depending on the position of the turn within the coil. The contribution to the turn hysteresis loss from the perpendicular component of field can be treated as an upper estimate, and that from the parallel component as a lower estimate. The actual

loss will lie somewhere between the two. To refine this estimate, Equations 6.7a and 6.7b may be used to calculate upper and lower limits for the loss of each turn [6.3].

$q_{h.tot}(high) = q_{\perp}.(B_{\perp}/B_a) + q_{//}.(B_{//}/B_a)$ Eq. 6.7a

$q_{h.tot}(low) = q_{\perp}.(B_{\perp}/B_a)$ Eq. 6.7b

Where $q_{\perp}$ is the calculated turn loss obtained if the net field at the turn, B_a, were perpendicular to the tape, and $q_{//}$ is the calculated turn loss if the net field were parallel to the tape. Greater insight, however, into the nature of the losses was obtained by summing the $q_{\perp}$ and $q_{//}$ components across the turns, and calculating overall perpendicular, $Q_{\perp}$, and parallel, $Q_{//}$, hysteresis loss components of the coils. The total hysteresis loss, $Q_{h.tot}$, can then be estimated as the sum of these two components. As shall be seen, this introduced little error, and over-estimates the coil hysteresis losses.

6.3.2 Iron loss and core temperature rise

The design assumes that the core is not part of the cryogenically cooled components, being separated from the windings by an electrically insulating cryostat. Hence, the iron loss for a particular design is calculated by simply using the specific iron loss for laminated cold rolled silicon steel at 1.75 T peak magnetisation.

Static air cooling was assumed, and the approximate temperature rise of the surface of the core and in the middle of the core was approximated by Equations 6.9 and 6.10, respectively, which employ the assumption of cylindrical symmetry in the core limbs and yoke.

$Q_{iron} = h.(T_{surface} - T_{amb}).A$ Eq. 6.9

$T_{centre} - T_{surface} = Q_{iron}R^2/2k$ Eq. 6.10

Where Q is the specific iron loss expressed in W/m^3,
R is the radius of the equivalent cylindrical iron core,
h is the static cooling co-efficient [W/m^2K]. An acceptable value to use is 10 [6.1],
A is the surface area of the iron core available fore effective cooling, and
k is the thermal conductivity in W/mK.

The core temperature of each design was checked using the maximum allowable limits which is 120 °C for the surface temperature and 145 °C anywhere else in the core. In this case, the core temperature rise is not a limiting factor in the design. Techniques of cooling the core to satisfy the AS2374 requirements are discussed in Chapter 5.

6.3.3 Eddy current loss in the sheathing material of the superconductor

Providing that an HTS tape is not in the skin effect regime, the eddy current loss in a portion of alloy sheathed HTS conductor is given by Equation 6.11 [2.6].

$$Q_{eddy} = f.(\pi/3).(2.\pi.f).B^2.a^2.(1/\rho).(1+3i^2/8) \quad [W/m^3] \quad \text{Eq. 6.11}$$

Where,
Q_{eddy} = eddy current loss per unit volume of sheathing material
ρ = resistivity at 77 K of the sheathing alloy
B = the magnetic field
2a = tape width for fields perpendicular to the tape or thickness for parallel fields
i = reduced transport current = (Irms*1.414)/Ic.

This component of loss is small compared to the hysteresis loss, and therefore, will not be included in this initial design study. Eddy current loss will become important compared to the hysteresis loss if high field amplitudes and frequencies are used. In addition, it has become common practice to include higher resistance alloys in superconducting sheaths to increase the resistivity, which in turn reduces the magnitude of the induced eddy currents and therefore eddy current losses.

6.3.4 Magnetic field distribution in transformer coils

Each one of the components of HTS tape AC loss discussed are significantly dependent on the relative direction and magnitude of the magnetic field generated. The magnetic field experienced by each turn of tape will be a complex function dependent on the position of the turn within the coils (r,z), the transport current present in the primary and secondary (I_p,I_s), the geometry of the transformer, the magnetising current, I_{mag}, and the orientation of the primary and secondary with respect to each other. In this analysis, the magnetic field of the magnetising current was ignored, as this is usually only a small fraction of the primary current. All non-fundamental components of the flux were also ignored.

The software package used to carry out the FEM analysis allowed multiple interconnected 3D objects to be drawn in 3D space, and their low frequency electromagnetic properties to be specified. The boundary conditions, although specifiable, were not required to be explicitly stated in the 3D version. The coils were drawn as perfect cylinders with a specified height, inner diameter, and outer diameter. This predetermined the field profiles to have cylindrical symmetry and this will be exploited later to simplify the calculations of the hysteresis losses.

The current terminals were drawn using a slice through the Z plane to create 2D planes intersecting the coil cross section. The number of turns was implicitly specified by assigning the current equal to the number of turns times the actual transport current in the coil. These assumptions gave an accurate calculation of the magnetic field at each position within the winding cross section. However, no details of the magnetic field in between tape turns can be obtained using this technique.

The iron core is drawn as a union of three perfectly cylindrical iron limbs and two perfectly cylindrical iron yokes of the same diameter, as shown in Figure 6.2. No

information regarding the joining technique, or laminations is specified in the FEM model. Since the exact field details outside the coils or very close to the iron cores are not of interest, only the correct volume and placement of iron is important, hence a cylindrical approximation is sufficient and will not give significant errors for the field inside the coil windings themselves.

A useful feature of the software was the ability to automate the whole procedure of drawing items by executing macros. In this project, many different designs were analysed before a optimised solution was found. By parameterising the transformer core and coils into nine variables, shown in Table 6.1, a general macro was written that allowed a new transformer design to be drawn rapidly.

Parameter	**Variable name in Macro**
Inside diameter of the primary coil	IDP
Outside diameter of the primary coil	ODP
Inside diameter of the secondary coil	IDS
Outside diameter of the secondary coil	ODS
Height of the primary coil	Hp
Height of the secondary coil	Hs
Length of the yoke	Yoke length
Height of the limb between yoke extremes	Height
Radius of iron core	Core radius

Table 6.1. Parameters used in the FEM macro to specify each transformer.

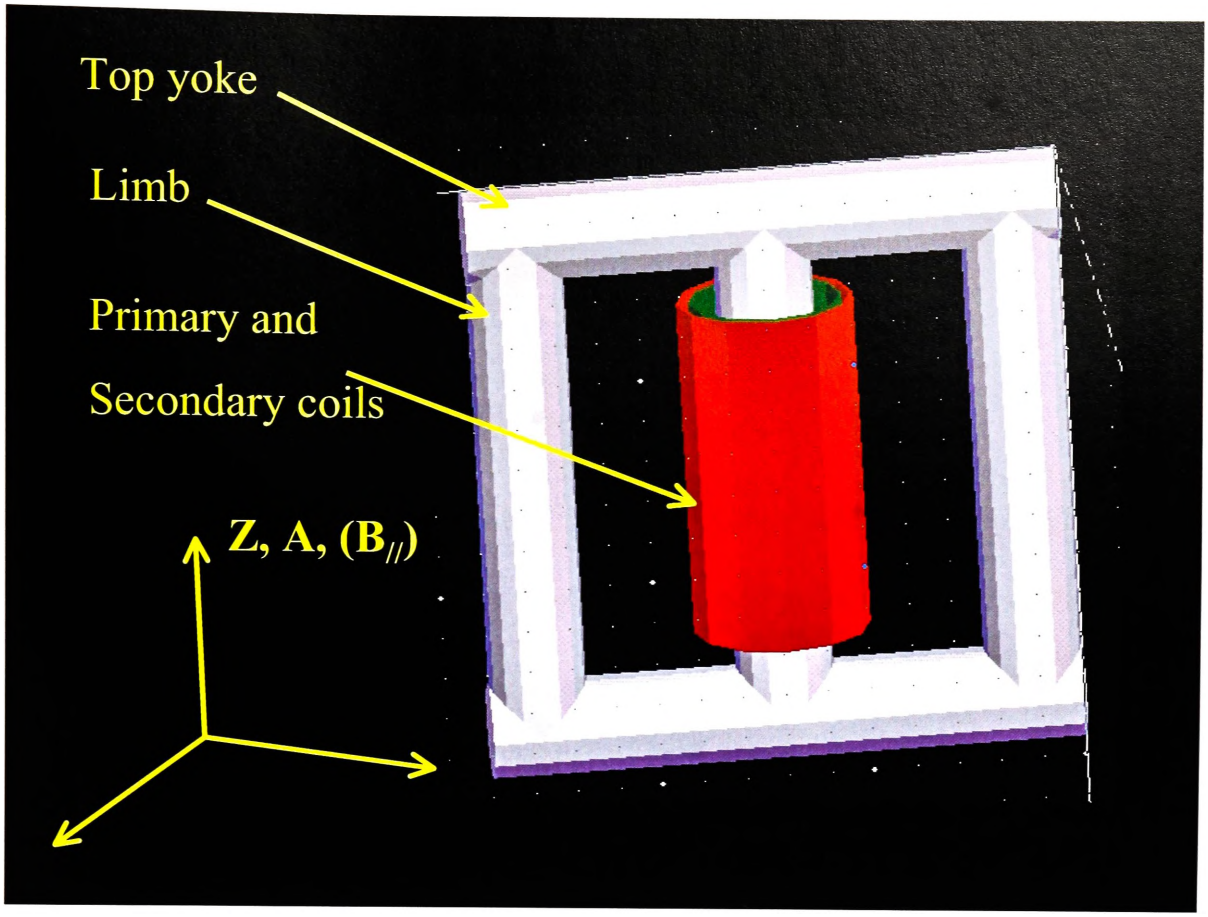

Figure 6.2. Drawing of the iron core and coil model used in the FEM analysis, showing the perfect cylinders used for the iron cores, and the cylindrical shells used to represent the windings. Primary coil is shown in green, secondary coil in red.

The cryostat was not included as it was intended to be made of a composite and therefore did not contribute or alter the magnetic fields.

The output of the FEM analysis was available as a three dimensional vector at any point on a three dimensional grid in the form of Equation 6.12.

$$B_{3D} = B_x\underline{\mathbf{i}} + B_y\underline{\mathbf{j}} + B_z\underline{\mathbf{k}} \quad \text{Eq. 6.12.}$$

Where B_x, B_y, B_z are the components in the x,y, and z directions, and

$\underline{\mathbf{i}}$, $\underline{\mathbf{j}}$, $\underline{\mathbf{k}}$ are the unit vectors along the x,y,z directions respectively.

The data was exported and manipulated in a Visual C program to convert it from a three dimensional to a two dimensional vector with components parallel and perpendicular to the tape surface, according to Equation 6.13.

$$B_{2D} = B_{//}\boldsymbol{\phi} + B_{\perp}\mathbf{r} \quad \text{Eq. 6.13}$$

Where
$B_{//} = f(B_x,B_y,B_z)$,
$B_{\perp} = g(B_x,B_y,B_z)$,

The unit vector **r** is perpendicular to the HTS tape at each point and is parallel to the C axis of each portion of tape. The unit vector $\boldsymbol{\phi}$ is defined as being parallel to the tape at each point, *i.e*, in the A-B plane of the tape.

The simplest way to transform the magnetic field profile from the three dimensional form of Equation 6.12 to Equation 6.13 was to utilise the cylindrical symmetry, and evaluate Equation 6.14 for each turn.

$$B_{2D} = (B_y^2+B_z^2)^{1/2}\,\boldsymbol{\phi} + B_x\,\mathbf{r} \quad \text{Eq. 6.14}$$

6.3.5 Estimated hysteresis losses from the field profile

The hysteresis losses associated with the parallel and perpendicular components of the magnetic field on each turn were calculated using the Equations 2.1-2.3. The loss was calculated for each turn, and then integrated over the entire coil. It has been shown that the specific losses associated with $B_{\perp}$ are about an order of magnitude greater than those from $B_{//}$ [6.3-6.5]. Hence, it is clear that any HTS coil design for a transformer should minimise the influence and extent of $B_{\perp}$ as far as possible, while at the same time keeping the cost, weight, and volume to an acceptable level.

Equation 6.14 is valid assuming a cylindrically symmetric field profile throughout the coil volume. If this approximation had not been made, then the complexity of calculating the hysteresis loss increased, and the loss would have to be integrated across the whole tape length.

6.3.6 Transport current loss

The ratings of the primary and secondary coils are 5.1 A and 140 A respectively. The Ic of the primary and secondary coils were designed so that the transport current amplitude was 85% of the Ic (77 K, self field). Hence, the required Ic of the tape in the coils was 10.3 and 282 A respectively which is about twice the rms transport current rating. This type of design has been shown to give reasonably small increases in the total loss of tapes subject to an external field less than 0.1 T and with a transport current compared to just the hysteresis loss component [1.43,6.6-6.8]. The results of Carr offer a first approximation for this component of loss in parallel fields if the hysteresis loss is independent of the transport current loss. Semi-empirical models, such as those used by Rabbers [6.5] and Hörnfeldt [6.8] or detailed FEM calculations such as those of Amemiya [6.9] and Passi [6.10] are the only way to estimate the total loss in the complex situation of a transformer coil. Due to the considerable work this would entail, the results of Carr were used to estimate the transport current loss for the final chosen transformer design only and hence only the hysteretic loss component of the transport current loss was considered and not the dynamic resistance component [see 1.2.8]

6.3.7 Total hysteresis losses in a HTS Transformer

The total hysteresis loss of each design was calculated using the following steps:

1. The magnetic field distribution across the coils was calculated using FEM analysis.

2. The magnetic field profile was transformed into $B_{//}$ and $B_{\perp}$ components on each turn according to equations 6.13 and 6.14.

3. Hysteresis loss figures due to the perpendicular, $q_{\perp}$, and parallel, $q_{//}$, components of the field were calculated for each turn using Equations 2.1 – 2.3.

4. The components found in (3) were summed over all the turns in the design to arrive at a total perpendicular, $Q_{\perp}$, and parallel, $Q_{//}$, hysteresis loss figure for the coil.

6.4 Final Design considerations

6.4.1 Leakage reactance calculations

The leakage reactance, although normally the factor which determines many features of a transformer design, was not made a specific design parameter that needed to be met. By relaxing this constraint, the possible ranges of reactance and its relationship to other parameters could be explored. In addition, the range of leakage reactance's in practical 100 kVA transformers can be between 2 and 20% and choosing one would be an artificial choice and a limitation on the design study. In conventional transformer design, leakage reactance is one of the first considerations, and is usually specified by the customer as a percentage impedance referred to the primary side, as in Equation 6.15.

$$X_l = Xl_p + a^2 Xl_s \quad \text{Eq. 6.15}$$

Where X_l is the total leakage reactance, Xl_p is the primary coil leakage reactance and Xl_s is the secondary coil leakage reactance, and a is the turns ratio, N_p/N_s.

In classical transformer design, a very simplified formula exists which calculates the leakage reactance very accurately for simple conventional designs of equal heights, H, as shown in Figure 6.3.

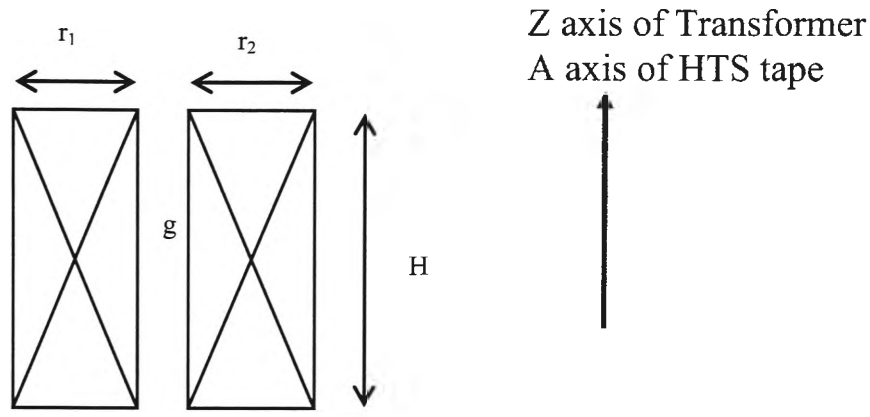

Figure 6.3. Profile view of a simple two winding transformer, showing one side of the coil sections in R-Z space.

The formula uses the simple geometry for the coils and the mean length per turn, L_{mt}, to calculate the leakage reactance of each coil within a phase according to Equation 6.16.

$$X_l = 2\pi f \mu_o N^2 L_{mt}(g/2+r/3)/H \quad \text{Eq. 6.16}$$

Where:
g is the primary to secondary coil gap,
r is the annular thickness of the coil under consideration, r_1 or r_2,
$N = N_p$ or N_s for the primary and secondary coil turns respectively, and
L_{mt} = mean length per turn for either coil.

Another Equation used by a transformer manufacturer is [5.5, 6.1]:

$$X_l = P*\pi/25.4*[D_1.(r_1/3)+D_2.g+D_3.(r_3/3)]/(3*H_e*q^2) \quad \text{Eq. 6.17}$$

Where all the dimensions are in millimetres, and:

r is the annular thickness of the coil under consideration, r_1 or r_2,
D_1 and D_2 are the mean diameter of each section,
P is the kVA of the transformer,
q is the volts/turn,
H_e is the effective length of the leakage flux path given by Equation 6.18.

$$H_e = H + (r_1+g+r_2)/3 \quad \text{Eq. 6.18}$$

There is no inherent reason why these formulas should not also apply to HTS coils, however, it was unknown whether they are a satisfactory approximation for the smaller annular thickness of the coils encountered in HTS designs. Hence, the leakage reactance was calculated from first principles as a check.

The leakage reactance was found from the inductance matrix of a primary and secondary coil, which was obtained directly from the FEM software from the total stored energy when each coil was energised in turn. The expression for the total energy stored when both coils were energised is as follows:

$$E_{tot} = (1/2)L_{pp}I_p^2 + L_{ps}I_pI_s + (1/2)L_{ss}I_s^2 \quad \text{Eq. 6.19}$$

Where:
L_{pp} is the self inductance of the primary winding,
L_{ss} is the self inductance of the secondary winding,
L_{ps} is the mutual inductance of the windings,
I_p and I_s are the primary and secondary rms transport current respectively.

The model used in the FEM analysis was a simple block of conductor with a forced even current distribution to simulate conductivity in a coil with insulated turns, the values of inductance obtained, L_{pp}',L_{ps}', and L_{ss}' from the software were converted to the actual values, L_{pp}, L_{ps}, and L_{ss} as follows:

$$L_{pp} = N_p^2L_{pp}' \quad \text{Eq. 6.20}$$
$$L_{ps} = N_pN_sL_{ps}' \quad \text{Eq. 6.21}$$
$$L_{ss} = N_s^2L_{ss}' \quad \text{Eq. 6.22}$$

The self inductance and the leakage inductances of the primary and secondary coil, L_{lp} and L_{ls}, were then found from the mutual inductance, L_{ps}, as follows:

$$L_{lp} = L_{pp} - aL_{ps} \quad \text{Eq. 6.23}$$
$$L_{ls} = L_{ss} - L_{ps}/a \quad \text{Eq. 6.24}$$

The net leakage inductance in the more familiar per unit (p.u.) form was calculated from Equation 6.25.

$$X_l = (2\pi f L_{lp} + a^2 2\pi f L_{ls})*(I_{ph}/V_{ph})*100 \quad \text{Eq. 6.25}$$

Where I_{ph} and V_{ph} are the current and voltage ratings of the transformer coil.

6.4.2 Iron core considerations

The main choices available for core shapes appropriate for a 3 phase transformer, and their advantages are described below. There are two problems which must be considered when choosing the core design, and these are also affected by the manner in which the three phases are connected, *i.e.* generally a star connection, with/or without a neutral.

The first problem is that of 50 Hz flux impinging on the windings. The components of 50 Hz flux from the secondary and primary coils oppose each other, and this reduces the magnetic field, B, on the coils considerably compared to that in the main leakage flux path where they enhance each other. If however, there are un-balanced loads, then the ampere-turns from the unbalanced phase will not necessarily be compensated in all cases with the equivalent ampere-turns in the primary. Hence, the magnetic field will be greater on those windings which will in turn increase the hysteresis loss as this is directly proportional to B and B^2.

The second problem is that of the odd third harmonics caused by the presence of the iron core. These can appear as third harmonic components in the transport current, or in the iron core flux, or in the leakage flux, or all three. The total AC losses of the coils basically follow a relationship such as $(\alpha f B + \beta B^2 f^2) i^2$, [W] therefore, clearly, it would

be best to minimise all third harmonic magnetic fields and transport current as far as possible.

There are two types of transformer core which were considered for this project, namely, the three limb core type and the shell type. Their particular advantages and disadvantages as they pertain to HTS transformers are discussed below.

The three limb core structure has a magnetic star connection, and the fundamental of the core fluxes are forced to balance out. Any un-balanced flux is compelled to take a leakage path (*i.e.*, through the air, and therefore the coils). The voltage phasors are forced to balance at the expense of the current phasors. In an unbalanced load situation, the un-compensated ampere-turns will lead to the windings of that phase being exposed to a larger than normal flux. This will increase the AC loss and this component will need to be minimised and designed for if it is found to be significant.

The disadvantage of the three limb core is also that there is no return path for the odd third harmonic flux, which therefore must return through a leakage path. Since the coil AC losses will follow a relationship $(\alpha fB + \beta B^2 f^2)i^2$, then this component of magnetic field must also be estimated and designed for in this situation. However, if the transformer were connected in a star - star arrangement without a neutral conductor, then the currents will be constrained to be perfectly sinusoidal, at the expense of distorting the phase voltage waveforms with third harmonics, (but not the line-line voltage).

In a shell type core, the 3 phasors of flux are not forced to balance when an un-balanced load exists. Instead, the voltage phasors take up an unbalanced distribution. The advantage of the shell type (and the 5 limb core type) is that these cores have a magnetic return path for the odd third harmonic core flux. This means there will only be

third harmonic transport current components to increase the loss, but negligible third harmonic magnetic field components.

A single phase on a three limb core or a shell type will provide a situation where there exists third harmonic magnetising currents and purely fundamental 50 Hz flux in the core. The leakage flux however, must have a third harmonic content (since the magnetising current has a third harmonic) and therefore the windings will be in a flux which contains a third harmonic component of magnetic field.

Figure 6.2 shows the basic design of the transformer considered. The cryostat and the other two phases are not shown for clarity. The spacing included in the dimensional analysis is sufficient for three individual cryostats each holding a primary coil at 6.6 kV and a secondary coil at 240 V.

6.4.3 Design of the current carrying conductors

There are three possible techniques to accomplish uniformity of current distribution, however, not all are appropriate for the HTS tapes. Each will be described with reference to a three tape conductor.

Asymmetric transpositioning, Figure 6.4, describes the case when the two outer wires are alternatively lapped over and under the centre wire.

Figure 6.4. Asymmetric transpositioning

The impedance of each layer is approximately the same as the central wire because the radius changes from slightly smaller than the average (giving a larger impedance for

that section) to slightly larger that the average (giving a smaller impedance for that section). To carry this out continuously would require specialised equipment and a very large pitch to reduce the lateral strain (bending within the plane of the tape) to acceptable values.

Plaiting, Figure 6.5, is referred to the case where the outer wire at any point is alternatively lapped over the centre wire.

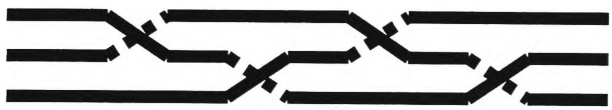

Figure 6.5. Plaiting of conductors

Symmetric transpositioning of conductors is where the wire on the outer side is alternatively place over the top of the other two wires in the plane of the tape.

Figure 6.6. Continuously transposed conductors.

This is analogous to the Litz or Roebel type conductors available for conventional transformers and is also referred to as continuously transposed conductor, or CTC. In all cases, the pitch must be sufficiently long to prevent degradation of the conductor Ic. Alternatively, only discrete transpositioning events need to be included during the winding in-order to accomplish a uniform current distribution [6.11]. This option was identified as the best for HTS tapes as it minimises the strain on the tape and the requirement for specialised winding equipment. To obtain a uniform current distribution in a conductor consisting of N tapes, a total of N-1 transpositioning events is required in each layer of a solenoid winding.

6.4.4 Deciding on a final design.

The iterative steps used in coming to a final design for a HTS transformer are shown in Figure 6.7. The coil losses ultimately governed the decision on the final design, although the other constraints were also simultaneously applied.

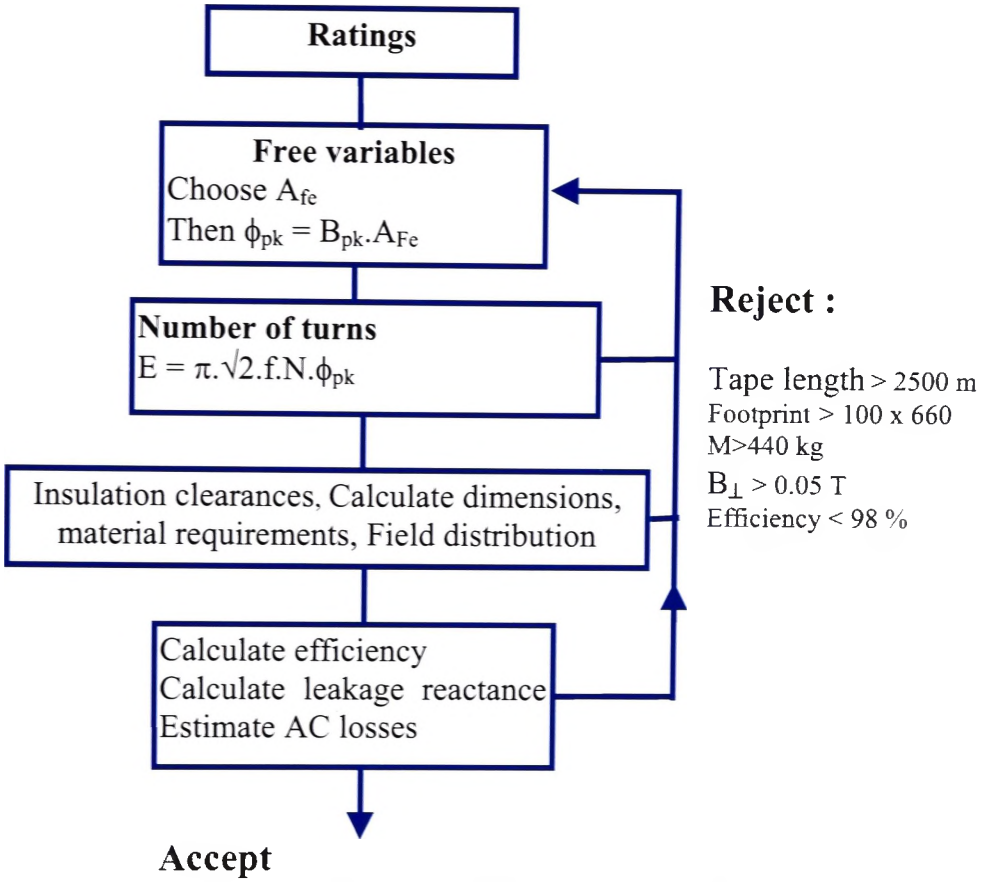

Figure 6.7 Iterative procedure for deciding on a final design of the HTS transformer

6.5 Results and Discussion

6.5.1 Results of the dimensional analysis

Figure 6.8 shows the plots of M,V, and L over a range of A for small shape factors (S = 1:2, 1:1 and 2:1). Figure 6.9 shows the plots of M,V, and L over a range of A and larger shape factors (8:1 and 1:10) with the 1:1 shape factor case included again for comparison. The range of core areas shown is equivalent to core diameter of 0 to 16 cm.

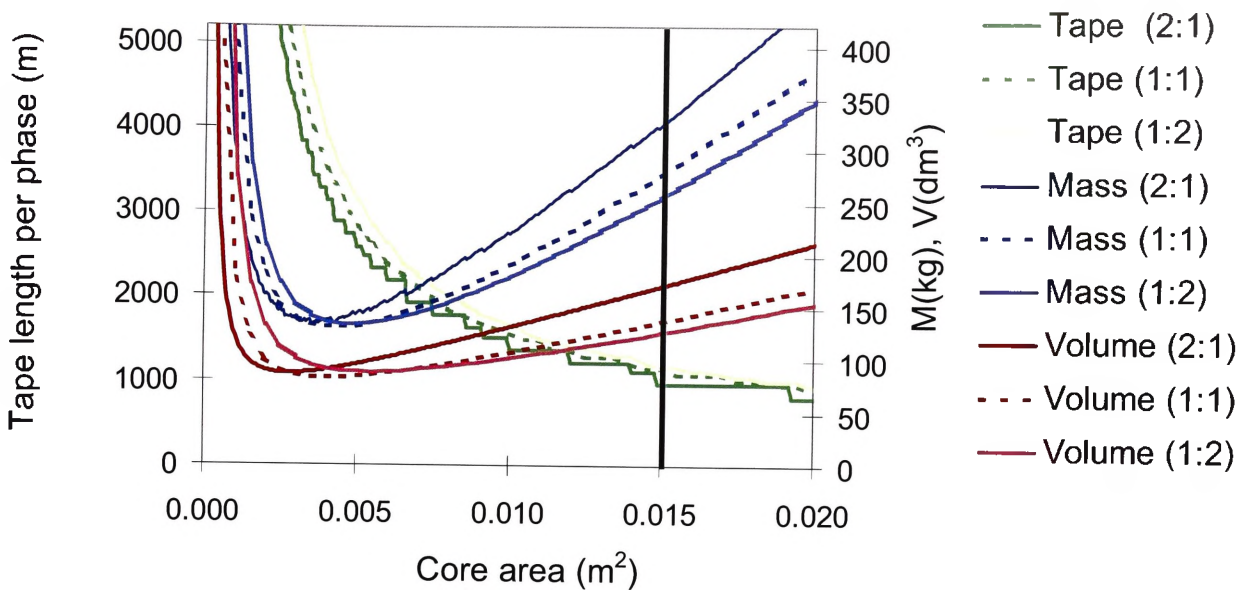

Figures 6.8. Results of the dimensional analysis for low shape factors.

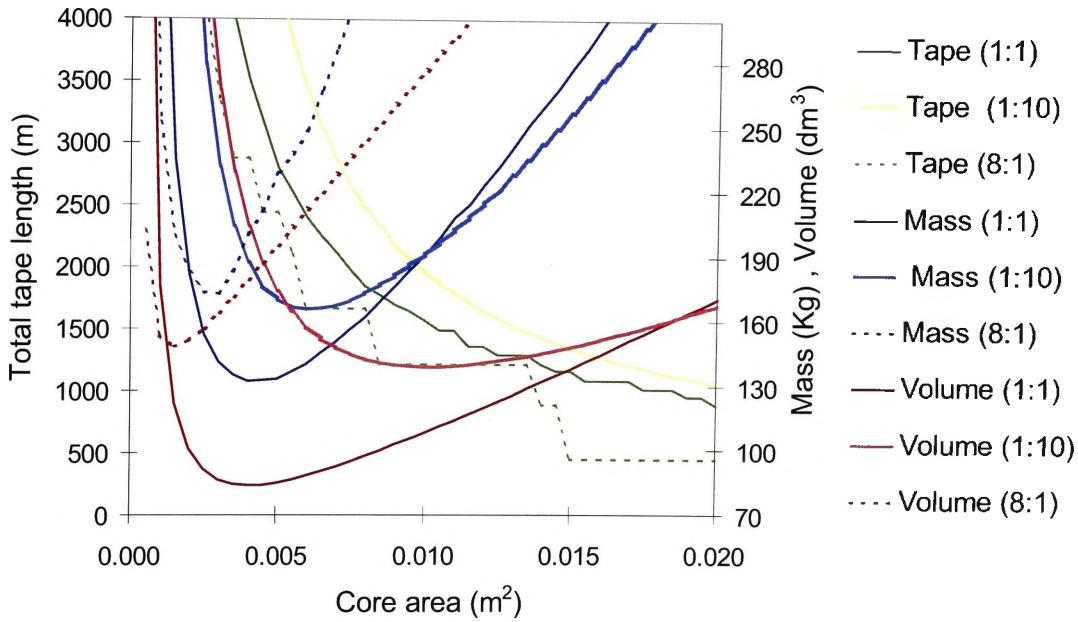

Figure 6.9. Results of the dimensional analysis for high and low shape factors.

Figures 6.8 & 6.9 show the presence of distinct minima in the mass and volume, for each shape factor, S, in the range of core cross sectional areas from 0.001m^2 to 0.010 m^2. To the left of each minimum, the largest contribution to the mass is from the HTS tape itself and is reflected in the large tape length requirement. To the right of each minimum, the high mass is a result of the large quantity of iron in the design. At each minimum, the mass of HTS tape and iron were equal.

Figures 6.8 and 6.9 show that the minima of the mass and volume do not match at the same core areas, so a design that fulfils exactly both minimum mass and volume was not possible. The minimum mass for a particular shape factor always occurs at a greater core area than the minimum volume. This was due to the fact that the minimum volume design required a larger amount of tape which in turn leads to coils with larger outer diameters, and therefore longer yokes to accommodate all three phases. The minimum mass design required less tape, which leads to a smaller outer diameter of the coils and consequently shorter and lighter yokes. Figure 6.10 shows the variables M,V,L,A at the minimum volume for each shape factor.

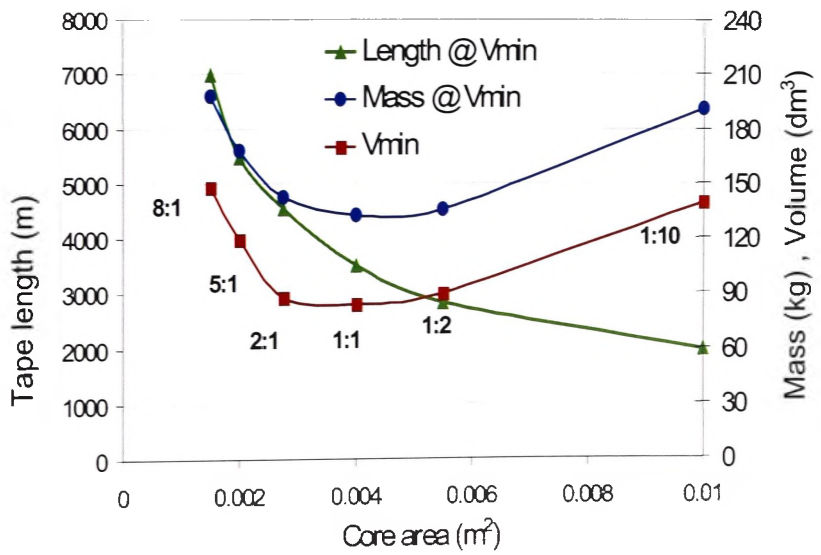

Figure 6.10. Plot of M, L, and V at the points of minimum volume for each S.

At first sight, it appears that the best choice of core area would be that which minimises the enclosed volume, that is, coils with a 1:1 shape factor and a core area of 0.004 m^2, however, as can be seen this would require a large amount of tape (~ 3500 m per phase). This would increase the cost of the transformer significantly. In addition, since iron is much cheaper than HTS tape, it is logical that a practical design would be to the right of the minima and have a larger than optimal core area. This compromises on minimum mass and volume for the sake of a cheaper design, but should still be smaller and lighter than a conventional transformer. It can also be seen that this does not necessarily increase the total volume significantly from the minima. For the low shape factor designs, figures 6.8 and 6.9 show that the increase in V with A is very slow to the right of the minima compared to the left. In addition, there is a considerable drop in tape length with only minor increases in A.

The shape factor played an important role in the design of the HTS transformer. For a low shape factor (1:10), the coils were flat and wide and have a relatively large annular thickness. This increased the yoke length and results in a shorter limb length. Hence the rise in mass with A is low compared with high shape factor coils (eg. S=10:1). The cryostat spacing requirements, particularly the space allowance from the top of the cryostat to the liquid level and from the liquid level to the top of the coils , and also the phase to yoke insulation gap are fixed for the voltage of the transformer. Therefore, the volume at the minimum point for low S coils is larger than for high S coils.

Tables 6.2 and 6.3 give the mass and volume of the transformer for minimum volume and minimum mass respectively for the range of shape factors considered.

Shape Factor (S)	Core area at minima Volume (m^2)	Mass at minimum volume(kg)	Minimum Volume (dm^3)	L @ min Volume (m)
8:1	0.0015	197.44	147.8	6978
5:1	0.002	167.97	119.3	5464
2:1	0.00275	142.1	87.4	4542
1:1	0.004	132.2	83.8	3508
1:2	0.0055	135.71	89.3	2827
1:10	0.01	190.86	139.0	1959

Table 6.2: The transformer designs for each shape factor which give minimum volume.

Shape Factor (S)	Core area at minima Mass (m^2)	Minimum Mass (kg)	Volume at Minimum Mass (dm^3)	L @ minimum mass (m)
8:1	0.00275	172.7	160.0	3711
5:1	0.0035	155.24	130.0	3028
2:1	0.0035	136.58	88.7	3544
1:1	0.0045	132.44	84.1	3157
1:2	0.005	134.84	89.4	3113
1:10	0.0065	165.6	157.0	3405

Table 6.3: The transformer designs for each shape factor that gives minimum mass.

To proceed towards the final design, a decision was made on the total acceptable cost and length of the conductor, and design chosen to meet these criteria while still being smaller and lighter than a conventional 100 kVA transformer. Tables 6.2 and 6.3, and Figure 6.10 show that low shape factor coils should be used (1:2, 1:1, and 2:1), however, there are still an infinite number of choices of core area to choose from. To fix this parameter, a decision must be made as to the total amount of tape which will be acceptable in the design and this was largely based on cost considerations. To analyse this, two different lengths of HTS tapes were used in the design study, in particular 1500 m and 2500 m per phase. Figure 6.11 shows the mass and volume variation with

core cross sectional area of a 100 kVA transformer with a fixed length of 1500m and 2500m of tape per phase.

Designs 4-6, with 2500 m of tape, allowed a smaller core area to be employed and therefore both the mass and volume of these designs for each shape factor were smaller than designs 1-3. It can be seen that reducing the amount of tape in the coils from 2500 m to 1500 m significantly increases the mass by 45 % (from 138 kg to 199 kg), however, the volume only increased by 27% (from 87.1 dm^3 to 110.0 dm^3).

From this exercise, the practical range of dimensions that specify the HTS transformer was reduced to the following set by using dimensional analysis alone and allowing for a reasonable cost represented by a HTS tape length of between 1500 and 2500 m.

$\{S\} \in (1{:}2 \leq S \leq 2{:}1)$
$\{A\} \in (0.005 \leq A \leq 0.011)\ m^2$
$\{L\} \in (1500 \leq L \leq 2500)$ m per phase

which has a range of transformer parameters:

$\{M\} \in (137.5 \leq M \leq 214.8)$ kg
$\{V\} \in (87.1 \leq V \leq 129)\ dm^3$

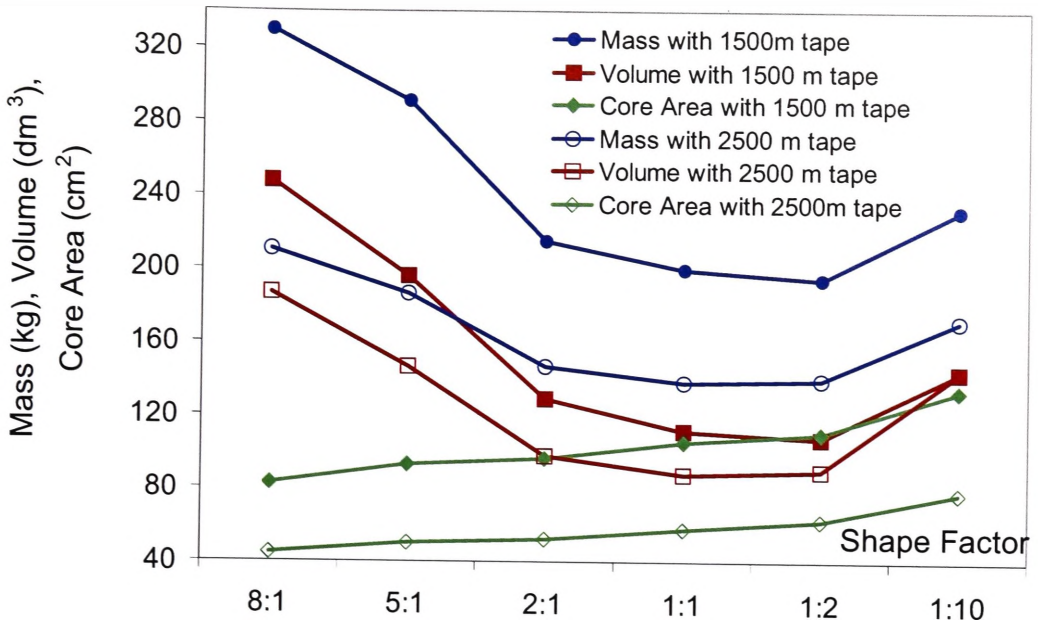

Figure 6.11. Mass, Volume, and tape length with a fixed 1500 m and 2500 m of tape for each coil versus the shape factor.

The dimensional analysis reduced the possible set of designs to six with the following parameters shown in Table 6.4. Each design has been adjusted to ensure an integer number of turns and equal turns ratio and A for each total tape length considered.

No.	L (m)	S	Np	Ns	A (m^2)	M (kg)	V (dm^3)
1	1500	2:1	1815	66	0.0094	215	129
2	1500	1:1	1815	66	0.0094	199	111
3	1500	1:2	1815	66	0.0094	194	107
4	2500	2:1	3300	120	0.0051	146	98
5	2500	1:1	3300	120	0.0051	138	87
6	2500	1:2	3300	120	0.0051	139	90

Table 6.4. Set of 6 candidate designs decided by dimensional analysis

6.5.2 Results of the FEM analysis

In order to assist in deciding on a final practical design, the magnetic field distribution on the tape turns within the coils of the six designs were mapped. This will ultimately determine the coil loss and therefore whether the design is practical from a cryogenic

point of view. The magnetic field FEM plot of a typical coil set considered here is shown in Figure 6.12.

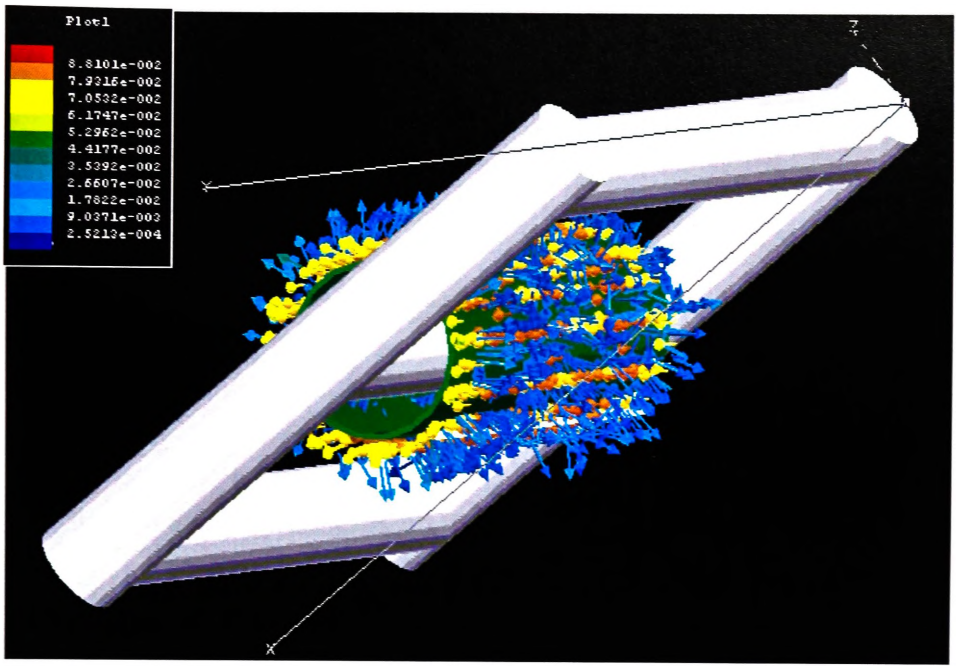

Figure 6.12. Typical graphic on the FEM software field plot screen.

The vectors are exported at every cubic millimetre and the components of field parallel and perpendicular to the tape at each of the points within the coil volumes were calculated using Equation 6.14. These components are shown plotted for designs 1 and 6 in Figures 6.13 and 6.14 respectively. These two cases represent the extremes of tape length and shape factor among the 6 chosen designs. Each point in Figure 6.13 and 6.14 represents the component of field on the tape within the coil at a particular grid point, r,z within the cross section of the coil. Appendix 4.4 gives the field profiles of the other designs.

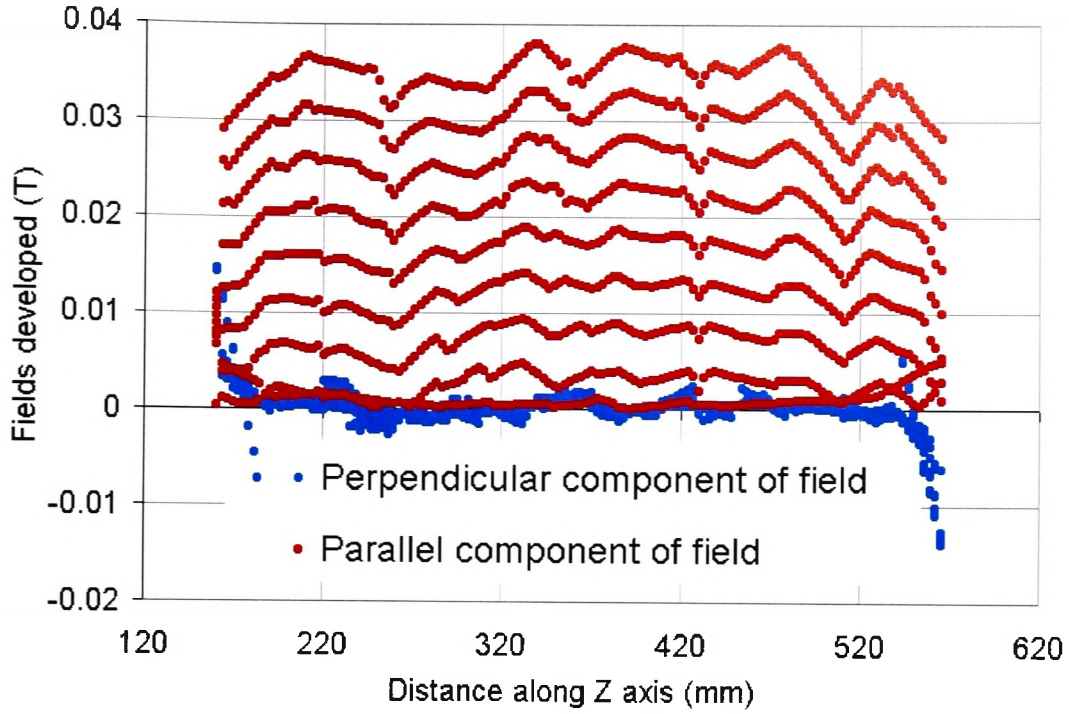

Figure 6.13. Field amplitude components developed on the primary coil in Design 1.

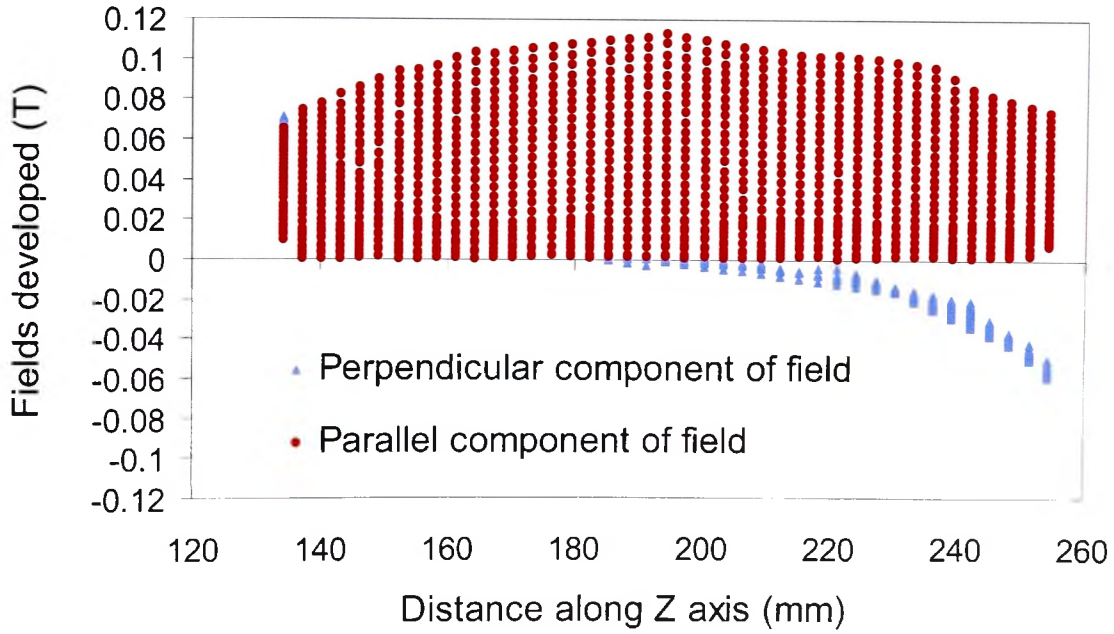

Figures 6.14. Field amplitude components developed on the primary coil in Design 6.

A summary of the results for each of the 6 chosen designs are shown in Table 6.4, along with the values of mass and volume, and plotted in Figure 6.15 to show the trend more clearly.

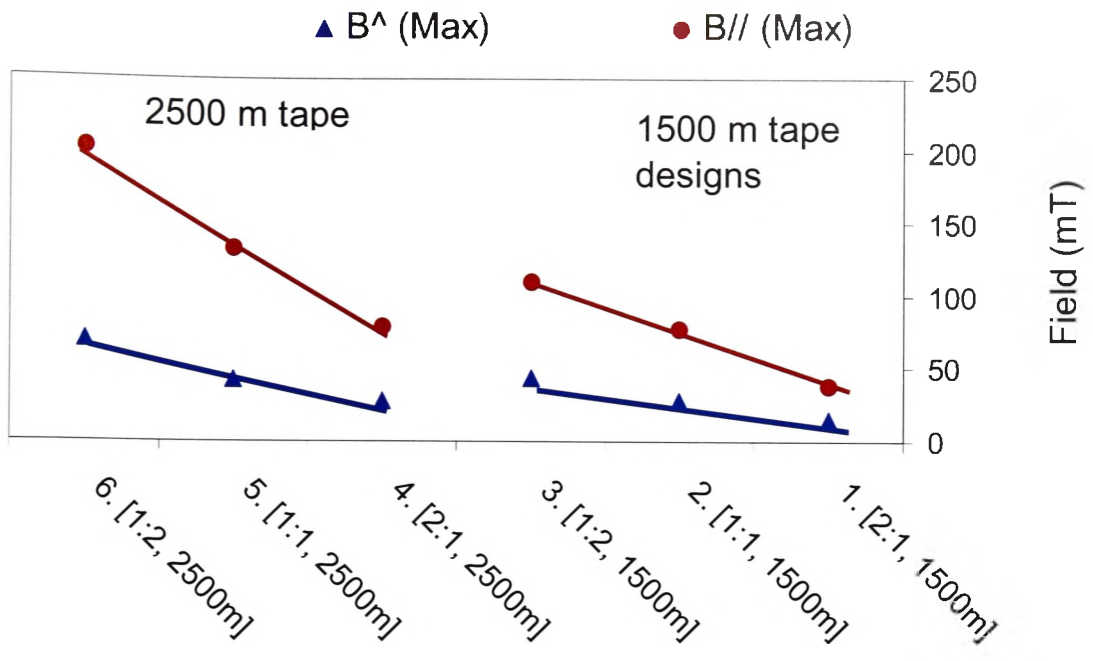

Figure 6.15. The maximum components of field amplitude on the primary coil for each of the six designs, $B_{//}$ and $B_{\perp}$.

No.	L	S	$B_{//}$ max Pri.	$B_{\perp}$ max Pri.	$B_{//}$ max Sec.	$B_{\perp}$ max Sec.
1	1500	2:1	38	15	31	10
2	1500	1:1	77	28	81	28
3	1500	1:2	110	44	120	44
4	2500	2:1	79	28	83	38
5	2500	1:1	133	43	144	52
6	2500	1:2	202	71	202	75

Table 6.5. Summary of magnetic field amplitude results for the 6 designs [mT].

The advantages of coils with S = 2:1 are clear from Table 6.5 and Figure 6.15. In longer coils (S = 2), both components of magnetic field are less than in shorter ones (S = 1/2). The parallel component of field decreased for longer coils because compared to shorter coils, long coils have less annular thickness. This means that each of the turns of the primary and secondary were closer to each other than if they were wound into short coils and hence, the fields that are produced individually cancel more effectively. In addition, comparing the data in Table 6.5 for coils of the same shape factor, but

differing tape lengths, designs with just 1500 m of tape had a maximum perpendicular field which was about 60% that of designs with 2500 m of tape.

In addition, the perpendicular component of the field is concentrated at the edge of the coils, with very little across the bulk of the turns. Hence, a much smaller relative portion of the longer coils are under the influence of this field component.

These effects, produced by the primary and secondary coils are only advantageous for the case for co-axial and concentric coils as previously shown in Figure 6.2. Primary and secondary coils placed in a sandwich arrangement (Co-axial, but not concentric) produce a situation where the perpendicular components of the magnetic field from each coil are additive within the winding volume of each coil. Figure 6.16, shows the magnetic field profile on the primary coil from a sandwich arrangement of coils in a 100-kVA transformer employing 2500 m of HTS tape/phase with S = 2.

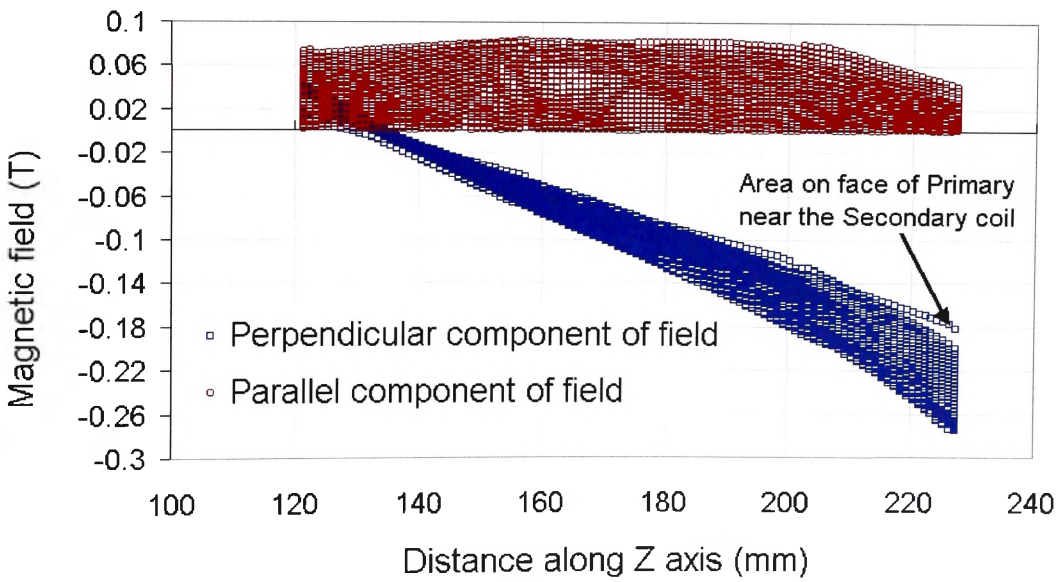

Figure 6.16. Magnetic fields generated in a sandwich coil arrangement.

The magnetic field profile that this arrangement produces in each coil winding is undesirable as the perpendicular fields are greater, with this component reaching 280

mT on the turns at the inner face of the primary coil, immediately opposite the secondary coil.

6.5.3 Results and discussion of hysteresis loss calculations

From the set of magnetic field data for each of the six designs the hysteresis losses were calculated for each turn of each coil and added to obtain the total hysteresis loss.

Table 6.6 summarises the results. The hysteresis loss of each full three phase transformer design is shown plotted in Figure 6.17, with the figures converted to the equivalent room temperature power required by a cryo-cooler. A cryogenic penalty of 16 was used.

No	L	S	$Q_{//}$ Pri.	$Q_{\perp}$ Pri.	$Q_{//}$ Sec.	$Q_{\perp}$ Sec.	$Q_{h.tot}$	$Q_{\perp tot}/Q_{h.tot}$	Iron loss
1	1500	2:1	5.87	1.88	3.50	0.68	**11.93**	0.21	330
2	1500	1:1	13.7	11.7	10.0	8.31	**43.72**	0.46	300
3	1500	1:2	40.4	83.8	15.4	29.8	**169.4**	0.67	293
4	2500	2:1	46.8	30.8	20.2	10.3	**108.1**	0.38	138
5	2500	1:1	42.9	61.2	33.7	42.2	**180.0**	0.57	128
6	2500	1:2	63.7	193.1	43.9	127.1	**427.7**	0.75	131

Table 6.6. Components of hysteresis loss for the six designs, [W/Phase].
$Q_{\perp tot} = Q_{\perp Pri} + Q_{\perp Sec.}$ The iron loss represents that for the full 3 phase device.

As can be seen, it was not necessary to calculate the full AC losses for each design (*i.e.* including transport current losses) to eliminate potential suitable candidates. An estimation of the hysteresis loss alone was sufficient for this purpose.

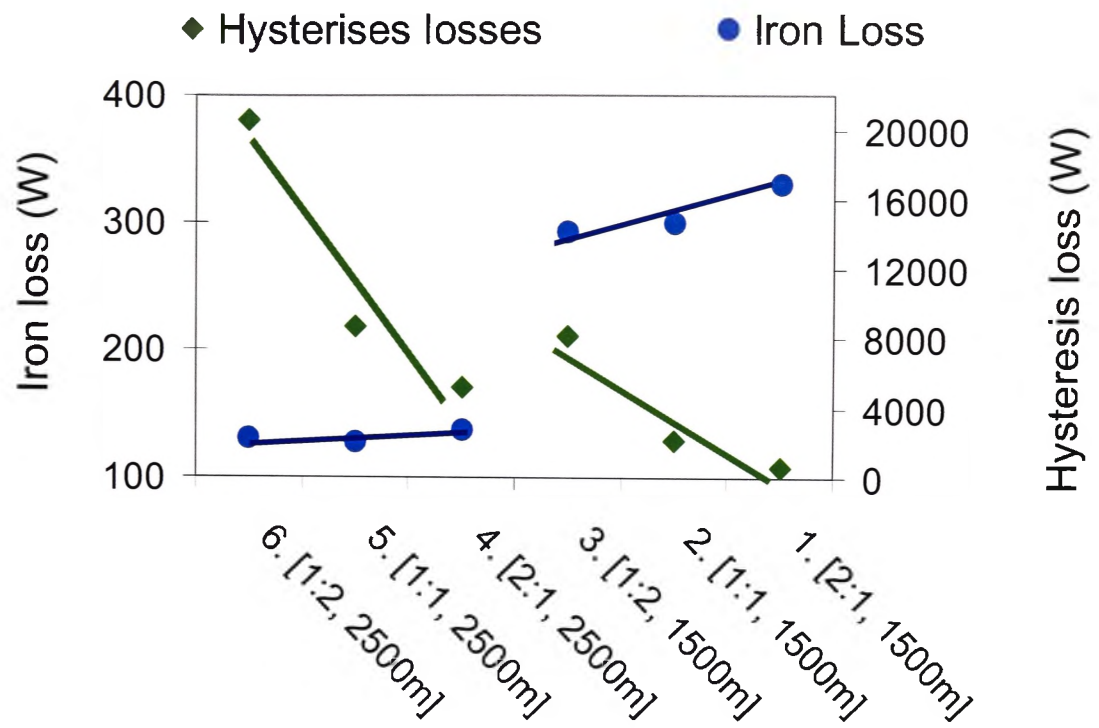

Figure 6.17. Losses for the six designs with the hysteresis loss now calculated as an equivalent wall power amount for a three phase device.

The benefit of coils with a shape factor of 2 as opposed to coils with lower aspect ratios is immediately obvious from Figure 6.17. The fact that each field component is reduced in this style of coil leads to the reduction in the hysteresis loss. The effect is most clearly demonstrated when comparing the differences between Design 1 and 6. When fully constructed, both of these designs would not look greatly different from each other. Design 1 would be slightly taller, and Design 6 would look a bit more squat in appearances, however, as can be seen Design 6 would be completely inappropriate to build because the hysteresis losses would be 36 times greater than Design 1.

The advantage in reducing the amount of tape in the design may also be seen in Table 6.6 and Figure 6.17. The total losses were reduced in the designs employing 1500m of HTS tape simply because there was less tape to contribute to the loss, and the fact that there were less ampere turns to produce the detrimental magnetic fields. These multiple factors reduced the coil hysteresis losses in long thin coils considerably, and will, as a

consequence reduce the transformer leakage reactance. The lower losses obtained by using 1500 m of tape instead of 2500 m, however, must be qualified against a suitable overall mass and volume. As Table 6.5 shows, with less tape used, the overall mass and volume of the transformer is higher with mass increasing quiet dramatically due to the higher cross sectional area of iron required. The increase in core loss that this extra iron produced is acceptable in the overall design because there is no cryogenic penalty associated with core losses.

The other major effect of using coils with a shape factor of 2:1 is that the ratio of $Q_{//}$ and $Q_{\perp}$ changes dramatically. For example, comparing Designs 1 and 3 which both employ 1500 m of HTS tape, it was found that $Q_{//}$ accounts for about 79% of $Q_{h\text{-}tot}$ in Design 1, while in Design 3, $Q_{//}$ accounts for only 33%. It is basically the perpendicular component of field which increases the hysteresis loss to an unacceptable amount in the designs with lower shape factors.

Owing to the nature of the magnetic field profile in co-axial, concentric coils, the hysteresis losses due to the perpendicular field component are severely concentrated at the top and bottom edges of the coil. Figure 6.18 shows the distribution of hysteresis losses in the Primary coil of design 1. This concentrated nature of $Q_{\perp}$ has lead some authors to propose ferro-magnetic rings, also know as flux diverters, to be used in close proximity to the windings to reduce this component of magnetic field and hence $Q_{\perp}$ [6.12-6.14]. Clearly, in the case of Design 1 here, such diverters would be of little benefit for significantly reducing the hysteresis loss, as $Q_{\perp}$ represents only 25% of the losses.

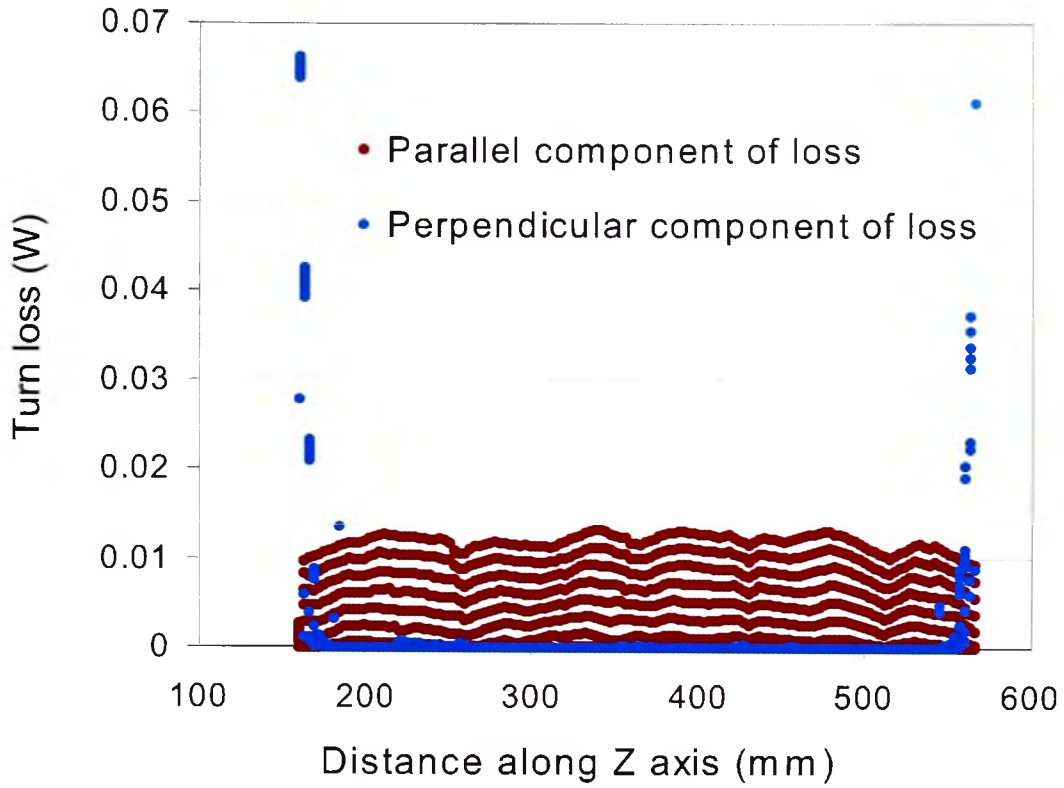

Figure 6.18. Hysteresis loss component distribution in the primary coil of Design 1.

6.5.4 Results of leakage reactance calculations

The leakage reactance results from the FEM analysis on the six designs considered here are shown in Table 6.7.

Design	L_{pp}	L_{ps}	L_{ss}	L_{lp}	L_{ls}
1500 m 2:1	158.1	5.80	0.213231	0.0355213	4.356e-5
1500 m 1:1	224.9	8.19	0.299452	0.0872618	1.077e-4
1500 m 1:2	242.8	8.88	0.326323	0.1441200	1.865e-4
2500 m 2:1	351.0	12.76	0.464524	0.1842734	1.568e-4
2500 m 1:1	426.4	15.57	0.569681	0.3505952	3.66e-4
2500 m 1:2	440.7	16.04	0.585350	0.5373912	6.05e-4

Table 6.7. Inductance of coils for the six designs from the FEM analysis [H].

The parameters used to estimate the leakage for all 6 designs are shown in Table 6.8.

Design	H (m)	r_1 (m)	r_2 (m)	g (m)
1500 m 2:1	0.405	0.0026	0.0042	0.01
1500 m 1:1	0.203	0.0053	0.00855	0.01
1500 m 1:2	0.121	0.0083	0.01335	0.01
2500 m 2:1	0.406	0.0053	0.00845	0.01
2500 m 1:1	0.203	0.0096	0.01545	0.01
2500 m 1:2	0.122	0.0146	0.02350	0.01

Table 6.8. Parameters used in Equations 6.16 and 6.17 to estimate the leakage reactance.

The results of the analysis using the three different techniques of leakage reactance calculation are shown in Table 6.9 after referring all values to the primary side and converting to p.u values. Equations 6.15 and 6.25 were used for this purpose.

No.	Design Code	X_l FEM (Eq. 6.19-6.25)	X_l (Eq. 6.16)	X_l (Eq. 6.17)	$Q_{h.tot}$ (W/phase)
1	1500 m 2:1	1.65	1.80	1.78	11.93
2	1500 m 1:1	4.07	4.59	4.38	53.72
3	1500 m 1:2	6.85	6.81	7.60	169.4
4	2500 m 2:1	7.35	7.45	7.22	108.1
5	2500 m 1:1	15.16	17.05	15.71	180.0
6	2500 m 1:2	24.10	31.94	27.13	427.7

Table 6.9. Per unit values (in %) of the leakage reactance of the six designs obtained by the three different techniques, compared to the hysteresis losses per phase.

As can be seen, the hysteresis loss increased as the leakage reactance increased because the leakage reactance depended strongly on the leakage flux density. The approximate leakage reactance calculation was suitable for lower values of reactance less than 0.15 p.u. where a better than 8% accuracy was obtained between the FEM result and Equation 6.17.

Power utilities installing new transformers in a sub-station will sometimes specify a high leakage reactance in order to assist in fault current limiting. This may typically be of the order of 15% [6.1]. Clearly, high shape factor designs are undesirable in this case, as it is difficult to achieve a high leakage reactance. Flux diverters, however, may assist in lowering the losses in high reactance coils with a low shape factor. For example, in Design 5 (see Appendix 4.4), the sum of the $Q_{\perp}$ components over 10 % of the winding volume of the complete coil accounts for 50 % of the total hysteresis losses. Hence, it is justified in these cases to reduce $B_{\perp}$ at the coil edges as far as possible in order to improve the efficiency of high reactance HTS transformers.

6.5.5 Effect of findings on the final design choice

Taking into consideration the issues of HTS tape length, and the transformer overall mass, volume, and efficiency, the final design was chosen with the following parameters. Shape factor = 2:1, Tape length = 1500 m per phase, Core area = 0.0094 m^2 which is Design 1 in Table 6.5.

These factors result in a transformer with a mass of 214.8 kg and a volume of 129.0 dm^3 and a full load 3 phase hysteresis loss of 36 W. Compared to the absolute minimum volume (S = 1:1, V = 83.8 dm^3, M = 132.2 kg, L = 3508 m), this design is 62% heavier and 54% larger in volume, but requires 2000 m less tape. The core and coil dimensions of this design are detailed in Table 6.10. It should be noted that this design employed tape with an assumed Je of 2000 A/cm^2, and further reductions in mass and volume will be possible if tape with a Je of 20,000 A/cm^2 was used. Design 5 would be suitable if a higher leakage reactance was required in a specification. however, this design would be significantly less efficient, and, due to the extra 1000 m of HTS tape. considerably more costly.

Dimension	Quantity	Unit
Coil arrangement	Core type	
Cross sectional core area	0.0094	m^2
Total Tape	1500	m/phase
Leakage reactance	1.78	%
Diameter of Core	0.1156	m
Inside diameter of secondary	0.1756 m	m
Outside diameter of secondary	0.1808 m	m
Inside diameter of primary	0.2008	m
Outside diameter of primary	0.2092	m
Coil Height	0.406	m
Boxed Volume	129	dm^3
Total Mass	214.8	kg
Limb Length	0.496	m
Yoke Length	0.6996	m
Primary turns	1815	Turns
Secondary turns	66	Turns
Primary phase current	5.1	A rms
Secondary phase current	140	A rms

Table 6.10. Full details of the 100-kVA transformer Design 1

Appendix 4.6 shows a graphical summary of the procedures which were followed here to arrive at this final design.

6.5.6 Results of full load efficiency calculations on Design 1

An estimate of the full load losses and efficiency of the 100 kVA transformer was made by including the transport current losses. This was approximated by using an expression for the total losses for each turn in terms of the field on each turn, the angle the field makes with the tape, and the transport current in the tape [1.39,6.3]. The transport current loss at full load was estimated to be 11 W per phase. The total coil losses at full load are therefore estimated to be 23 W. Table 6.10 shows all the loss contributions in Design 1 required to calculate the full load efficiency of this design. The current lead

loss of 13 W is an approximation gained from experience with the MBC where leads were designed with 0.045 W/A loss.

Variable	Amount (W)
Hysteresis losses per phase	12
Transport current loss per phase	11
Core loss	330
Heat leak losses	12
Current lead losses	13

Table 6.11. Summary of the estimated losses in Design 1.

The total losses in terms of the power required by a cryocooler operating at a 1:16 efficiency to re-condense the LN may then be calculated from the expression,

$$Q_{tot} = \{[(12 + 11)*3]+13+12\}*16 + 330 = 1834 \text{ W} \quad \text{Eq. 6.26}$$

Hence the full load efficiency of the three phase device is estimated to be 98.2%.

There is ample evidence in the literature and from the work in this thesis (Chapter 2) to show that twisted filament HTS tapes can significantly lower the parallel field component of hysteresis loss owing to power frequency AC magnetic fields in the range of 10 to 60 mT [2.3,2.5]. In Design 1, if the hysteresis loss component were reduced by a factor of three, and the transport current loss halved, which is reasonable based on the evidence found in this work and others, then the loss would be reduced to 1210 W as shown in the expression,

$$Q_{tot} = \{[(4 + 6)*3]+13+12\}*16 + 330 \quad = \quad 1210 \text{ W} \quad \text{Eq. 6.27}$$

and therefore the overall efficiency of Design 1 would increase to 98.8%.

Hence, the use of twisted filament HTS tape in appropriately designed transformer coils will be of benefit in improving the full load efficiency of HTS transformers.

6.6 Conclusions

A dimensional analysis for the design of a 100 kVA, 3 phase, iron core, 6.6 kV/240 V, Wye-Wye connected transformer employing HTS tapes has been carried out and a systematic design procedure was developed and implemented. The mass, volume and tape length requirements were calculated over a range of core cross sectional areas. The analysis of mass and volume with core area variation showed the presence of distinct points that minimise these quantities. However, it was found that that these designs were impractical in reality owing to the significant length and cost of tape that they would entail. It was also shown that the coil electrical losses in these designs were too high owing to the length of tape required and from the higher hysteresis loss. By considering the factors of mass, volume, hysteresis loss, shape factor, and tape length, a suitable design was found which gave an overall three phase transformer efficiency of 98% and a leakage reactance of 1.8%.

For the purposes of analysing HTS transformer coils, it was found useful to introduce a new parameter, the coil shape factor, S, in order to characterise coils. The analysis revealed that the most appropriate coils to use had a shape factor of 2:1 and required a total of 1500 m of tape per phase. High shape factor coils were found to have a low leakage reactance and the major component of the hysteresis loss was determined to be due to the parallel field component. Low shape factor coils were found to have a high

leakage reactance and the major loss component was that owing to the perpendicular field component. Hence, flux diverters could be of benefit in reducing hysteresis losses of low shape factor, high reactance HTS transformers, but not for high shape factor, low reactance designs. The use of twisted filament HTS tape could be beneficial for reducing hysteresis losses in HTS transformers employing high shape factor coils.

References

[6.1] Private communication, Ravii Ravindran, transformer design engineer, ABB Australia, Ex. Alsthom U.K. (Retired).

[6.2] B.W.Connell, S.P.Mehta, M.S.Walker, "HTS Transformers", IEEE Power Engineering Review, pp 7-11, 2000.

[6.3] M.P Oomen, J. Rieger, M. Leghissa, H.H.J ten Kate, "Field angle dependence of alternating current loss in multifilamentary high – Tc superconducting tapes", Applied Physics Letters, Vol. 70, pg 3038, 1997.

[6.4] P. Kummeth, R. Schlosser, P. Massek, H. Schmidt, C.Albrect, D. Breitfelder, H-W Neumüller, "Development and Test of a 100 kVA superconducting transformer operated at 77K", Applied Superconductivity, Vol. 1, No. 167, pp 1099-1102, 1999.

[6.5] J.J Rabbers, B ten Haken, O.A Shevchenko, H.H.J ten Kate, "Total AC loss of BSSCO/Ag tape in different orientations of the external AC magnetic field", Inst. Phys.Conf. Ser., No. 167, pg 859, 2000.

[6.6] K.Kajikawa, A.Takenaka, K.Kawasaki, M. Iwakuma, K. Funaki, "Numerical simulation for AC losses of HTS tapes in combined alternating transport current and external AC magnetic field with phase shift", IEEE Transactions on Applied Superconductivity, Vol. 11 Issue: 1 Part: 2, pp 2240-3, 2001.

[6.7] M.Iwakuma, K.Funaki, *et al*, "Ac Loss Properties of a 1MVA Single-Phase HTS Power Transformer", IEEE Transactions on Applied Superconductivity, Vol. 11, No.1, 99 1482-1485, 2001.

[6.8] N.Magnusson, S.Hörnfeldt, "Losses in HTS Carrying AC Transport Currents in AC External Magnetic fields", IEEE Transactions on Applied Superconductivity, Vol. 9, No.2, 1999.

[6.9] N.Amemiya, K.Miyamoto, S.Murasawa, H.Mukai, K.Ohmatsu, "Finite Element analysis of AC loss in non-twisted Bi-2223 tape carrying AC tranport current and/or exposed to DC or AC external magnetic field", Physica C, No. 310, pp 30-35, 1998.

[6.10] J.Paasi, J.Lehtonen, M.Lahtinen, L.Kettunen, "Computation of AC losses in high-temperature superconductors", Physica C, No. 310, pp 62-66, 1998.

[6.11] M.Iwakuma, K.Funaki, H.Shinohara, T.Sadohara, M.Takeo, K.Yamafuji, "Electromagnetic Properties in Parallel Conductors Composed of Bi-2223 Multifilamentary wires for Power Transformer windings", IEEE Transactions on Applied Superconductivity, Vol. 7, No. 2, pp 298-301, 1997.

[6.12] F.Zizek, Z.Jelinek, Z.Timoransky, H.Piel, F.Chovanec, P.Mozola, M.Polak, "End-Winding Region Configuration of an HTS Transformer", IEEE Transactions on Applied Superconductivity, Vol. 12, No. 1, pp 904-906, 2002.

[6.13] J.K.Sykulski, K.F.Goddard, R.L.Stoll, "High temperature superconducting demonstrator transformer: design considerations and first test results", IEEE Transactions on Magnetics, Vol. 35 Issue: 5, Part: 2, pp 3559 –61, 1999.

[6.14] M.K. Al-Mosawi, C.Beduz, Y.Yang, M.Webb, A.Power, "The effect of flux diverters on AC losses of a 10 kVA high temperature superconducting demonstrator transformer", IEEE Transactions on Applied Superconductivity, Vol. 11, Issue: 1 Part:

1, pp 2800-3, 2001.

Chapter 7

Assembly and testing of a 100 kVA HTS LN transformer

7.1 Introduction

A primary and secondary coil forming a single phase of a 100 kVA three phase transformer was constructed using the results gained from the dimensional and FEM analysis (described in Chapter 6), the AC loss measurements (described in Chapter 4 and 5), and the coil winding experiments (described in Chapter 3). A total of 1500 m of tape was used to wind both coils of the phase into solenoids. The coils were subsequently cured and tested in LN. Due to practical construction considerations, the details varied slightly from the optimum found in Chapter 6, however, the design was essentially that of design 1, *i.e.* 1500 m 2:1. Owing to the small size of the transformer, it was only practical to obtain a 3 limb core from a limited choice of sizes, rather than a purpose built core. A four step cruciform type core with a cross sectional area of 0.011 m^2 was obtained, rather than one with an optimised 0.0096 m^2 as described in Chapter 6. The design of the coils were subsequently altered to suit this area. In addition, to save on the HTS tape requirement, the primary coil was placed inside the secondary against convention. Owing to the relatively low voltage of operation, and the clearances allowed for, this had no consequence on the insulation co-ordination.

7.2 Phase coil winding and arrangement

The secondary conductor was composed of a stack of 6 tapes, each with a nominal Ic of 50 A, to give a total conductor Ic of 300 A. At the time of winding the secondary, it was not

possible to individually insulate each HTS tape, and hence, the tapes were simply stacked on top of each other allowing resistive conduction between them. A total of 58 turns of this conductor was wound across a 405 mm coil length and terminated to form the secondary coil. The turn to turn insulation on both phase coils was provided by insulation system A.

The primary coil was wound with a single HTS tape with a nominal Ic of 30 A. A total of 1600 turns were wound over 16 layers with 2 resistive joints required. Again, turn to turn insulation was provided by insulation system A. The layer to layer insulation of the primary coil was provided by the same insulation material. In addition, each layer of the high voltage coil had an additional 10 mm overlap of insulation to increase the creep distance between turns of adjacent layers at the coil ends.

Both coils were further insulated to provide sufficient coil to coil insulation for 6.6 kV operation. Each coil was potted according to the best techniques found in this work, Chapter 3, to ensure robustness, immunity to the effects of LN, and maintenance of Ic after repeated thermal cycles.

The coils were each separately cooled in LN using the slow thermal technique and the Ic measured using a standard 4 point DC technique as described in chapter 4. The measured Ic of the secondary coil was 214.5 A, in the self field of the coil. It was estimated that the parallel component of the field was 40 mT at the Ic and the perpendicular component was 5 mT. The estimated field free Ic was calculated to be 270 A close to that required, and sufficient for a low loss 100 kVA design [7.1]. Table 7.1 summarises the electrical and dimensional details of the coils. The voltage to current relationships of each coil are shown in Figures 7.1 and 7.2 respectively.

Quantity	Primary	Secondary
Turns [-]	1600	58
Nominal turns ratio	27.59	27.59
Measured turns ratio	27.47±0.1	27.47±0.1
Length of tape [m]	1190	270
Length of coil [m]	0.400	0.405
Measured terminal resistance at 300 K [Ω]	40.5	0.19
Measured self inductance in air [H]	0.24	4.08×10^{-4}
Tape Ic (77 K, self field)	23	50
Coil Ic (self field of coil, 77 K) [A]	11.4	214.5
Coil n (self field of coil, 77 K) [-]	11	13.85

Table 7.1. Details of the primary and secondary coils wound. Self inductances were measured at 120 Hz.

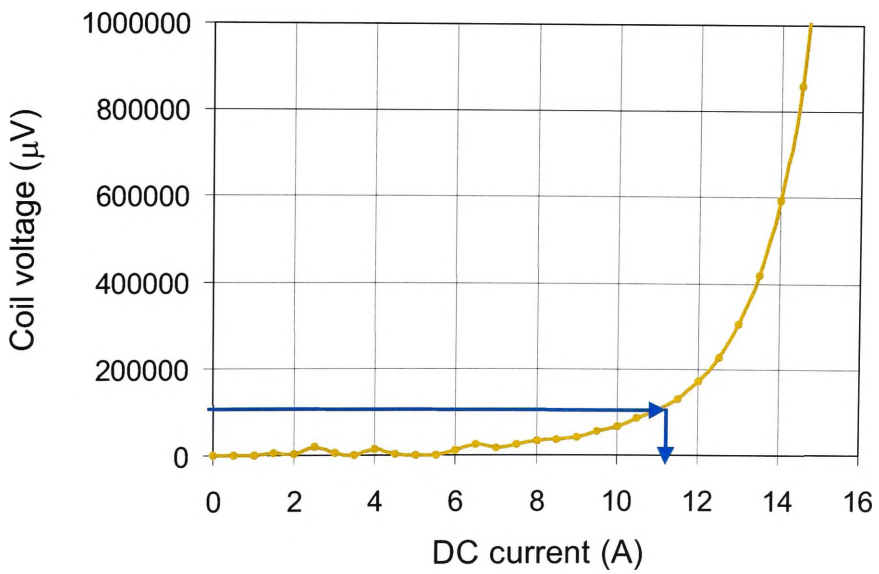

Figure 7.1. Self field I-V curve of the primary coil, over 1200 m, at 77 K.

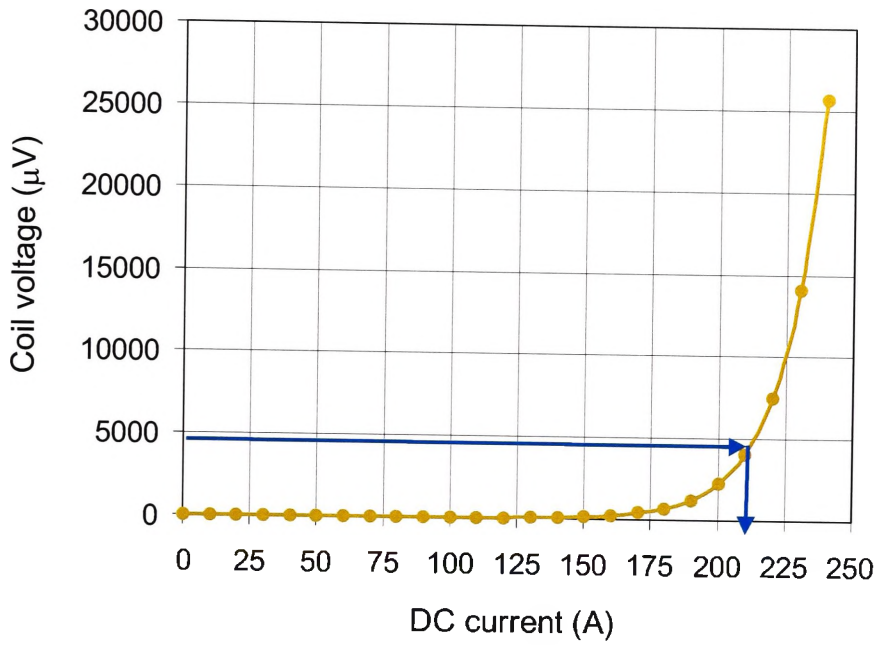

Figure 7.2. Self field I-V curve of the secondary coil over 50 m at 77 K

The phase coils were arranged on the iron core according the clearance diagram shown in Figure 7.3. As can be seen, non uniform insulation between the coils and core was used as the initial design specification was for a star : star transformer. This is particularly advantageous for superconducting transformers as it leaves a greater level of coolant (LN) at the top of the coil, and a greater distance between the coil and cryostat lid. It is usual for the high voltage winding to be connected in star arrangement and the lower voltage winding in delta arrangement to take advantage of the reduced insulation requirements to the bottom yoke, while still limiting harmonics into the secondary line.

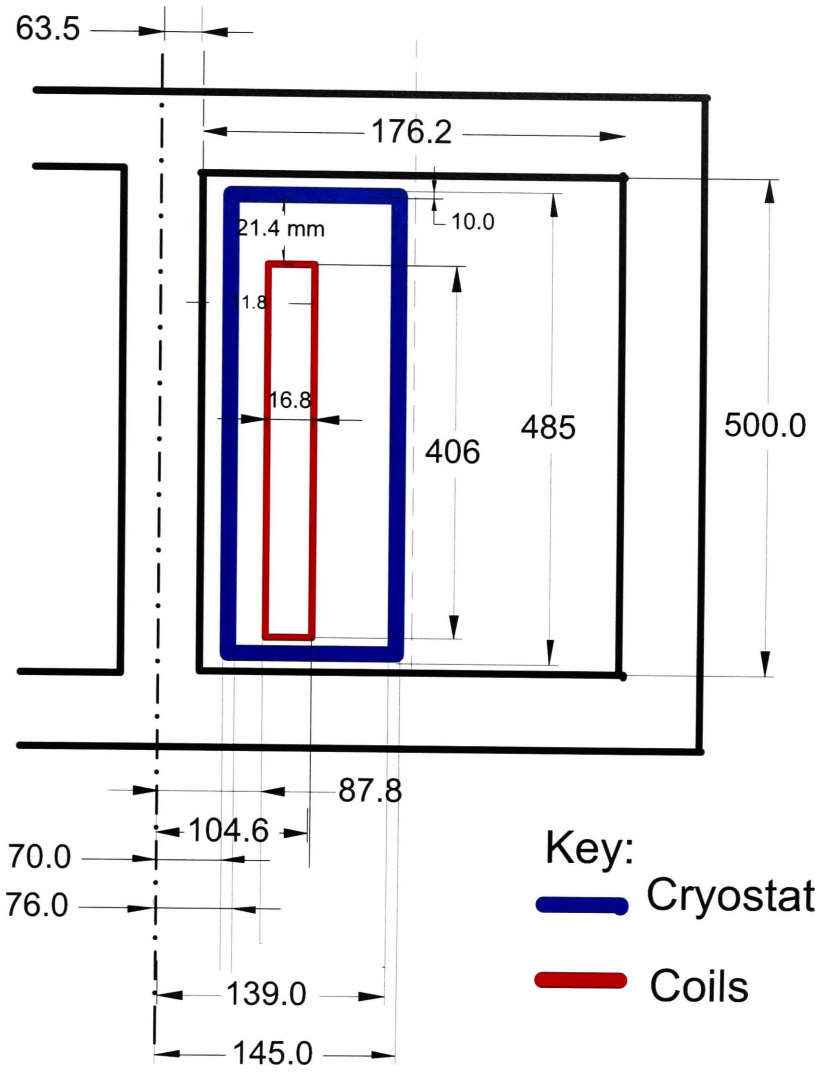

Figure 7.3. Clearance diagram (mm) of the constructed transformer.

7.3 Testing of the transformer

No suitable warm bore cryostat was available to carry out testing of the complete transformer in LN. However, room temperature measurement of the open circuit and short circuit characteristics were performed to obtain the turns ratio and leakage reactance which are independent of the temperature of operation. The room temperature equivalent circuit diagram was drawn, and an approximate equivalent circuit diagram at 77 K inferred from

this by eliminating the DC resistance. Figure 7.2 shows the equivalent circuit, the symbols used, and the placement of meters for testing. The results are shown in table 7.2, including the re-calculated leakage reactance and the iron core losses for the final constructed coil/core arrangement.

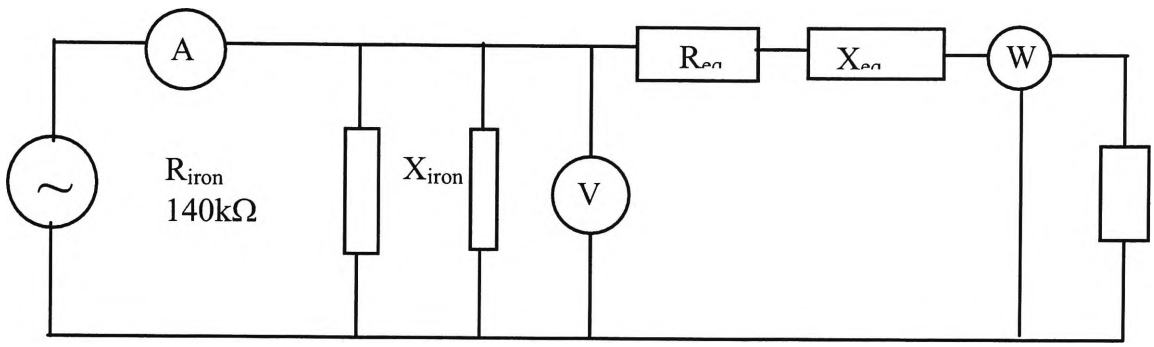

Figure 7.2. The equivalent circuit at room temperature and the conventions used.

Quantity	Primary	Secondary
Turns [-]	1600	58
Calculated turns ratio	27.59	27.59
Measured turns ratio	27.47±0.1	27.47±0.1
Calculated DC Req [Ω]	183.2	-
Measured AC Req, short circuit test [Ω]	203	-
Measured AC Req, p.u	0.157	
Calculated Xeq [p.u] (Method 2)	1.56	
Measured Xeq [p.u] (O/C test)	1.78	

Table 7.2. Results of the room temperature tests. The p.u values are on a 100 kVA base

The open circuit test was performed on the secondary side to reduce the supply voltage required. At room temperature, it was not possible to apply full secondary voltage during

the open circuit test and hence the core was not fluxed to 1.75 T. The equivalent circuit parameter representing iron loss, R_{iron}, and reactive VAR's were approximated from the data supplied by the manufacturer.

The phase coil insulation and clearances were tested at room temperature and by applying up to 90 V rms on the secondary side and thereby inducing an open circuit voltage of 2.5 kV rms on the primary side. By taking the 10 mm coil to coil clearance into consideration, this level of voltage was considered safe. No collapse of the voltage was observed during this test. It should be noted, however, that the AS2374 documentation specifies a test voltage of up to 28 kV, which would require a secondary voltage of 1000 volts. The insulation clearances were insufficient to carry out this test in air.

The turns ratio was checked by applying a 50 Hz AC voltage signal to the secondary coil with the primary open circuited. The average measured value of 27.47 was 0.47 % below that calculated from the turns ratio of 27.59, however, this is within the AS guidelines which allow a 0.5% deviation.

7.4 Conclusions

An HTS primary and secondary coil were manufactured for the construction of a single phase of a low loss 100 kVA LN HTS transformer. The coil winding techniques developed in this work were found suitable for the construction of robust coils which were immune to the temperature effects of LN, and thermal quenching.

The measured Ic (at 77 K in self field) of each of the coils was found suitable to construct a low loss transformer with a 6.6 kV/240 V rating. The turns ratio was measured to be within 0.5% of that designed, and the leakage reactance was close to that predicted

by the approximation formulae.

References

[7.1] F.Darmann, R.Zhao, G.McCaughey, M.Apperley, T.P.Beales, "Calculation of the critical current in pancake coiled long length Bi-2223/Ag tapes in non-uniform local magnetic fields perpendicular to the grain alignment axis", Cryogenics, Vol. 39, pp 445-451, 1999.

Chapter 8

Summary and Conclusions

8.1 Conclusions

A manufacturing technique for making short lengths and potentially long lengths of twisted filament tape with different sheath and matrix alloys was investigated and optimised over the period of two years as part of this work and is described in Chapter 2 and Appendix 1. Samples of twisted filament tape with Ic values the same as the control samples were manufactured with twist pitches as low as 8 mm and Ic's of 40 A (77K, Zero applied field). HTS tapes with shorter twist pitches of 4 mm were also investigated and a variety of matrix materials were also included in these investigations.

In Chapter 3, a technique for the winding, insulating, and potting of pancake and solenoid type coils suitable for transformers and other applications was investigated. Several pancake coils and proto-type solenoid coils for the transformer were manufactured to establish the technique. A variety of insulation materials and techniques of application were investigated for this purpose and the benefits of each for different applications were assessed. It was found in section 3.3 that up to 45 double quenches could be performed on pancakes with negligible decrease in Ic. Under the severe double quench test, the Ic of pancake coils degraded consistently by a very small 0.1 A/double quench. Under the less severe thermal cycle testing, the Ic of coils and pancakes was found not to degrade at all.

In Chapter 4, the twisted filament tape samples prepared in the work described in Chapter 2 were characterised for AC losses in a purpose built "short length" AC loss rig at 77 K against control samples. Through this work, a suitable matrix material and twist pitch

combination was found which could lower the hysteresis loss of the tapes by a factor of two to six in a suitable window. The sample which showed the most benefit from twisting of the many tested had a unique alloy matrix and a twist pitch of 4 mm, (Section 4.2.3).

A cryogenic calorimeter to investigate the AC losses of coils under a variety of magnetic fields and transport current was built over a period of three years and described in section 4.3. It was found that the calorimeter was suitable for resolving losses in solenoid wound coils and pancakes with an uncertainty as low as ±0.5 W. The main conclusion found from AC loss data gathered from the calorimeter is that induced currents dominated the self field losses of a solenoid coil at 55 Hz, and hysterises losses dominated at 110 – 200 Hz. [See section 4.4.6]. In an applied parallel field, however, hysterises losses dominated at 55 Hz. In a pancake coil, the analytical solutions of Carr for the hysteresis losses of an infinite slab with transport current and applied parallel field provided the closest approximation for the transport AC losses.

Investigations into the electrostatic, thermal, and various other design issues in transformers were described in Chapter 5. It was found that LN HTS transformers could solve many of the current problems facing design engineers. In particular, it was found that LN performs better as a dielectric than transformer oil with higher breakdown characteristics under all circumstances and it has no partial discharge by-products [See section 5.3].

In section 5.3 it was also found that the electrostatic design of transformer coils is not substantially different from conventional transformers due to the favourable ratio of dielectric constants of the materials used. Finite element analysis showed that the small radius of curvature of the HTS tapes does not considerably influence the field enhancement

effect at the surface, and is almost completely masked by the coil edge enhancement effect [Figures 5.6,5.9].

The subject of keeping the iron core cool in ambient air was analysed in section 5.5. By setting up a simplified model of cylinders in a cross flow of air with reasonable velocity, it was shown, using the established equations, how a three limb iron core structure could remain sufficiently cool even without the benefit of oil as a coolant. In addition, the sound level due to the magnetostriction of this structure was found in section 5.6 to be at least 2 dB less than that calculated for an equivalently rated conventional transformer.

In Chapter 6 it was shown that practical coils of sufficiently low ac loss could be manufactured from HTS tape with characteristics suitable for transformers that could benefit from a reduction in the overall losses, size, and mass [Section 6.5]. In particular, it was shown in section 6.2 that the shape factor of the coils, rather than the volts/turn was an important parameter and that this could be used as a variable to summarise the properties of a particular design. Significant insight into HTS transformer design was gained by plotting variables such as mass, volume, hysteresis losses, and leakage reactance in terms of the coil shape factor [Section 6.2]. The shape factor is such an important parameter because of the anisotropic properties of the HTS conductor [Section 6.3]. It was found that by using coil shape factors of around S = 2, the parallel field hysteresis losses dominated the loss [Section 6.5.3]. Twisted filament tape could be of further benefit in lowering the hysteresis losses of high shape factor coils, but not flux diverters. The hysteresis loss due to perpendicular fields was found to dominate the total hysteresis loss in coils with shape factors of S=1, and hence flux diverters could be of benefit. In this case, only 10 % of the winding volume was responsible for about half the total coil losses.

Using the knowledge and experience gained from the work described in Chapter 3, two fully insulated and potted solenoid type coils for the transformer primary and secondary were wound with a total of 1500 m of tape as per the found optimised solution in Chapter 6. Chapter 7 describes how these were designed and constructed with terminations, and insulation sufficient for both the over voltage and LI test levels appropriate for a voltage of 6.6 kV. The Ic values in self field, which was significant, were found to be 11 A and 235 A respectively, which is more than adequate for this rating of transformer.

8.2 Equipment and measurement systems built

The research for this thesis required the design and development of a considerable amount of new manufacturing and measurement equipment and systems. These are summarised in this section.

1. Short length AC loss measurement system based on lock-in amplifier

Section 4.1 – 4.2

This rig was built from components such as a lock-in amplifier, audio amplifier, copper coil, and sample holder. Labview™ software was used to control the data acquisition and the various components using a GPIB card and IEEE protocols.

2. Mass boil off calorimeter.

Section 4.3 – 4.5

A liquid nitrogen calorimeter with field coil, mass flow meters, and PWM power supply. was built up in stages over two and a half years. Most components were drawn in turbo-

Cad™ for a machinist to manufacture. A manufacturer of glass cryostats capable of handling the required dimensions was also located and one ordered. The field coil was designed, specified, and the insulated strip specified. Due to the large size and power of the field coil, a third party carried out the winding, however, the thermal and electromagnetic design was part of the research work reported here as was then construction of the safety housing around the cryostat and field coil and the final assembly of the whole device.

Suitable mass flow meters were sourced and two finally purchased after about 6 months of investigations. The software was written in Labview™ to communicate between the lock-in amplifier, PWM supply, audio amplifier control, and the mass flow meters.

3. One phase of a liquid nitrogen cooled HTS 100 kVA transformer

The Iron core for the transformer, its frame, the bushings, current feed throughs, and coil holder were designed and specified as part of this work, and manufactured by a third party. However, the timber frame to constrain it was designed and constructed as part of the research work.

The materials for a GFRP cryostat were investigated, tested, and sourced as part of this work. The coils (1 phase, Primary and Secondary) were designed and wound from tape supplied by AS. Considerable input to the specification of the tape was also provided as part of this research.

4. Coil winder

A coil winder/tape wrapper specification was written. The device was built by a third party but research was required to define the transpositioning details and mechanics and the tolerances of stresses and strain which the tapes could safely handle. A number of commissioning trials, carried out over 12 months, were required as part of this work to improve the functionality of the coil winder. This involved winding several solenoids and pancakes and modifications and improvements were made to the insulation application technique and the HTS tape guiding system.

5. Cryostat testing rig

A roughing pump and differential pump arrangement was re-commissioned in order to set up a rig for the testing of warm bore cryostats. A small iron core (5 cm diameter, 3 limb) arrangement in a wooded structure was constructed for this purpose.

6. GFRP warm bore cryostat development

In conjunction with a third party, the development of a warm bore, vacuum insulated double wall GFRP cryostat was undertaken during this work. The design and project was conceived and run as part of this work. Testing of the cryostat for vacuum tightness, and LN boil off rate was also conducted as part of the research work. Using a simple epoxy resin system, the insulation vacuum space reached better than $5x10^{-5}$ Torr.

8.3 Suggestions for further work

Measurements of the AC loss of coils in the MBC is currently on-going to confirm the results obtained in this research work, and also to more fully characterise the frequency

response of pancake coil self field losses. In addition, the AC losses of coils with the combined action of applied AC field and AC transport current needs to be characterised. It is understood that many different possible types of measurements are possible including the addition of a DC background field and current, and various phase differences between applied field and transport current.

The characterisation of AC losses of coils which have been wound with low loss HTS tapes needs to be investigated as well as this is the driving force behind their development.

At the time of writing, a suitable stainless steel warm bore cryostat was being procured, but due to delays in its development and specification, it was unable to be incorporated in the final transformer construction. When this arrives, the AC losses under different load conditions will be measured.

It is also intended to model high reactance HTS transformers, with flux diverters in place. Based on the literature, and the hysteresis loss distribution throughout the modeled coils, this technique seems the best way of achieving both a high reactance and low loss HTS transformer.

Betta Book Binding Printing
M & D Morrisey 4261 2998
26 Fields Street
Kanahooka NSW 2530